HIGH-RESOLUTION REMOTE SENSING APPLIED TO MINERAL EXPLORATION IN AUSTRALIA

VOLUME II

ANDREW R. GABELL

DEPARTMENT OF GEOLOGY AND GEOPHYSICS, UNIVERSITY OF ADELAIDE

April, 1986

A Thesis submitted for the Degree of Doctor of Philosophy

LIST OF FIGURES

Figure 1.1 Location of test sites.

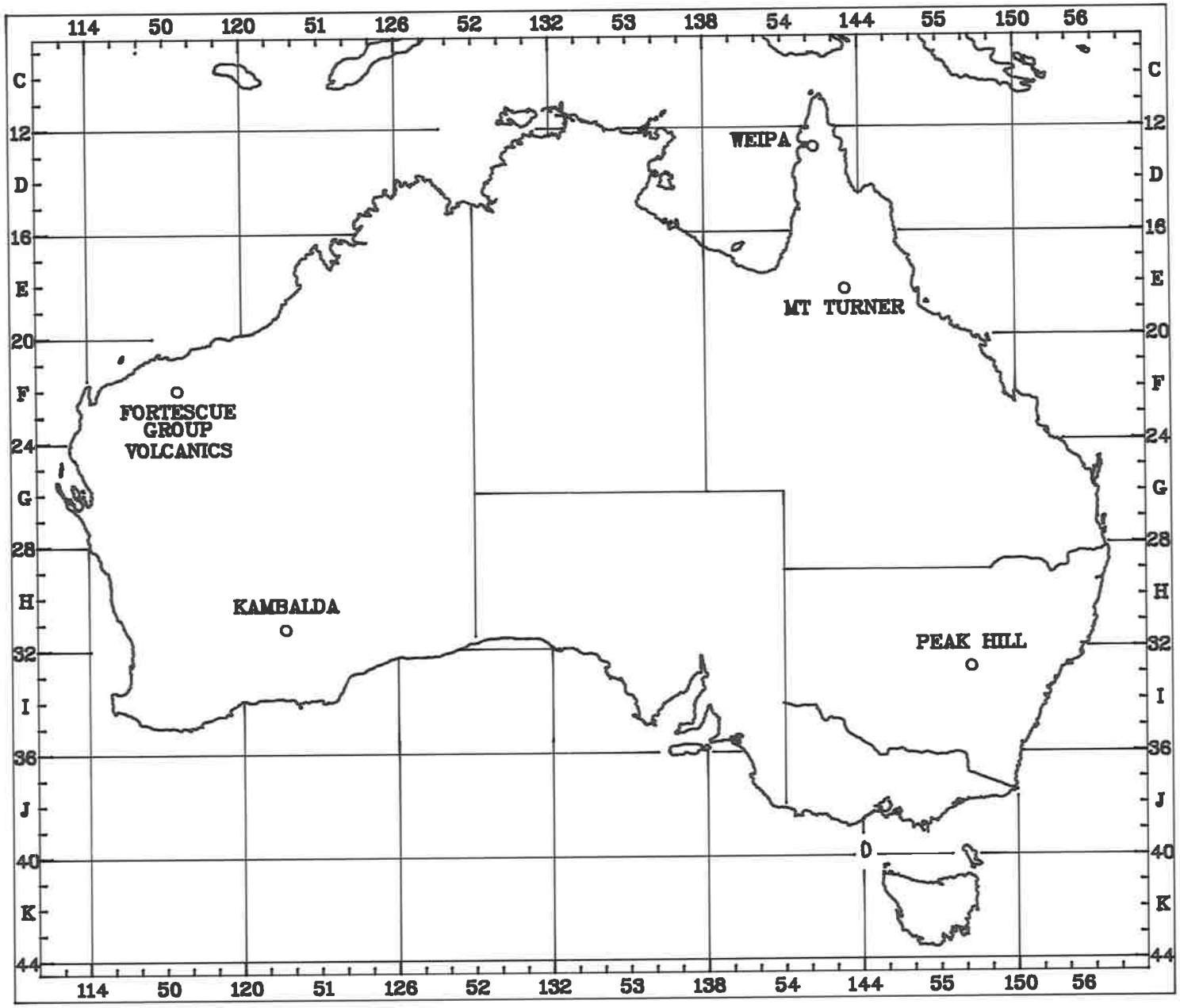
114 50 120 51 126 52 132 53 138 54 144 55 150 56
C 12 D 16 E 20 F 24 G 28 H 32 I 36 J 40 K 44
WEIPA
MT TURNER
FORTESCUE GROUP VOLCANICS
KAMBALDA
PEAK HILL

FIGURE 1.1

Figure 2.1 The electromagnetic spectrum and atmospheric transmission.

The wavelength regions defined in section 1.5 are shown, with their percentage atmospheric transmission. Landsat MSS and TM bandpasses are also shown for reference. The regions most utilised for remote sensing are the VNIR (.4 to 1.1μm), SWIR (1.1 to 2.5μm) and MIR (8 to 14μm).

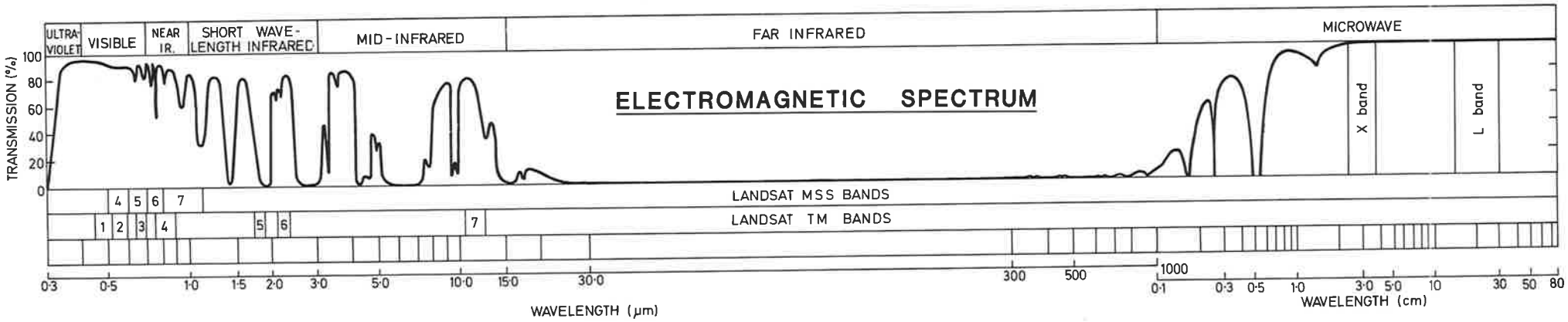
ULTRA-VIOLET
VISIBLE
NEAR IR.
SHORT WAVE-LENGTH INFRARED
MID-INFRARED
FAR INFRARED
MICROWAVE
ELECTROMAGNETIC SPECTRUM
TRANSMISSION (%)
100
80
60
40
20
0
X band
L band
LANDSAT MSS BANDS
LANDSAT TM BANDS
4 5 6 7
1 2 3 4 5 6 7
0·3 0·5 1·0 1·5 2·0 3·0 5·0 10·0 15·0 30·0 300 500 1000
WAVELENGTH (μm)
0·1 0·3 0·5 1·0 3·0 5·0 10 30 50 80
WAVELENGTH (cm)

Figure 2.2 The spectral response of green vegetation in the VNIR and SWIR.

In addition to the reflectance of green vegetation,the cause of the spectral features in each region is shown. The spectral regions where mineralogical effects occur are also depicted, as are Landsat MSS and TM bandpasses.

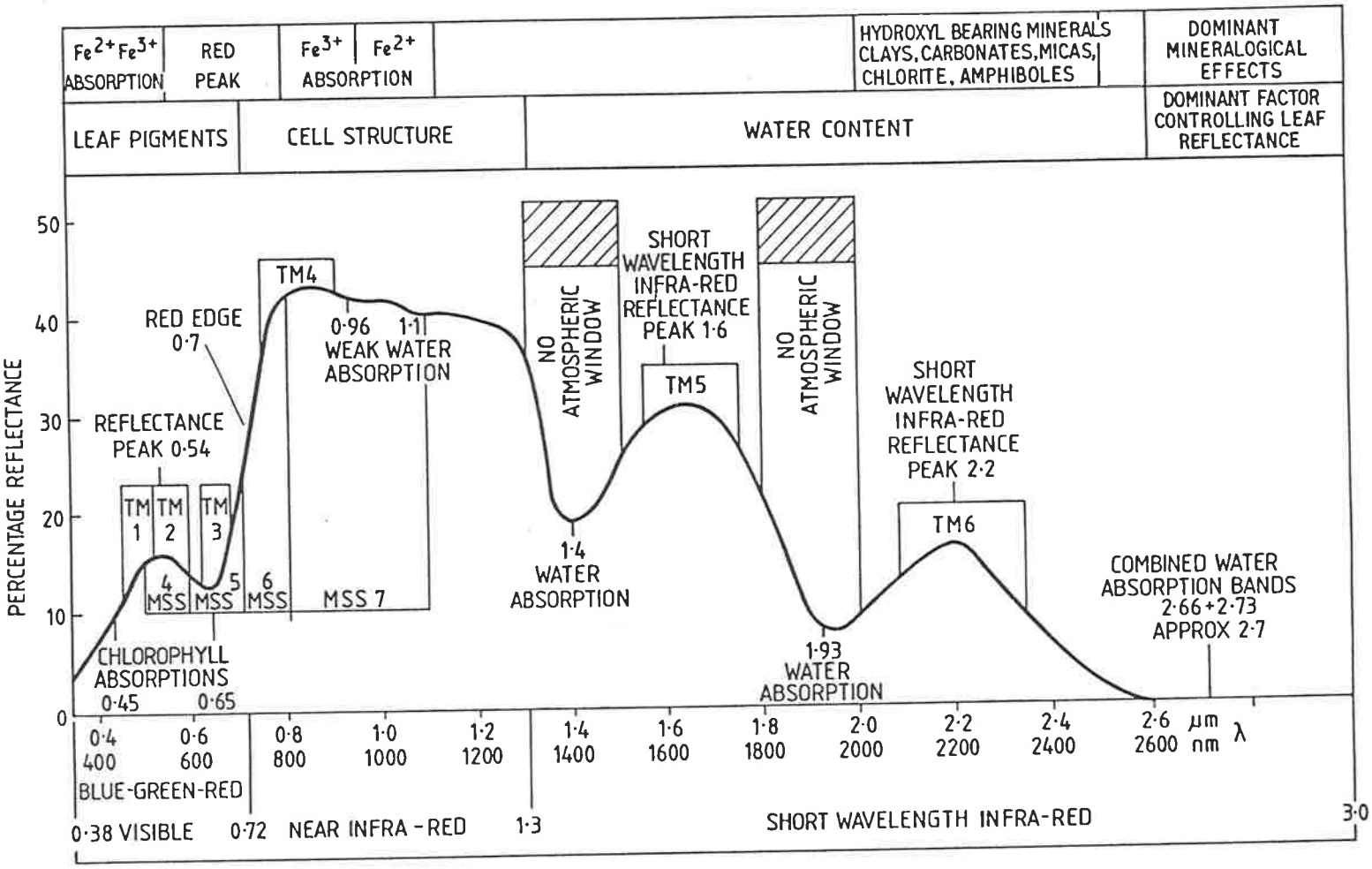

SPECTRAL RESPONSE OF GREEN VEGETATION AND LANDSAT BANDS

Figure 2.3 Typical VNIR spectra of the iron oxides.

The absorption features in iron-bearing rocks occur at wavelengths that vary slightly because of crystal field or charge transfer effects. Typical absorption wavelengths are shown for some iron oxides and the sulphate, jarosite. Note the absence of diagnostic features in the spectra of the iron-free shale and carbonate rocks. Landsat MSS and TM bandpasses are included for reference.

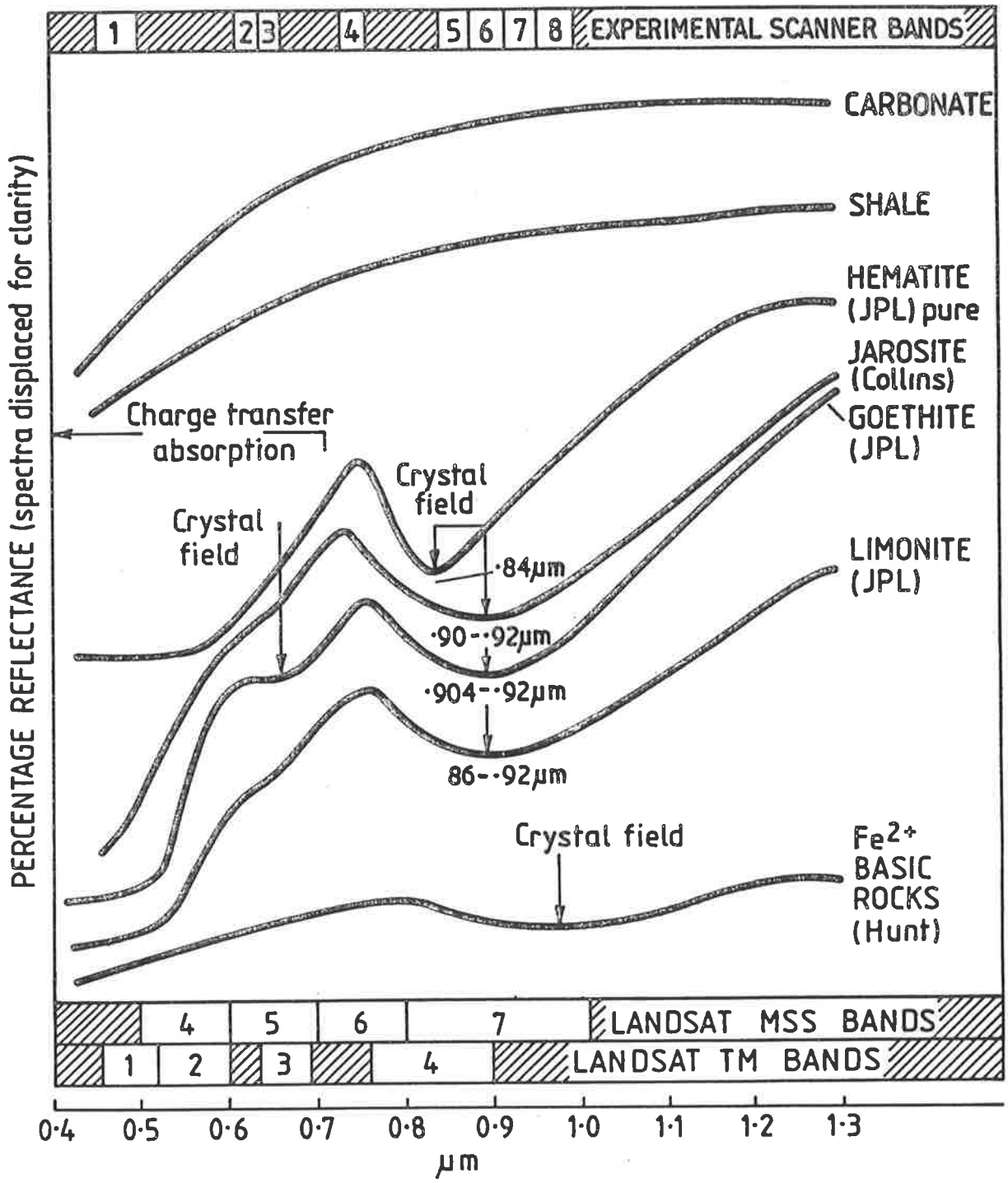

TYPICAL VISIBLE AND NEAR INFRARED SPECTRA OF THE IRON OXIDES

Figures 2.4a&b MIR kaolinite transmission spectra.

Figure 2.4a depicts the fundamental O-H stretching absorption features (ν_{OH}).

Figure 2.4b shows the fundamental O-H bending absorption doublet, near 900 cm^{-1}. The doublet structure is due to the occupation by hydroxyls of two non-equivalent lattice sites.

KAOLINITE INFRARED TRANSMISSION SPECTRA

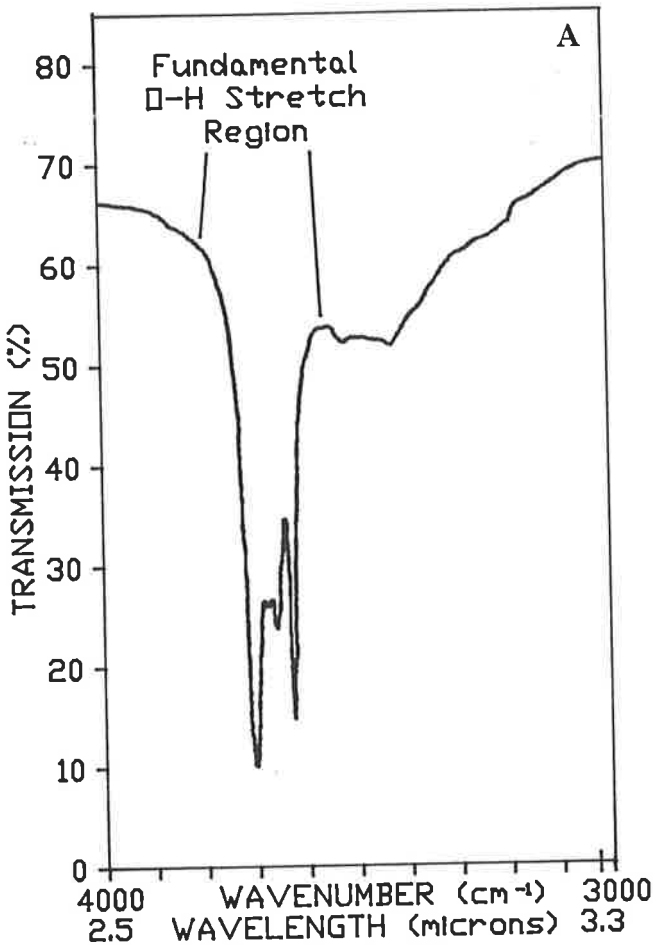

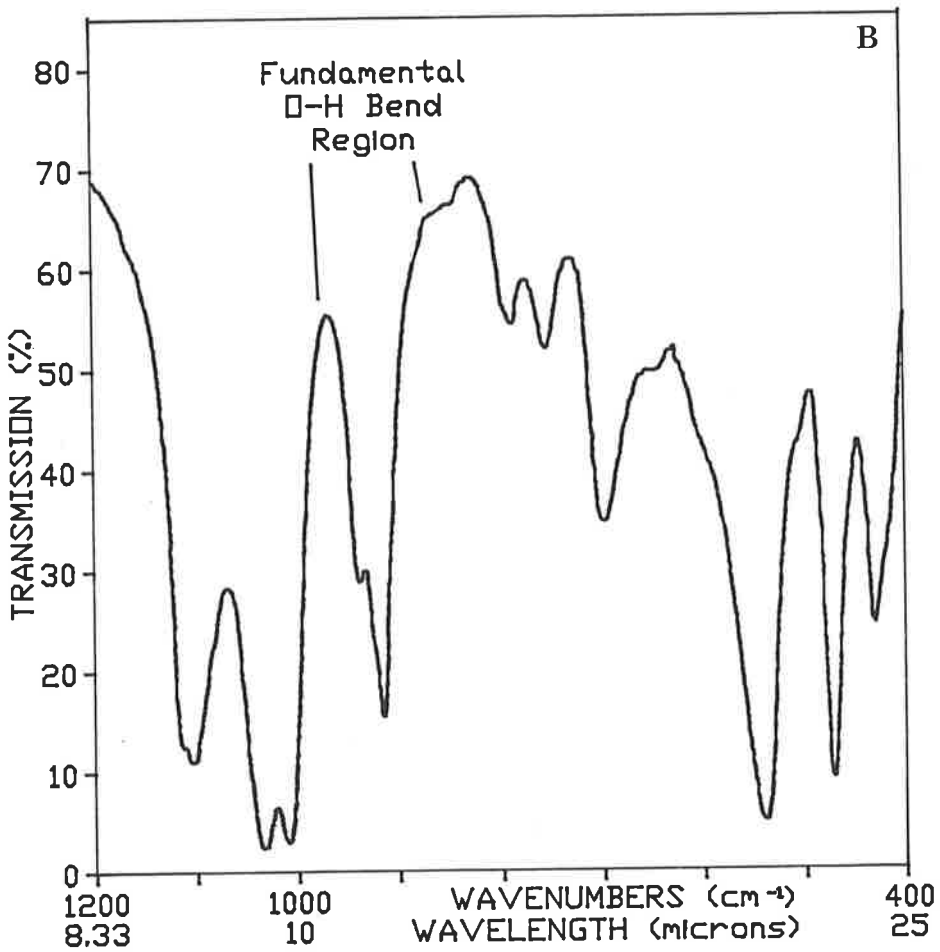

Figure 2.5 SWIR reflectance spectra - Al-OH minerals.

The SWIR reflectance spectra of some important dioctahedral (Al-OH) phyllosilicates are shown. In a remote sensing mode, the features at 1.4 and 1.9μm are largely obscured by atmospheric absorption. The major absorption feature between 2.0 and 2.5μm is caused by the combination of fundamental bending and stretching vibration frequencies. It is this region that is most useful for remote sensing. Note that the doublet structure exhibited by kaolinite is very similar to that of its fundamental O-H bending feature (Fig. 2.4b). The spectra are from the CSIRO/MXY spectral library, and have been displaced vertically for clarity.

REFLECTANCE SPECTRA - AL-OH MINERALS

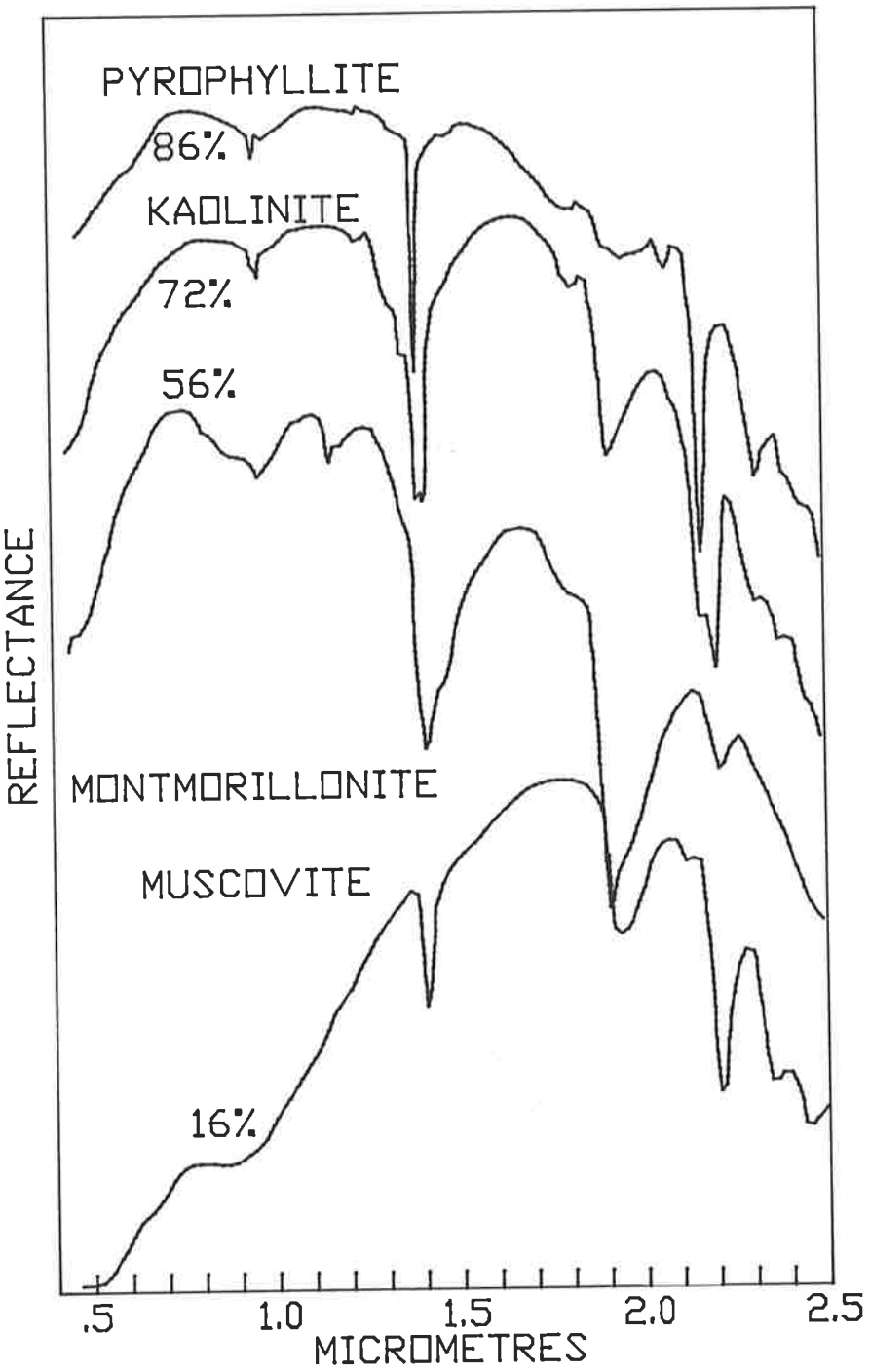

Figure 2.6 SWIR reflectance spectra - Mg-OH minerals.

The SWIR reflectance spectra of the trioctahedral (Mg-OH) phyllosilicates, talc and chlorite, and the Ca,Mg-bearing amphibole, tremolite, are depicted. These spectra are also from the CSIRO/MXY spectral library, and have been displaced vertically.

REFLECTANCE SPECTRA - MG-OH MINERALS

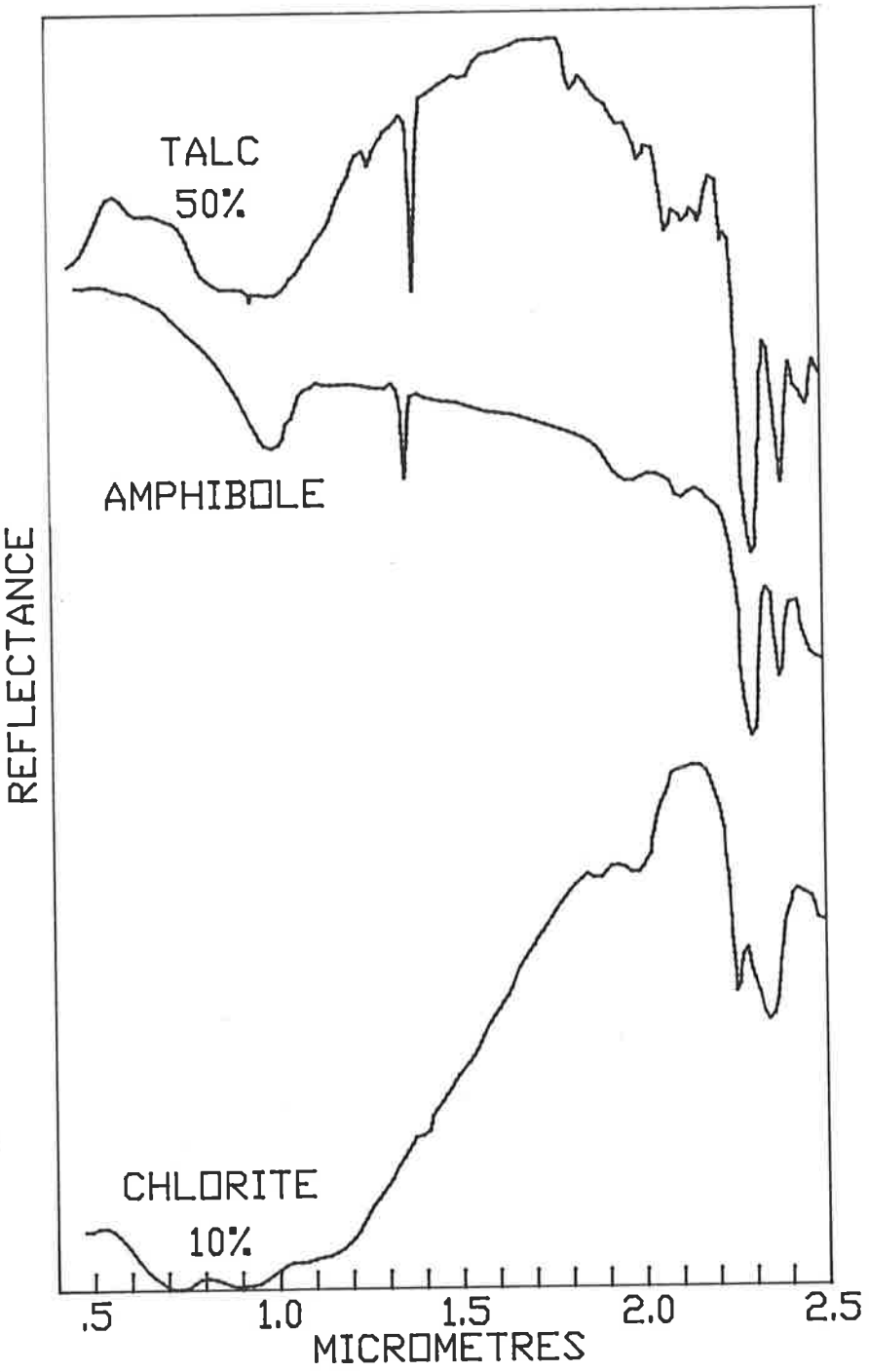

Figures 2.7a&b VNIR reflectance spectra of kaolinite.

Figure 2.7a shows the VNIR reflectance spectrum of a kaolinite sample from Alum Mountain, NSW. The $3\nu_{OH}$ absorption appears as a doublet centred on .952μm and .964μm.

Figure 2.7b depicts the magnified inset of Fig. 2.7a. The absorption feature at .75μm is barely detectable, but does represent significantly greater variation than the noise level. Although the theoretical position of the third overtone is .71μm, it is likely that this minimum represents the $4\nu_{OH}$ absorption feature.

VNIR REFLECTANCE SPECTRA OF KAOLINITE

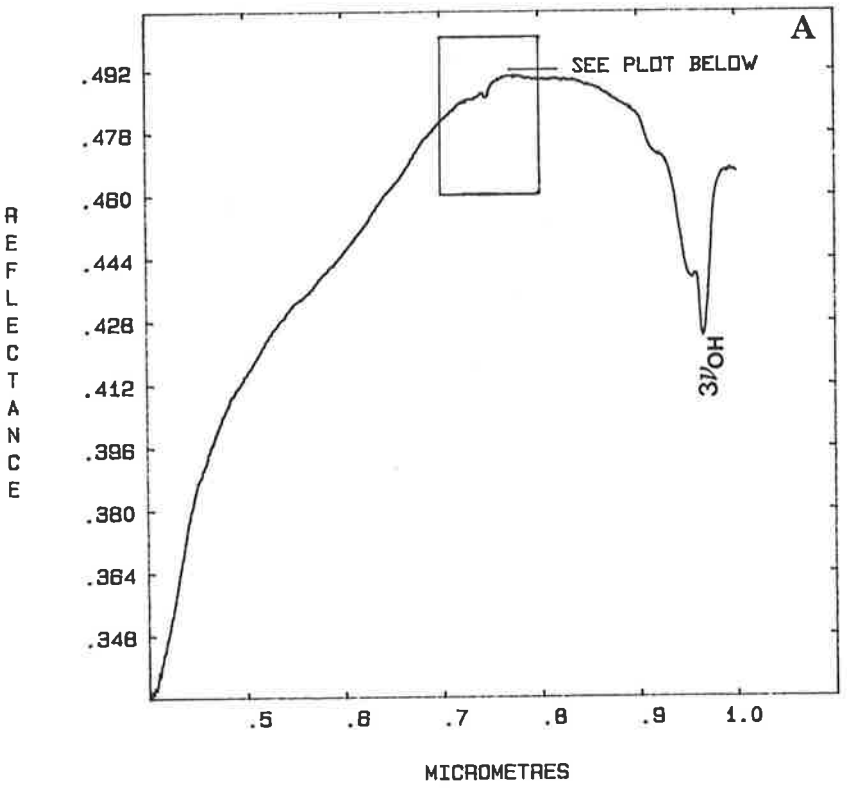

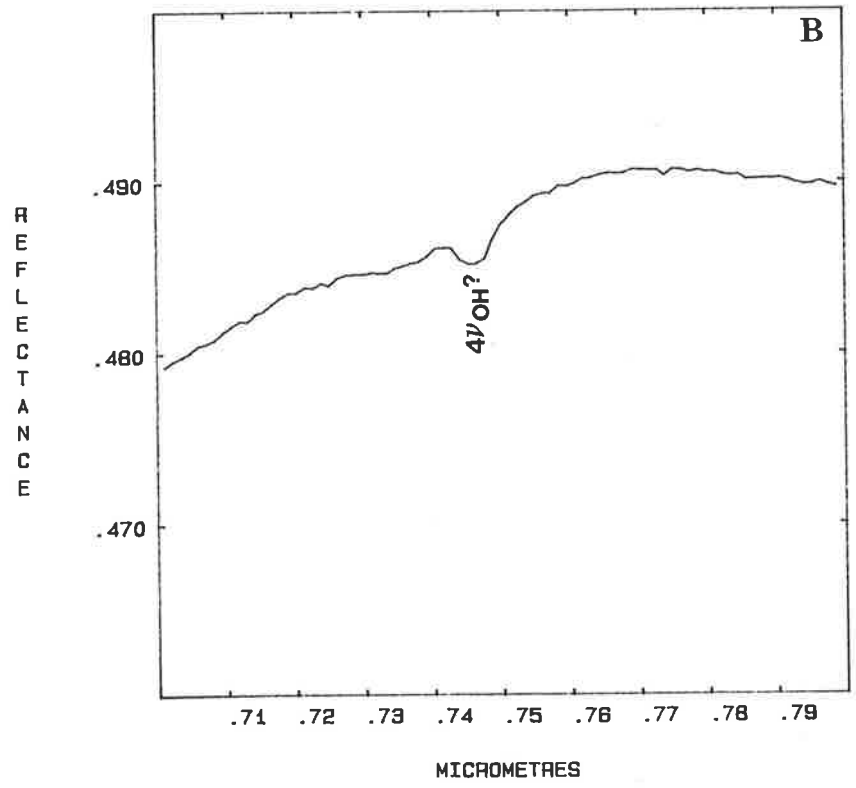

Figure 2.8 SWIR reflectance spectra - carbonates.

The SWIR reflectance spectra of magnesite ($MgCO_3$), dolomite ($(Ca,Mg)CO_3$) and calcite ($CaCO_3$) are shown. Hunt and Salisbury (1971) ascribe the major absorption feature near 2.3μm to the third overtone of the antisymmetric mode of the carbonate ion ($3\nu_3$). The vertical line on the plot is centred on 2.32μm, and is included as a reference point to highlight the progressive shift of the $3\nu_3$ minimum to longer wavelengths with increasing Ca content. The higher atomic weight of Ca relative to Mg leads to the slight decrease in frequency (or increase in wavelength) at which the carbonate ion vibrates. The spectra are from the CSIRO/MXY spectral library, and have been displaced vertically.

REFLECTANCE SPECTRA - CARBONATES

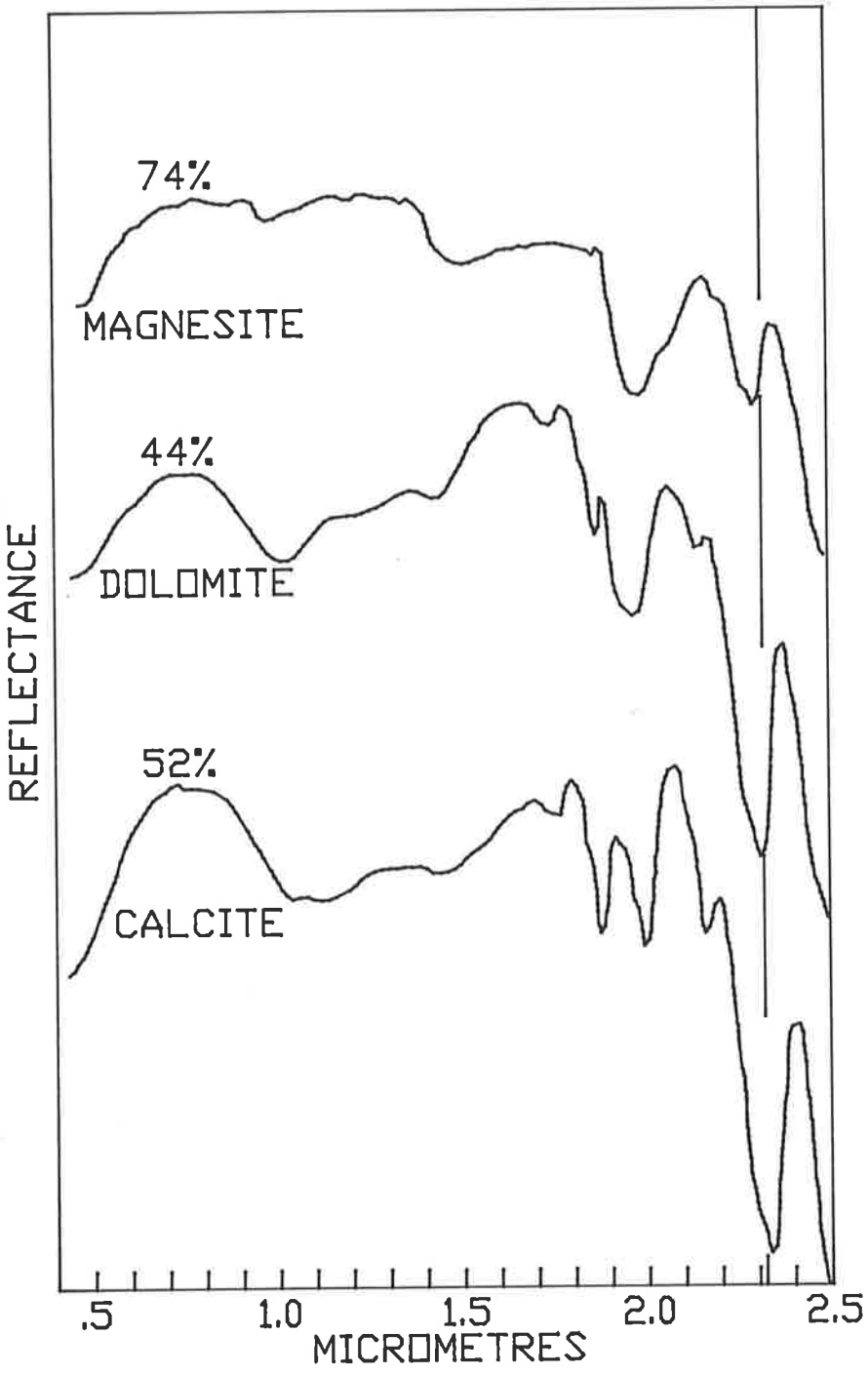

Figure 2.9 SWIR reflectance spectra - sulphates.

The SWIR reflectance spectra of jarosite ($KFe(OH)_6(SO_4)_2$), alunite ($Al_3(SO_4)_2(OH)_6$) and gypsum ($CaSO_4.2H_2O$) are depicted. Hunt et al. (1971) attribute all of the absorption features in alunite to various overtones and combination tones of Al-O-H, and those of gypsum to overtones and combination tones of water. The jarosite spectrum measured by Hunt et al. showed almost no absorption features, but those of the spectrum shown here are consistent with an origin due to Fe-O-H. (The absorption features of jarosite correlate well with those of alunite, but are shifted to longer wavelengths). Because the sulphate fundamentals occur at low frequencies (the highest being only $1100cm^{-1}$), at least the fourth overtone would be required to produce features in the SWIR, making their detection unlikely. The spectra are from the CSIRO/MXY spectral library, and have been displaced vertically.

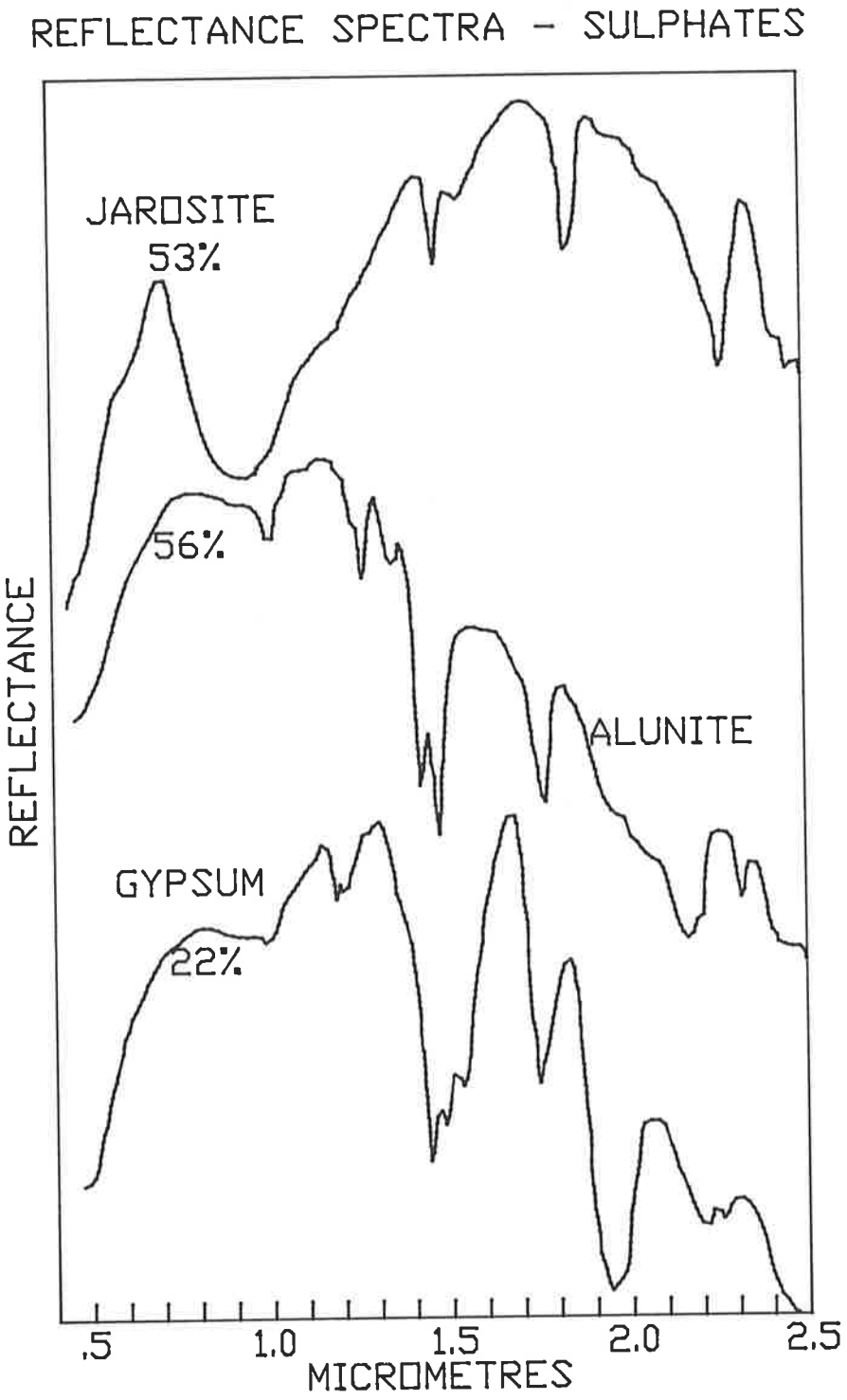
REFLECTANCE SPECTRA - SULPHATES
JAROSITE
53%
56%
ALUNITE
GYPSUM
22%
REFLECTANCE
.5
1.0
1.5
2.0
2.5
MICROMETRES

Figure 2.10 MIR spectra of felsic rocks (after Eberhardt et al., 1984).

The solid lines are emissivity curves for felsic rocks, which have an increasing feldspar content from the top curve downwards. They have been displaced for clarity, and superimposed on reflectance plots of a granite (crosses) and a quartzite (triangles).

Figure 2.11 MIR spectra of intermediate rocks (after Eberhardt et al., 1984).

The solid line is the emissivity spectrum of an andesite (plotted with a scale factor of 3). The reflectance spectrum of a diorite (diamonds) is shown for comparison.

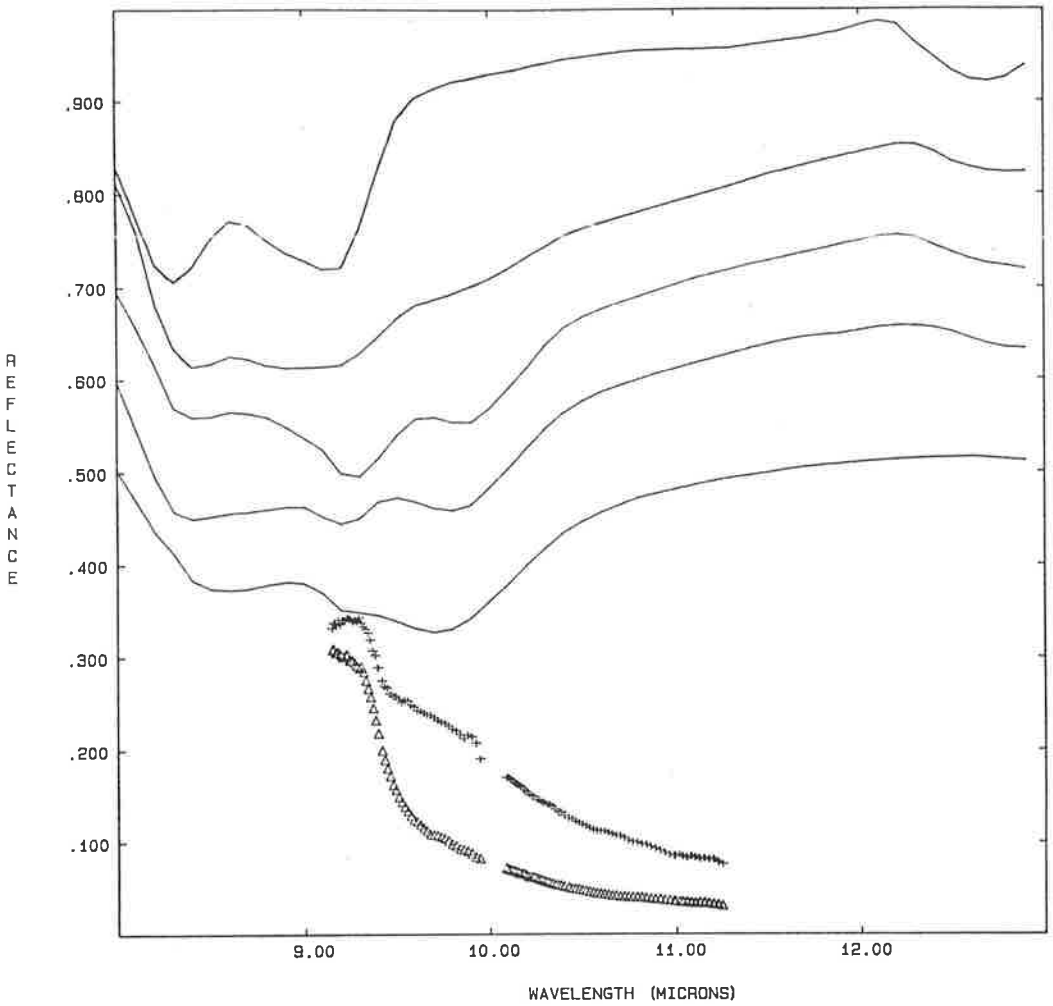
REFLECTANCE
.900
.800
.700
.600
.500
.400
.300
.200
.100
9.00
10.00
11.00
12.00
WAVELENGTH (MICRONS)

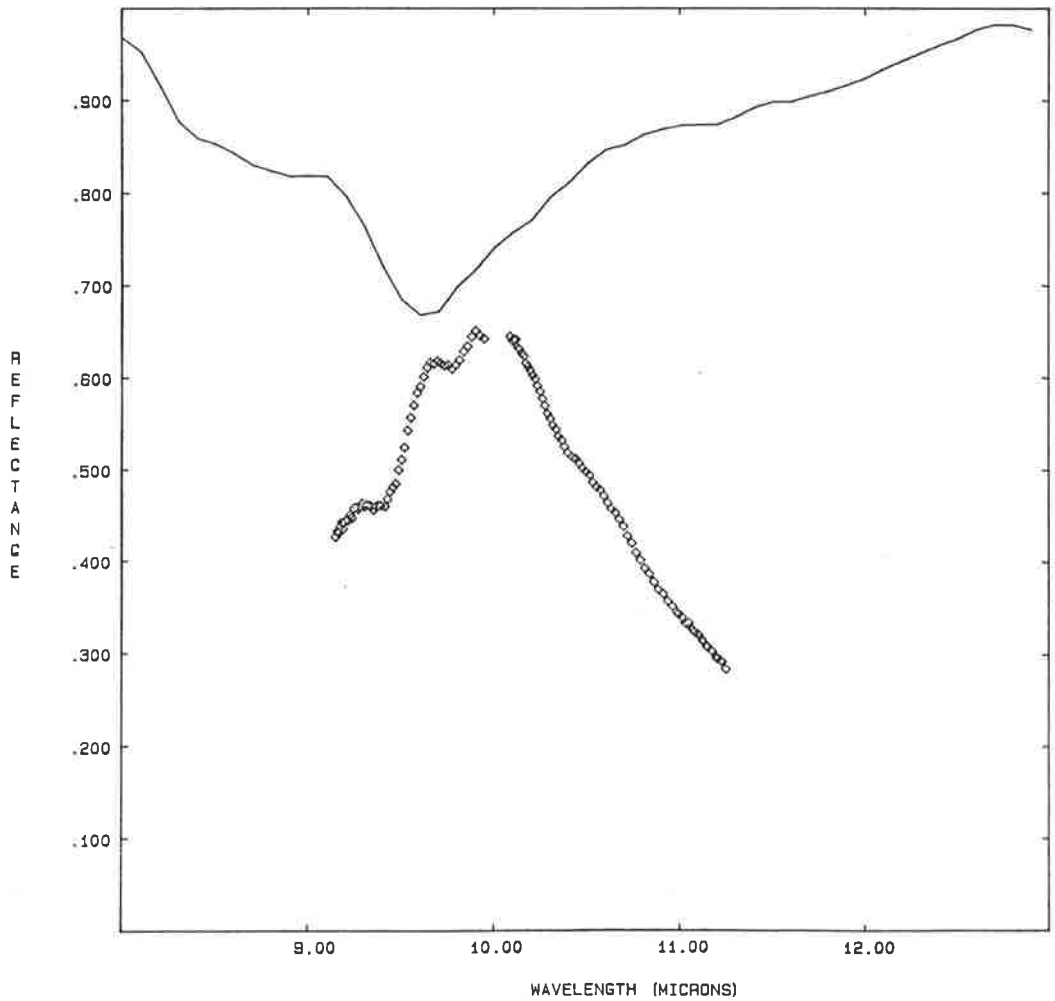
REFLECTANCE
.900
.800
.700
.600
.500
.400
.300
.200
.100
9.00
10.00
11.00
12.00
WAVELENGTH (MICRONS)

Figure 2.12 MIR spectra of serpentinites (after Eberhardt et al., 1984).

The emissivity spectrum (scale factor 3) shows very similar structure to the reflectance spectra of both the weathered (diamonds) and the fresh (crosses) surfaces of the serpentinite sample (both plotted with a scale factor of 2).

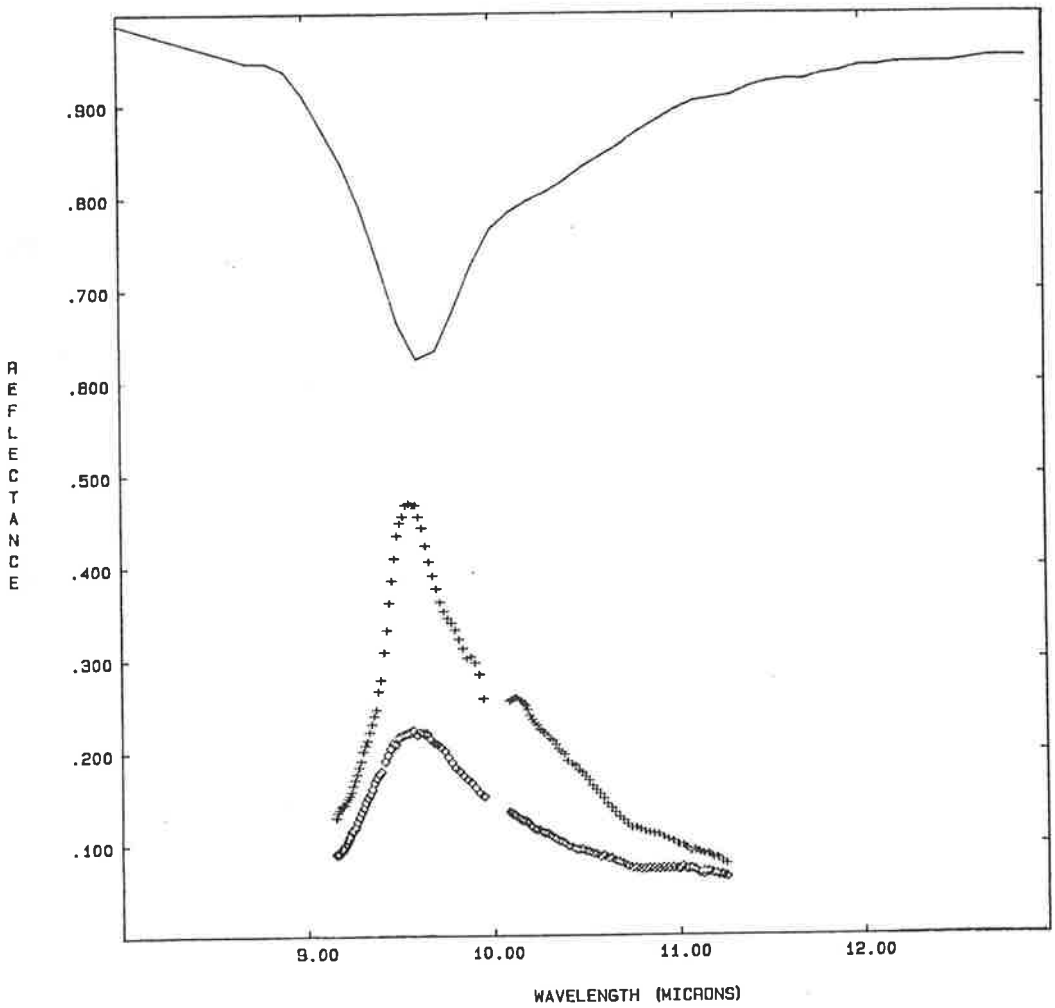
.900
.800
.700
.800
.500
.400
.300
.200
.100
REFLECTANCE
9.00
10.00
11.00
12.00
WAVELENGTH (MICRONS)

Figure 2.13 MIR spectra of ultramafic rocks (after Eberhardt et al., 1984).

The solid line is an emissivity curve for a pyroxenite (scale factor 3). The reflectance spectra of a talc-carbonate rock (diamonds, scale factor 3.2) and a picrite, comprising amphibole and chlorite (crosses, scale factor 3) are shown for comparison.

Figure 2.14 MIR spectra of garnet-rich rocks (after Eberhardt et al., 1984).

The emissivity spectrum (scale factor 5) and reflectance spectra (both scale factor 2.5) of weathered (diamonds) and fresh (crosses) surfaces of a garnetite are shown.

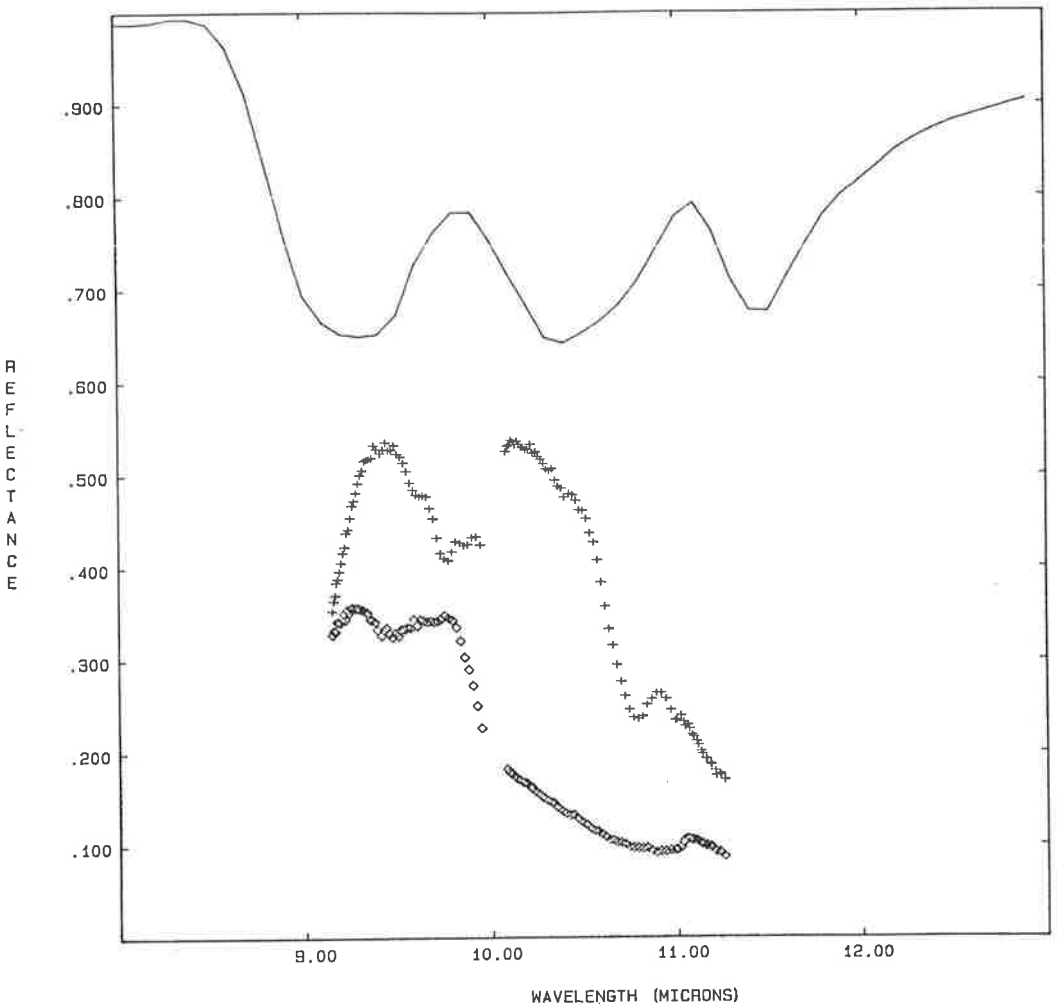
.900
.800
.700
.600
.500
.400
.300
.200
.100
REFLECTANCE
9.00
10.00
11.00
12.00
WAVELENGTH (MICRONS)

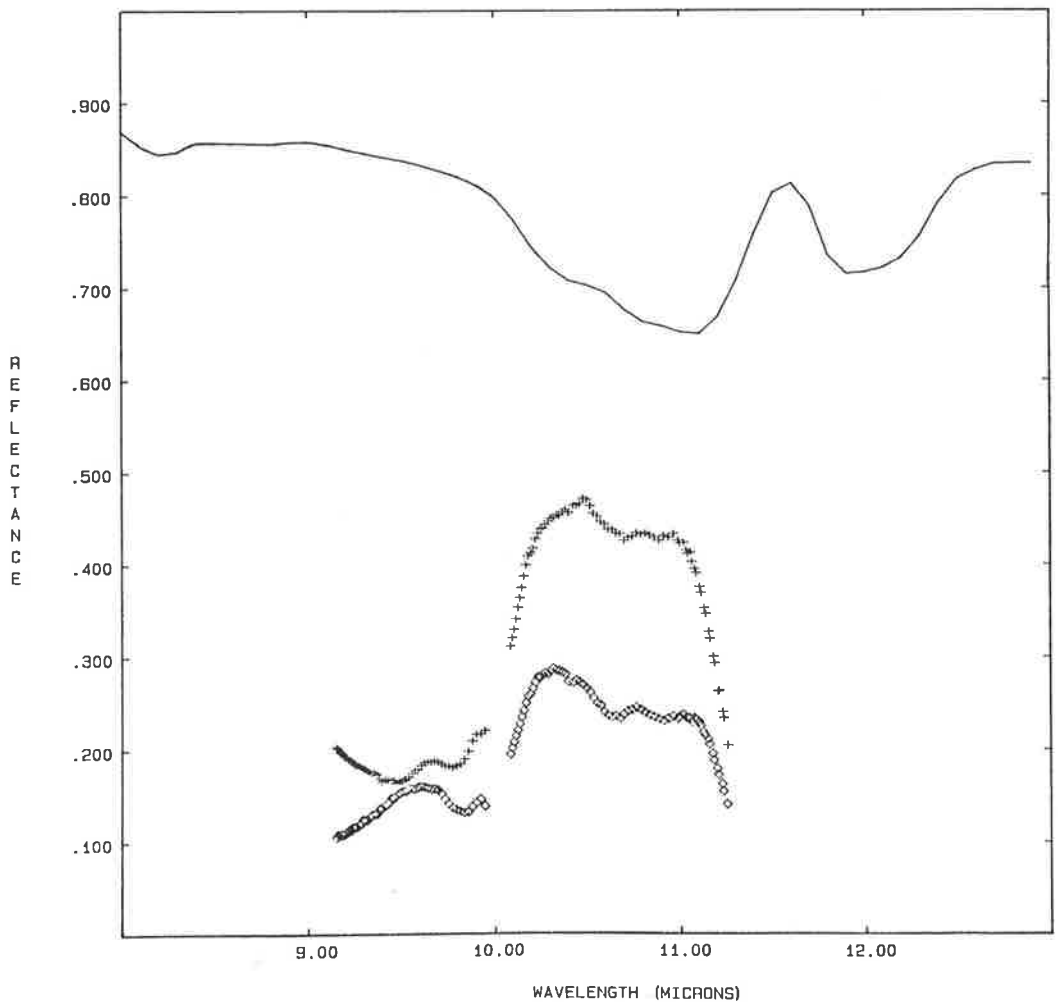
.900
.800
.700
.600
.500
.400
.300
.200
.100
REFLECTANCE
9.00
10.00
11.00
12.00
WAVELENGTH (MICRONS)

Figure 2.15 MIR reflectance spectra of minerals (after Eberhardt et al., 1984).

The reflectance spectra of quartz (crosses), plagioclase (triangles) and olivine (diamonds). The spectra have been rescaled (scale factors 4, 1 and 1.3 respectively) and offset (-5%, -10% and 0% respectively) for ease of display. Note that once again the wavelengths of the reflectance maxima increase with decreasing SiO_2.

Figure 2.16 MIR reflectance spectra of minerals (after Eberhardt et al., 1984).

The reflectance spectra of muscovite (crosses), hornblende (x), calcite (squares), magnesite (diamonds) and dolomite (triangles). Spectra are rescaled (scale factors 2, 3, 2.5, 1.5 and 1.7 respectively) and offset (-10%, -10%, -15%, -7% and -25% respectively). Note the sharp reflectance maximum displayed by the carbonates near 11.1μm, moving to progressively longer wavelengths with increasing Ca content (a similar effect to that observed in the SWIR ; see Fig. 2.8).

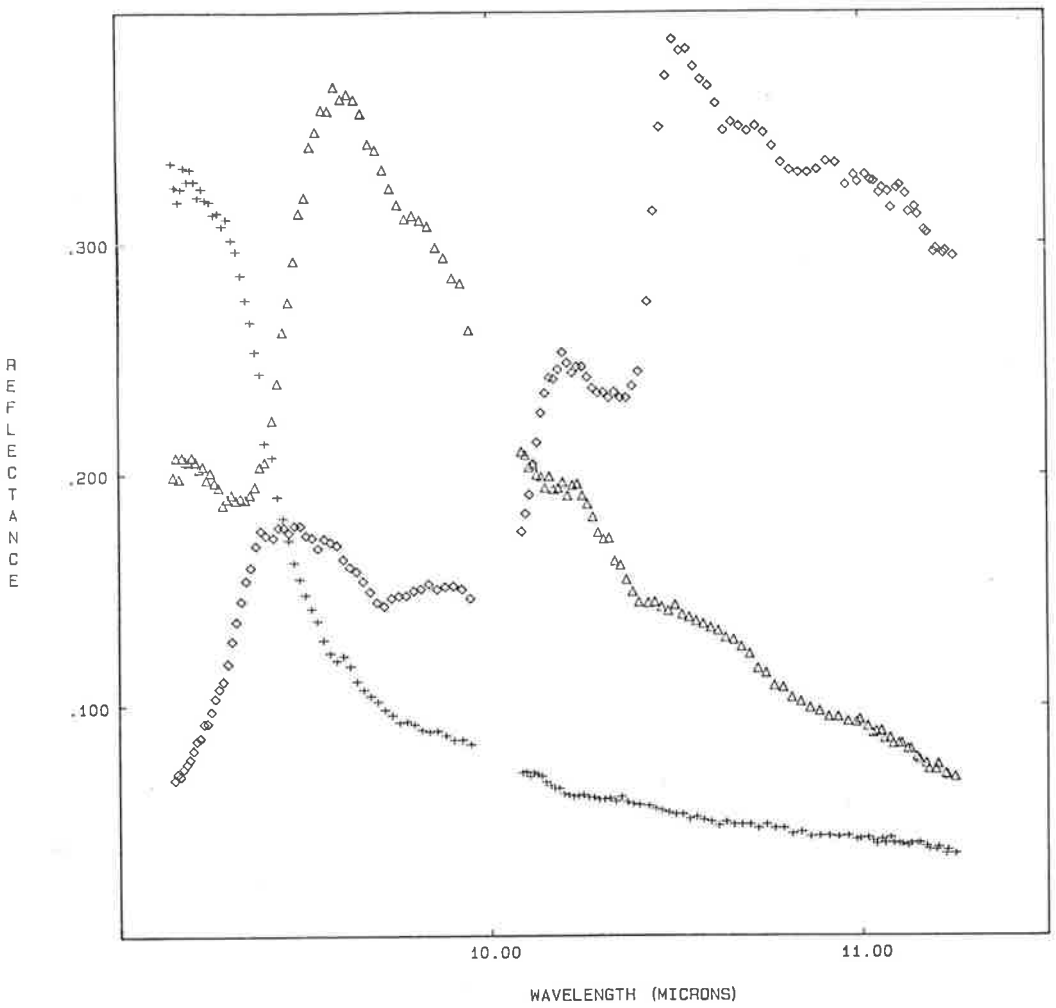
REFLECTANCE
.300
.200
.100
10.00
11.00
WAVELENGTH (MICRONS)

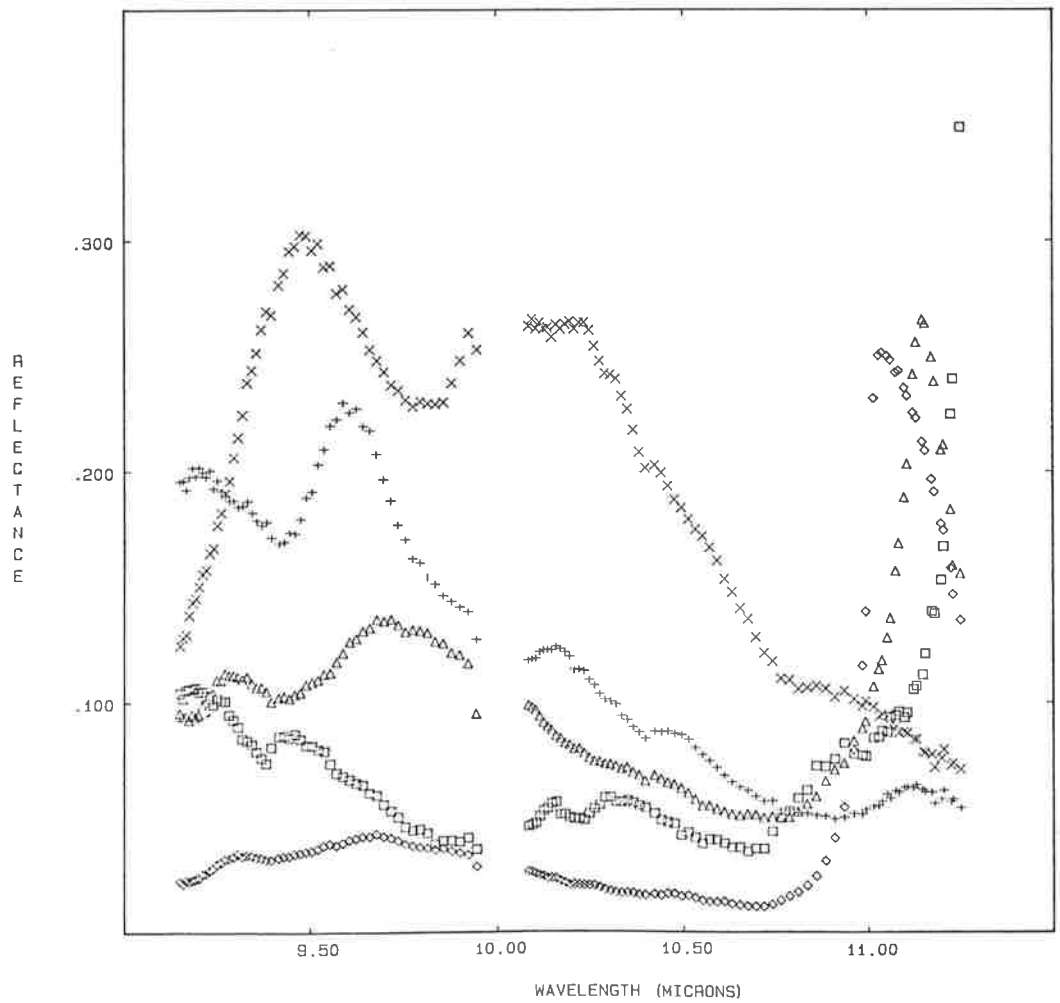
REFLECTANCE
.300
.200
.100
9.50
10.00
10.50
11.00
WAVELENGTH (MICRONS)

Figures 2.17a-c VNIR reflectance spectra of altered and unaltered rocks (after Rowan et al., 1974).

Figure 2.17a shows spectra of felsic rocks, rhyolite (12), granite (14), rhyolite (4) and granodiorite (2), all showing increasing reflectance with increasing wavelength.

Figure 2.17b depicts selected mafic rocks, serpentinite (15), gabbro (9), peridotite (8) and basalt (13) exhibiting overall decreasing reflectance with increasing wavelength.

Figure 2.17c shows reflectance of some alteration minerals. The hematitic limonite spectrum was recorded in situ at Goldfield, Nevada ; other spectra are from various sources. Note the absorption features in the .8 to 1.0μm region.

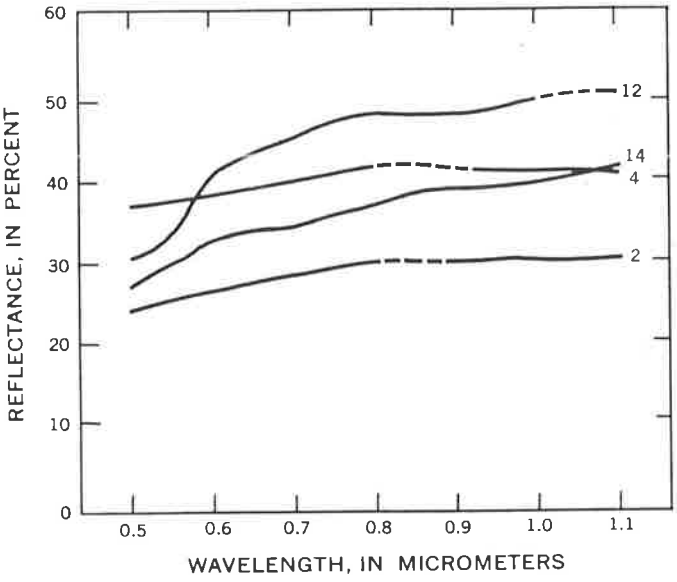
REFLECTANCE, IN PERCENT
60
50
40
30
20
10
0
0.5
0.6
0.7
0.8
0.9
1.0
1.1
WAVELENGTH, IN MICROMETERS
12
14
4
2

A

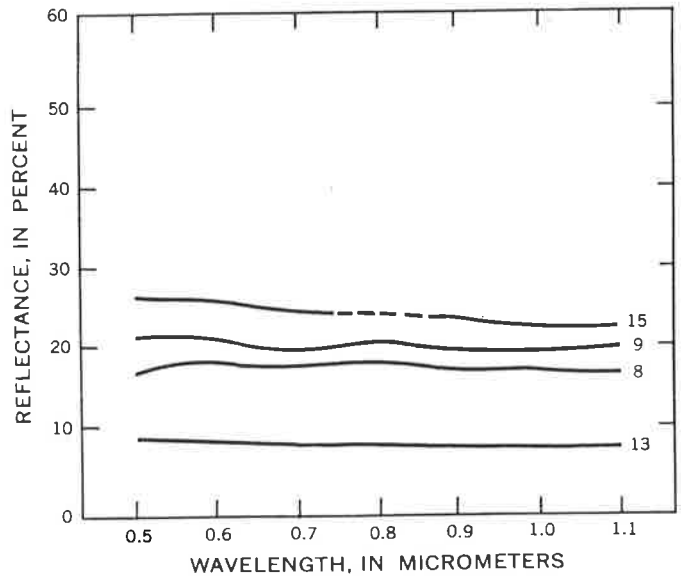
REFLECTANCE, IN PERCENT
60
50
40
30
20
10
0
0.5
0.6
0.7
0.8
0.9
1.0
1.1
WAVELENGTH, IN MICROMETERS
15
9
8
13

B

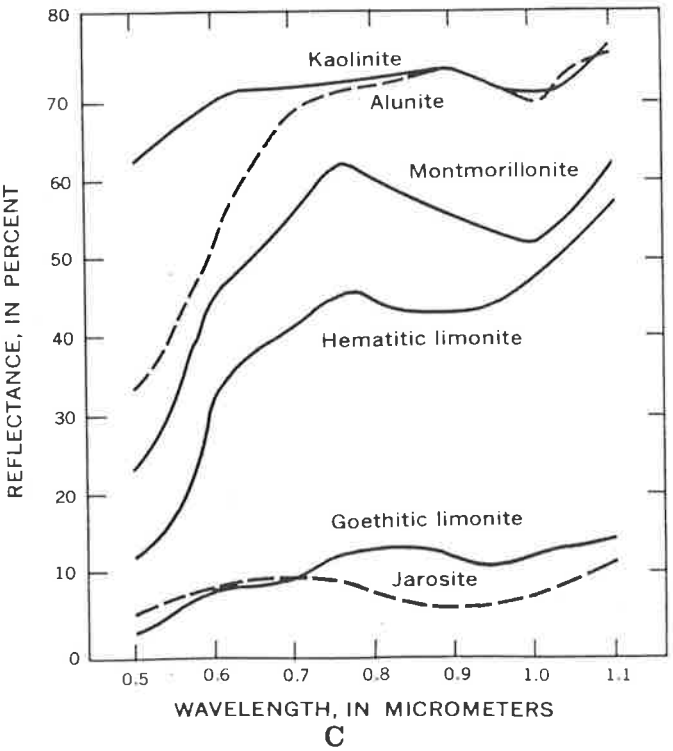
REFLECTANCE, IN PERCENT
80
70
60
50
40
30
20
10
0
0.5
0.6
0.7
0.8
0.9
1.0
1.1
WAVELENGTH, IN MICROMETERS
Kaolinite
Alunite
Montmorillonite
Hematitic limonite
Goethitic limonite
Jarosite

C

Figure 2.18 VNIR and SWIR spectral reflectance curves of altered and unaltered rocks from Cuprite, Nevada (after Abrams et al., 1977).

These spectra show the presence of VNIR iron absorption features in argillically altered samples only. SWIR clay absorption features are present in opalite containing alunite, and in argillized rocks. Note that silicified rocks (no clays) and unaltered rocks (top curve) have no distinctive absorption features.

Figures 2.19a&b Aircraft spectra illustrating removal of atmospheric effects (after Marsh and McKeon, 1983).

Figure 2.19a shows a single airborne spectrum (solid line) and the average spectrum (dotted line) of an entire survey.

Figure 2.19b shows the difference (residual) of the two plots in Fig. 2.19a. The intensity scale is in mW/cm sq/steradian.

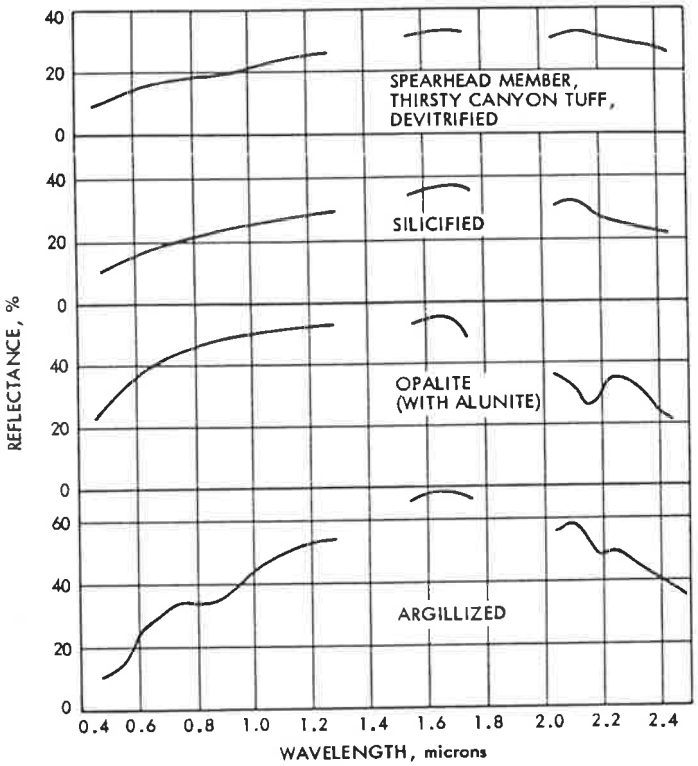
SPEARHEAD MEMBER, THIRSTY CANYON TUFF, DEVITRIFIED
SILICIFIED
OPALITE (WITH ALUNITE)
ARGILLIZED
REFLECTANCE, %
WAVELENGTH, microns

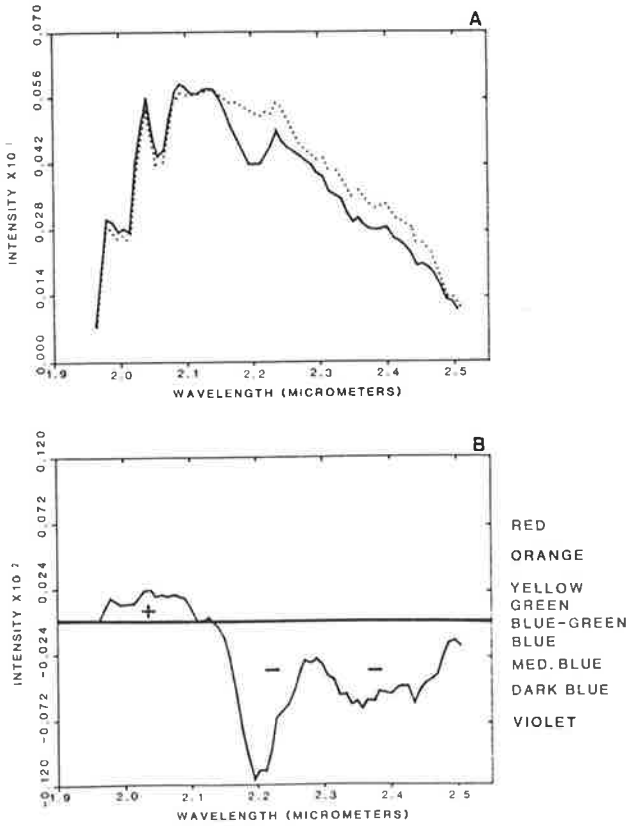
A
B
INTENSITY X10
WAVELENGTH (MICROMETERS)
RED
ORANGE
YELLOW
GREEN
BLUE-GREEN
BLUE
MED. BLUE
DARK BLUE
VIOLET

Figure 2.20 Classification of alteration at Oatman, Arizona (after Marsh and McKeon, 1983).

Ratio of 2.16μm to 2.20μm bands of flight line OA2A. Categories A, B and C were delineated using a waveform analysis technique.

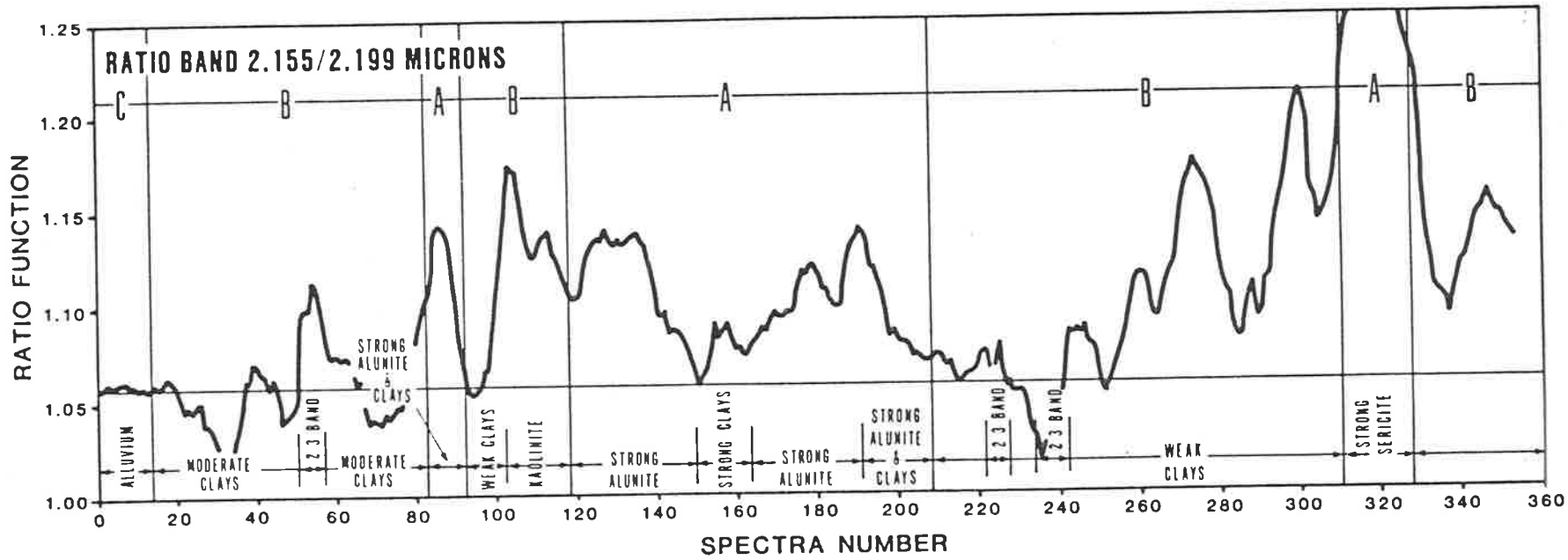
RATIO BAND 2.155/2.199 MICRONS
C
B
A
B
A
B
A
B
RATIO FUNCTION
1.25
1.20
1.15
1.10
1.05
1.00
0
20
40
60
80
100
120
140
160
180
200
220
240
260
280
300
320
340
360
SPECTRA NUMBER
ALLUVIUM
MODERATE CLAYS
2 3 BAND
MODERATE CLAYS
STRONG ALUNITE & CLAYS
WEAK CLAYS
KAOLINITE
STRONG ALUNITE
STRONG CLAYS
STRONG ALUNITE
STRONG ALUNITE & CLAYS
2 3 BAND
2 3 BAND
WEAK CLAYS
STRONG SERICITE

Figure 2.21 AIS data from Cuprite, Nevada (after Goetz, 1984).

Spectra derived from flight data are compared to laboratory spectra (dashed lines) of alunite and kaolinite samples collected from Cuprite, Nevada.

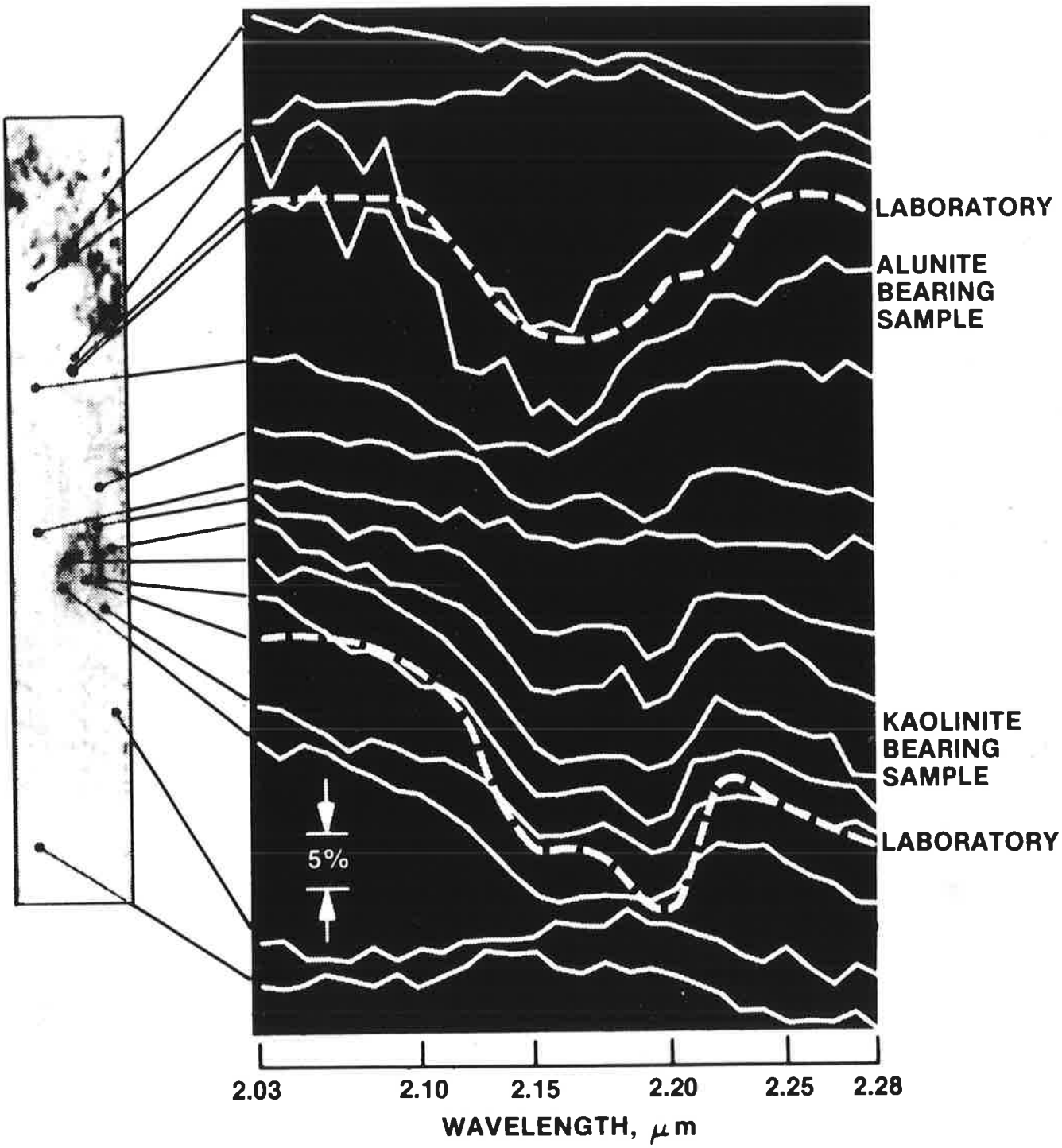
LABORATORY
ALUNITE BEARING SAMPLE
KAOLINITE BEARING SAMPLE
LABORATORY
5%
2.03
2.10
2.15
2.20
2.25
2.28
WAVELENGTH, μm

Figure 2.22 AIS data from the Wind River Basin, Wyoming (after NASA, 1985).

The spectra shown were derived from AIS data over ground corresponding to the geologic units indicated in the statigraphic column.

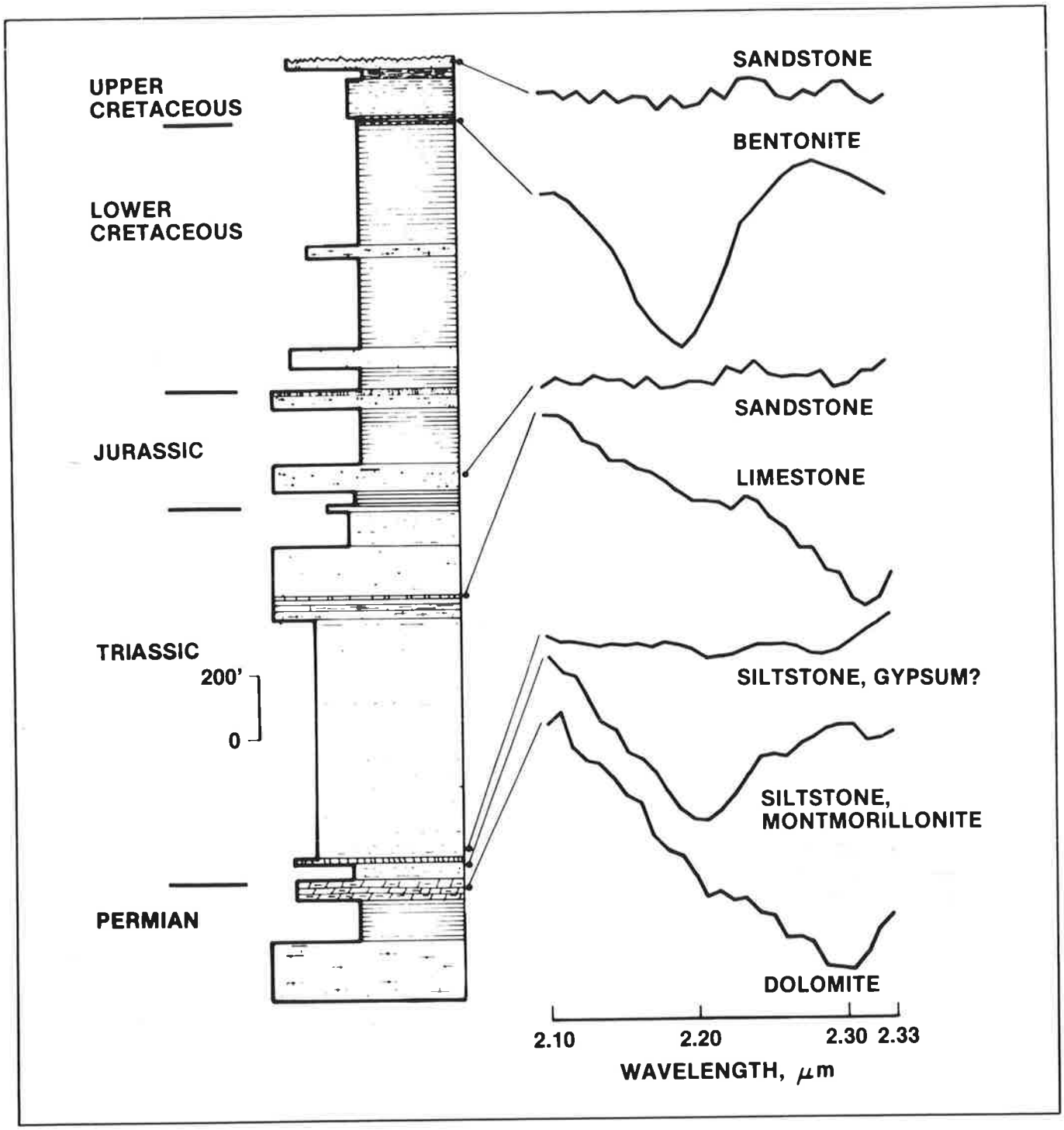
UPPER CRETACEOUS
LOWER CRETACEOUS
JURASSIC
TRIASSIC
200'
0
PERMIAN
SANDSTONE
BENTONITE
SANDSTONE
LIMESTONE
SILTSTONE, GYPSUM?
SILTSTONE, MONTMORILLONITE
DOLOMITE
2.10
2.20
2.30
2.33
WAVELENGTH, μm

Figure 2.23 Preservation of the deep weathering profile in Australia (after Butt and Smith, 1980).

The full profile is most commonly preserved in areas of low to moderate relief, as plateau remnants or beneath transported overburden. The weathered profile is vestigial or absent mainly in humid regions of moderate to high relief.

Figure 2.24 Development of the weathering profile (after Butt,1983).

Figure 2.24 depicts profile formation, during lateritic weathering, modelled on the SW coast of Western Australia. The profiles are applicable to acid and basic rocks.

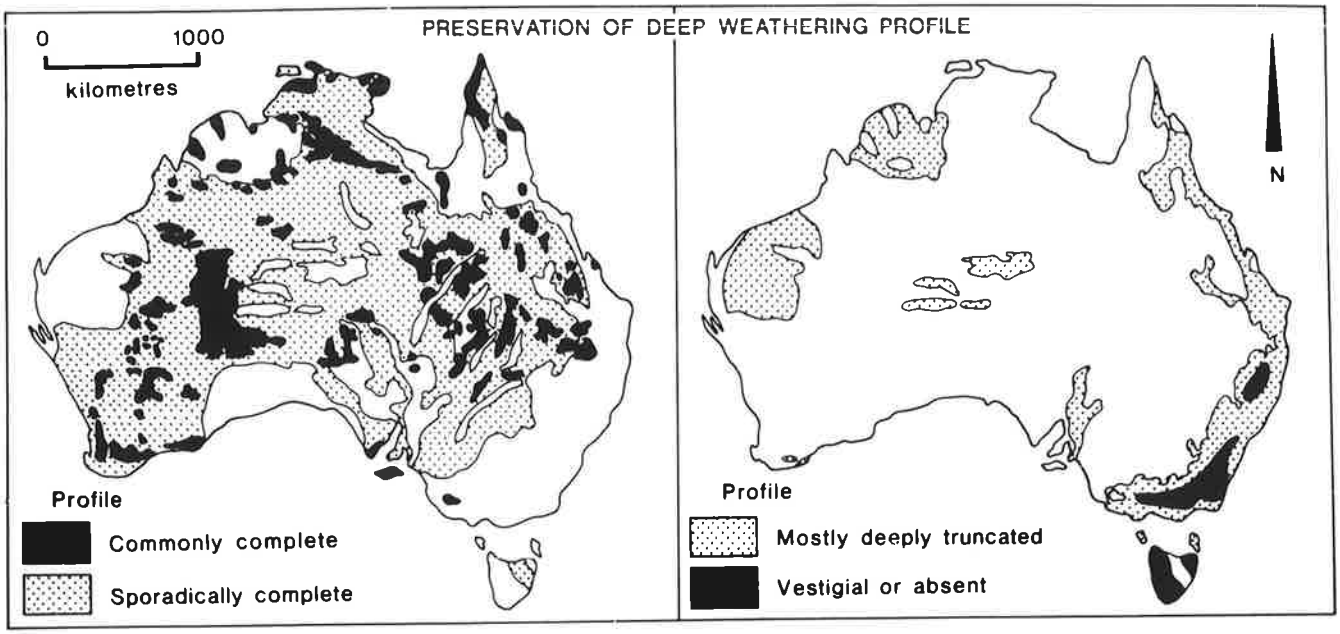
PRESERVATION OF DEEP WEATHERING PROFILE
0
1000
kilometres
N
Profile
Commonly complete
Sporadically complete
Profile
Mostly deeply truncated
Vestigial or absent

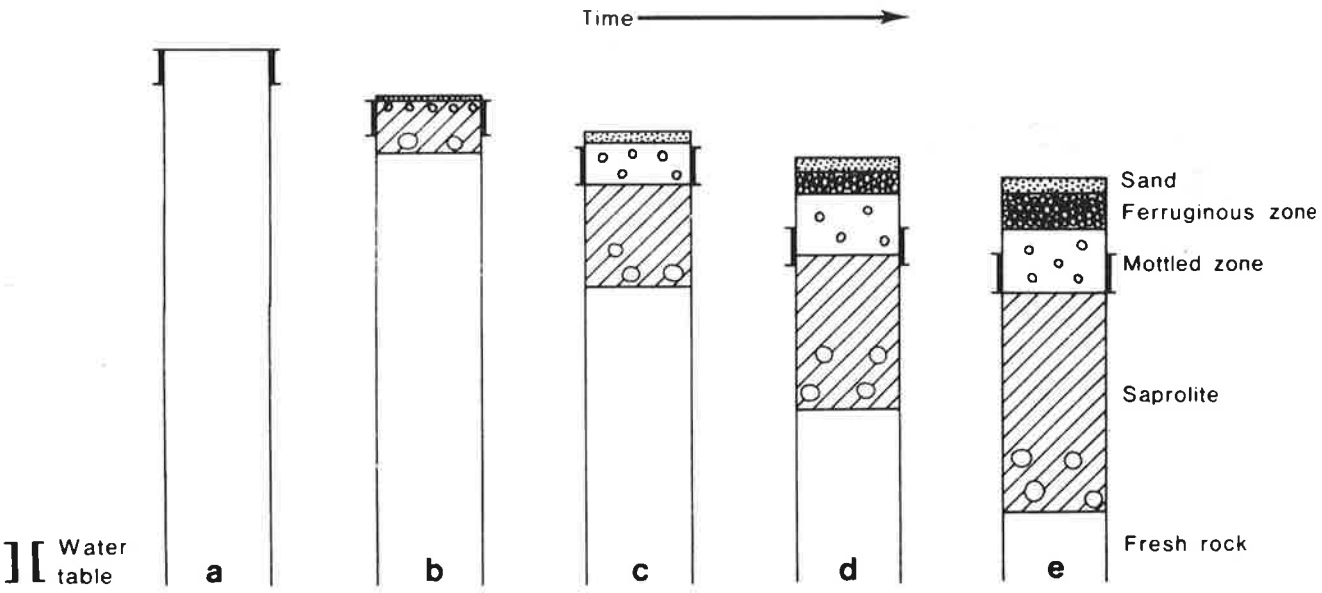
Time
Water table
a
b
c
d
e
Sand
Ferruginous zone
Mottled zone
Saprolite
Fresh rock

Figure 2.25 Composition of lateritic duricrusts (after Schellmann, 1979).

The triangular diagrams represent the various compositions of duricrusts derived from five different precursors. The compositions are expressed in terms of Fe_2O_3, Al_2O_3 and SiO_2 end-members. Information about each of these end-members is available from the VNIR, SWIR and MIR portions of the spectrum, respectively, using remote sensing techniques.

AFTER SCHELLMANN 1981

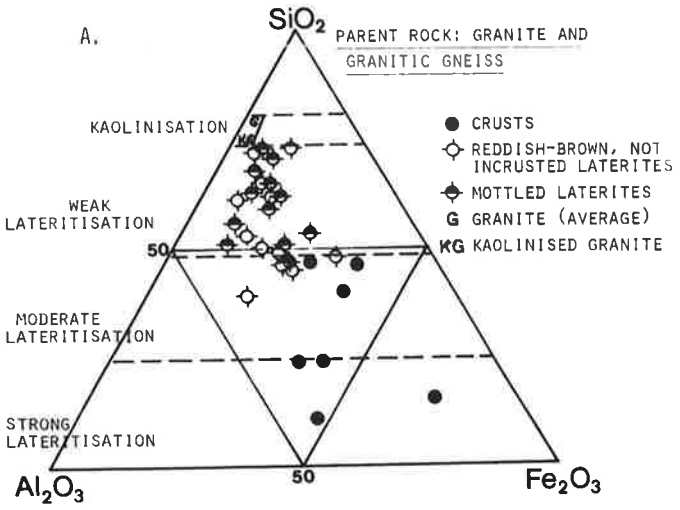

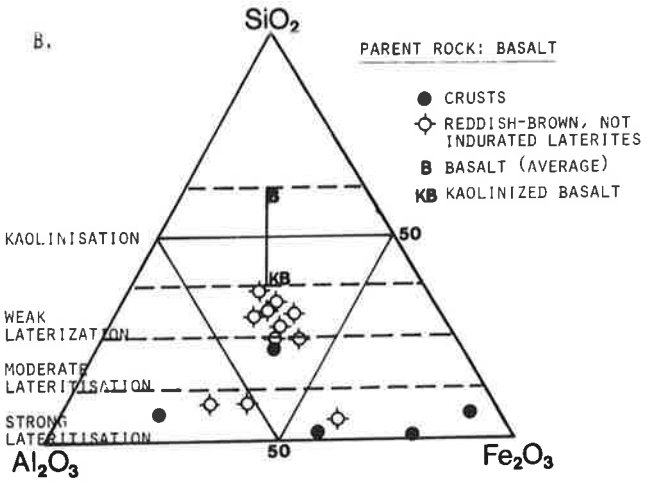

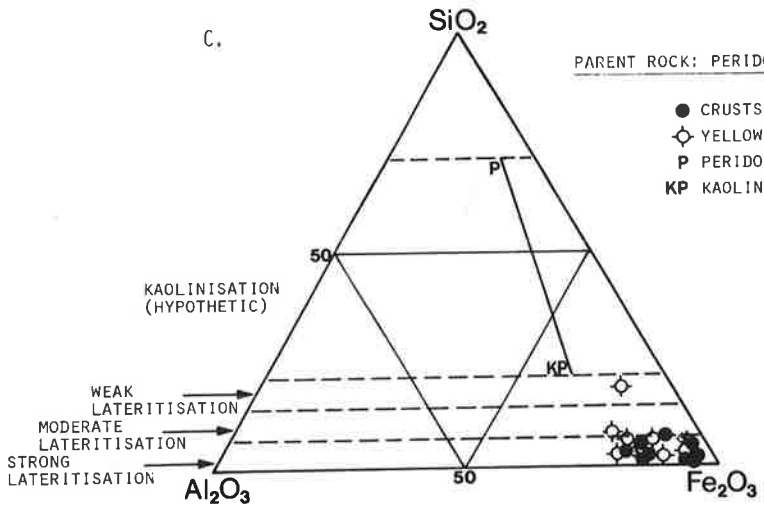

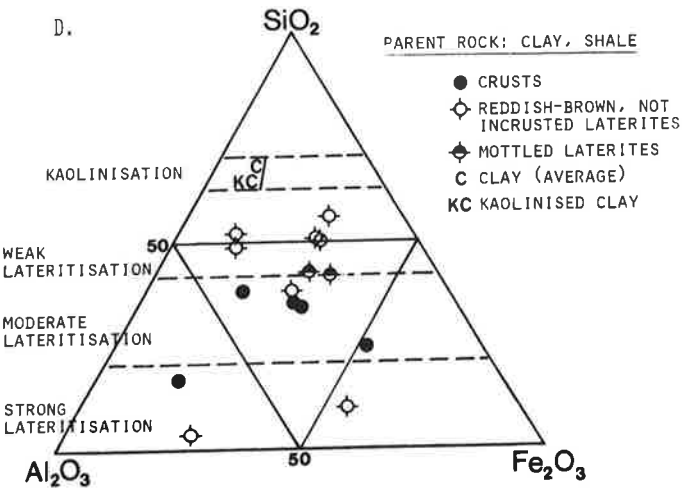

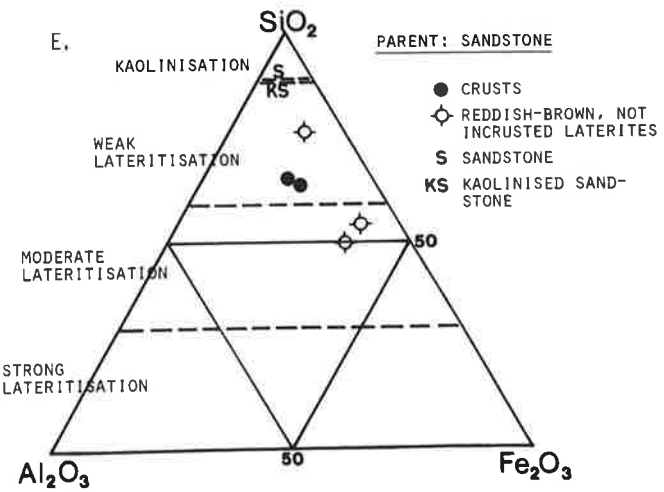

Figure 2.26a-c Weathering profiles developed on felsic, mafic and ultramafic rocks (after Butt, 1983).

The effects of convergent evolution are most pronounced near the top of each profile, mineralogical differences becoming greater with depth. A partially stripped profile will therefore offer a better chance of identifying the precursor by remote sensing techniques.

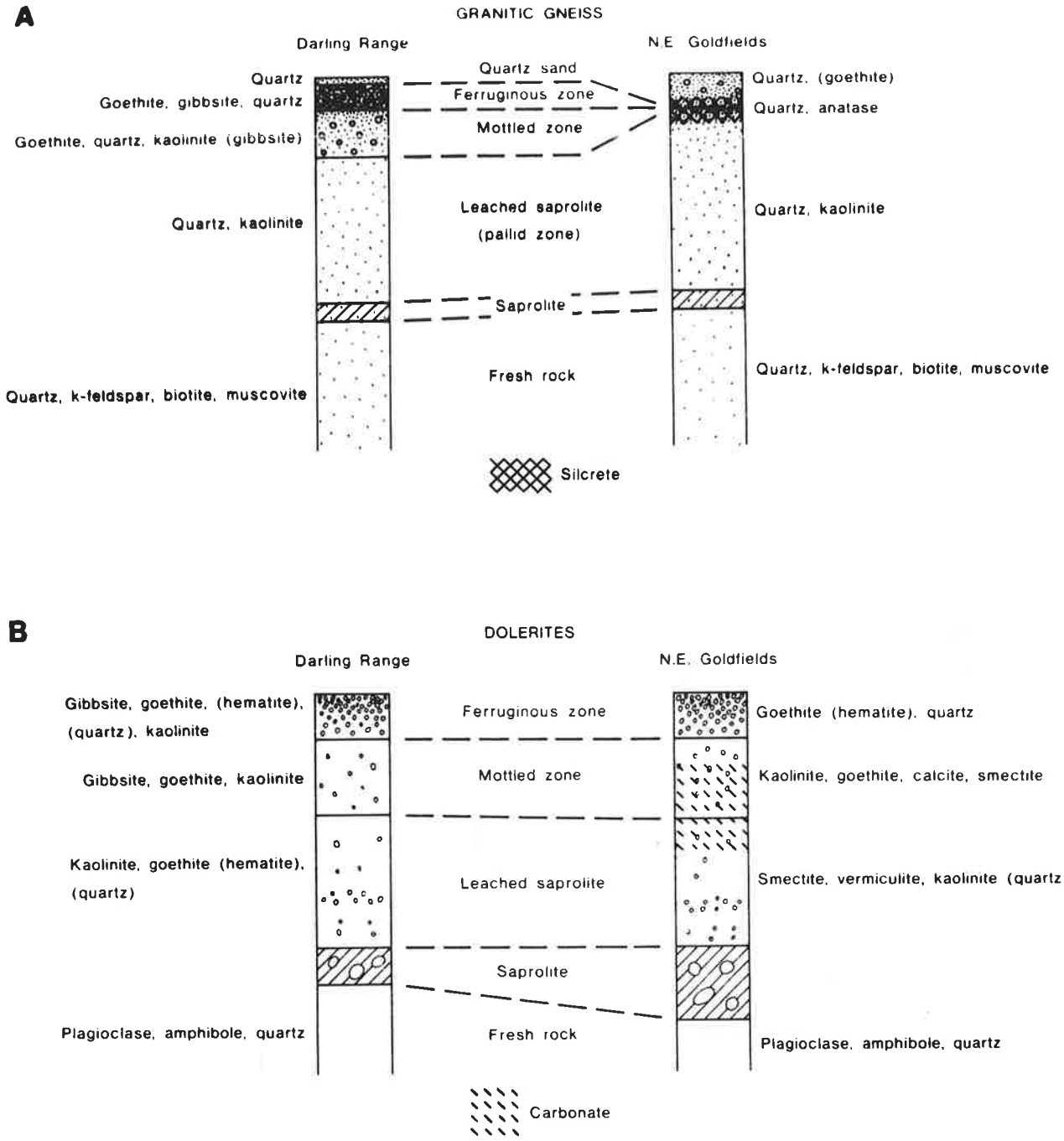
A
GRANITIC GNEISS
Darling Range
N.E Goldfields
Quartz
Goethite, gibbsite, quartz
Goethite, quartz, kaolinite (gibbsite)
Quartz, kaolinite
Quartz, k-feldspar, biotite, muscovite
Quartz sand
Ferruginous zone
Mottled zone
Leached saprolite
(pallid zone)
Saprolite
Fresh rock
Quartz, (goethite)
Quartz, anatase
Quartz, kaolinite
Quartz, k-feldspar, biotite, muscovite
Silcrete
B
DOLERITES
Darling Range
N.E. Goldfields
Gibbsite, goethite, (hematite), (quartz), kaolinite
Gibbsite, goethite, kaolinite
Kaolinite, goethite (hematite), (quartz)
Plagioclase, amphibole, quartz
Ferruginous zone
Mottled zone
Leached saprolite
Saprolite
Fresh rock
Goethite (hematite), quartz
Kaolinite, goethite, calcite, smectite
Smectite, vermiculite, kaolinite (quartz)
Plagioclase, amphibole, quartz
Carbonate
C
DUNITE
PERIDOTITE
Goethite (hematite), (quartz)
Goethite, smectite, serpentine
Quartz, (serpentine), (smectite), (goethite)
Serpentine, carbonate, goethite
Serpentine
Ferruginous zone
Mottled zone
Ferruginous silicified saprolite
Saprolite
Fresh rock
Goethite (hematite), (talc)
Goethite, smectite, serpentine, (talc)
Serpentine, goethite, smectite, (talc), carbonate
Plagioclase, pyroxene, amphibole, serpentine, (talc), (carbonate)

Figure 3.1 Experimental arrangement for measurement of VNIR and SWIR spectra in the laboratory.

EXPERIMENTAL ARRANGEMENT FOR MEASUREMENT OF SPECTRA

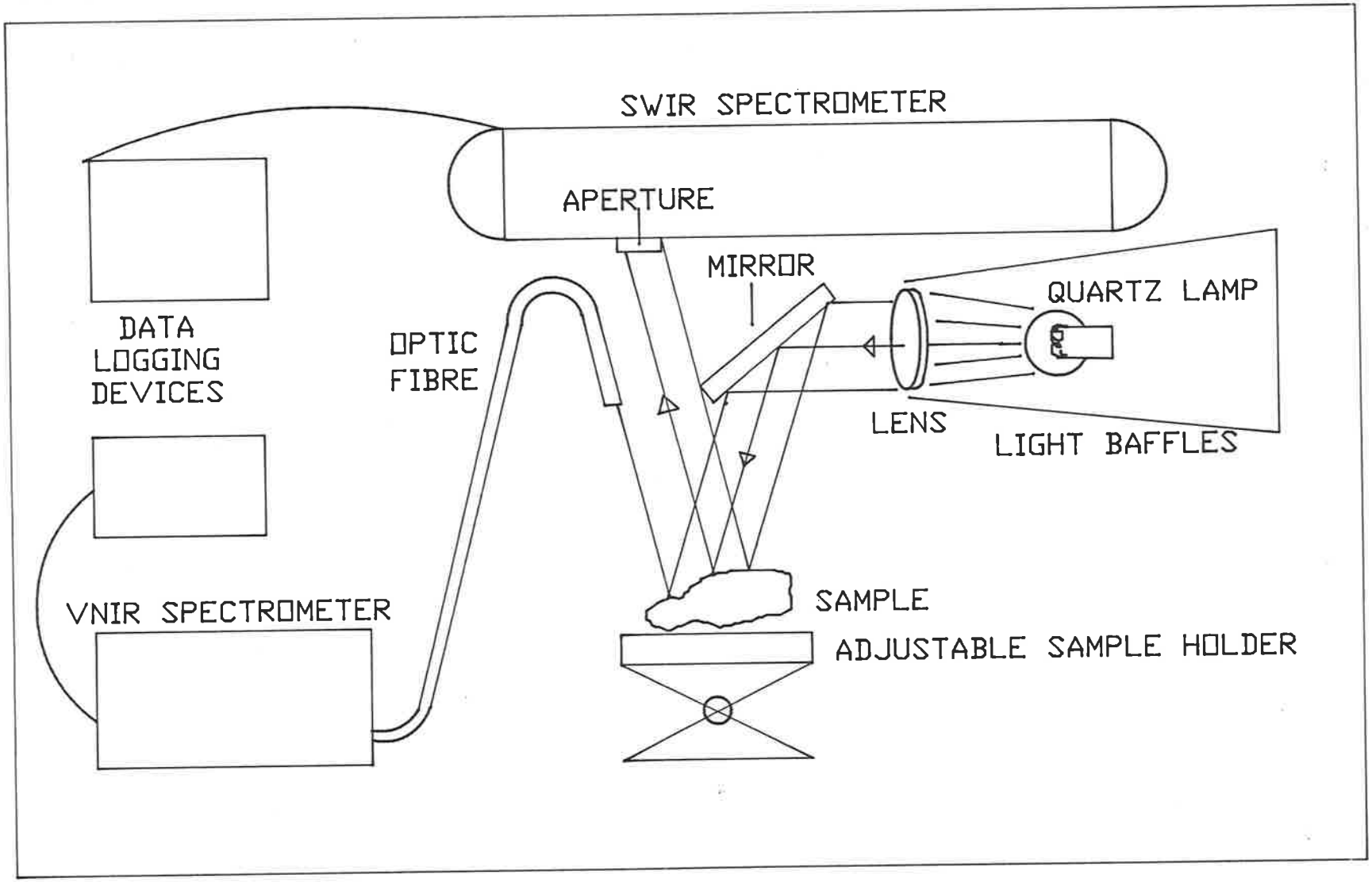

Figure 3.2 The Tracor Northern VNIR spectrometer.

The blue box (middle right) is a multichannel analyser, linked to the spectrometer head (grey box, centre of picture) by the thick, grey cable. An optic fibre bundle runs from the input slit of the spectrometer head to a position above the adjustable sample holder.

Figure 3.3 The SWIR spectrometer.

The CVF spectrometer is mounted on the inside (right-hand side) of the pod which can be attached to the exterior of an aircraft. The CVF has a resolution of approximately 1% of wavelength. A SWIR radiometer occupies the left-hand side of the pod, but was not used in the laboratory. A movable mirror allows the instrument to be used in eiher an upward-looking, or a downward-looking mode. The pod is approximately 1.8m long.

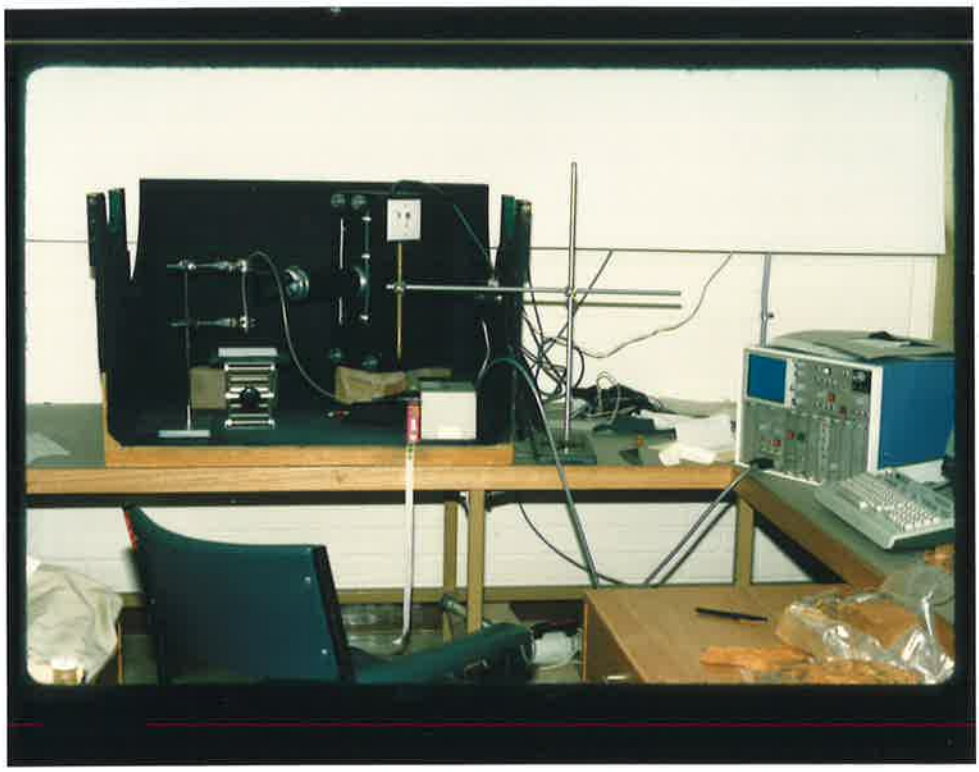

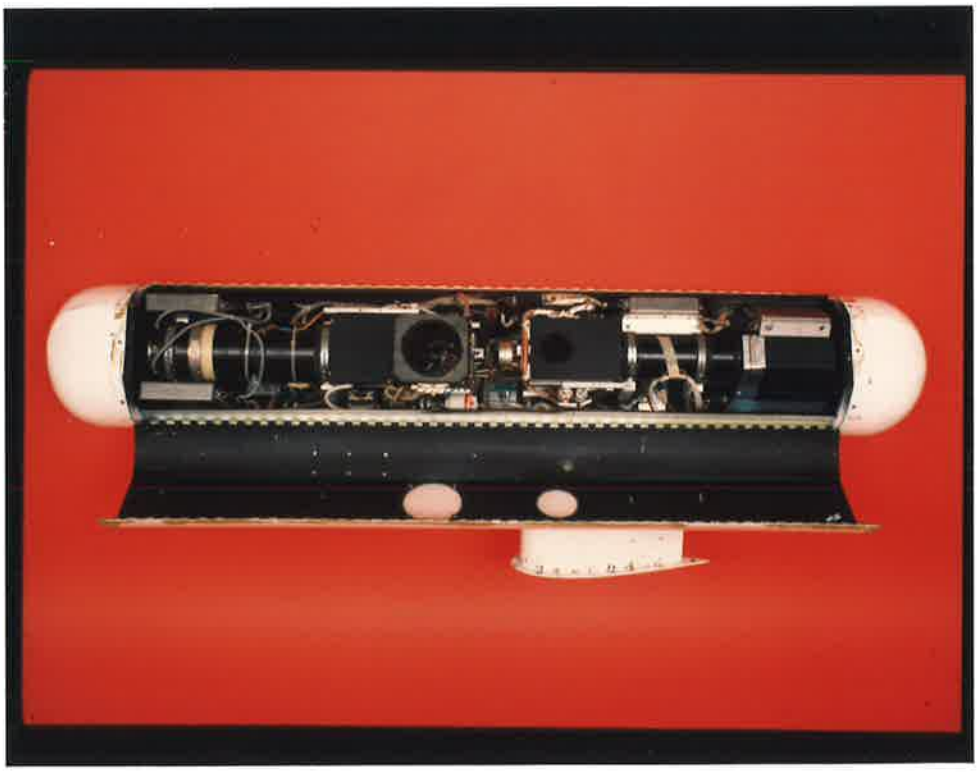

Figure 3.4 The CO_2 laser spectrometer (after Eberhardt et al., 1984).

The various components of the system are listed below :

1. Line-tuned continuous CO_2 laser.
2. Calorimeter
3. Visible He-Ne laser
4. ZnS splitter
5. Ge lens
6. HgCdTe photoconductive detector
7. Photoelectric trigger
8. Samples
9. Hexagonal mirror
10. Oscillation of hexagonal mirror axis

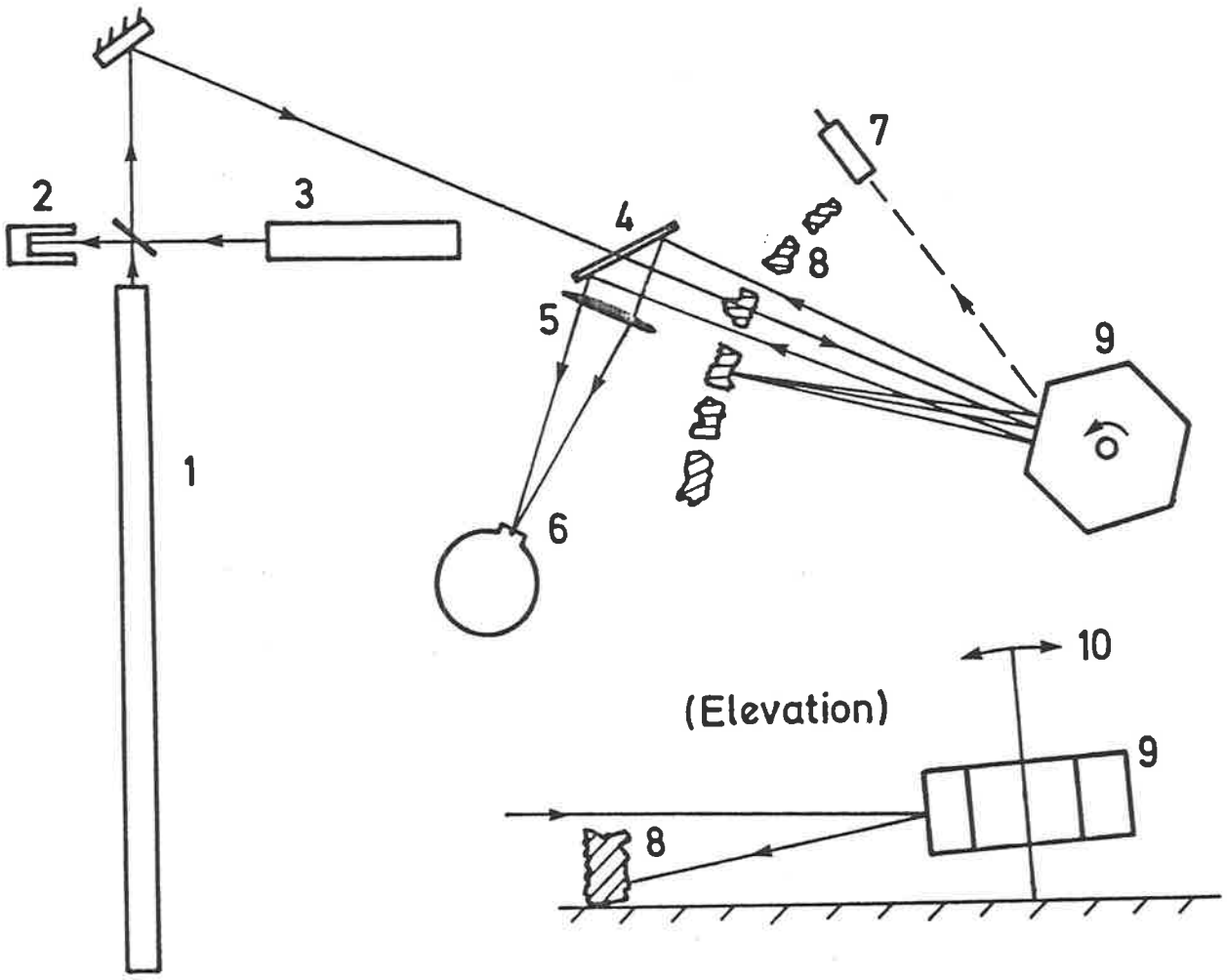
1
2
3
4
5
6
7
8
9
10
(Elevation)

Figure 3.5 The image processing system.

The components of the system are the colour television monitor (left), a computer terminal (centre) and a remote operator panel (right). The remote operator panel controls cursor movement and graphics display. Refresh memory is housed with the host computer, located behind a wall to the left of the picture.

Figure 3.6 Typical structure of an XPUT file sample.

Each sample comprises a header, containing a label, and any number of groups (four are shown here). Each group contains a number of channels, and can consist of spectral data, derived data, or non-spectral information (such as coded geology). The trailer for each group can contain a flag used by several XBOSS programs when analysing the data.

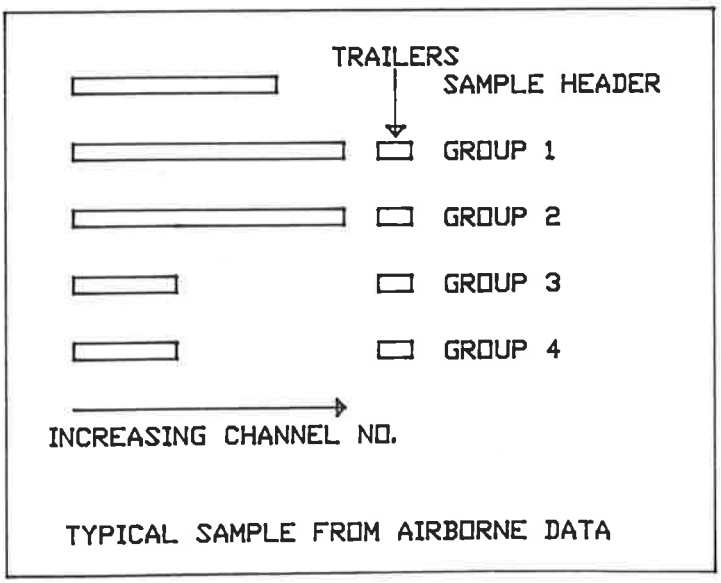

TYPICAL SAMPLE FROM AIRBORNE DATA

Figure 3.7 XBOSS menus (after Craig et al., 1984).

The three menus show the different types of operations which can be performed on XPUT files. Operations vary from simple display of data, to complex analysis and classification.

```
TL OR DL,FNAME.............ABRIDGED FILE PARAMETERS
PL,FNAME...................COMPLETE FILE PARAMETERS
LI,FNAME...................LIST FILE DATA
MO,FNAME...................MODIFY FILE DATA
SL,FNAME OR SL,FNAME,M,N..PRINT SAMPLE HEADERS M TO N
HL,FNAME OR HL,FNAME,N....PRINT HEADER INFORMATION
HS,FNAME...................MODIFY SAMPLE HEADER INFO
HM,FNAME,N.................MODIFY GROUP HEADER INFO
CR.........................CREATE XPUT FILE
PU,FNAME...................PURGE XPUT FILE
LL,LU#.....................CHANGE LIST DEVICE LU
ZC,FNAME...................ZAP BAD CHANNEL
BK,FNAME...................LIST PARBLOCK
EX (OR /)..................EXIT PROGRAM

SA.........................SAVE FILE ON MAG TAPE
RE.........................RESTORE FILE FROM MAG TAPE
VI,FNAME...................COMPUTE VOLTAGE INTEGRAL
PB,FNAME...................SCHEDULE PROGRAM COLNS
FN.........................SCHEDULE PROGRAM FINX
TU,FNAME...................SCHEDULE PROGRAM TUCOL
OK,FNAME...................SCHEDULE PROGRAM XFIX
LN,FNAME...................TAKE LOG NATURAL
XP,FNAME...................TAKE EXPONENTIAL
NT,FNAME...................EQUALIZE FLIGHT LINES (XTEND)
RC,FNAME...................RECONSTRUCT SPECTRUM (XPLIN)
RX,FNAME...................FLIGHT-LINE STAVES (XBRIX)
PN,FNAME...................GENERATE TCHEBYCHEV POLYNS
MP.........................SCHEDULE PROGRAM XMAP
NX,FNAME...................ZEROS OF SPECTRA (XNIX)

CO,FNAME...................COPY GROUP TO ANOTHER FILE
SM,FNAME...................SMOOTH (SAMPLES OR CHANNELS)
AV,FNAME...................FILL NEW GROUP WITH LOC AV
MX,FNAME...................FILL NEW GROUP WITH LOC MAX
GF,FNAME...................GRAPHING FACILITY (XPOSE)
SC,FNAME...................SCATTER DIAGRAMS (XCAT)
RS.........................SCHEDULE PROGRAM RSXXP
LR.........................LOGARITHMIC RESIDUALS (XLOG)
XA,FNAME...................SPECTRAL STATISTICS (XTAT)
FU,FILEOUT.................ARITHMETIC FACILITY (XFUN)
D1,FNAME...................FIRST DERIVATIVE
D2,FNAME...................SECOND DERIVATIVE
TC,FNAME...................TCHEBYCHEV ANALYSIS
YZ,FNAME...................SPECTRAL ANALYZER
PR,FNAME...................SPECTRAL CLASSIFIER
ST,FNAME...................MULTIVARIATE STATS (XMVAR)
PC,FNAME...................PRINCIPAL COMPONENTS
CC,FNAME...................INTERPOLATE (CHANGE # CHANNELS)
TV,FNAME...................SCHEDULE PROGRAM XTV
TP,FNAME...................SCHEDULE PROGRAM XTVP
KT,FNAME...................SCHEDULE PROGRAM XDECT
KR,FILEOUT.................SCHEDULE PROGRAM XDECR
```

Figures 3.8a-d The log residual technique.

Figures 3.8a&b show airborne radiance spectra from the Kambalda region. The overall shape of the curve is influenced by the energy available to the detectors, and is controlled largely by atmospheric water absorption at both ends of the spectrum shown. In addition, sharp absorption features due to CO_2 and H_2O occur between 1.9 and 2.5μm. The log residual technique removes these effects, and variations due to terrain brightness, resulting in the enhancement of subtle mineralogical features, as shown in Figs.3.8c&d.

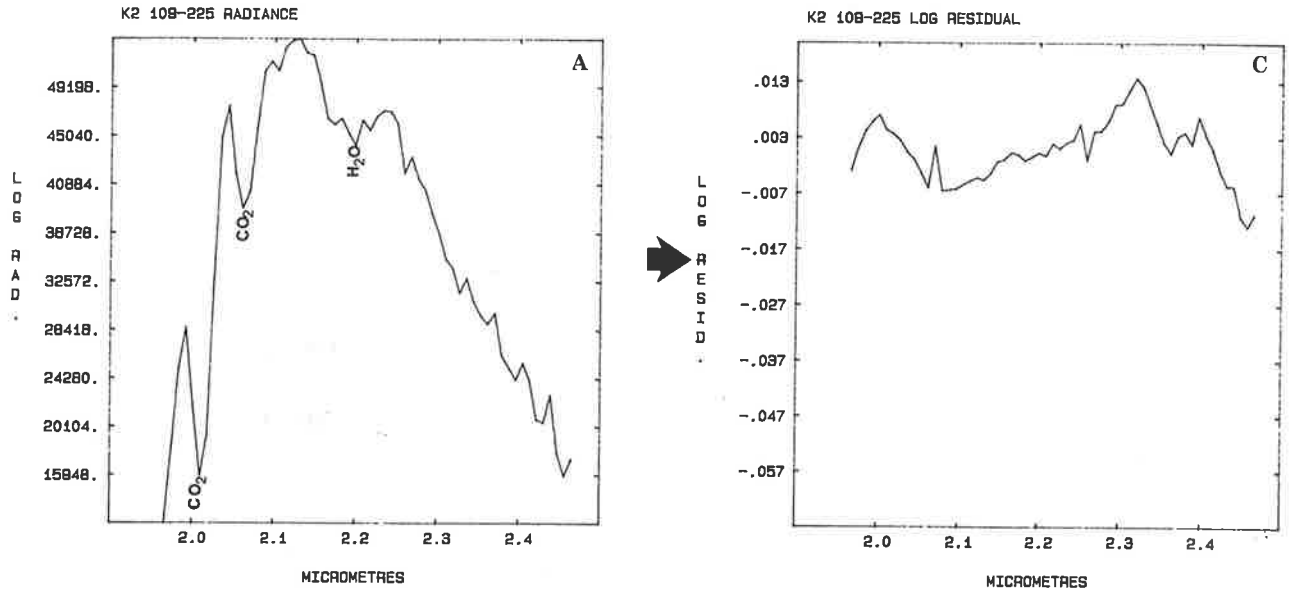
K2 108-225 RADIANCE
A
49198.
45040.
40884.
38728.
32572.
28418.
24280.
20104.
15848.
LOG RAD.
CO_2
CO_2
H_2O
2.0
2.1
2.2
2.3
2.4
MICROMETRES
K2 108-225 LOG RESIDUAL
C
.013
.003
-.007
-.017
-.027
-.037
-.047
-.057
LOG RESID.
2.0
2.1
2.2
2.3
2.4
MICROMETRES

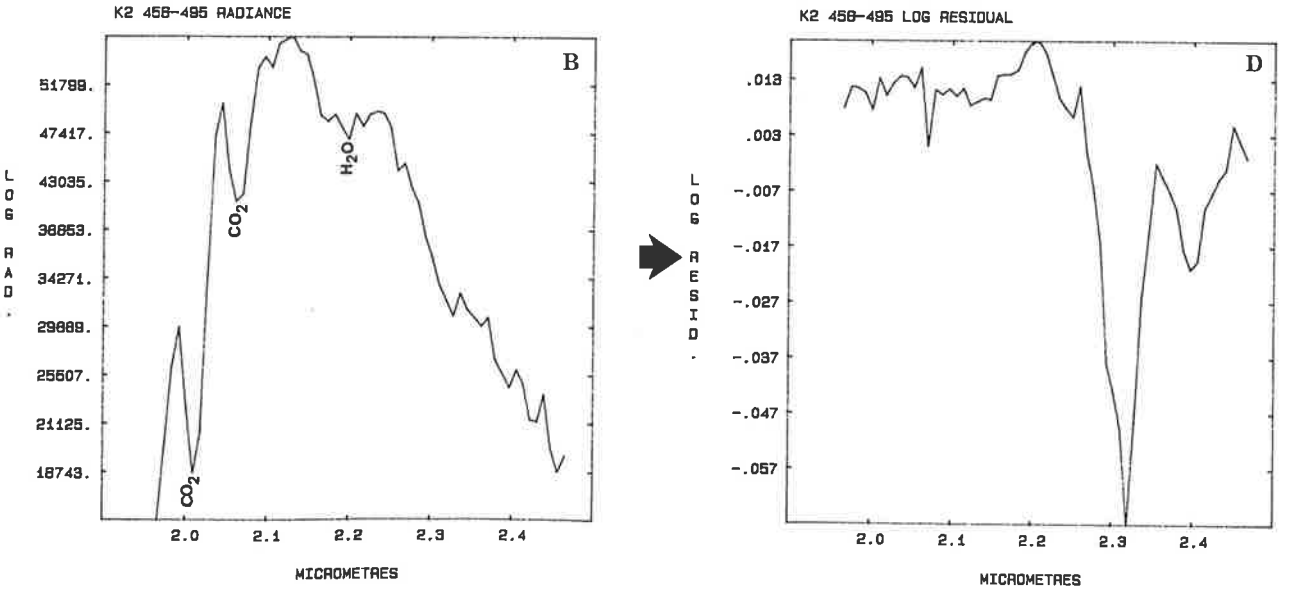
K2 458-495 RADIANCE
B
51799.
47417.
43035.
38653.
34271.
29889.
25507.
21125.
18743.
LOG RAD.
CO_2
CO_2
H_2O
2.0
2.1
2.2
2.3
2.4
MICROMETRES
K2 458-495 LOG RESIDUAL
D
.013
.003
-.007
-.017
-.027
-.037
-.047
-.057
LOG RESID.
2.0
2.1
2.2
2.3
2.4
MICROMETRES

Figures 3.9a&b Positive and negative log residuals.

These plots show the effect of removing the flight-line mean during the log residual process. Muscovite is widespread throughout the flight line, and its effects (2.2μm absorption) are contained in the line mean. Figure 3.9a is derived from an area that contains more muscovite than the flight-line average, so it exhibits a log residual minimum (greater absorption) at 2.2μm. Figure 3.9b is derived from an area that contains less muscovite than the flight-line average, so it has a log residual maximum (less absorption) at 2.2μm.

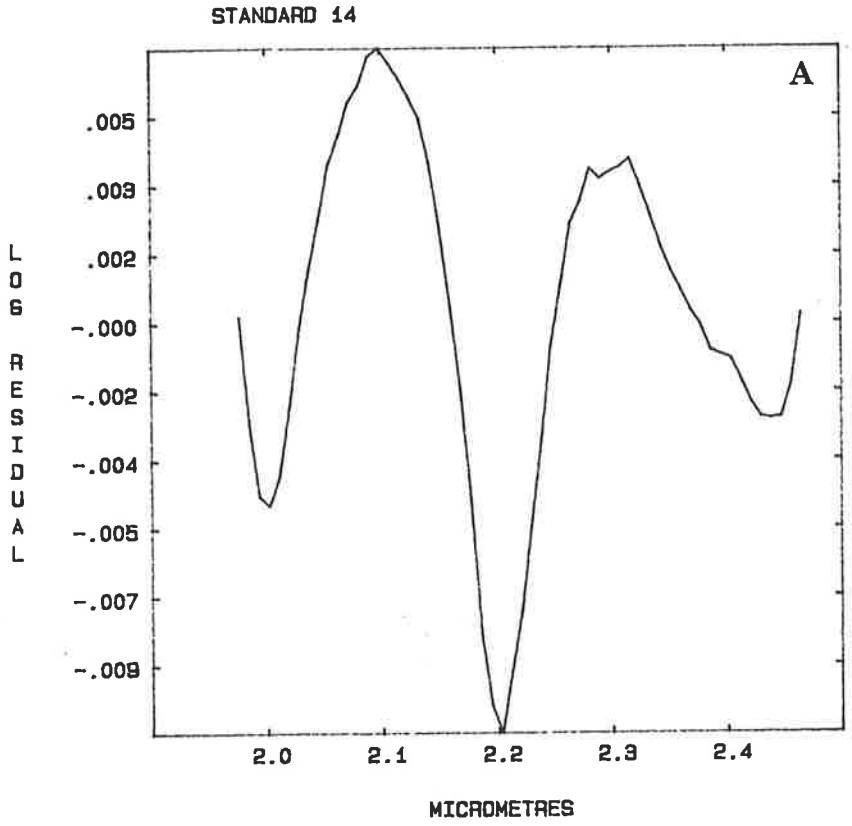
STANDARD 14
A
.005
.003
.002
-.000
-.002
-.004
-.005
-.007
-.009
LOG RESIDUAL
2.0
2.1
2.2
2.3
2.4
MICROMETRES

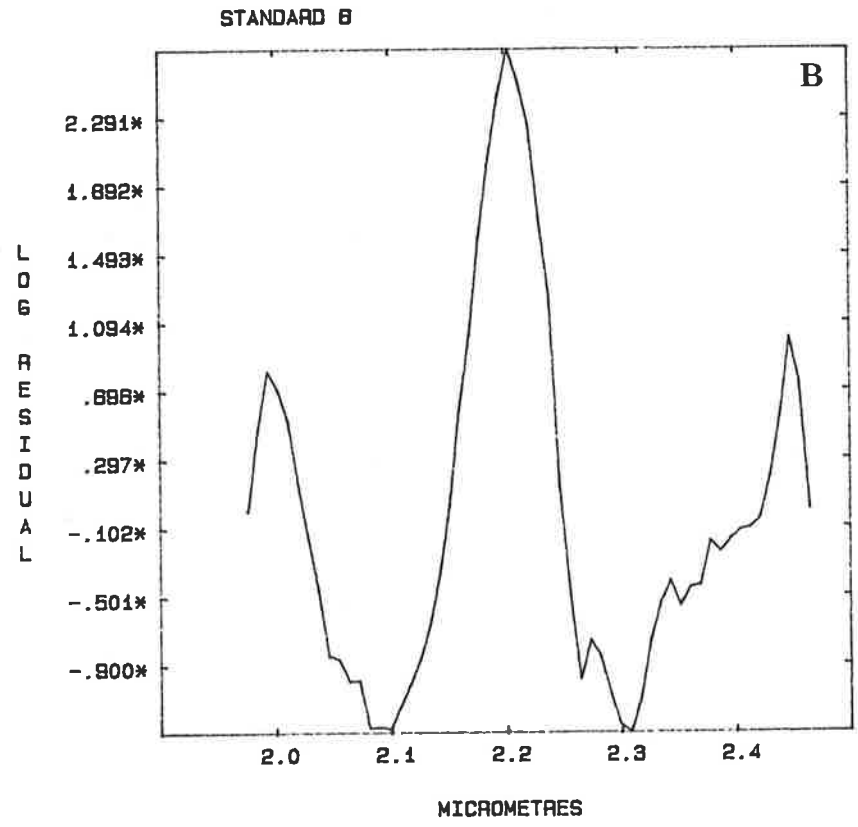
STANDARD 8
B
2.291*
1.892*
1.493*
1.094*
.696*
.297*
-.102*
-.501*
-.900*
LOG RESIDUAL
2.0
2.1
2.2
2.3
2.4
MICROMETRES

Figure 3.10 Log residual data in image format.

There are four columns of data in Fig. 3.10. From left to right they are VNIR log residuals, VNIR albedo (labelled V A), SWIR log residuals and SWIR albedo (labelled S A).

The data have been density sliced. Dark blue colours represent the lowest log residual values (deepest absorption features), the mid-green colours (see vertical strips at extremities of the SWIR log residuals) represent zero values, and deep red colours represent the highest log residual values. The block boundaries (horizontal lines) outline changes in the nature of the data along the flight line.

The data fall naturally into a number of 'bands' defined by the wavelength limits of the absorption features. The vertical lines outline these bands. Wavelengths of the band boundaries are ;

VNIR	1	0.327μm (start)
	2	0.635μm
	3	0.784μm
	4	1.012μm (end)
SWIR	5	1.954μm (start)
	6	2.147μm
	7	2.216μm
	8	2.302μm
	9	2.328μm
	10	2.353μm
	11	2.422μm
	12	2.500μm (end)

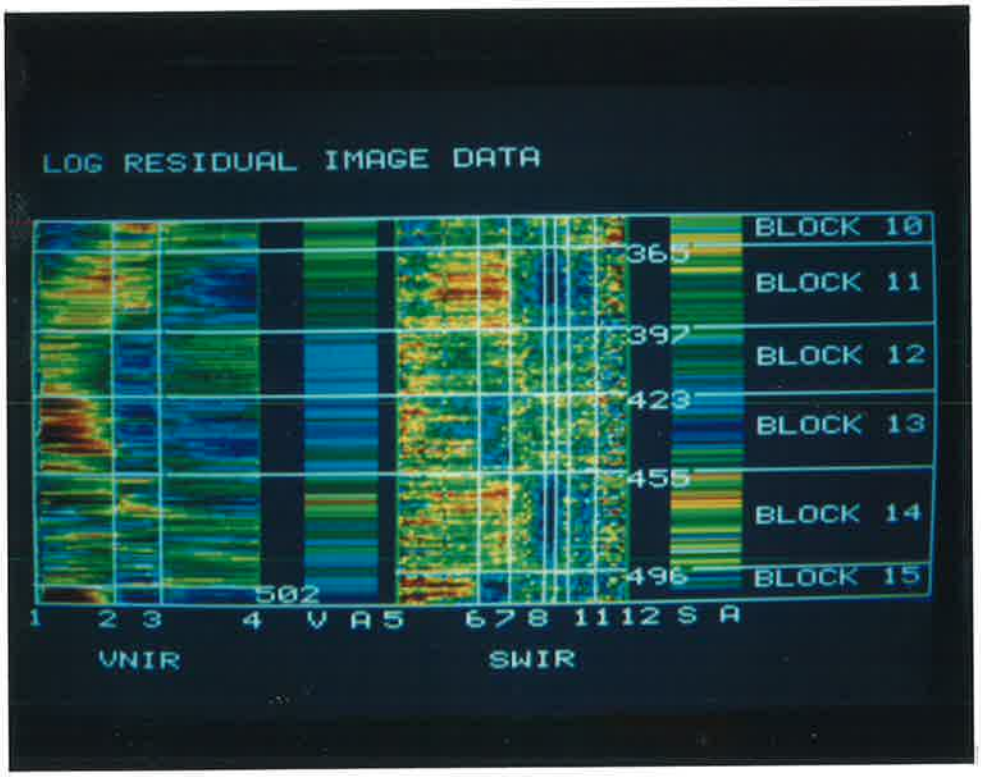
LOG RESIDUAL IMAGE DATA
BLOCK 10
365
BLOCK 11
397
BLOCK 12
423
BLOCK 13
455
BLOCK 14
496
BLOCK 15
502
1 2 3 4 V A 5 6 7 8 11 12 S A
VNIR
SWIR

Figures 3.11a-f Tchebychev polynomial functions - degree 0 to 5.

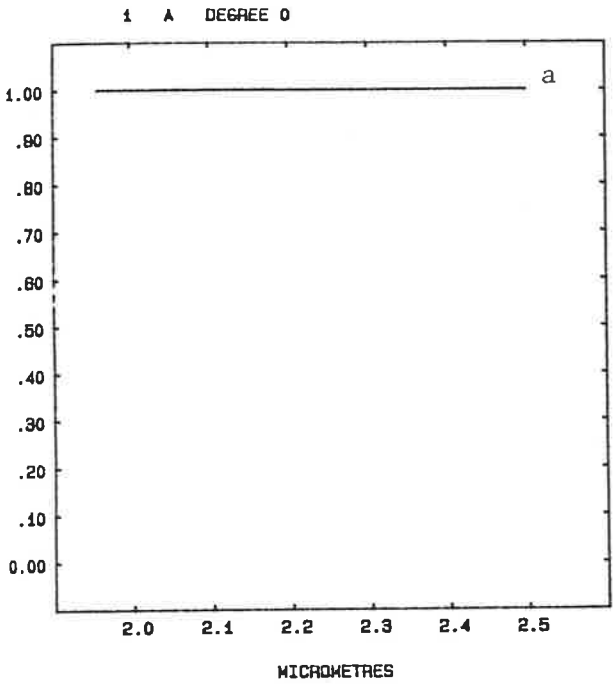
1 A DEGREE 0
a
1.00
.90
.80
.70
.60
.50
.40
.30
.20
.10
0.00
2.0 2.1 2.2 2.3 2.4 2.5
MICROMETRES

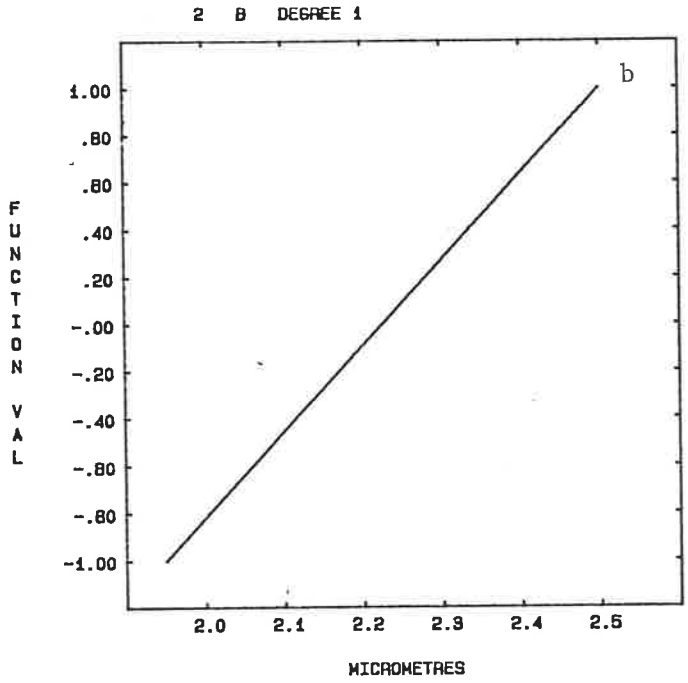
2 B DEGREE 1
b
FUNCTION VAL
1.00
.80
.60
.40
.20
-.00
-.20
-.40
-.60
-.80
-1.00
2.0 2.1 2.2 2.3 2.4 2.5
MICROMETRES

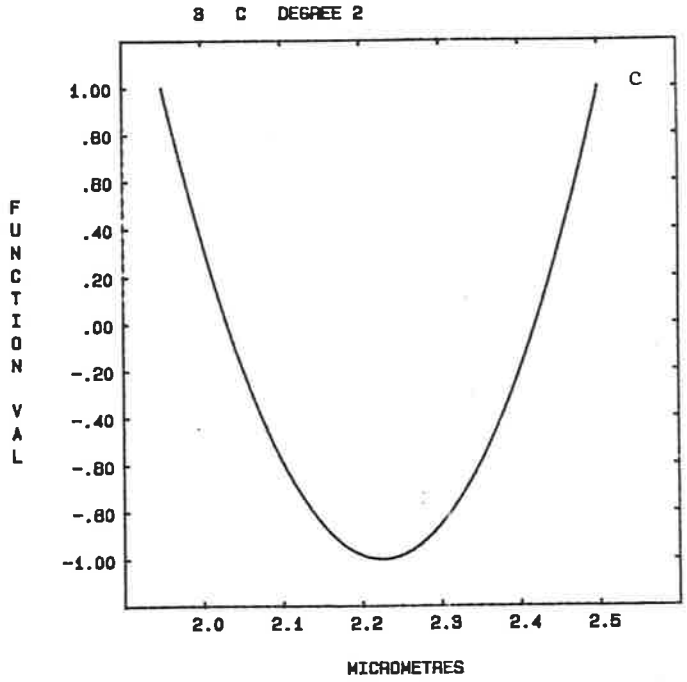
3 C DEGREE 2
c
FUNCTION VAL
1.00
.80
.60
.40
.20
.00
-.20
-.40
-.60
-.80
-1.00
2.0 2.1 2.2 2.3 2.4 2.5
MICROMETRES

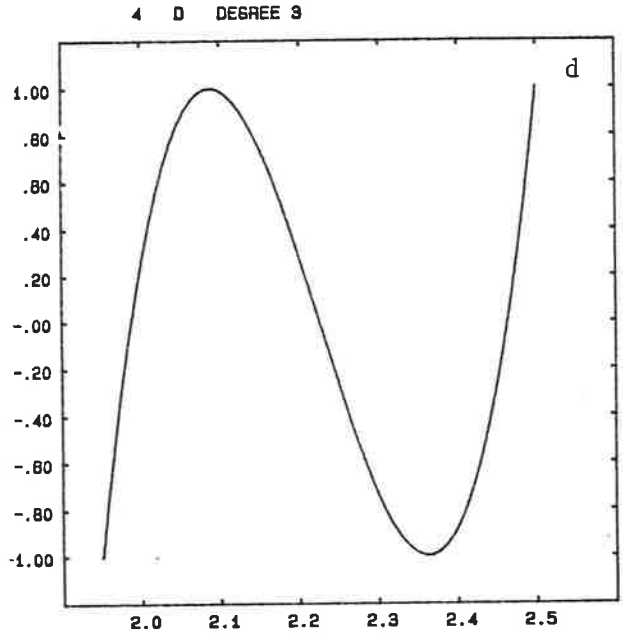
4 D DEGREE 3
d
1.00
.80
.60
.40
.20
-.00
-.20
-.40
-.60
-.80
-1.00
2.0 2.1 2.2 2.3 2.4 2.5

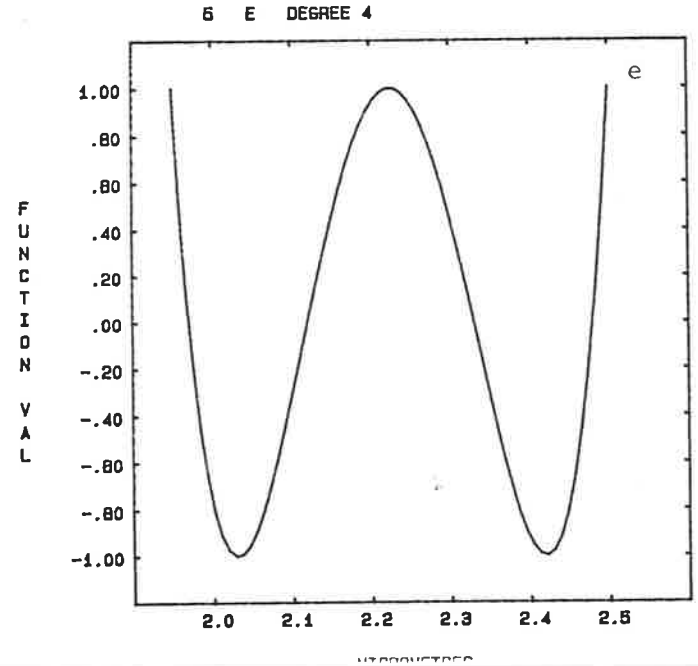
5 E DEGREE 4
e
FUNCTION VAL
1.00
.80
.60
.40
.20
.00
-.20
-.40
-.60
-.80
-1.00
2.0 2.1 2.2 2.3 2.4 2.5

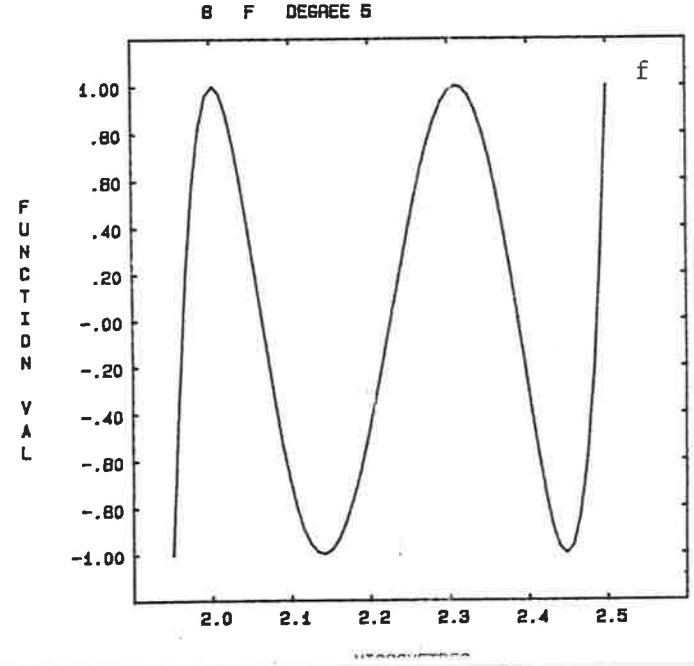
6 F DEGREE 5
f
FUNCTION VAL
1.00
.80
.60
.40
.20
-.00
-.20
-.40
-.60
-.80
-1.00
2.0 2.1 2.2 2.3 2.4 2.5

Figures 3.11g-1 Tchebychev polynomial functions - degree 6 to 11.

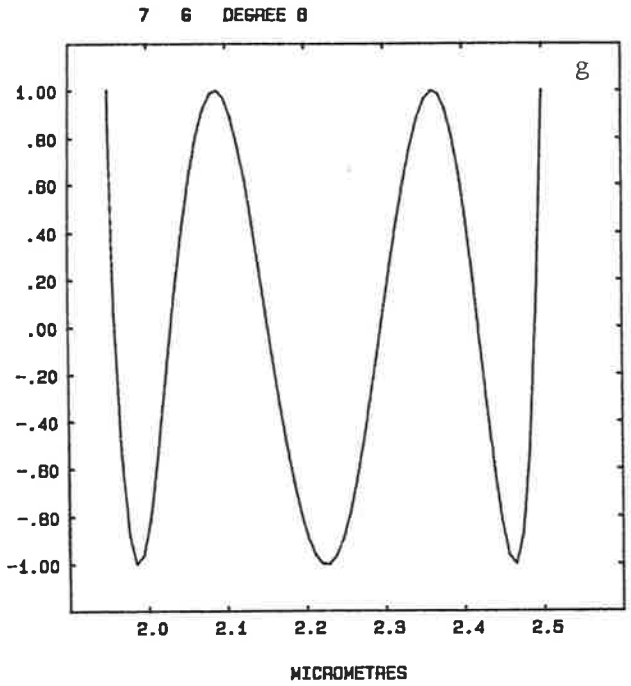
7 G DEGREE 8
g
1.00
.80
.60
.40
.20
.00
-.20
-.40
-.60
-.80
-1.00
2.0
2.1
2.2
2.3
2.4
2.5
MICROMETRES

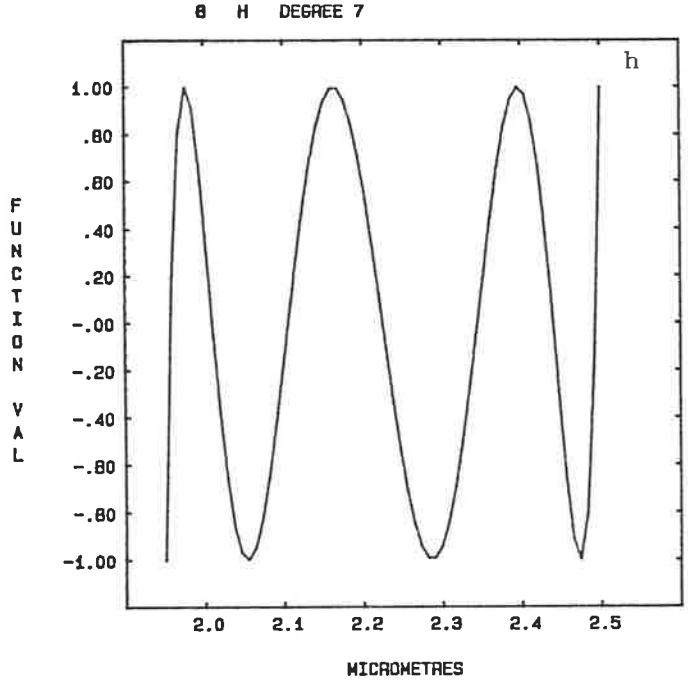
8 H DEGREE 7
h
FUNCTION VAL
1.00
.80
.60
.40
.20
-.00
-.20
-.40
-.60
-.80
-1.00
2.0
2.1
2.2
2.3
2.4
2.5
MICROMETRES

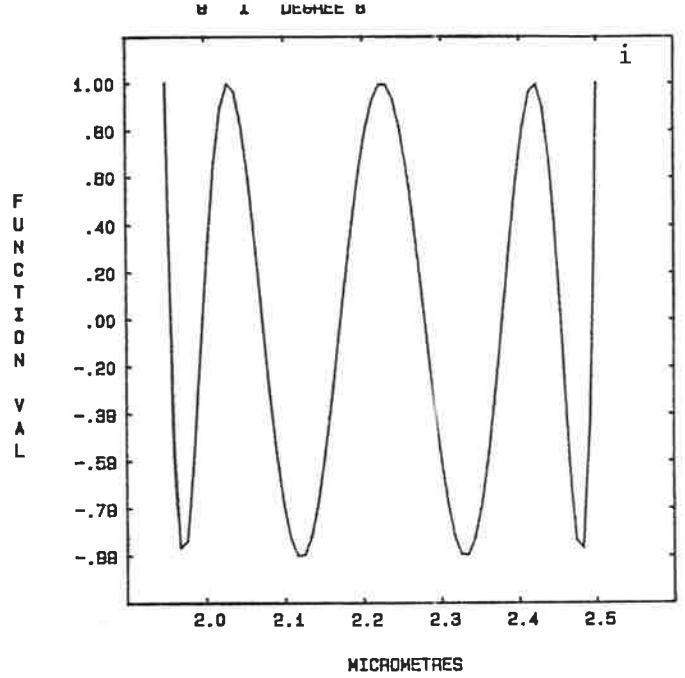
i
FUNCTION VAL
1.00
.80
.60
.40
.20
.00
-.20
-.38
-.58
-.78
-.98
2.0
2.1
2.2
2.3
2.4
2.5
MICROMETRES

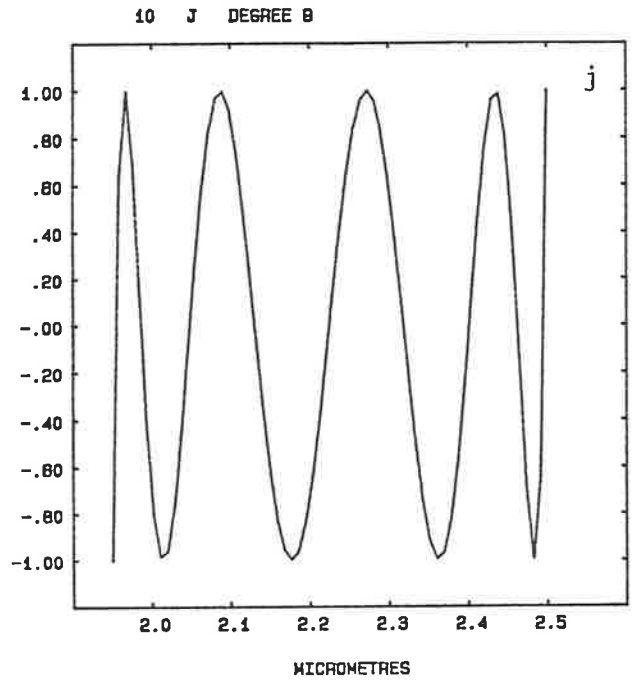
10 J DEGREE 9
j
1.00
.80
.60
.40
.20
-.00
-.20
-.40
-.60
-.80
-1.00
2.0
2.1
2.2
2.3
2.4
2.5
MICROMETRES

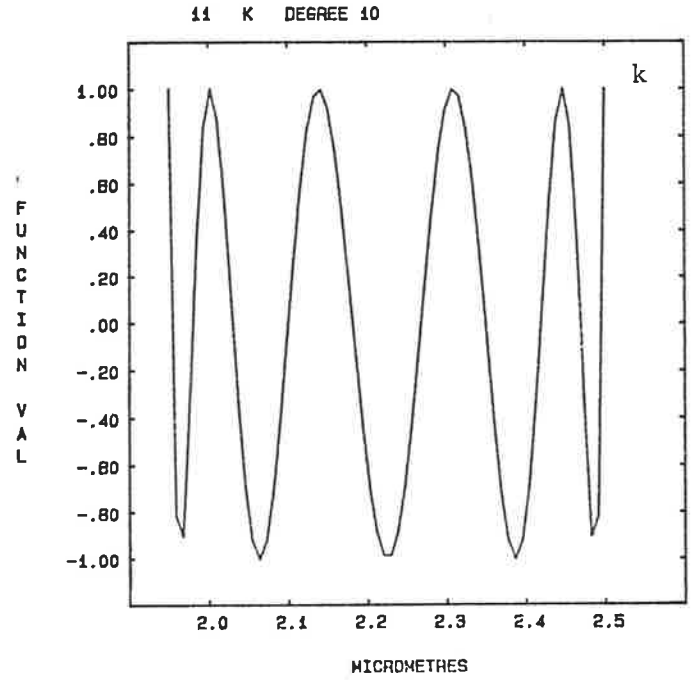
11 K DEGREE 10
k
FUNCTION VAL
1.00
.80
.60
.40
.20
.00
-.20
-.40
-.60
-.80
-1.00
2.0
2.1
2.2
2.3
2.4
2.5
MICROMETRES

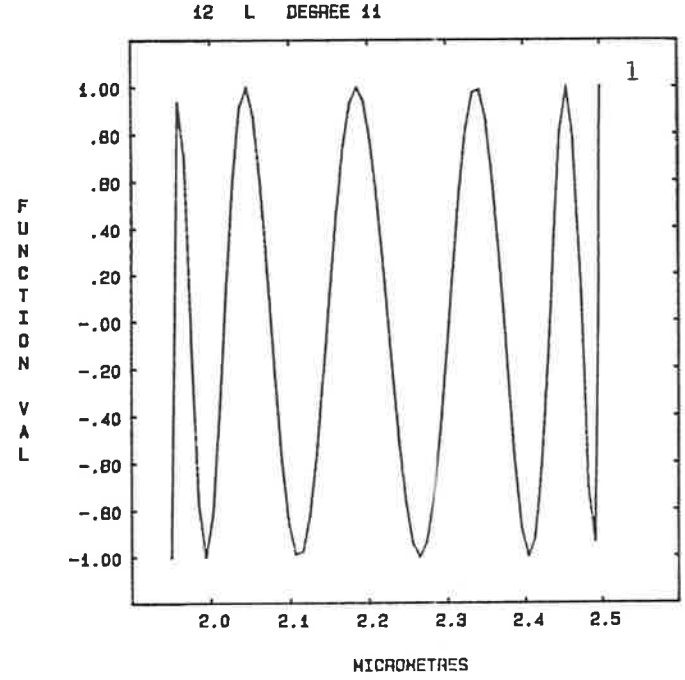
12 L DEGREE 11
l
FUNCTION VAL
1.00
.80
.60
.40
.20
-.00
-.20
-.40
-.60
-.80
-1.00
2.0
2.1
2.2
2.3
2.4
2.5
MICROMETRES

Figures 3.12a-d Interpretation of spectra by smoothing using Tchebychev polynomials and calculation of first and second derivatives.

Figure 3.12a is a VNIR laboratory reflectance spectrum consisting of 512 data channels. It has been smoothed by Tchebychev 'reconstruction' (using 12 polynomial terms) to produce Fig. 3.12b. Figure 3.12c&d are the first and second derivatives, respectively, of Fig. 3.12b. Zero values for the first derivative represent inflection points in the original spectrum, while zero values for the second derivative represent maxima or minima in the original spectrum (thus defining the positions of absorption features).

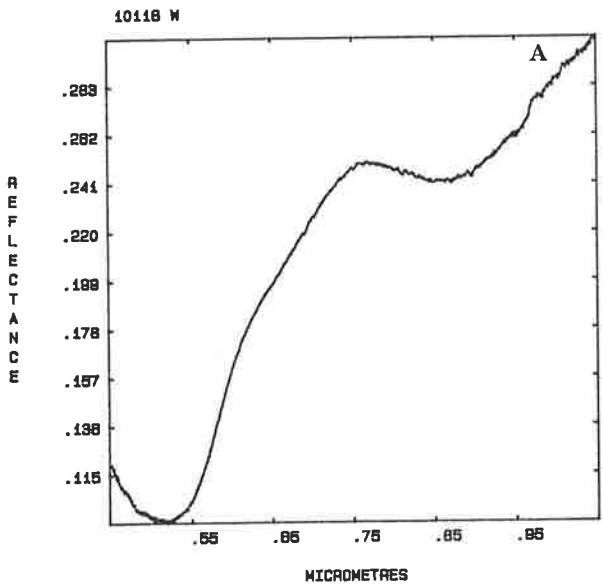
10118 W
A
.283
.262
.241
.220
.199
.178
.157
.136
.115
REFLECTANCE
.55
.65
.75
.85
.95
MICROMETRES

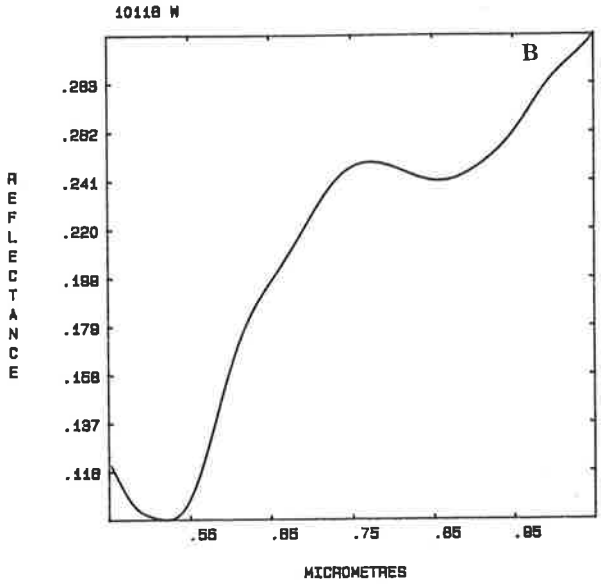
10118 W
B
.283
.262
.241
.220
.199
.179
.158
.137
.116
REFLECTANCE
.55
.65
.75
.85
.95
MICROMETRES

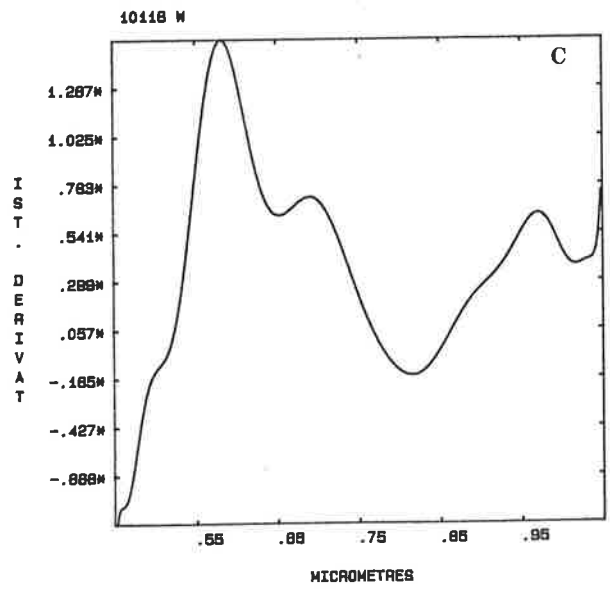
10118 W
C
1.287M
1.025M
.783M
.541M
.299M
.057M
-.185M
-.427M
-.668M
1ST. DERIVAT
.55
.65
.75
.85
.95
MICROMETRES

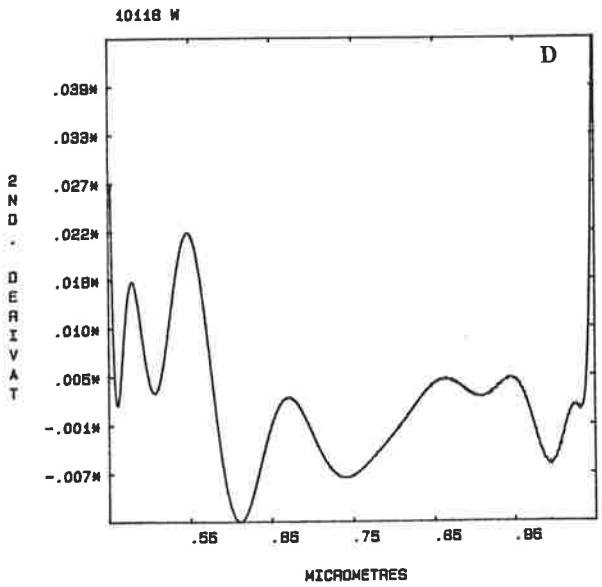
10118 W
D
.038M
.033M
.027M
.022M
.018M
.010M
.005M
-.001M
-.007M
2ND. DERIVAT
.55
.65
.75
.85
.95
MICROMETRES

Figure 4.1 Summary of stratigraphy on Cape York Peninsula (after Doutch et al., 1973).

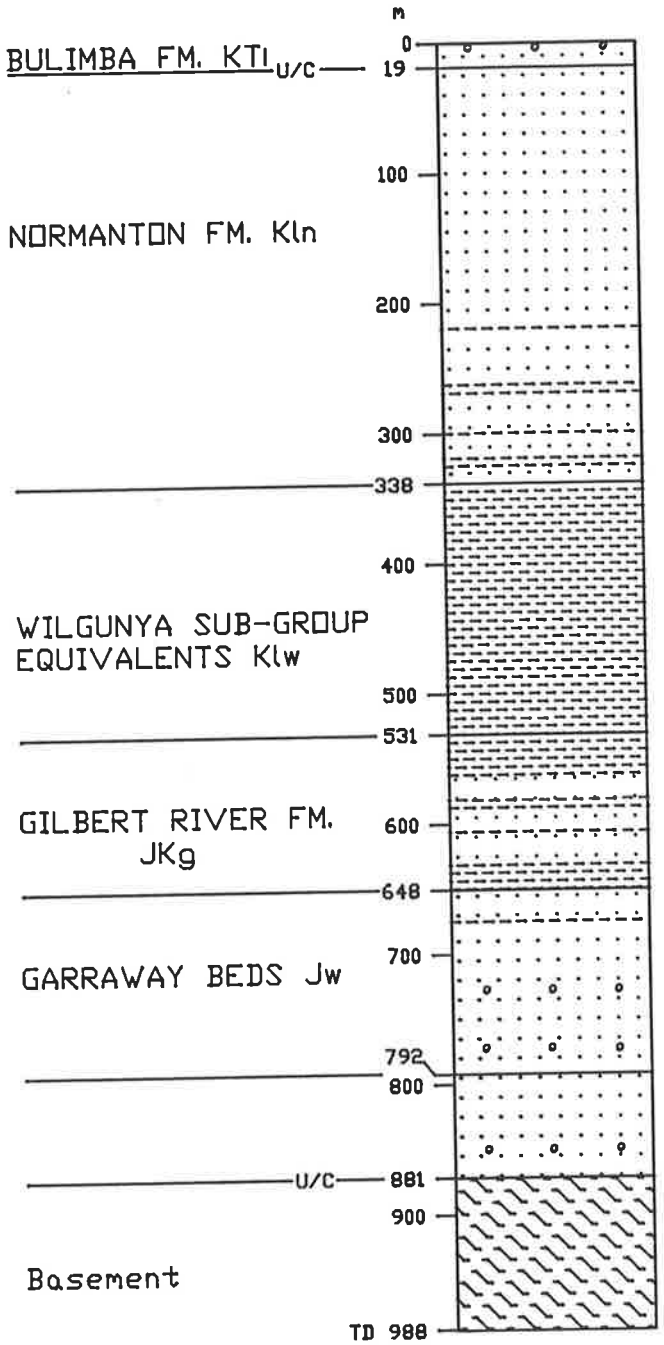

0–3m Bauxite and ferricrete
3–19m Poorly sorted, angular, very clayey quartz sandstone.
19–26m Yellow-brown stained, labile sandstone.

26–338m Fine to medium-grained grey-green glauconitic labile sandstone with minor inter-beds of grey silty shale

338–531m Grey micaceous silty shale

531–656m Grey marine silty shale with interbeds of medium-grained, grey-green glauconitic quartzose sandstone.

656–709m Grey-green, well-bedded glauconitic quartzose sandstone with minor pyrite, mica. Some interbeds of silty shale.

709–792m Coarse-grained poorly sorted, subangular clayey feldspathic quartzose sandstone, a few conglomerate and clay bands. Minor coal below 783m.

792–881m Sandstone as above, some conglomerate and clay. Becoming increasingly coaly and micaceous towards basement.

881–988m Deeply weathered metamorphic sediments composed of quartz, chlorite, muscovite, magnetite and pyrite, with

Figure 4.2 Distribution of laterite on Cape York Peninsula (after Evans, 1972).

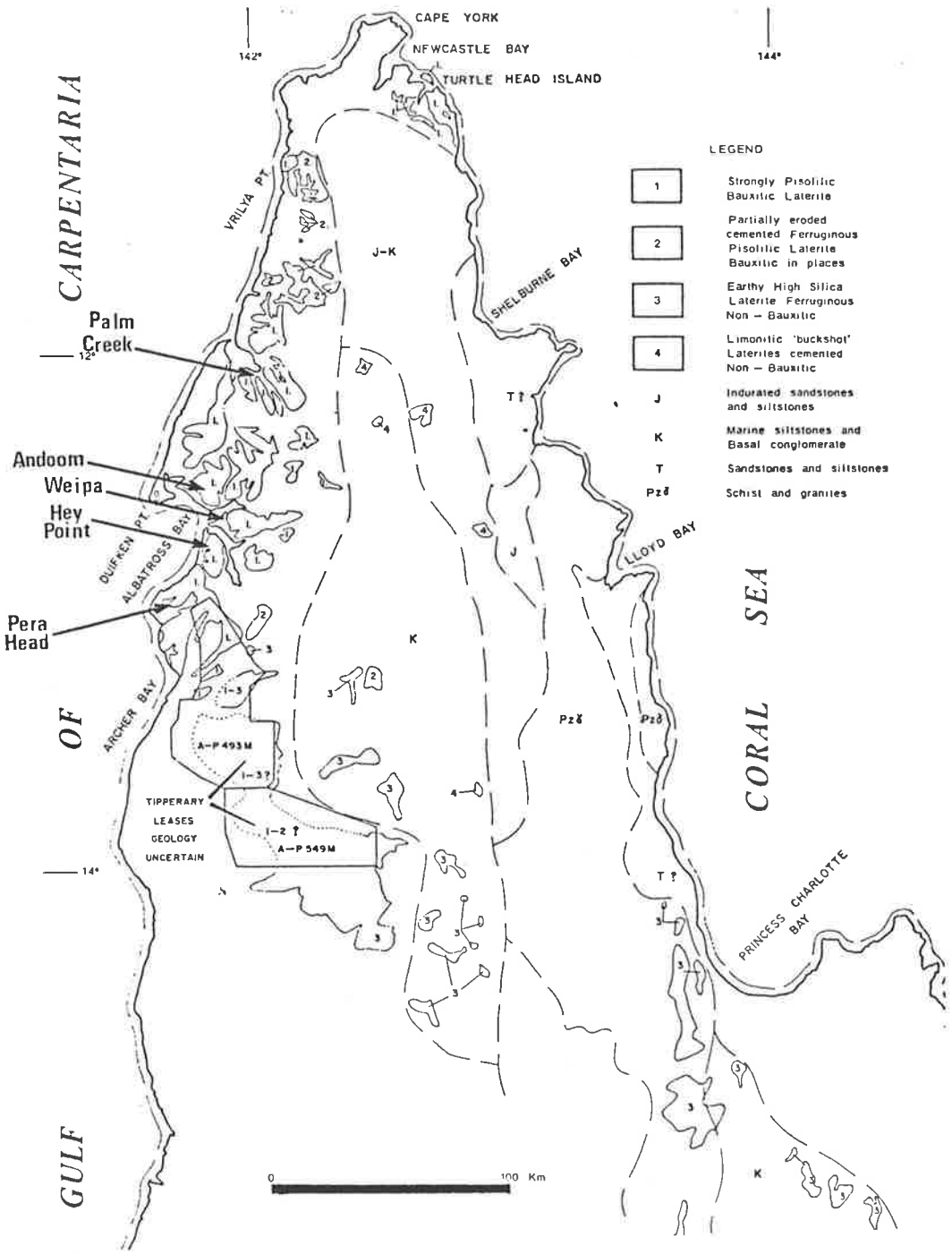
CAPE YORK
NEWCASTLE BAY
TURTLE HEAD ISLAND
142°
144°
12°
14°
CARPENTARIA
GULF OF
CORAL SEA
VRILYA PT
SHELBURNE BAY
LLOYD BAY
PRINCESS CHARLOTTE BAY
QUIFKEN PT
ALBATROSS BAY
ARCHER BAY
Palm Creek
Andoom
Weipa
Hey Point
Pera Head
A-P 493M
A-P 549M
TIPPERARY LEASES GEOLOGY UNCERTAIN
J-K
K
T?
Pzǒ
Q
J
0
100 Km
LEGEND
1 Strongly Pisolitic Bauxitic Laterite
2 Partially eroded cemented Ferruginous Pisolitic Laterite Bauxitic in places
3 Earthy High Silica Laterite Ferruginous Non – Bauxitic
4 Limonitic 'buckshot' Laterites cemented Non – Bauxitic
J Indurated sandstones and siltstones
K Marine siltstones and Basal conglomerate
T Sandstones and siltstones
Pzǒ Schist and granites

Figure 4.3 Typical stratigraphic log from the Weipa Peninsula (after Coffey and Hollingsworth, 1971).

Figure 4.4 Cross section through the Weipa Peninsula from hydrologic bore data (after Coffey and Hollingsworth, 1971).

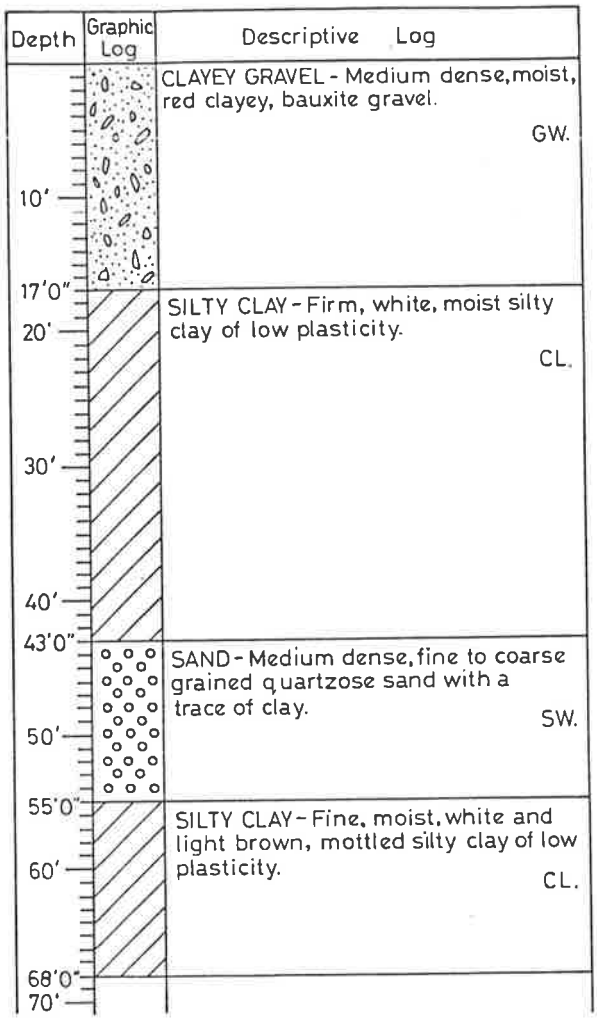
Depth
Graphic Log
Descriptive Log
CLAYEY GRAVEL - Medium dense, moist, red clayey, bauxite gravel.
GW.
10'
17'0"
20'
SILTY CLAY - Firm, white, moist silty clay of low plasticity.
CL.
30'
40'
43'0"
SAND - Medium dense, fine to coarse grained quartzose sand with a trace of clay.
SW.
50'
55'0"
SILTY CLAY - Fine, moist, white and light brown, mottled silty clay of low plasticity.
CL.
60'
68'0"
70'

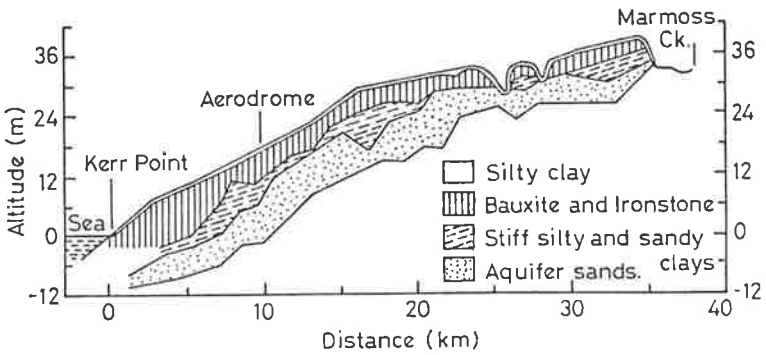
Marmoss Ck.
Aerodrome
Kerr Point
Sea
Altitude (m)
36
24
12
0
-12
0
10
20
30
40
Distance (km)
Silty clay
Bauxite and Ironstone
Stiff silty and sandy clays
Aquifer sands.

Figure 4.5 Weipa area vegetation map (after Specht et al., 1977).

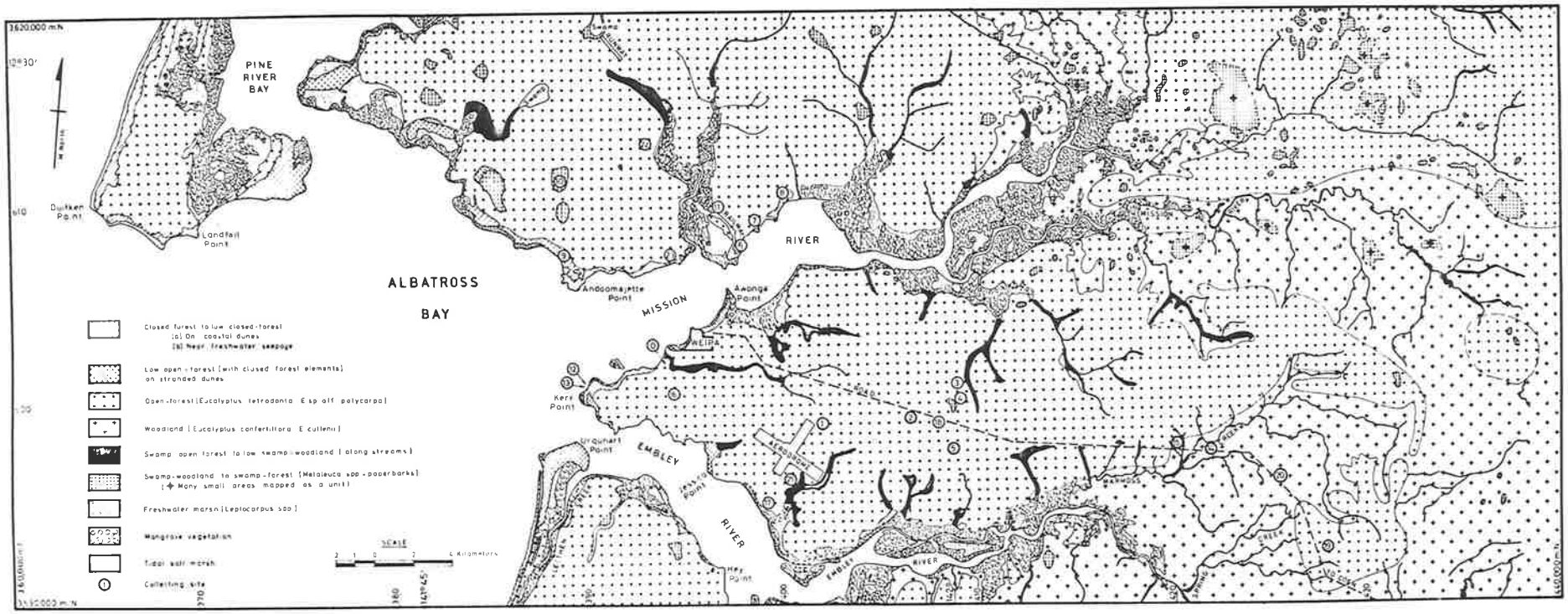
3620000 m N
12°30'
PINE RIVER BAY
Duiken Point
Landfall Point
ALBATROSS BAY
Andoomajette Point
MISSION
Aaonga Point
RIVER
WEIPA
Kerr Point
Urquhart Point
EMBLEY
RIVER
Hey Point
Closed forest to low closed-forest
(a) On coastal dunes
(b) Near freshwater seepage
Low open-forest (with closed forest elements) on stranded dunes
Open-forest (Eucalyptus tetrodonta E sp aff polycarpa)
Woodland (Eucalyptus confertiflora E cullenii)
Swamp open forest to low swamp-woodland (along streams)
Swamp-woodland to swamp-forest (Melaleuca spp - paperbarks)
(✦ Many small areas mapped as a unit)
Freshwater marsh (Leptocarpus spp)
Mangrove vegetation
Tidal salt marsh
Collecting site
SCALE
2 1 0 2 4 Kilometers
3510000 m N

Figure 4.6 Graph of Moisture Index and Net Photosynthetic Index from Weipa Peninsula (after Specht et al., 1977).

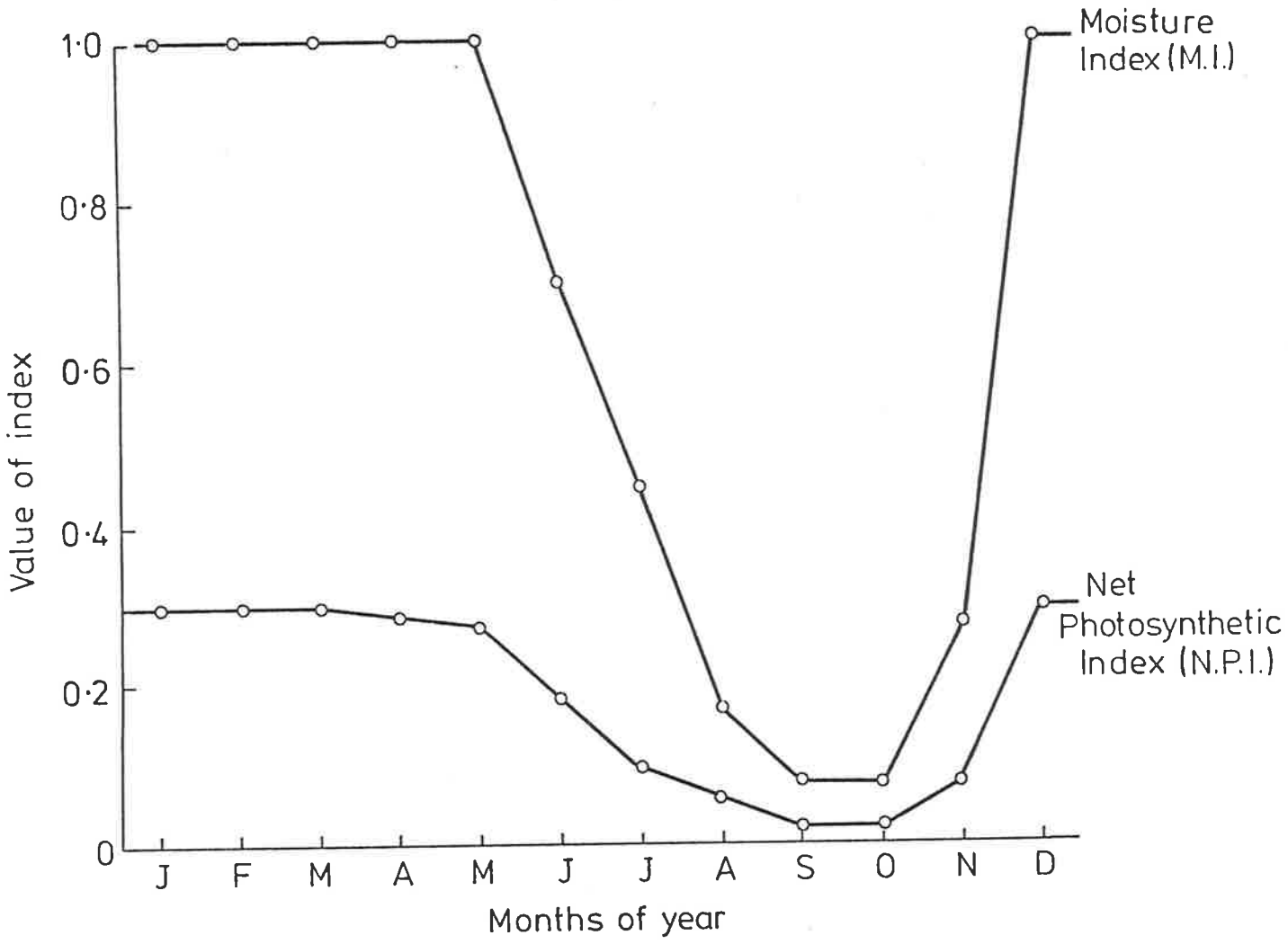
Moisture
Index (M.I.)
Net
Photosynthetic
Index (N.P.I.)
Value of index
1·0
0·8
0·6
0·4
0·2
0
J
F
M
A
M
J
J
A
S
O
N
D
Months of year

Figure 4.7 Landsat false colour composite - sub-scene of Cape Weymouth - linear stretch of raw bands 4, 5 and 7, dry season image (after Huntington et al., 1982).

Image ID No. 01036-00004, 26 July, 1973. Scale is approximately 1:1,000,000, or 10km between scale ticks along top and bottom of the image. The large central white area is Weipa mine site, while black to green-brown patches to the east and southeast are bushfire burn scars. The bauxite plateaux boundaries are just detectable on this image.

Stretch limits for this scene were derived from the land subscene shown on the overlay, corresponding to: FL 600, LL 2340, FP 900, LP 2100. DS stretch limits used were: 4 17-34, 5 9-29, 7 0-20.

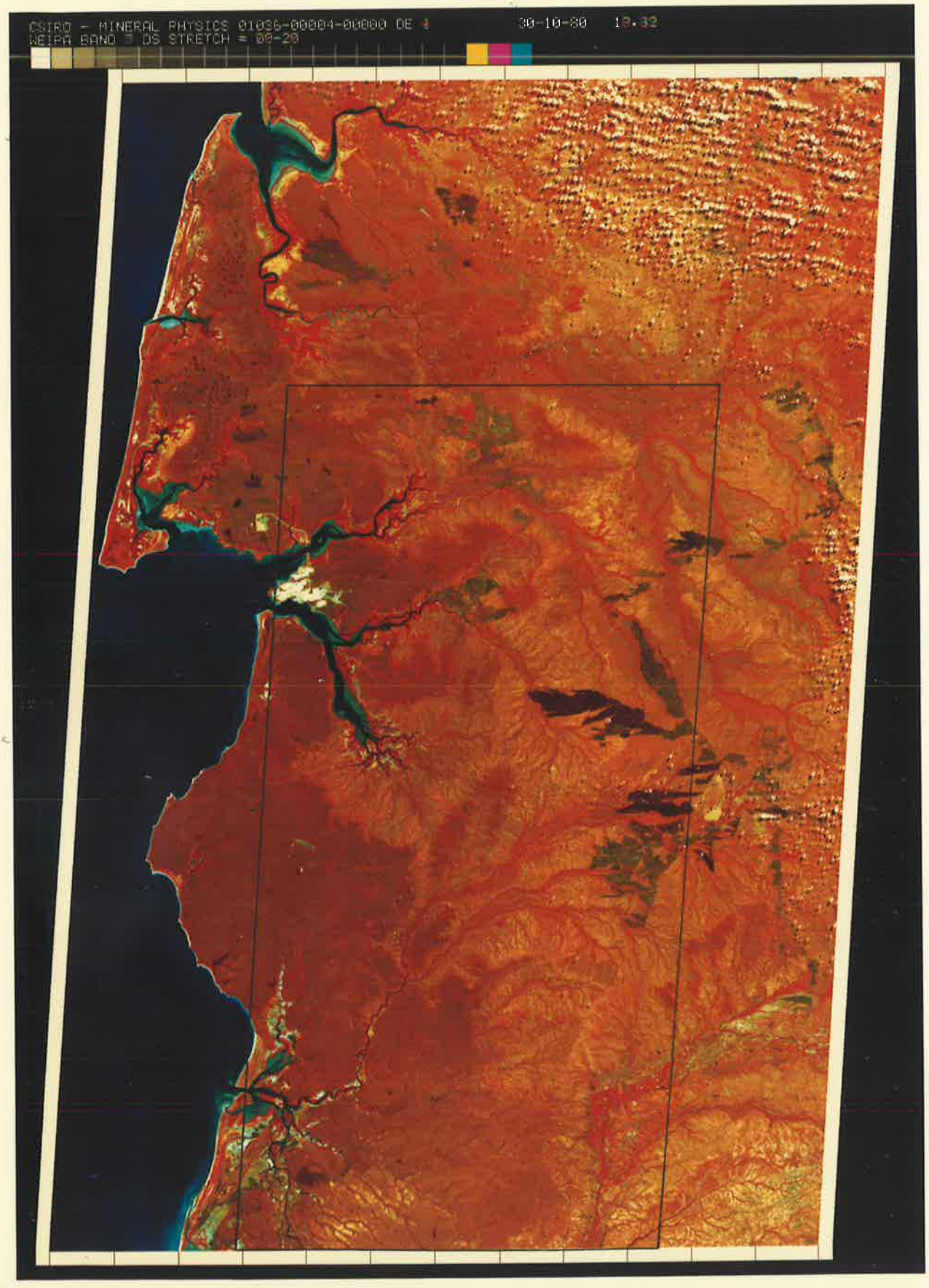
CSIRO - MINERAL PHYSICS 01036-00004-00000 DE 4
30-10-80 13:32
WEIPA BAND 3 DS STRETCH = 00-20

Figure 4.8 Landsat false colour composite - Cape Weymouth scene - histogram normalised, bands 4, 5 and 7, dry season image (after Huntington et al., 1982)

This image is the optimum enhancement of the Cape Weymouth scene, produced by histogram normalisation. The input file used for this process includes all data from the rectangular area shown on the overlay. Image ID and scale as for Fig. 4.7. The improvement over Fig. 4.7 is dramatic. The bauxite surfaces are clearly delineated (boundaries are shown on the overlay), and individual plateaux show variations in red and green colour tones. Intense red along creeks are mostly mangrove swamps.

KEY

1 Palm Creek Block

2 Andoom Block

3 Weipa Block

4 Hey Point Block

5 Pera Head Block

6 Watson River

7 Watson River Block

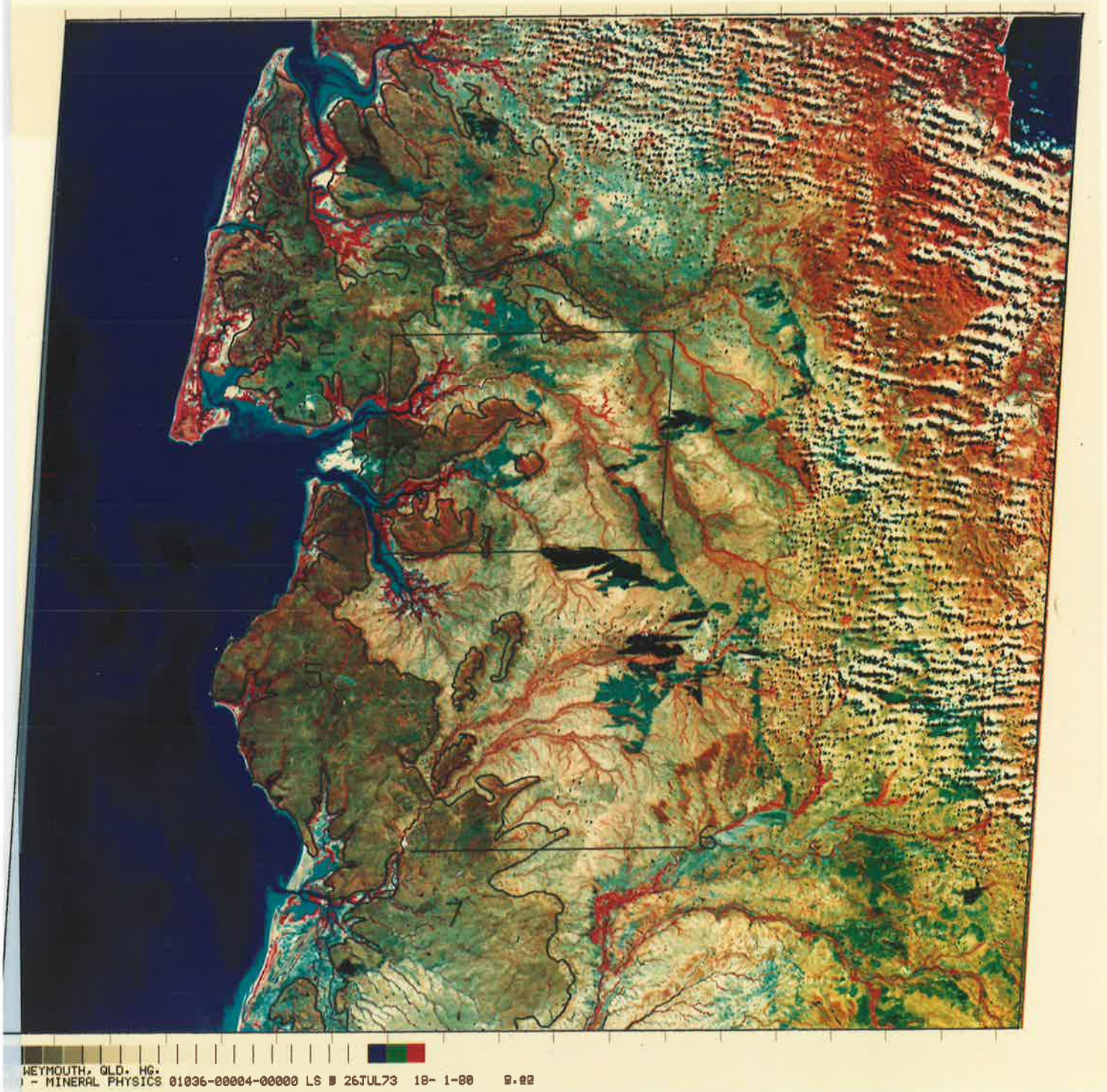

WEYMOUTH, QLD. HG.
- MINERAL PHYSICS 01036-00004-00000 LS B 26JUL73 18- 1-80 B.02

Figure 4.9 Density sliced Transformed Vegetation Index image of the Weipa Peninsula (after Huntington et al., 1982).

The image has been smoothed with a low-pass filter. Note the east-west trend in the index on the plateau top. Blue = low TVI7 values, dark red = high TVI7 values. High values depict areas of most intense (most luxuriant, most dense) vegetation response. M = mangrove areas. Image ID as for Figs. 4.7 and 4.8. Scale as shown.

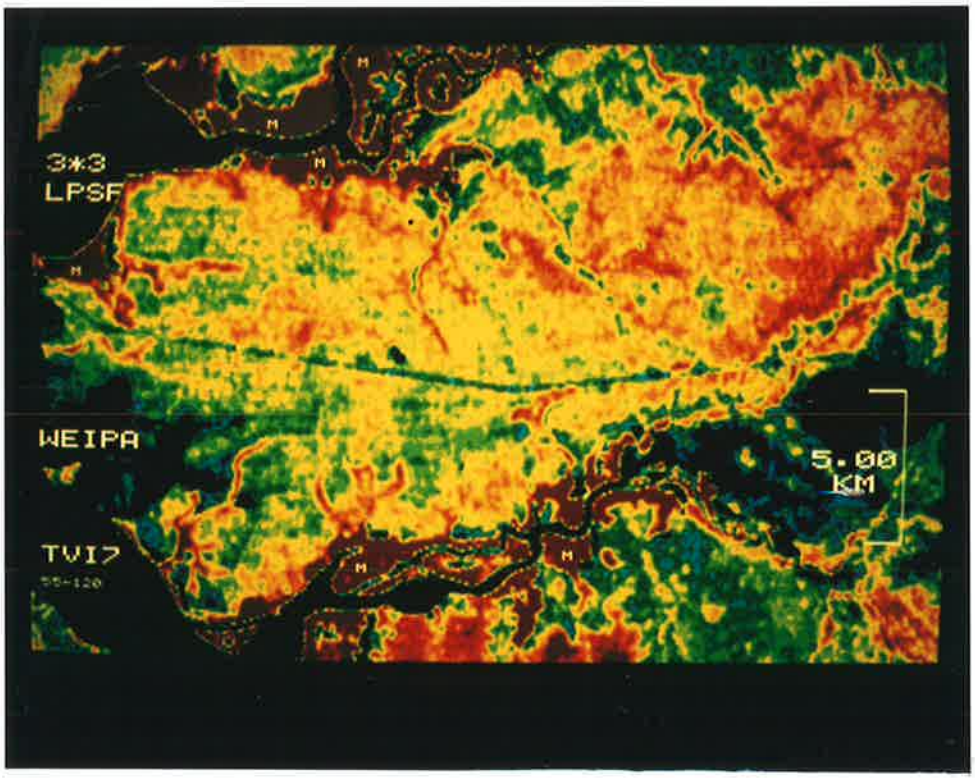
3*3
LPSF
WEIPA
TVI?
5.00
KM

Figure 4.10 Landsat false colour composite - sub-scene of Cape Weymouth - linear stretch of bands 4, 5 and 7, wet season image.

Image ID No. 22289-23511, 29 April, 1981. Technique used for production of this image is essentially the same as for Fig. 4.8, but the image shown is sub-sampled and photographed from a TV screen. Note overall increased redness of the image compared to Fig. 4.8, and larger black 'swamp' areas on Weipa Peninsula.

Figure 4.11 Landsat false colour composite - Weipa Peninsula - linear stretch, bands 4, 5 and 6.

Image ID as for Figs. 4.7 and 4.8. The image has been photographed from a full resolution TV display. The same trends are present as in Fig. 4.8, but they are not as well defined.

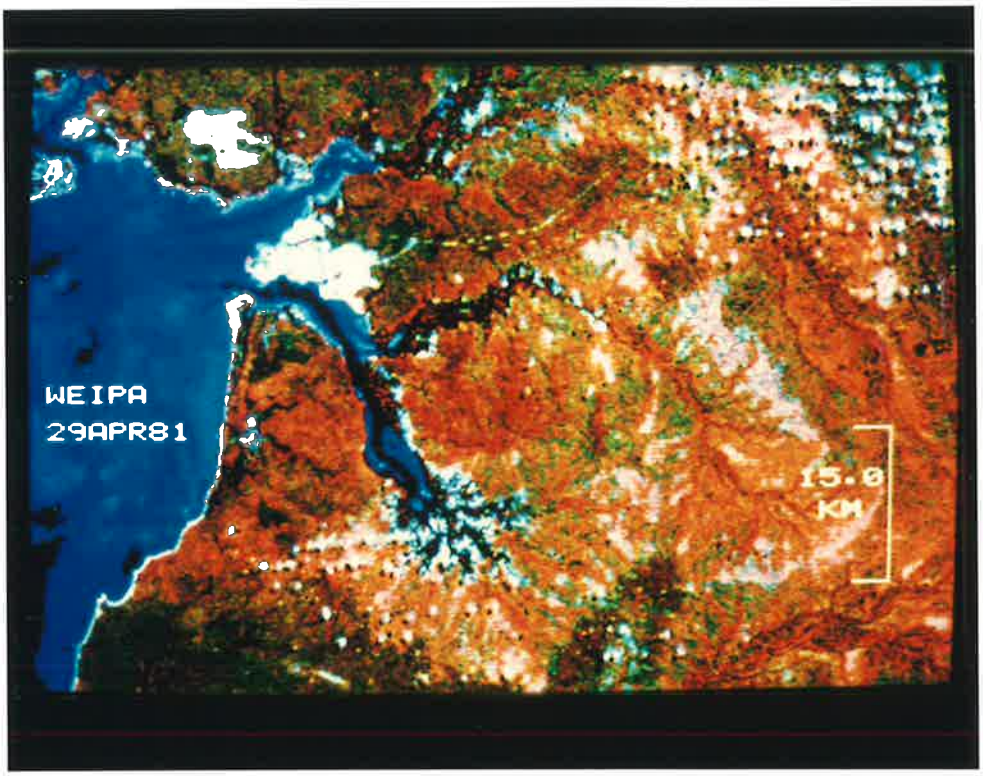
WEIPA
29APR81
15.0
KM


KM
WEIPA
CM4=4-107 CM5=12-136 CM6=96-210

Figure 4.12a&b Bauxite isopachs from a portion of Weipa Peninsula (after Evans, 1972 and O'Sullivan, pers. comm.,1982).

Figure 4.12a shows the interpretation of Evans (1972), indicating a structural control (fold axes) on ore thickness.

Figure 4.12b depicts Evans' 'synclinal axes' in highlighted colour. The 'synclinal axes' are more likely to be channels of an older drainage system, while 'anticlinal axes' would be interfluves (K. O'Sullivan, pers. comm., 1982).

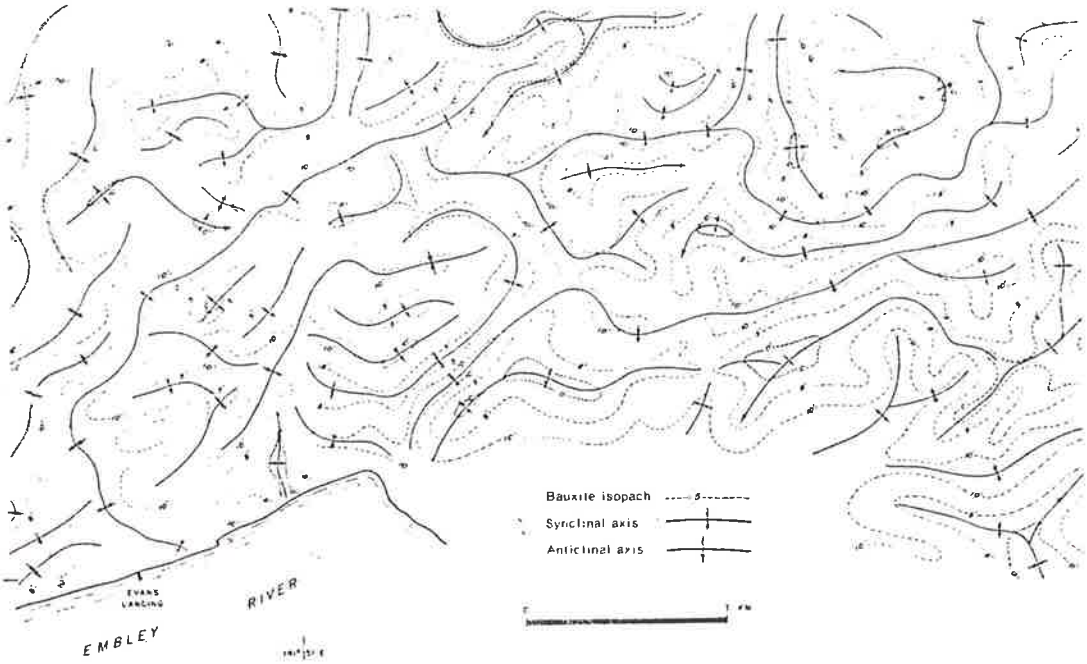
Bauxite isopach
Synclinal axis
Anticlinal axis
EVANS LANDING
RIVER
EMBLEY

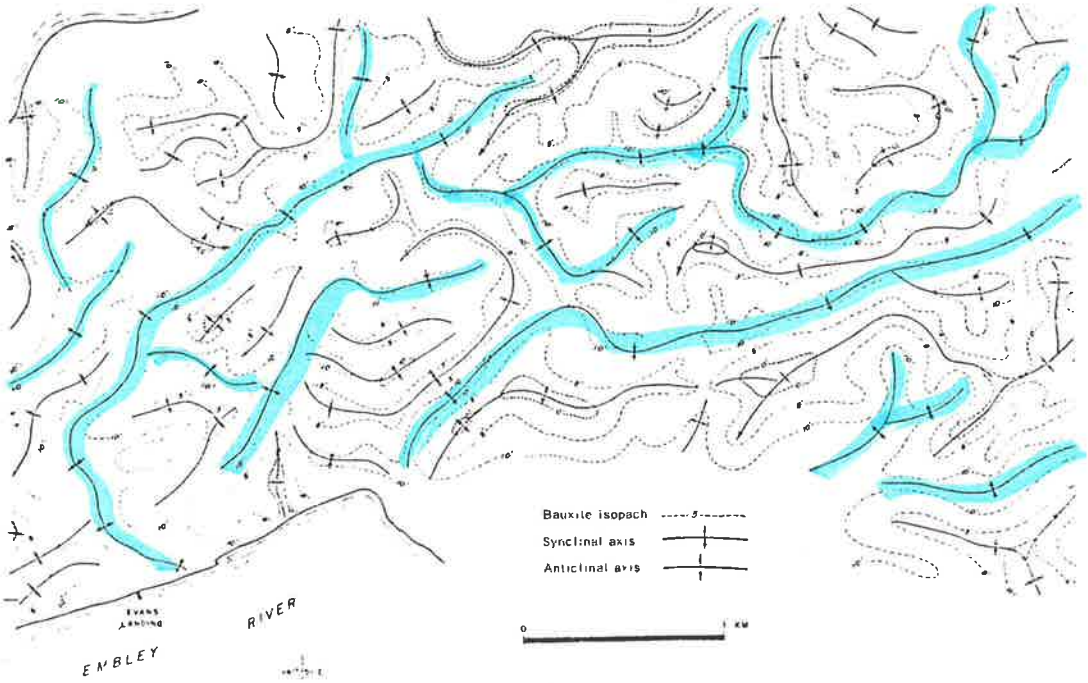
Bauxite isopach
Synclinal axis
Anticlinal axis
EVANS LANDING
RIVER
EMBLEY

Figure 4.13 Landsat false colour composite - Weipa Peninsula - linear stretch, bands 4, 5 and 7, dry season image.

Image ID as for Fig. 4.7. Contrast modification limits as shown. Arrows point to drilling-grid lines. East-west arrows are aligned along coordinate 20,000N. Note again the gradational colour change from B (green) to A (red) along the peninsula. BF = bush fire scar. The overlay indicates NNW-SSE linear trend.

Figure 4.14 Landsat false colour composite - Weipa Peninsula - linear stretch, bands 4, 5 and 7, wet season image.

Band 4 has been smoothed with a 4*4 low pass box filter to reduce residual striping. Image ID as for Fig. 4.10. Note the red fringe to the bauxite plateau.

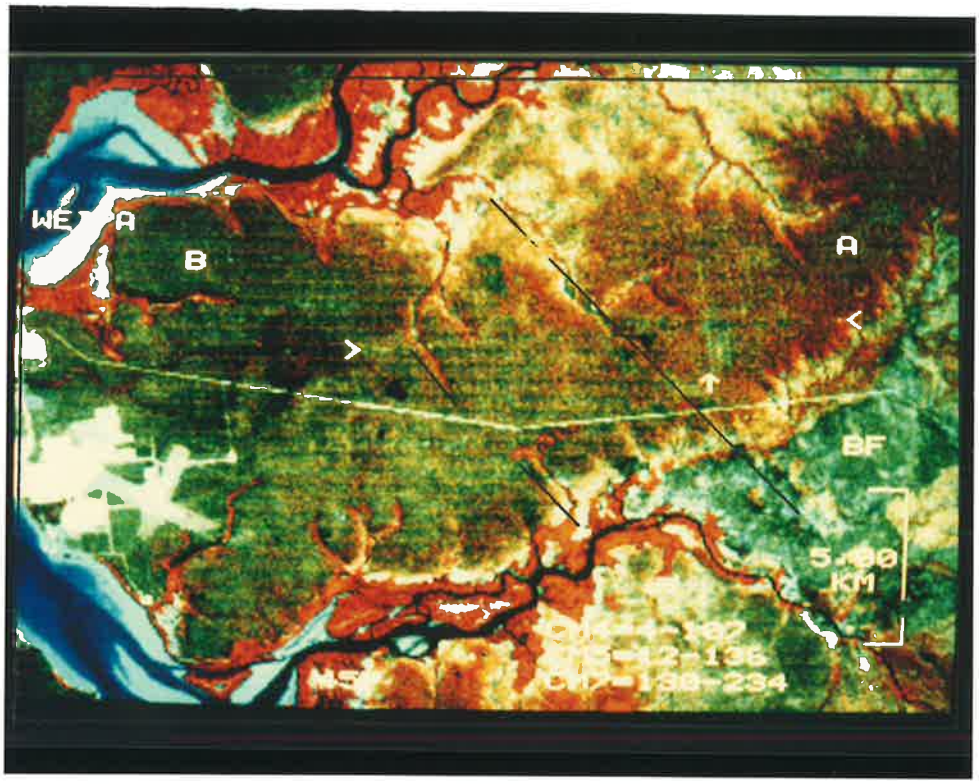
WE
A
B
A
BF
KM

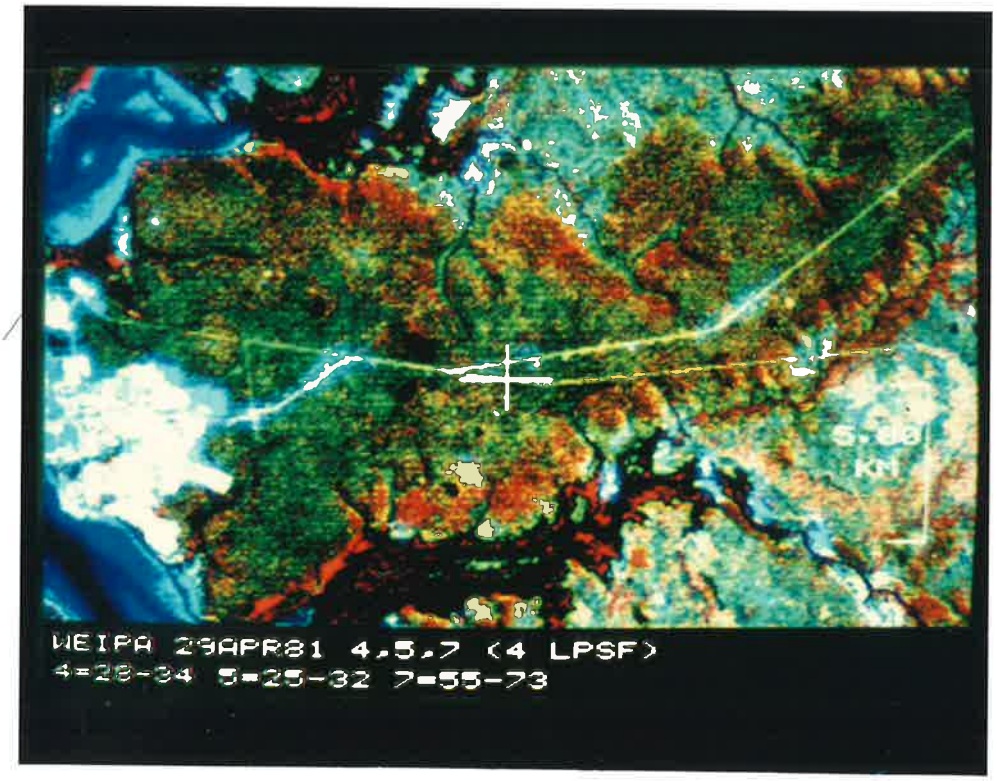
KM
WEIPA 29APR81 4,5,7 (4 LPSF)
4=28-34 5=25-32 7=55-73

Figure 4.15 Landsat colour ratio composite - Weipa Peninsula - histogram normalised, wet season image.

The ratios used were 4/5 (blue), 5/6 (green) and 6/7 (red). Note that the colour variation is mainly from the edges towards the centre of the plateau, rather than along the peninsula (as is the case with dry season imagery).


5.00
KM

Figure 4.16 Average annual wet season water table rise over Weipa Peninsula (after Coffey and Hollingsworth, 1971).

Note the similarity of the shape of the contours and the distribution of colour variations in Fig. 4.15.

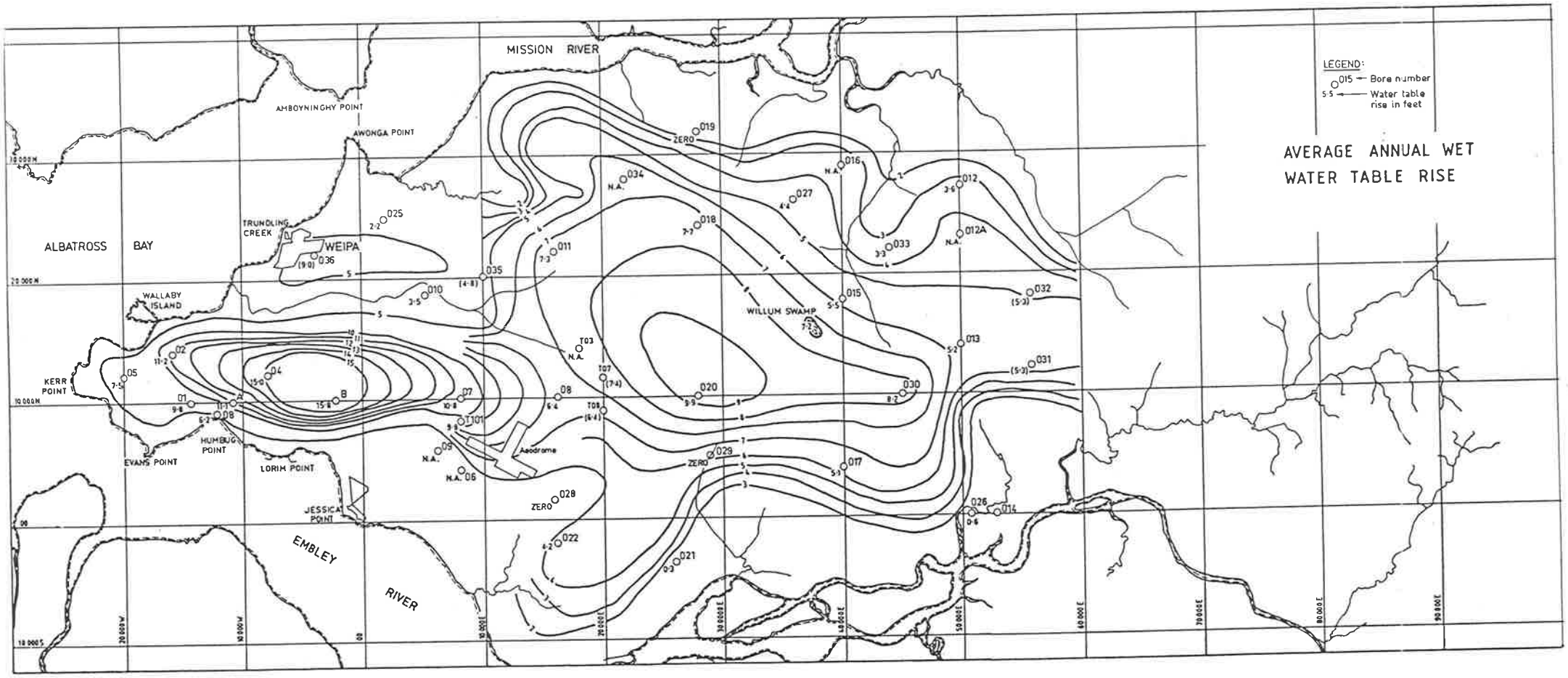
MISSION RIVER
AMBOYNINGHY POINT
AWONGA POINT
ALBATROSS BAY
TRUNDLING CREEK
WEIPA
WALLABY ISLAND
KERR POINT
EVANS POINT
HUMBUG POINT
LORIM POINT
JESSICA POINT
EMBLEY RIVER
WILLUM SWAMP
Aerodrome
ZERO
N.A.
LEGEND:
015 — Bore number
5·5 — Water table rise in feet
AVERAGE ANNUAL WET WATER TABLE RISE

Figure 4.17 Variation of SiO_2 content of soil samples along Weipa Peninsula.

For Figs. 4.17 to 4.20 data come predominantly from the 20,000N line (east of 50,000E), and the 10,000N line (west of 50,000E). Precise locations are documented in Table 4.1 The regression lines have been calculated for the y-direction.

SiO_2 values show a strong trend to increasing values from west to east along the peninsula.

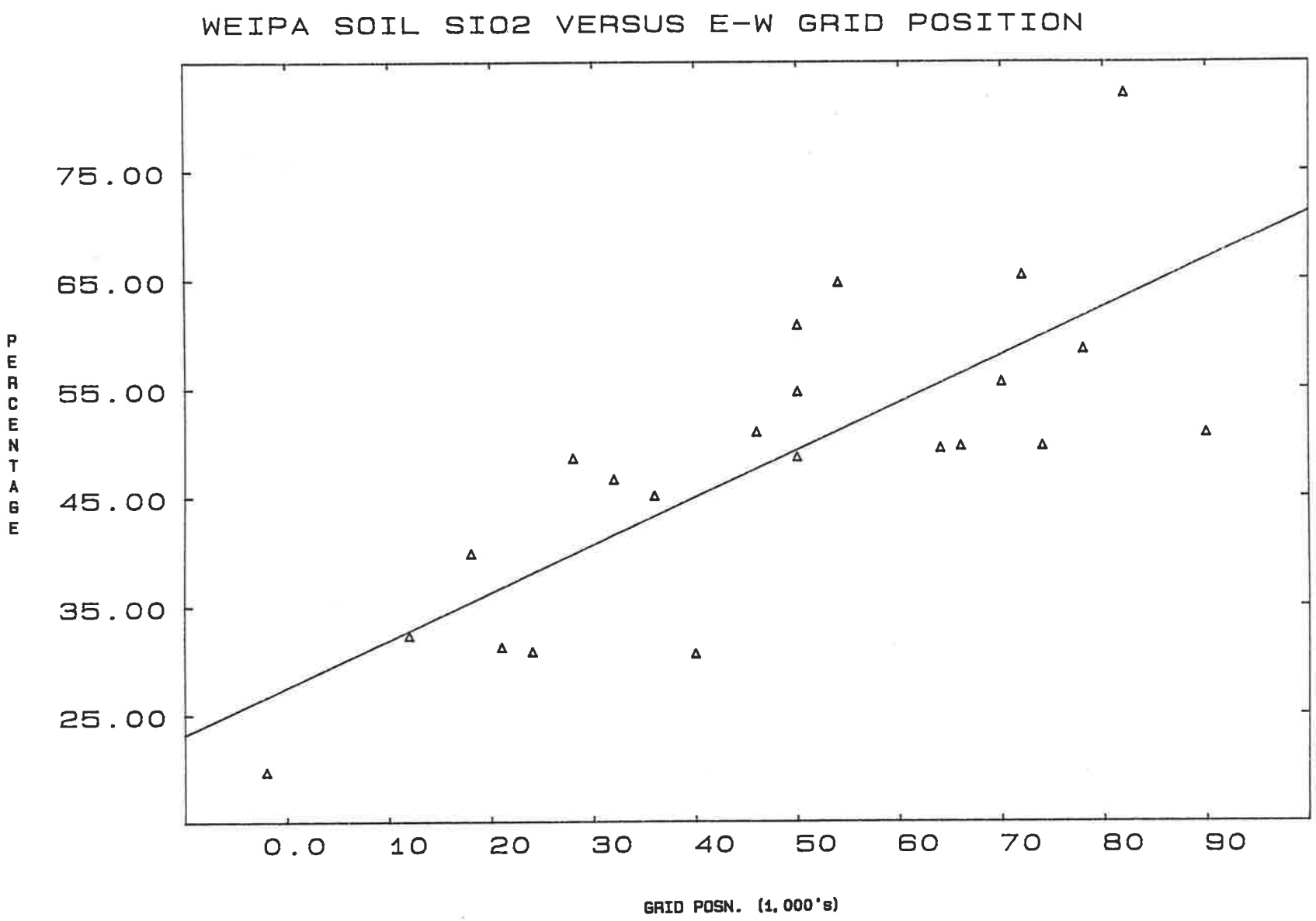
WEIPA SOIL SIO2 VERSUS E-W GRID POSITION
PERCENTAGE
75.00
65.00
55.00
45.00
35.00
25.00
0.0
10
20
30
40
50
60
70
80
90
GRID POSN. (1,000's)

Figure 4.18 Variation of Al_2O_3 content of soil samples along Weipa Peninsula.

Note that the trend is the inverse of that exhibited by SiO_2 in Fig. 4.17.

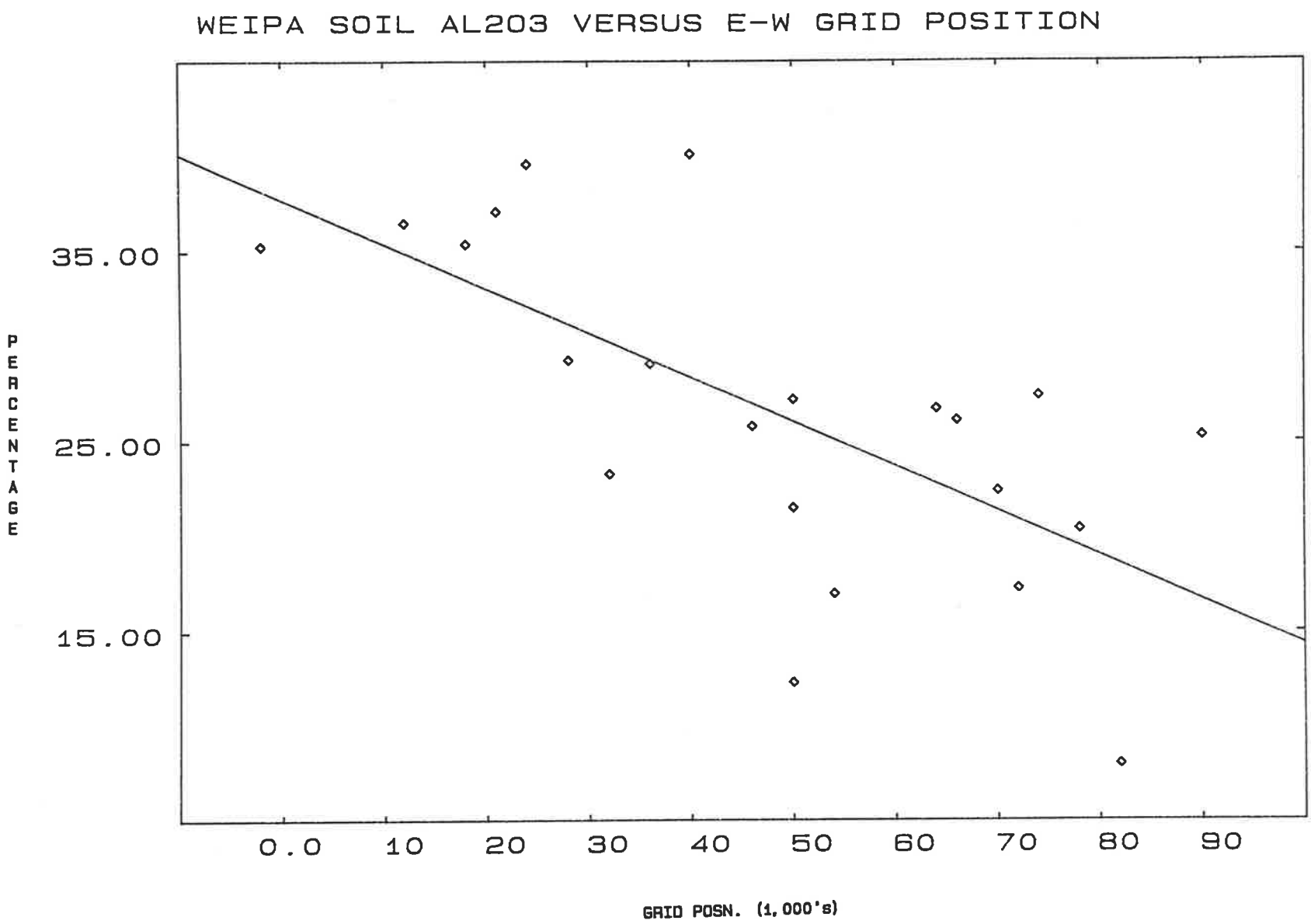
WEIPA SOIL AL203 VERSUS E-W GRID POSITION
PERCENTAGE
35.00
25.00
15.00
0.0
10
20
30
40
50
60
70
80
90
GRID POSN. (1,000's)

Figure 4.19 Variation of TiO_2 content of soil samples along Weipa Peninsula.

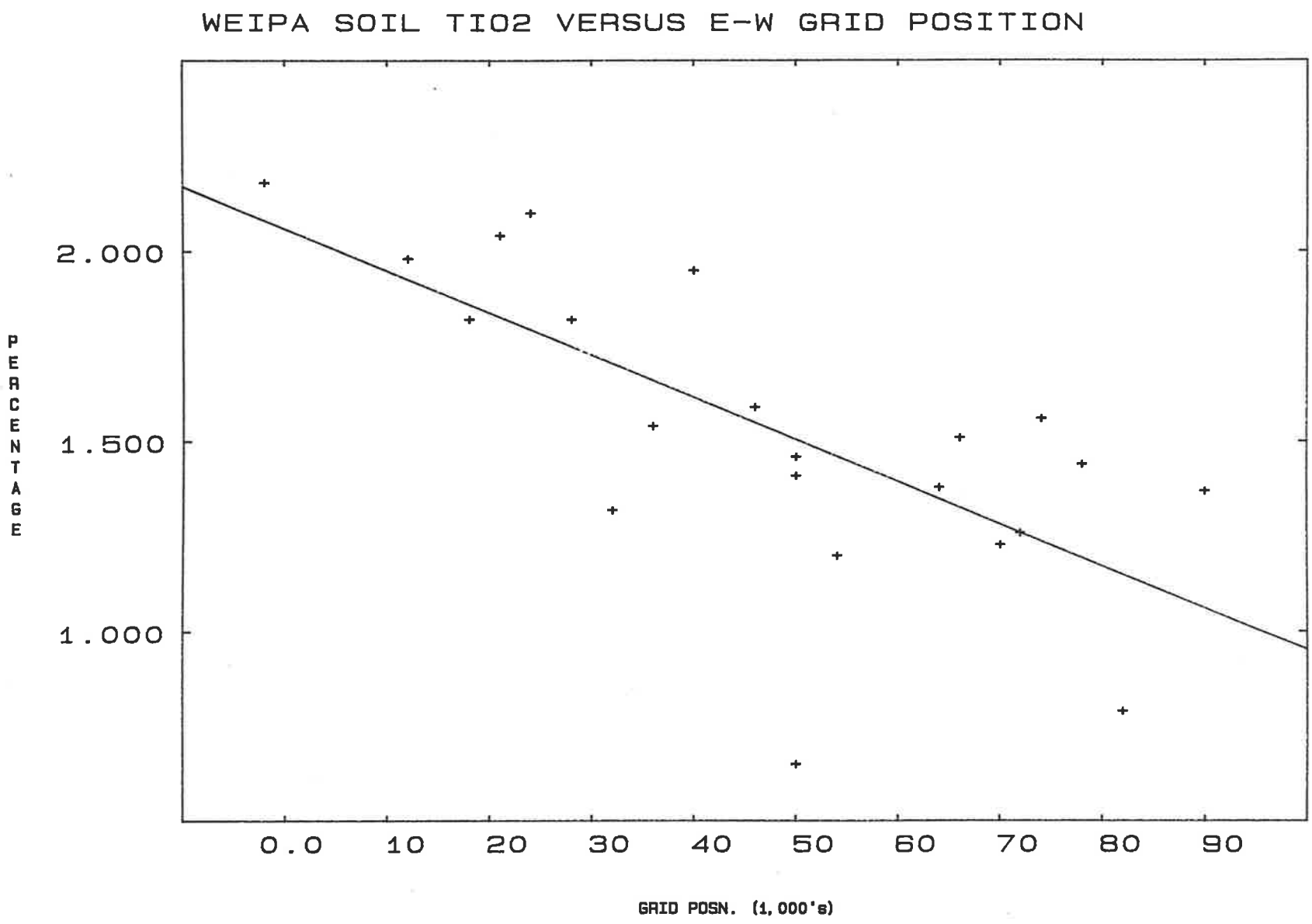
WEIPA SOIL TIO2 VERSUS E-W GRID POSITION
PERCENTAGE
2.000
1.500
1.000
0.0
10
20
30
40
50
60
70
80
90
GRID POSN. (1,000's)

Figure 4.20 Variation of Fe_2O_3 content of soil samples along Weipa Peninsula.

Note that the two outliers at 2,000W and 50,000E have been included in the regression calculation. Exclusion of these values will decrease the slope of the line, but still leave a weak trend in the same direction. All trends in Figs. 4.17 to 4.20 are compatible with decreased leaching of residual soil from west to east along the peninsula.

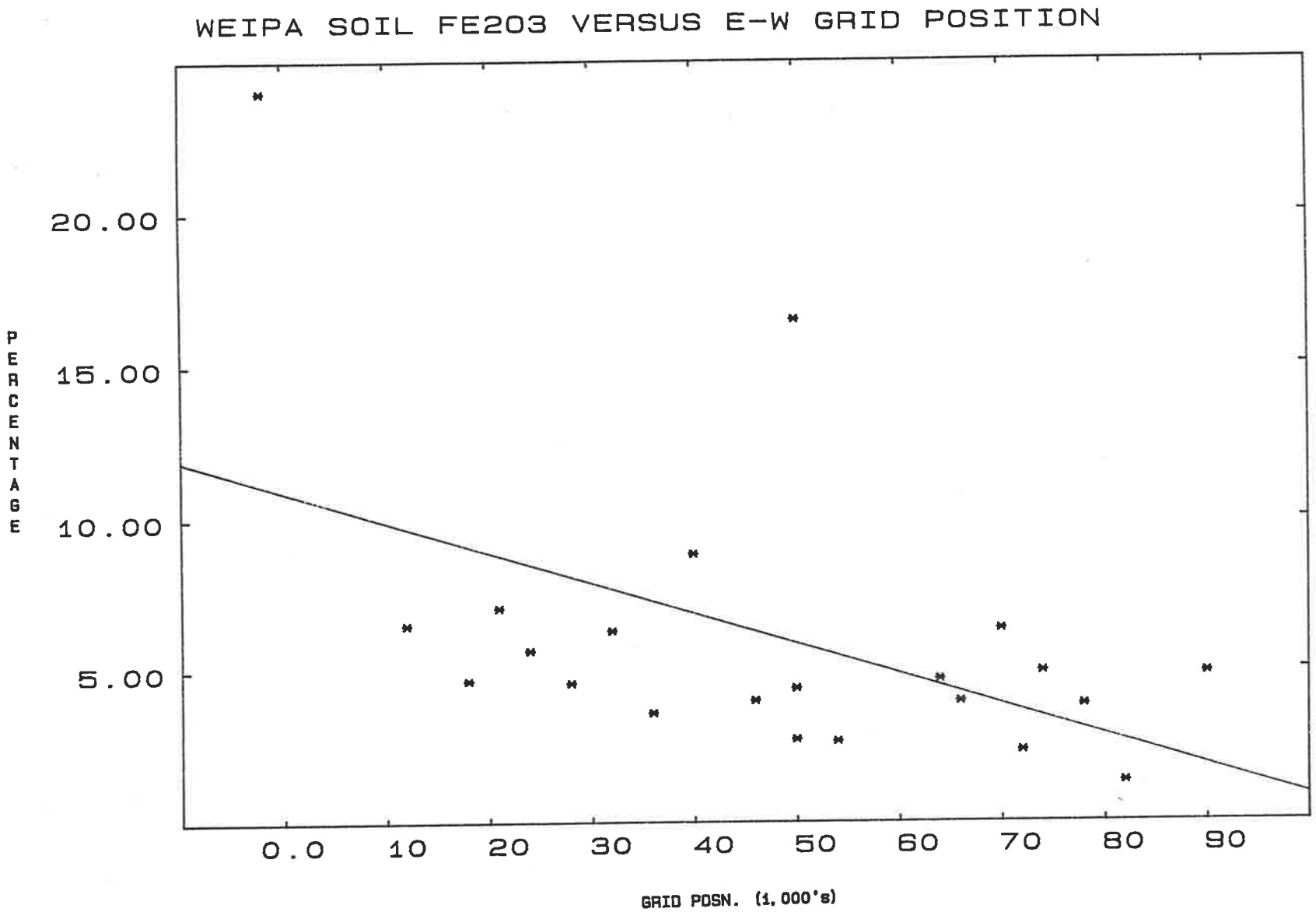
WEIPA SOIL FE203 VERSUS E-W GRID POSITION
PERCENTAGE
20.00
15.00
10.00
5.00
0.0
10
20
30
40
50
60
70
80
90
GRID POSN. (1,000's)

Figure 4.21 SWIR spectrum of synthetic gibbsite powder.

The spectrum shown was measured from a synthetic sample of gibbsite (aluminium trihydrate ($Al(OH)_3$)). The spectral shape is almost identical to that of the gibbsite sample measured by Hunt et al., 1971. Note the unusual wavelength of the major absorption feature (2.27μm).

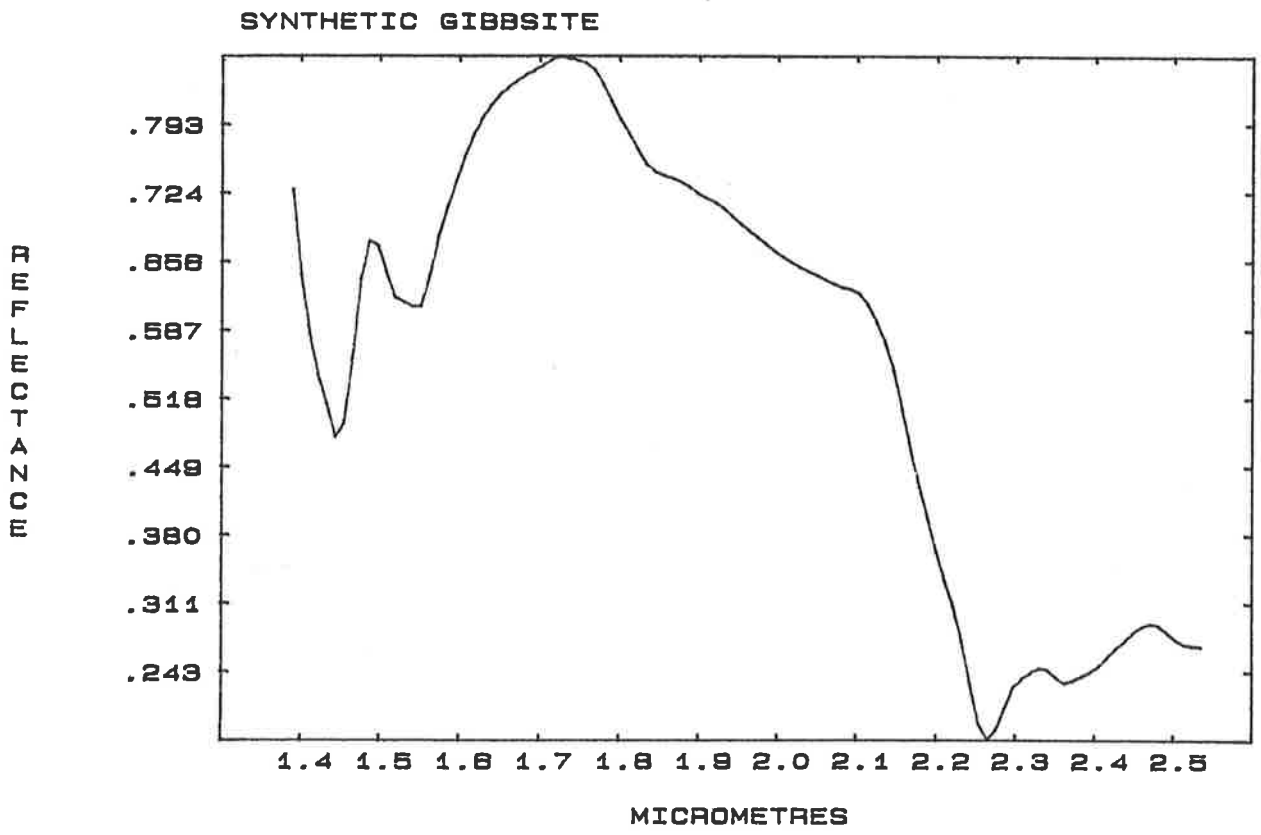
SYNTHETIC GIBBSITE
REFLECTANCE
.793
.724
.656
.587
.518
.449
.380
.311
.243
1.4 1.5 1.6 1.7 1.8 1.9 2.0 2.1 2.2 2.3 2.4 2.5
MICROMETRES

Figures 4.22a-c Representative VNIR laboratory spectra of Weipa soils.

All spectra have been smoothed by reconstruction using Tchebychev polynomials.

Figure 4.21a is representative of the majority of VNIR soil sample spectra, with increasing reflectance from .5 to 1.0μm, and no iron absorption features. All samples containing less than about 6% Fe_2O_3 fall into this category.

Figure 4.21b is an example of one of the few spectra which exhibit any iron oxide spectral features. Even so, the absorption is is very subtle, and takes the form of a minor dip centred near .85μm.

Figure 4.21c is the spectrum of a haematite-rich sample of cemented pisolite ore. This sample contains 24% Fe_2O_3.

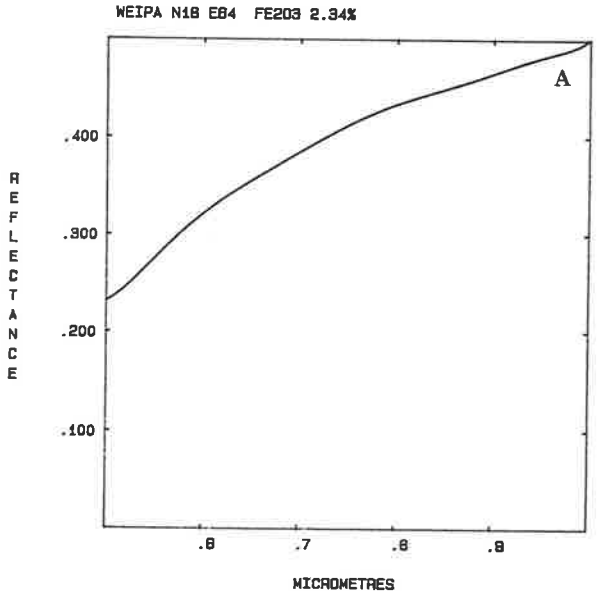
WEIPA N18 E84 FE203 2.34%
A
REFLECTANCE
.400
.300
.200
.100
.6
.7
.8
.9
MICROMETRES

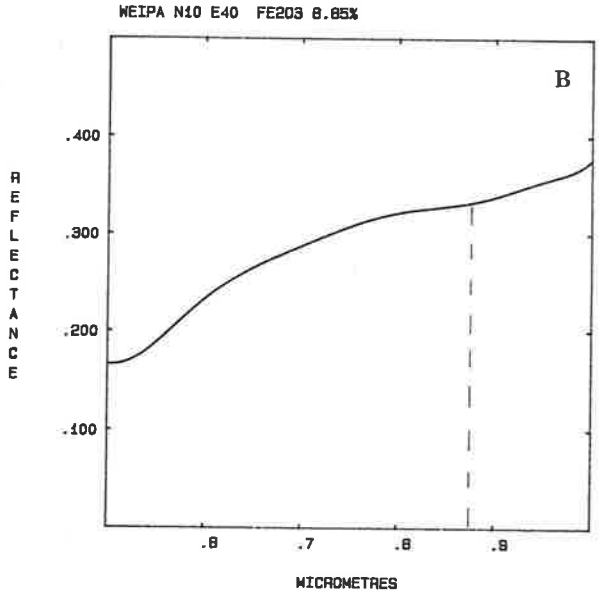
WEIPA N10 E40 FE203 8.85%
B
REFLECTANCE
.400
.300
.200
.100
.6
.7
.8
.9
MICROMETRES

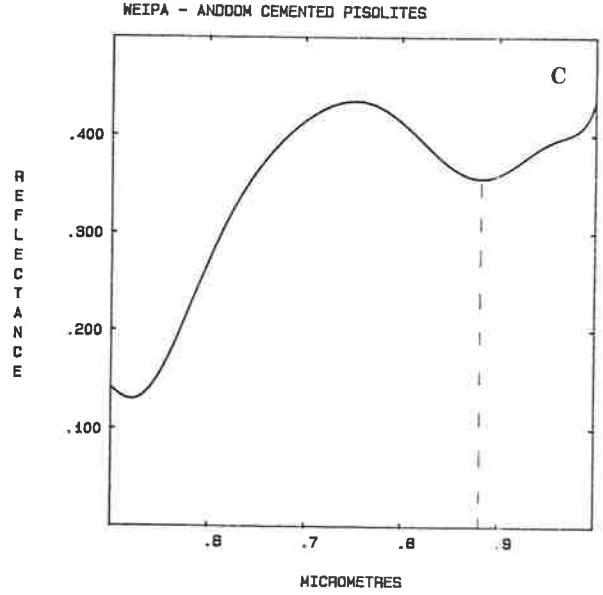
WEIPA - ANDOOM CEMENTED PISOLITES
C
REFLECTANCE
.400
.300
.200
.100
.6
.7
.8
.9
MICROMETRES

Figures 4.23a-d Representative SWIR laboratory spectra of Weipa soils.

Figure 4.23a depicts a spectrum which has a particularly strong (for the Weipa samples) absorption feature in the 2.27μm region, indicative of the presence of bauxite minerals.

Figure 4.23b shows an unusually strong 2.2μm absorption feature, with a weak shoulder developed at 2.17μm. These features are attributed to kaolin.

Figure 4.23c is representative of the majority of the Weipa soil samples. It falls between the extremes depicted in Figs. 4.23a&b, and has only weak to moderate absorption in both the 2.2 and 2.27μm regions.

Figure 4.23d is the spectrum of a pisolitic ore sample from Andoom, which is composed largely of gibbsite, boehmite and iron oxides.

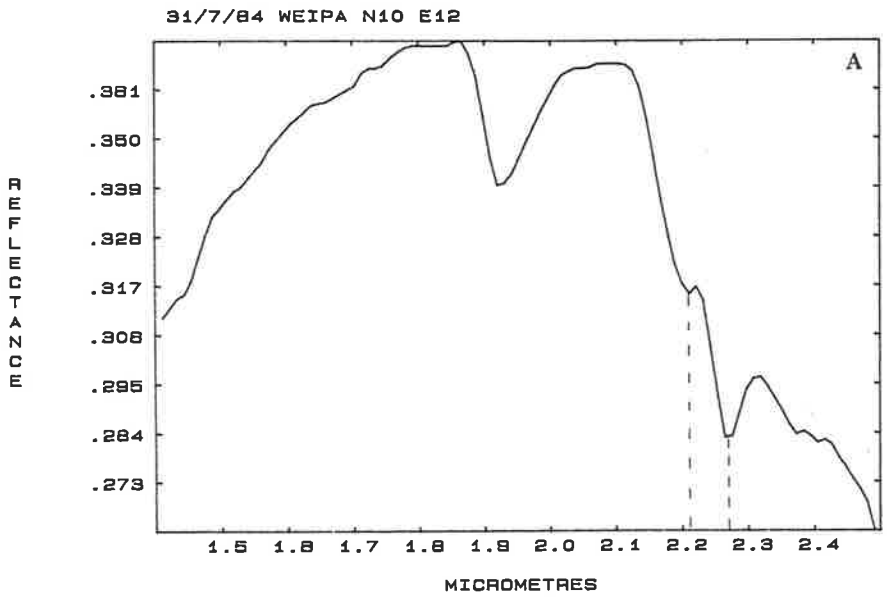
31/7/84 WEIPA N10 E12
A
REFLECTANCE
.381
.350
.339
.328
.317
.308
.295
.284
.273
1.5 1.6 1.7 1.8 1.9 2.0 2.1 2.2 2.3 2.4
MICROMETRES

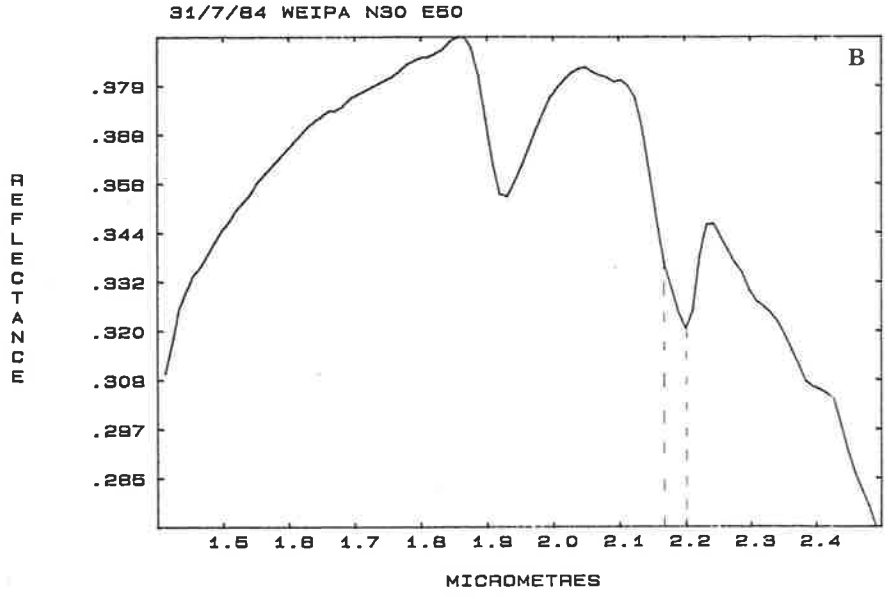
31/7/84 WEIPA N30 E50
B
REFLECTANCE
.378
.368
.358
.344
.332
.320
.308
.297
.285
1.5 1.6 1.7 1.8 1.9 2.0 2.1 2.2 2.3 2.4
MICROMETRES

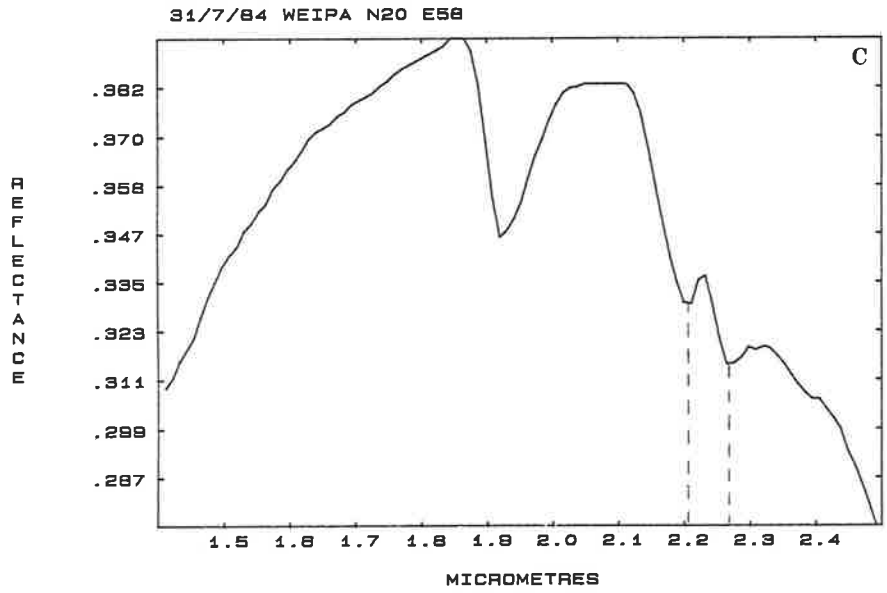
31/7/84 WEIPA N20 E58
C
REFLECTANCE
.382
.370
.358
.347
.335
.323
.311
.299
.287
1.5 1.6 1.7 1.8 1.9 2.0 2.1 2.2 2.3 2.4
MICROMETRES

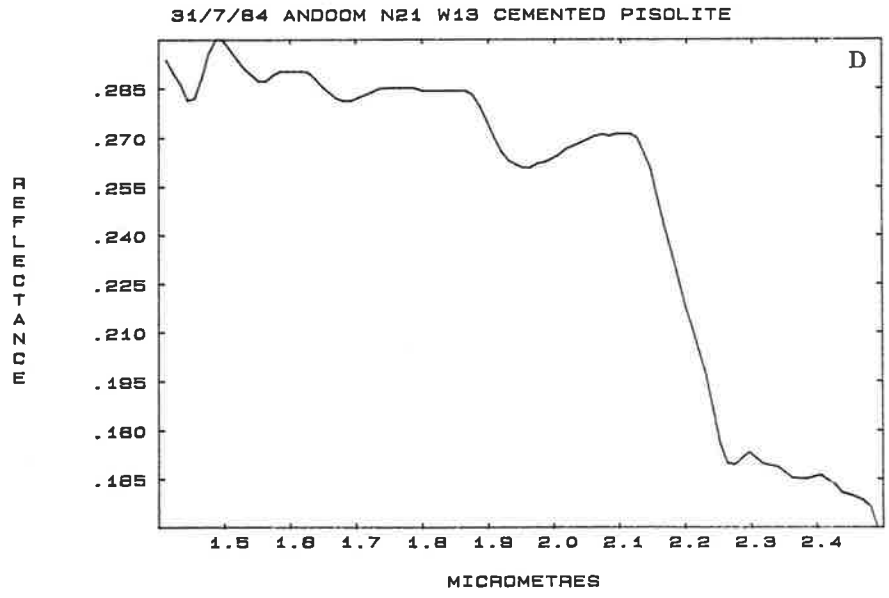
31/7/84 ANDOOM N21 W13 CEMENTED PISOLITE
D
REFLECTANCE
.285
.270
.255
.240
.225
.210
.195
.180
.165
1.5 1.6 1.7 1.8 1.9 2.0 2.1 2.2 2.3 2.4
MICROMETRES

Figure 4.24 Variation of SiO_2 content of ore on the 2000N line along Weipa Peninsula (Comalco drilling data).

Data points plotted in Figs. 4.24 and 4.25 are averages of multiple analyses of samples taken from each drill hole. Each point should therefore be representative of the entire ore zone at that location. In both plots the thick line represents a line of best fit.

Although there is considerable scatter in the SiO_2 data, a trend of increasing silica content from west to east is evident.

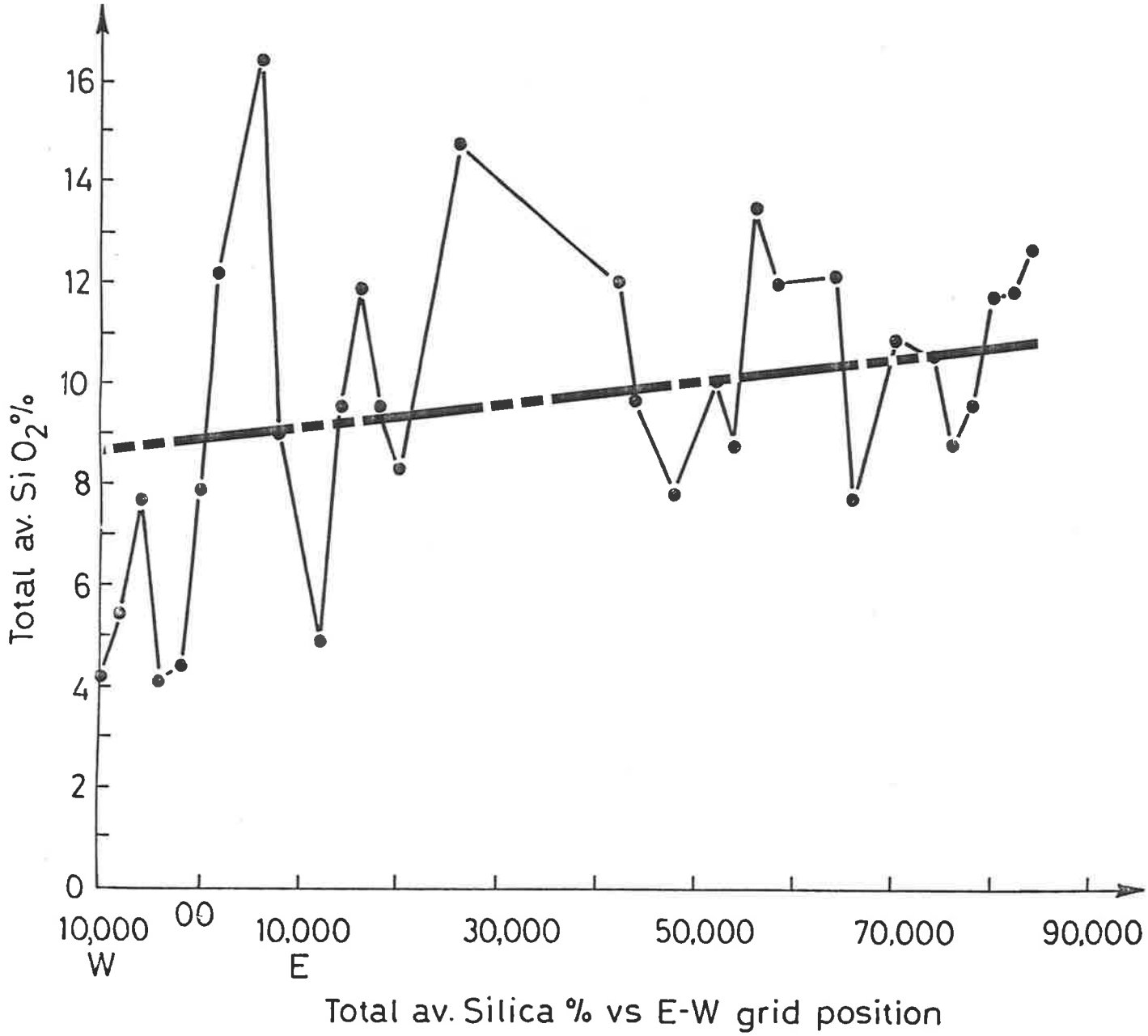

Total av. Silica % vs E-W grid position

Figure 4.25 Variation of Al_2O_3 content of ore on the 2000N line along Weipa Peninsula (Comalco drilling data).

Like Fig. 4.24 there is considerable scatter in the data, but an inverse trend is apparent, with decreasing alumina content from west to east.

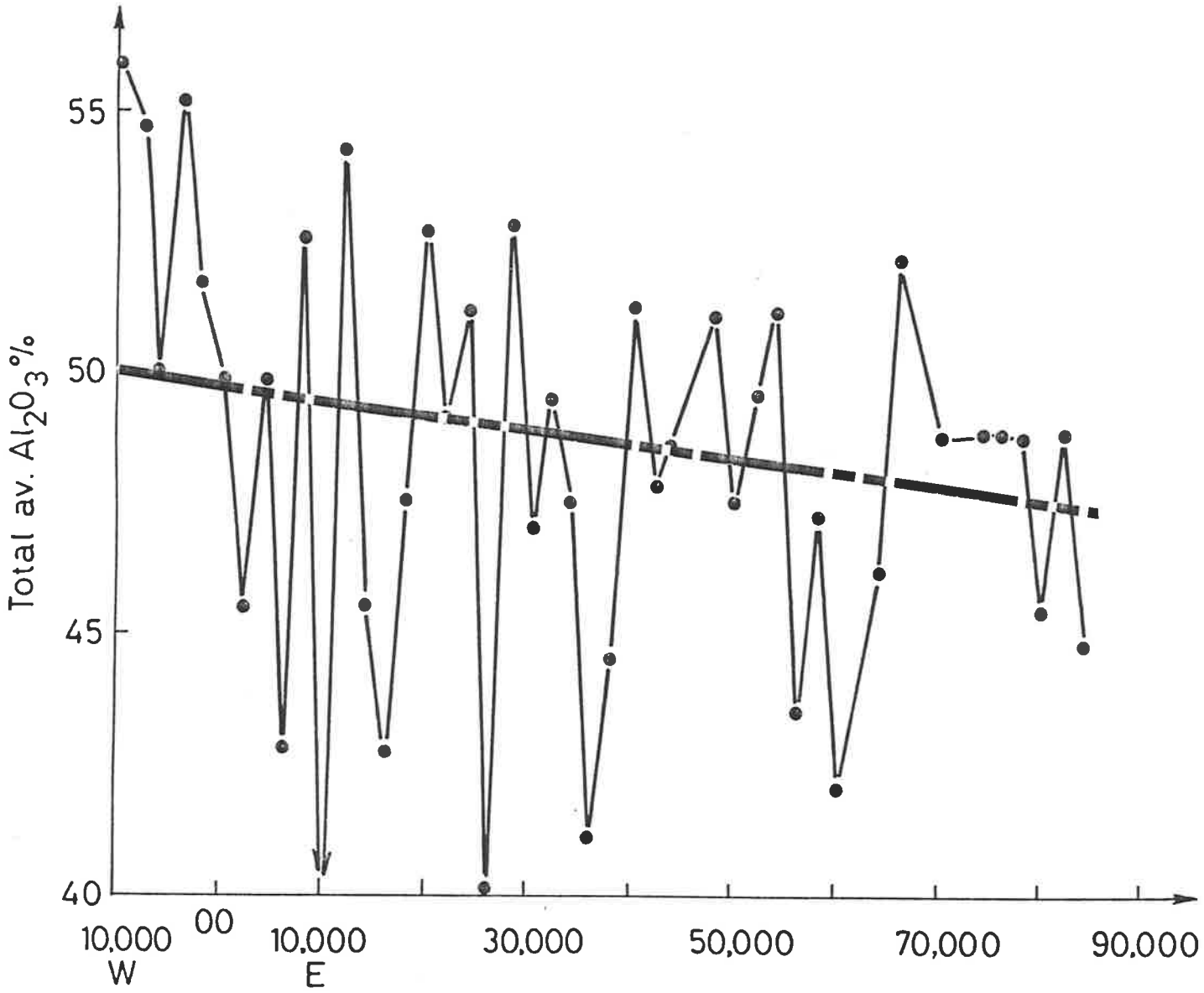

Total av. Al_2O_3% at 180°C (nearest avail. data) vs E-W grid positn.

Figure 4.26 Variation of SiO_2 content of ore (N-S lines averaged) along Weipa Peninsula (Comalco drilling data).

Figures 4.26 and 4.27 are plots of ore geochemistry, but all data for each north-south grid line has been averaged to a single value. In both plots the thick line is a line of best fit.

For SiO_2 the trend of increasing values to the east is stronger, and there is less scatter in the data.

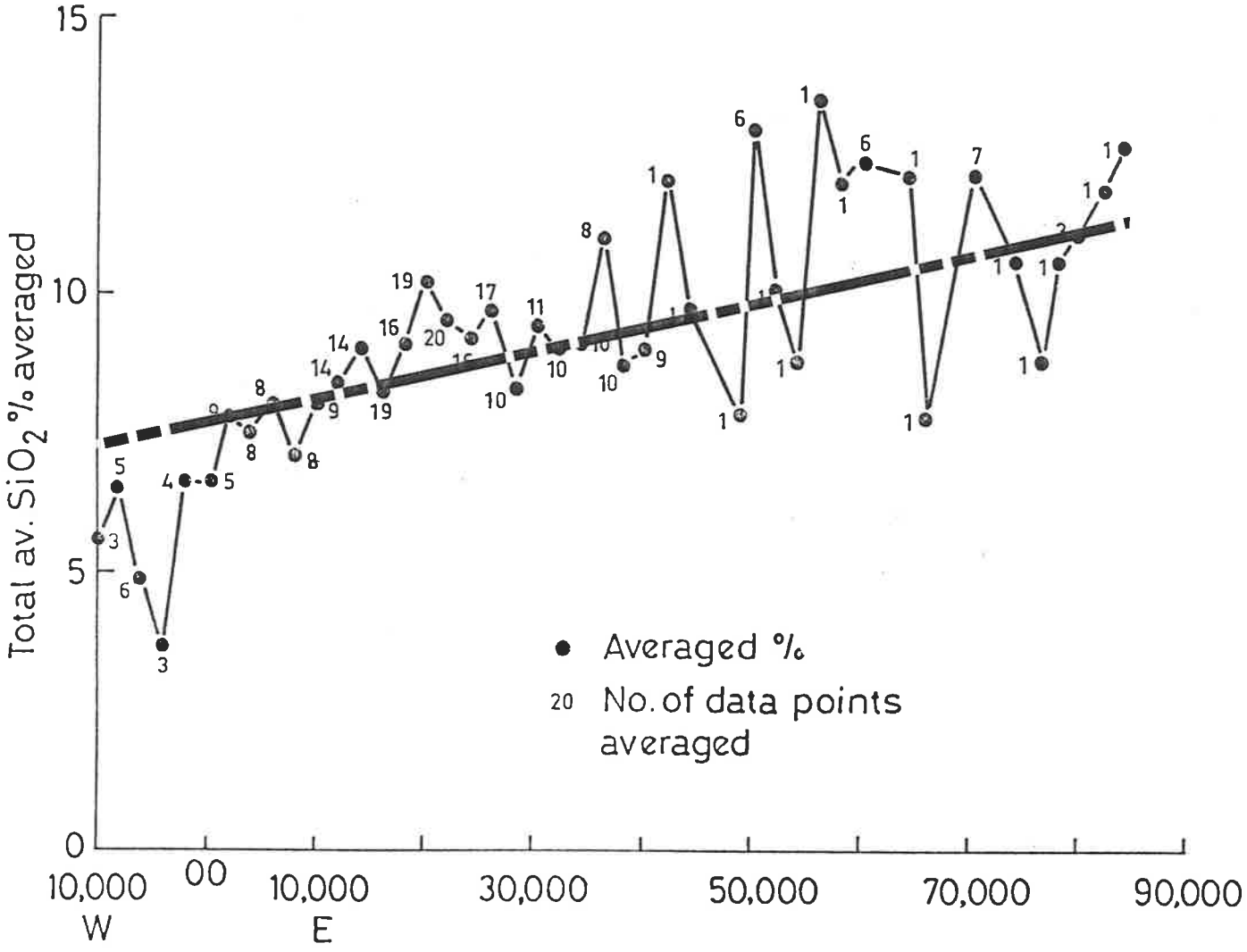
15
10
5
0
Total av. SiO_2 % averaged
10,000 W
00
10,000 E
30,000
50,000
70,000
90,000
Averaged %
20 No. of data points averaged

Figure 4.27 Variation of Al_2O_3 content of ore (N-S lines averaged) along Weipa Peninsula (Comalco drilling data).

Like SiO_2 the Al_2O_3 values show a stronger trend, with less scatter in the data, once th north-south lines have been averaged.

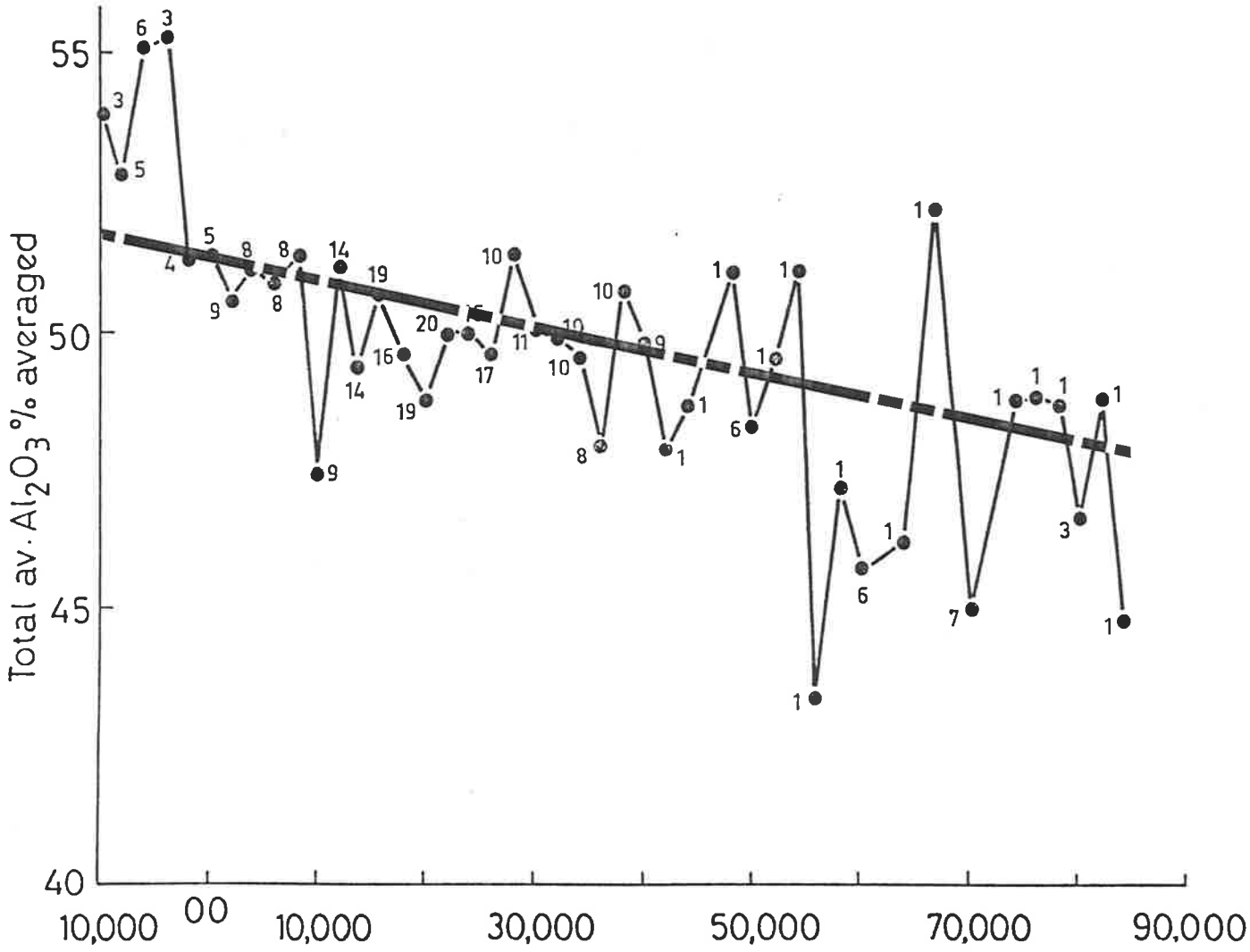
Total av. Al_2O_3 % averaged
55
50
45
40
10,000
00
10,000
30,000
50,000
70,000
90,000

Figure 4.28 Image representation of Al_2O_3 content of ore over Weipa Peninsula (Comalco drilling data).

The image has been contrast stretched and density sliced. Each coloured pixel represents one 2,000 foot drilling block. Al_2O_3 values range from 36 to 55%. Red equals high values, yellow medium values and green and blue low values. Note the gradient from high to low values from west to east. The longest east-west data line is located on the 20,000N grid line. North is vertical.

Figure 4.29 Geometrically resampled image of Al_2O_3 content of ore over Weipa Peninsula (Comalco drilling data).

Same as Fig. 4.29, but the data has been geometrically resampled and registered to fit Landsat scene 1036-00004. North is now roughly 10° west of the vertical.

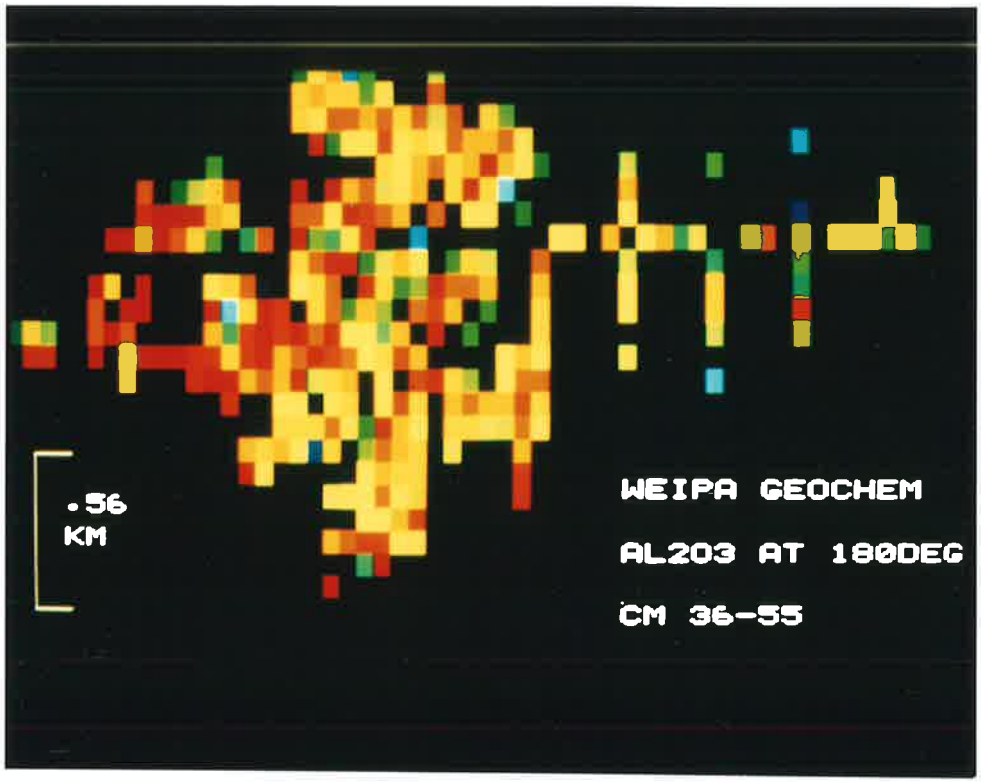
.56
KM
WEIPA GEOCHEM
AL203 AT 180DEG
CM 36-55

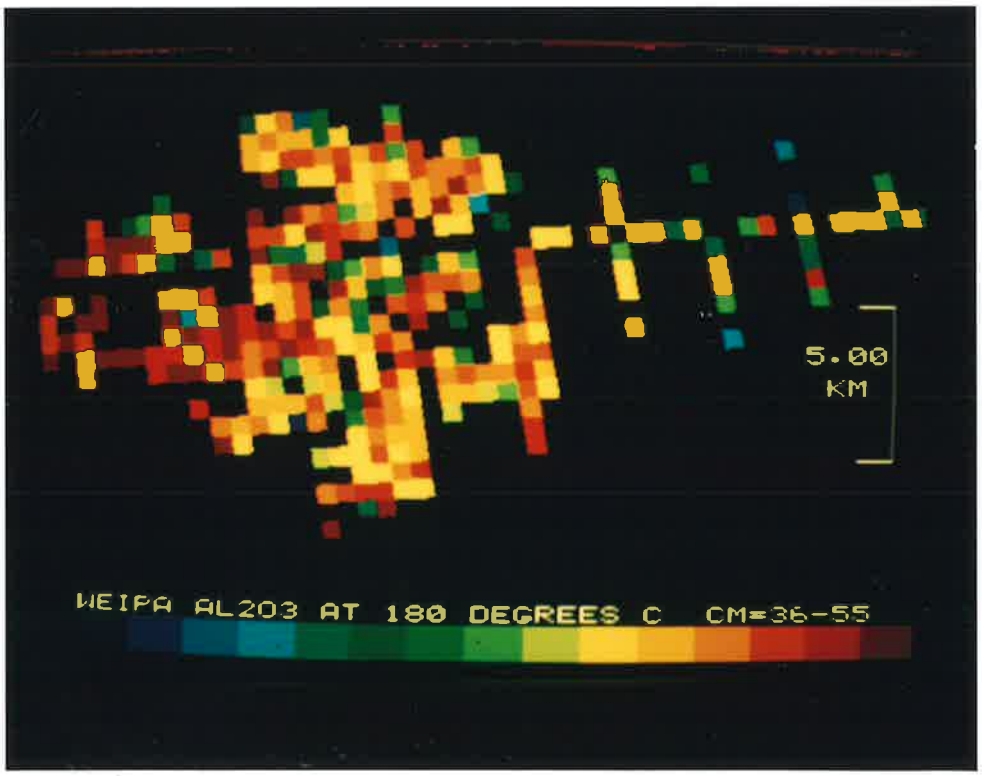
5.00
KM
WEIPA AL203 AT 180 DEGREES C CM=36-55

Figure 4.30 Geometrically resampled image of SiO_2 content of ore over Weipa Peninsula (Comalco drilling data).

The image has been density sliced, and values range from 15% (red) to 3% (blue). Note the inverse trend to Fig. 4.29.

Figure 4.31 Geometrically resampled image of ore thickness over Weipa Peninsula (Comalco drilling data).

The image has been density sliced, with values ranging from 14 feet (red) to 1 foot (blue). Where local variations in ore thickness are likely to be related to palaeotopography (see Fig. 4.12b), the regional trend depicted here could either be due to regional palaeotopographic variation or to a weak structural deformation post-dating ore formation. The author favours the latter alternative.

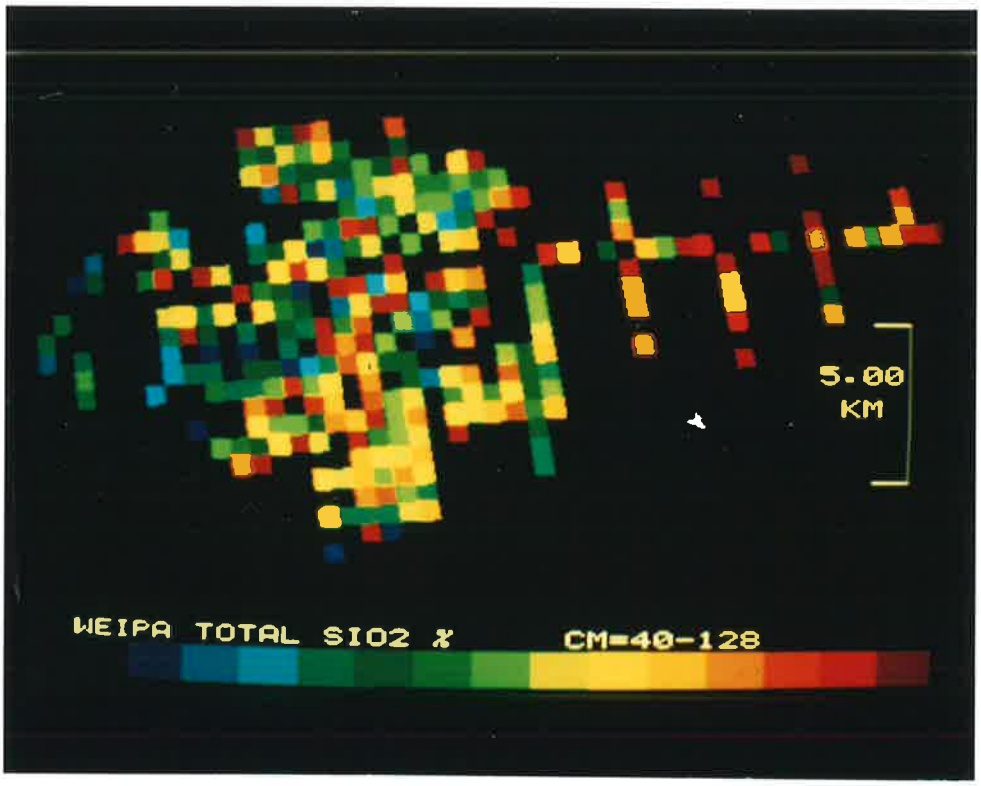
5.00
KM
WEIPA TOTAL SIO2 %
CM=40-128

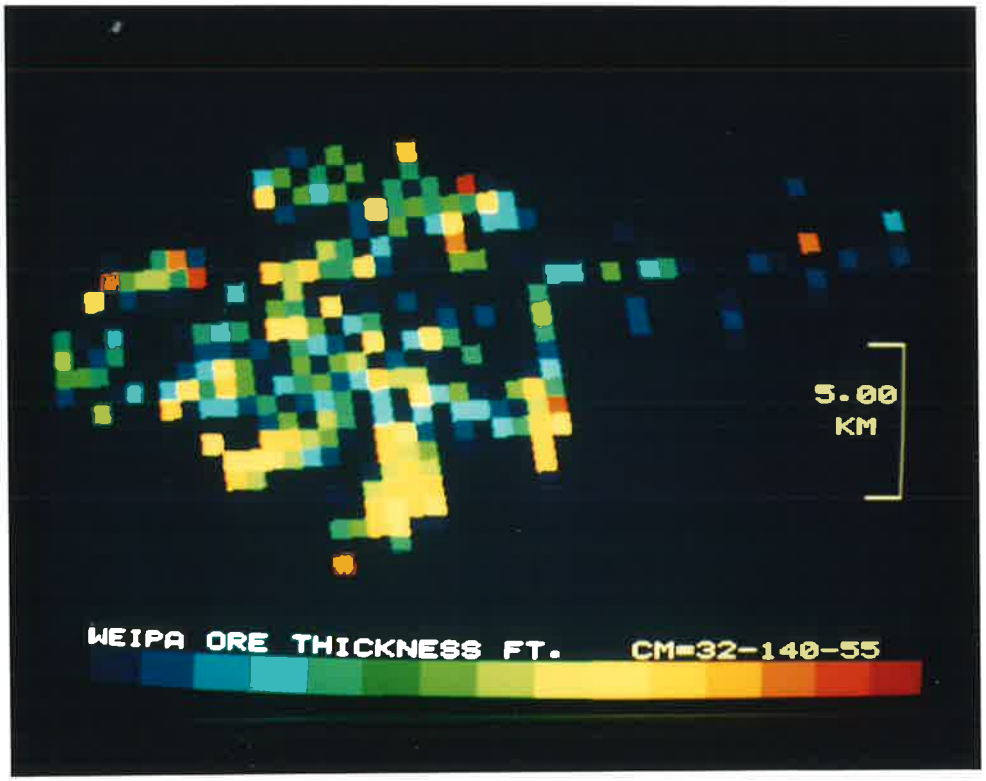
5.00
KM
WEIPA ORE THICKNESS FT.
CM=32-140-55

Figure 4.32 Landsat and geochemistry training areas and geochemical grid over Weipa Peninsula.

Training areas are shown as numbered, white boxes, while geochemistry grid is shown in blue. Landsat MSS bands 5 and 7 are displayed as green and red, respectively.

Figure 4.33 Landsat false colour composite - Weipa and Andoom mine sites - highlighting vegetation regeneration - linear stretch, bands 4, 5 and 7, wet season image.

The image ID No. is 22289-23511 (29th April,1981). The different stages of regeneration are evident as areas of varying shades of red on the white background of the mines. Grey-blue areas have recently had their tree cover felled, but not removed.

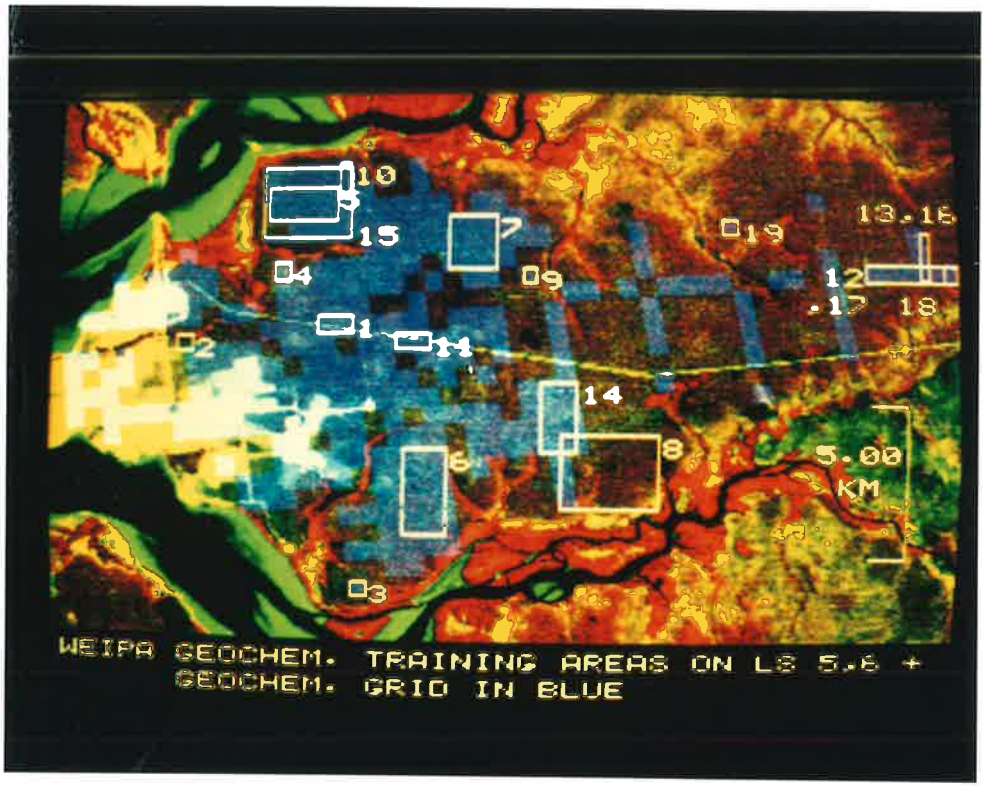
10
15
4
9
19
13.18
12
18
2
1
11
14
8
6
3
5.00
KM
WEIPA GEOCHEM. TRAINING AREAS ON LS 5.6 +
GEOCHEM. GRID IN BLUE


WEIPA 29/4/81
22289-23511
5.00
KM

Figure 5.1 Geology map of Mt Turner.

The map has been compiled and simplified from BMR 1:25,000 compilation sheets. White mica (muscovite from the weathering of Proterozoic granites and Robertson River Formation metasediments) and sericite (from altered felsic intrusives) are widespread throughout the map area.

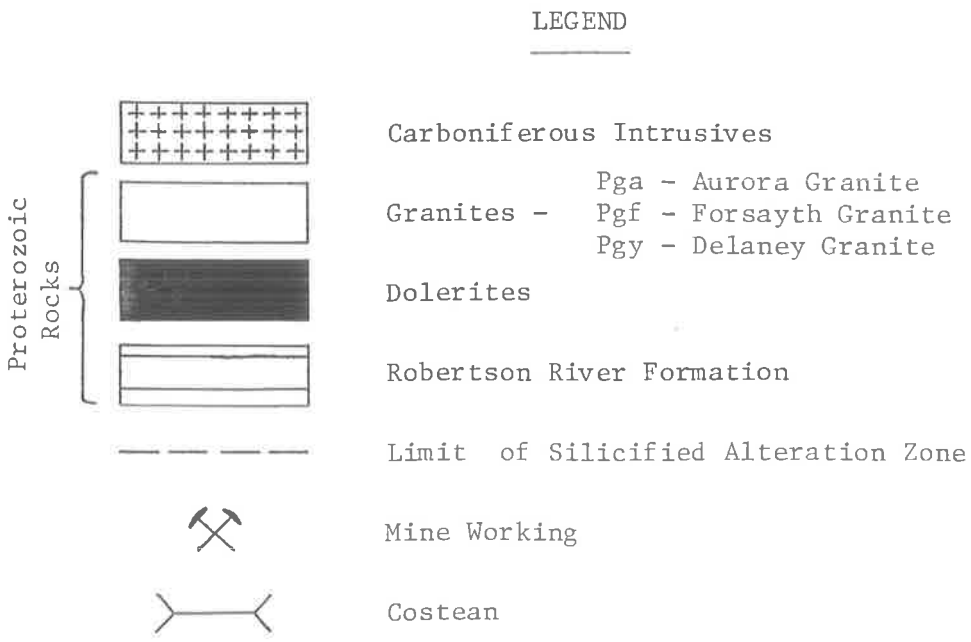

MOUNT TURNER GEOLOGY

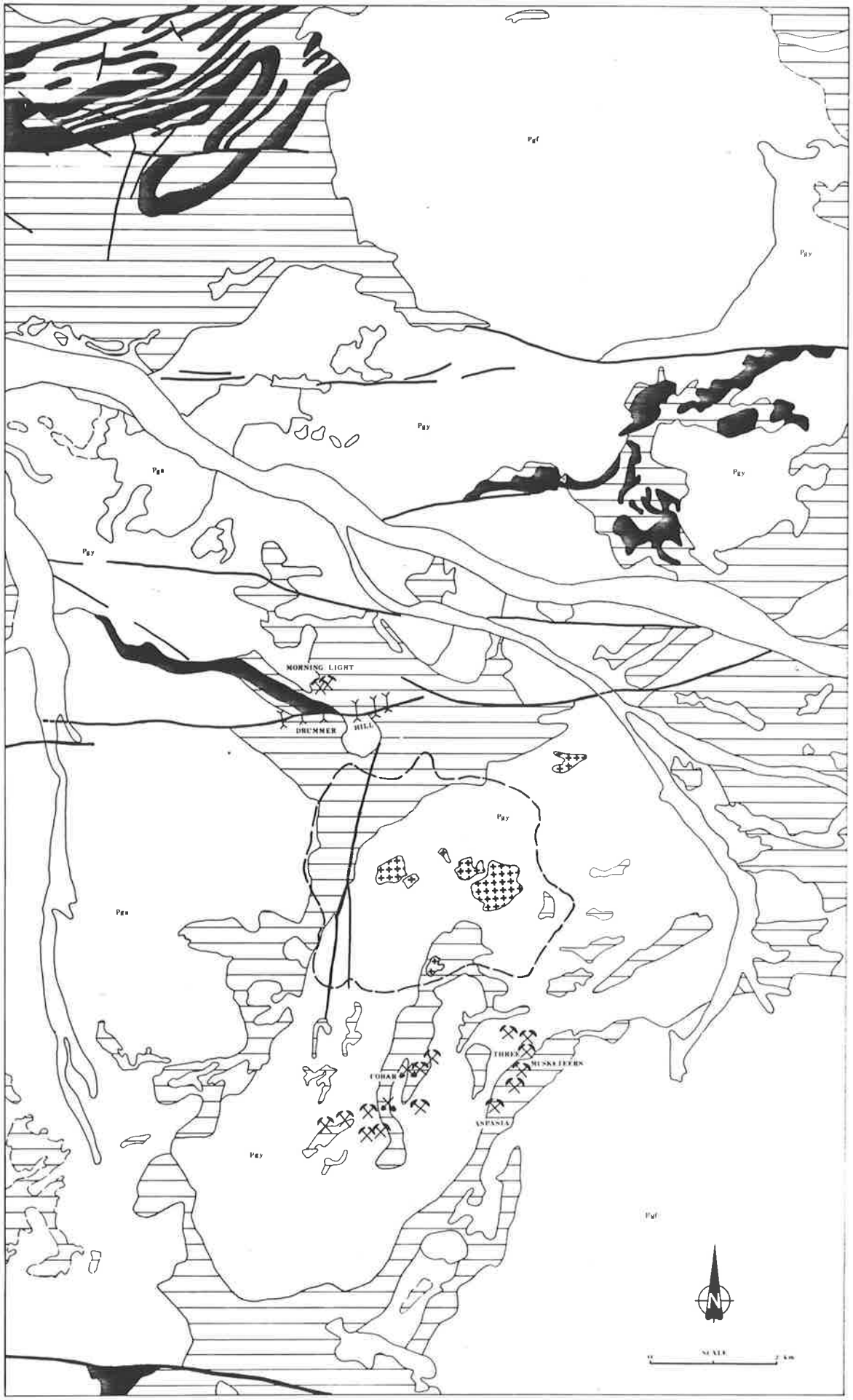

Figure 5.2 Photocopy of RC9 1:80,000 black and white aerial photograph of Mt Turner, with alteration (A) and flight line location (B) overlays.

Note that fissure veins and rhyolite dykes are best developed within the silicified zone, but have been omitted from the overlay for clarity.

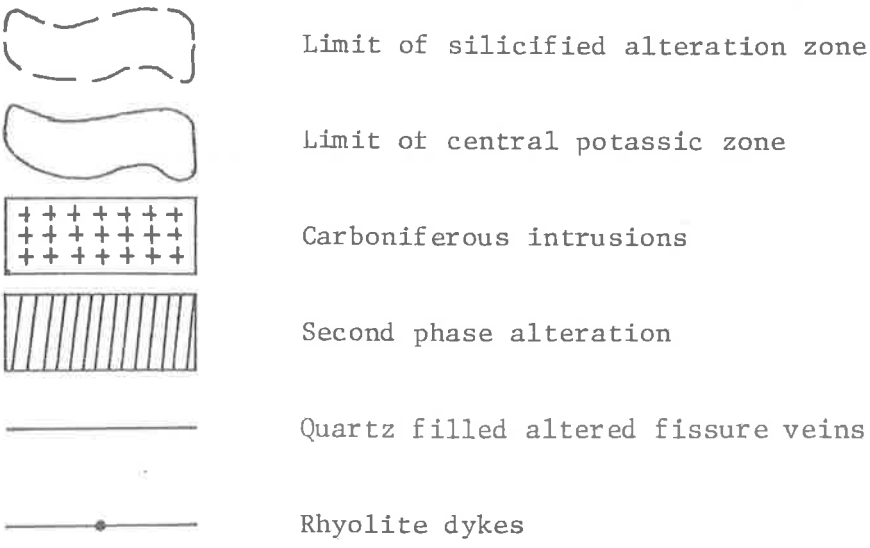


2
RGETOWN
49-99
RUN 3
27-8-1,67
CAB
330
25,000
Ca 612
SAg 65
f-68.41
MT
MT 1
MT 2
MT 3

Figure 5.3 Landsat false colour composite - Mt Turner area - linear stretch, bands 4, 5 and 7 (after Huntington, pers. comm. 1983).

The vegetation anomaly over Mt Turner results in the high band 7 (red) response. The dark green areas are bushfire scars.

Figure 5.4 Landsat band ratio image - Mt Turner area - density slice, ratio bands 5/6 (after Huntington, pers. comm., 1983).

The vegetation anomaly over Mt Turner stands out as blue colours. Also shown is the boundary of most intense "limonite" (derived from a Landsat MSS 4/5, 4/6, 6/7 ratio image) resulting from alteration, mafic intrusives and Robertson River Formation metasediments.


MT TURNER 1005-23544 4,5,7 LIN
2.50
KM

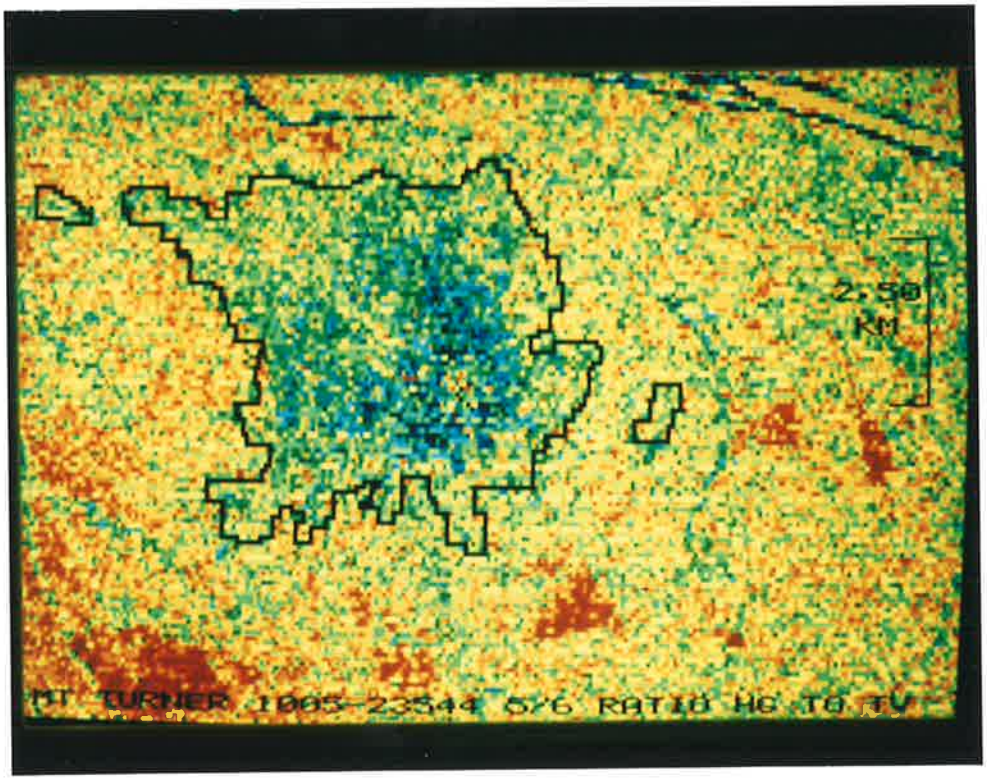
2.50
KM
MT TURNER 1005-23544 5/6 RATIO HG TO TV

Figure 5.5 Landsat colour ratio composite - Mt Turner area - histogram normalisation of bands 4/6 (blue), 6/7 (green) and 4/5 (red), (after Huntington, pers. comm., 1983).

The image depicts limonite in shades of green, and vegetation in shades of red. Mt Turner (arrowed to the east), is differentiated from its immediate surrounds, but not from other iron-rich rocks (for instance dolerites in the Robertson River Formation to the NW). The Phyllis Mae area (arrowed to the west) shows no anomalous features.


GEORGE -
TOWN QLD
4/5=R
4/6=B
6/7=G
1972
20.0
KM

Figures 5.6a&b SWIR laboratory reflectance spectra of weathered and fresh surfaces of the same altered sample.

Figure 5.6a is the spectrum of the weathered surface, while Fig. 5.6b is the fresh surface spectrum. The sample contains quartz, sericite and minor kaolin. Note the similarity of the spectral features in both plots.

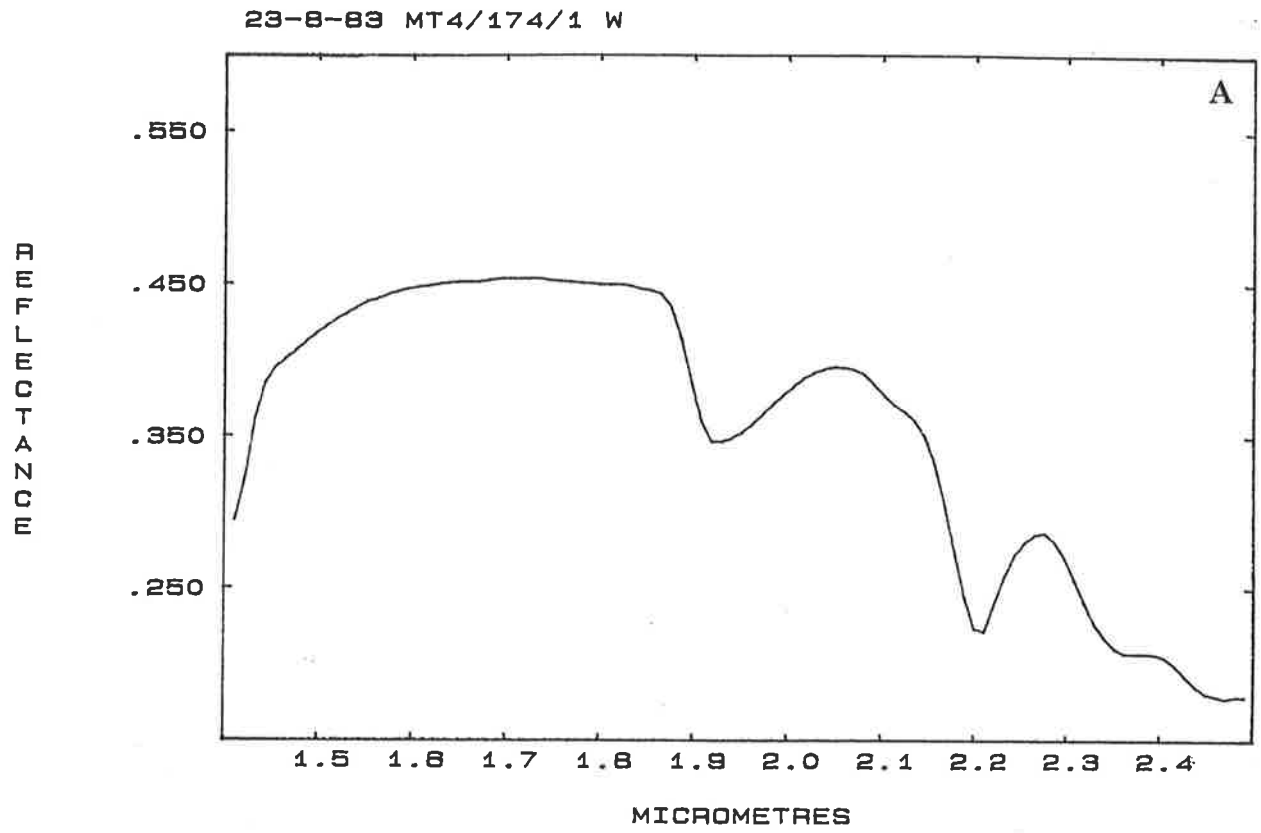
23-8-83 MT4/174/1 W
A
.550
.450
.350
.250
REFLECTANCE
1.5 1.6 1.7 1.8 1.9 2.0 2.1 2.2 2.3 2.4
MICROMETRES

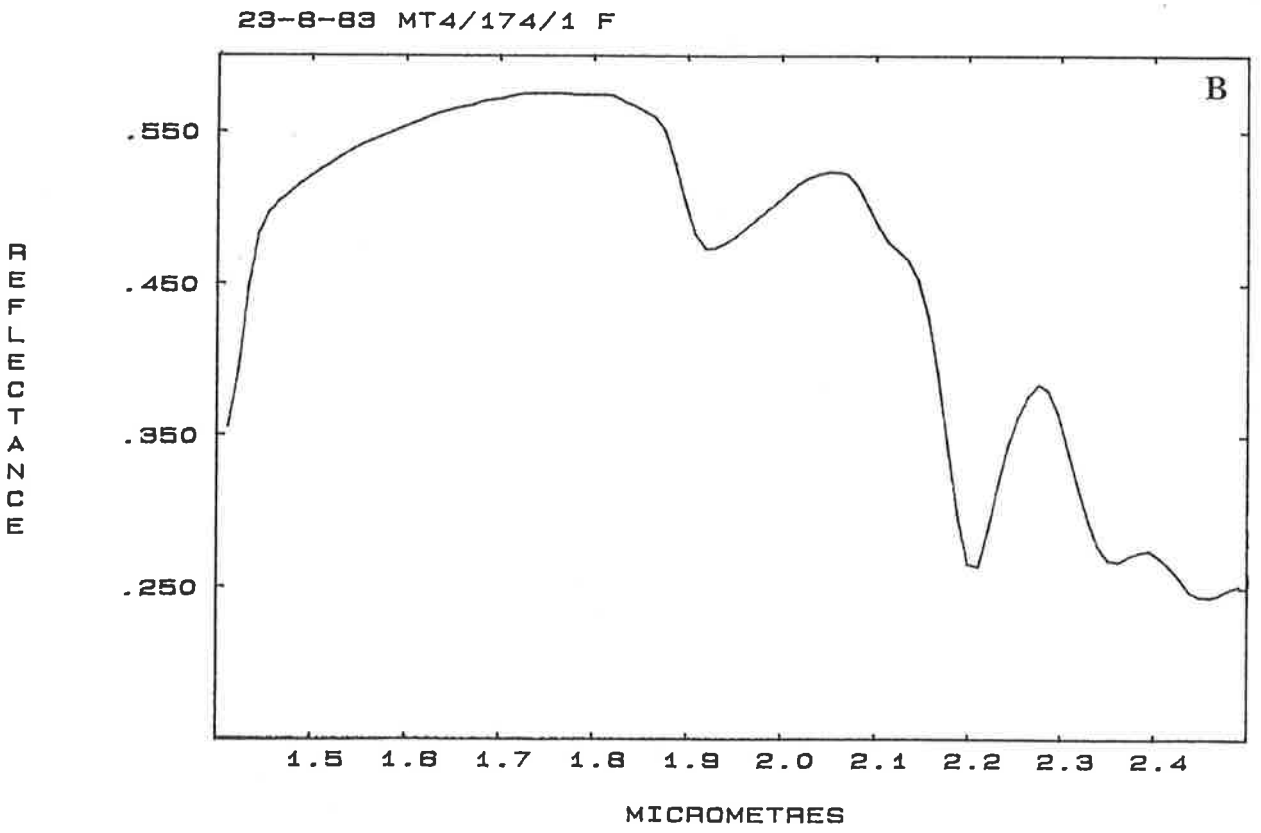
23-8-83 MT4/174/1 F
B
.550
.450
.350
.250
REFLECTANCE
1.5 1.6 1.7 1.8 1.9 2.0 2.1 2.2 2.3 2.4
MICROMETRES

Figures 5.7a&b SWIR laboratory reflectance spectra of a weathered, lichen-covered surface and a fresh surface of the same altered sample.

Figure 5.7a depicts the spectrum of the weathered surface and shows the effects of an even cover of black lichen.

Figure 5.7b depicts the fresh surface spectrum, with strong 2.2μm absorption. This sample is an altered rhyolite composed of quartz and sericite.

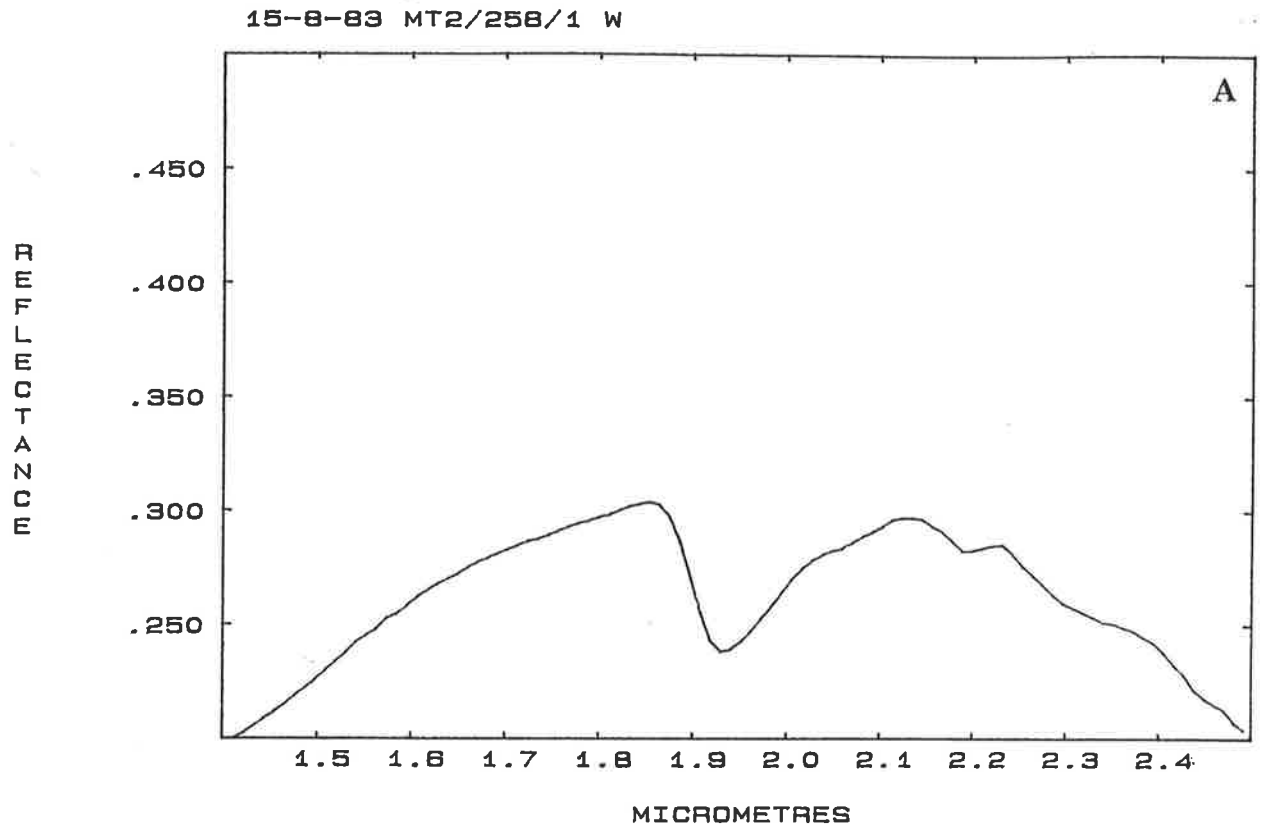
15-8-83 MT2/258/1 W
A
.450
.400
.350
.300
.250
REFLECTANCE
1.5 1.6 1.7 1.8 1.9 2.0 2.1 2.2 2.3 2.4
MICROMETRES

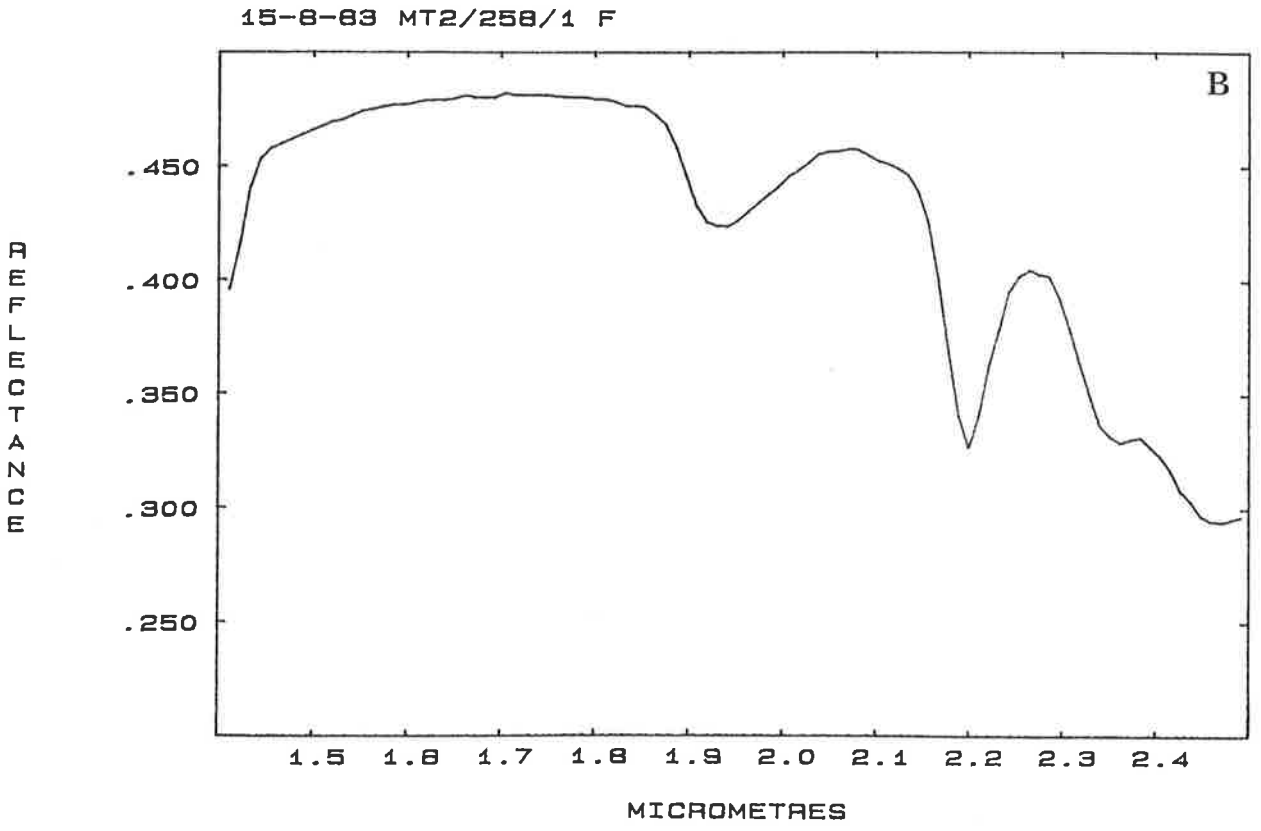
15-8-83 MT2/258/1 F
B
.450
.400
.350
.300
.250
REFLECTANCE
1.5 1.6 1.7 1.8 1.9 2.0 2.1 2.2 2.3 2.4
MICROMETRES

Figure 5.8 SWIR laboratory reflectance spectra of healthy and dry vegetation.

The spectrum of healthy vegetation is affected mainly by the moisture in the foliage. The absorption features at 2.1 and 2.3μm in the spectrum of dry vegetation are caused by the cellulose present in the plant. These features become apparent only when the water content is low.

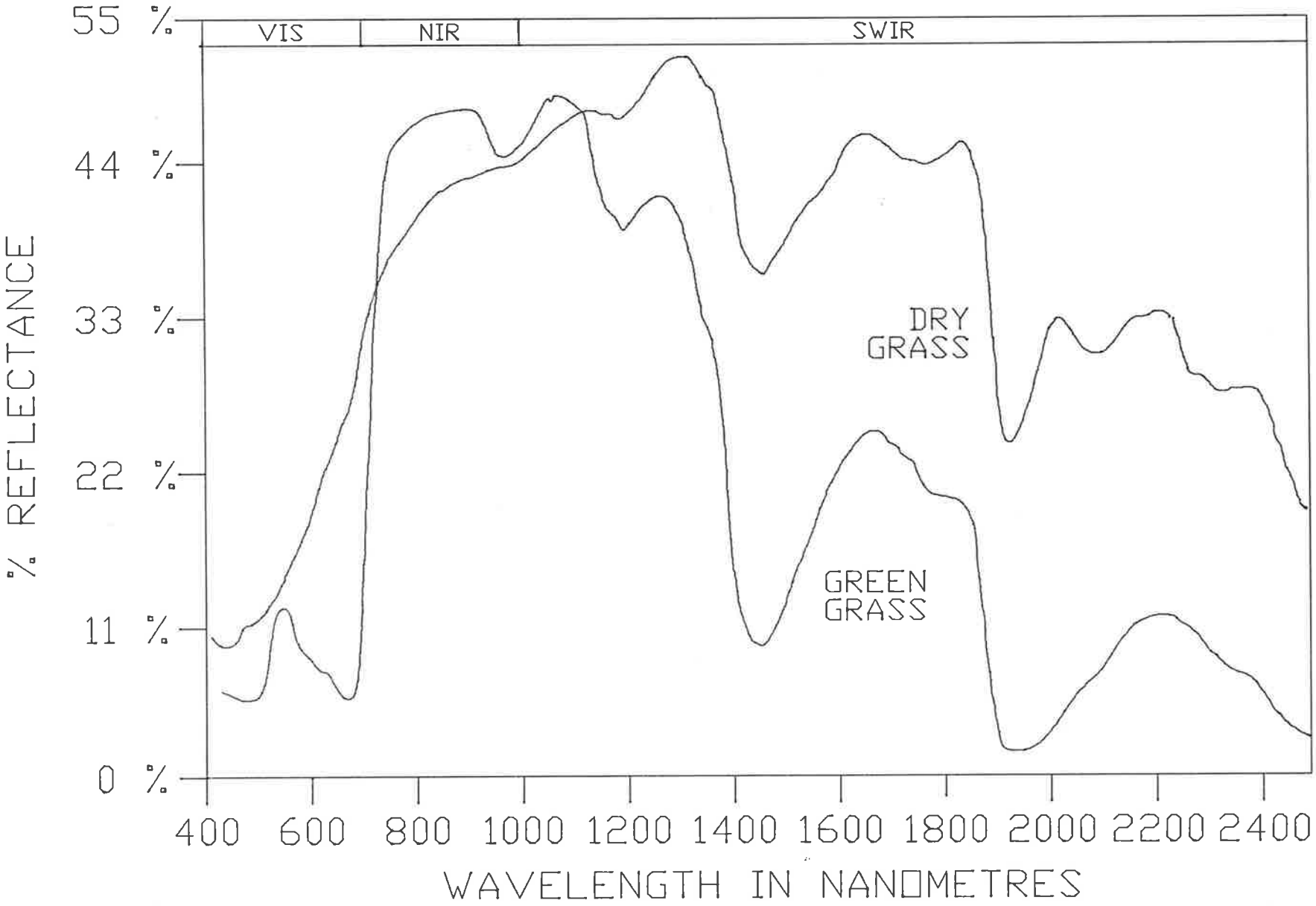
55 %
44 %
33 %
22 %
11 %
0 %
% REFLECTANCE
VIS
NIR
SWIR
DRY GRASS
GREEN GRASS
400 600 800 1000 1200 1400 1600 1800 2000 2200 2400
WAVELENGTH IN NANOMETRES

Figures 5.9a-d The four major spectral types from SWIR laboratory reflectance measurements of Mt Turner samples.

Kaolin-type (a) occurs only when there is significant kaolin in the sample. Sericite-type (b) is from altered rocks, and has secondary absorption features near 2.35 and 2.45μm. Muscovite-type (c) is similar to Sericite-type, but does not have strong secondary absorption features. Mafic-type spectra (d) have their major absorption features in the 2.3 μm region, and can result from a variety of primary mafic or propylitic alteration minerals.

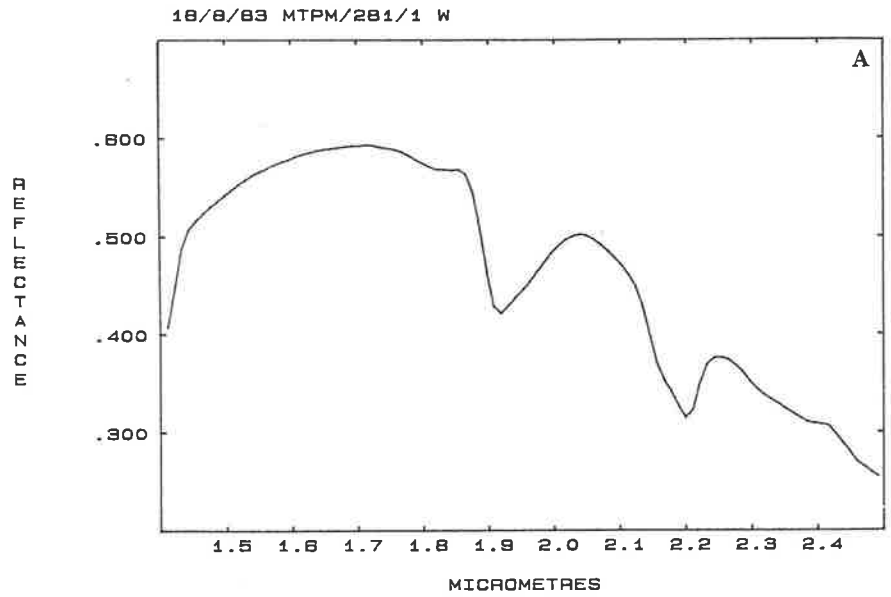
18/8/83 MTPM/281/1 W
A
.800
.500
.400
.300
REFLECTANCE
1.5 1.6 1.7 1.8 1.9 2.0 2.1 2.2 2.3 2.4
MICROMETRES

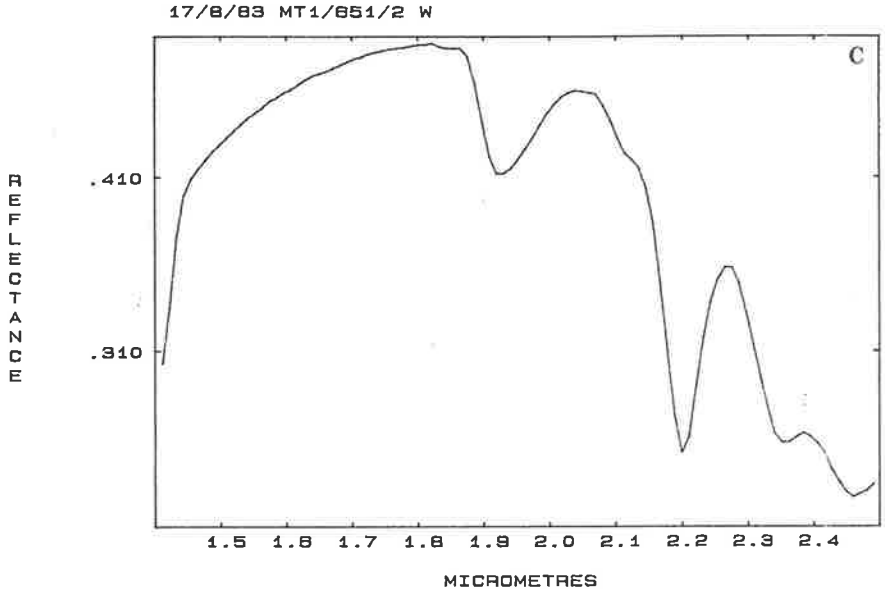
17/8/83 MT1/651/2 W
C
.410
.310
REFLECTANCE
1.5 1.6 1.7 1.8 1.9 2.0 2.1 2.2 2.3 2.4
MICROMETRES

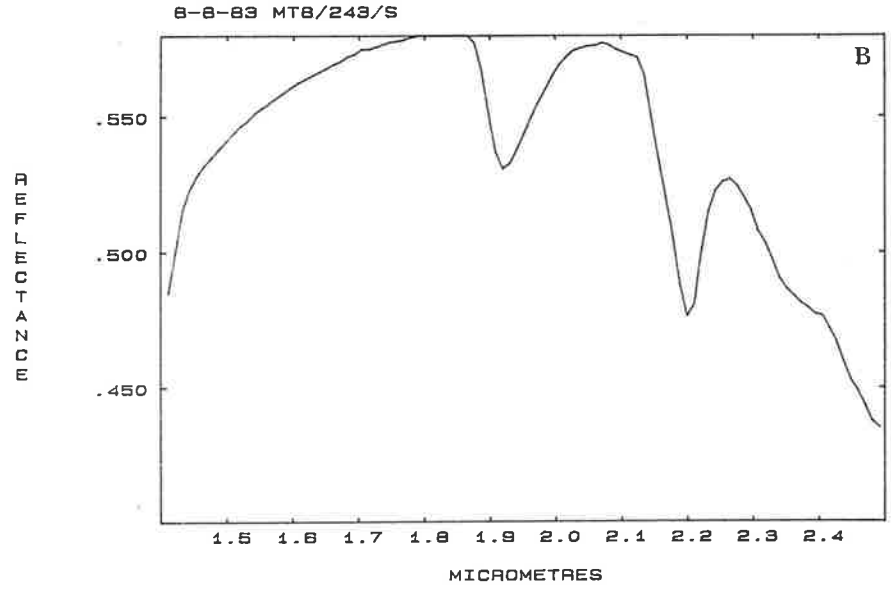
8-8-83 MT8/243/S
B
.550
.500
.450
REFLECTANCE
1.5 1.6 1.7 1.8 1.9 2.0 2.1 2.2 2.3 2.4
MICROMETRES

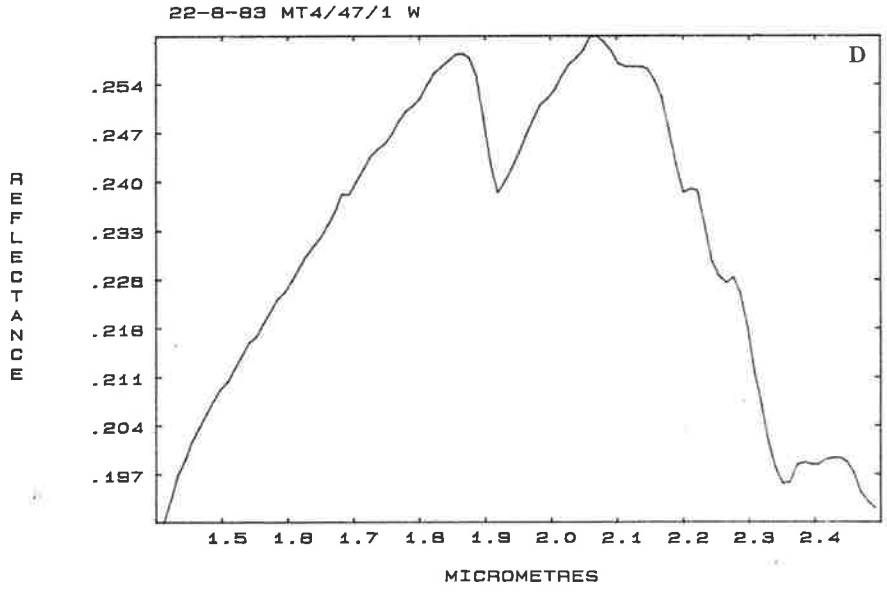
22-8-83 MT4/47/1 W
D
.254
.247
.240
.233
.228
.218
.211
.204
.197
REFLECTANCE
1.5 1.6 1.7 1.8 1.9 2.0 2.1 2.2 2.3 2.4
MICROMETRES

Figures 5.10a&b Averages of 'altered' and 'unaltered' SWIR laboratory reflectance spectra of Mt Turner samples.

The major absorption feature at 2.2μm is deeper in the spectrum of the averaged altered samples (10% for altered versus 4% for unaltered). Secondary features near 2.35 and 2.45μm are also better developed in the altered spectrum.

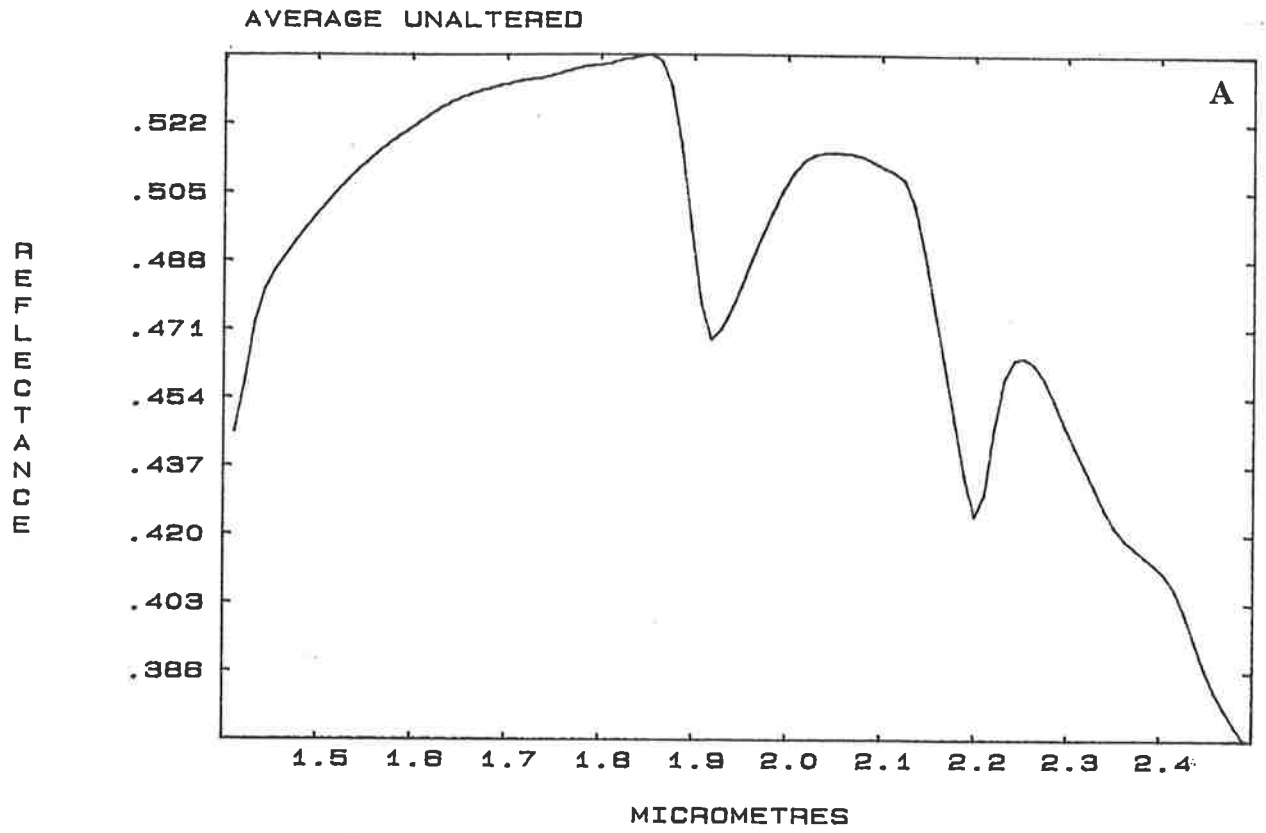
AVERAGE UNALTERED
A
REFLECTANCE
.522
.505
.488
.471
.454
.437
.420
.403
.388
1.5 1.6 1.7 1.8 1.9 2.0 2.1 2.2 2.3 2.4
MICROMETRES

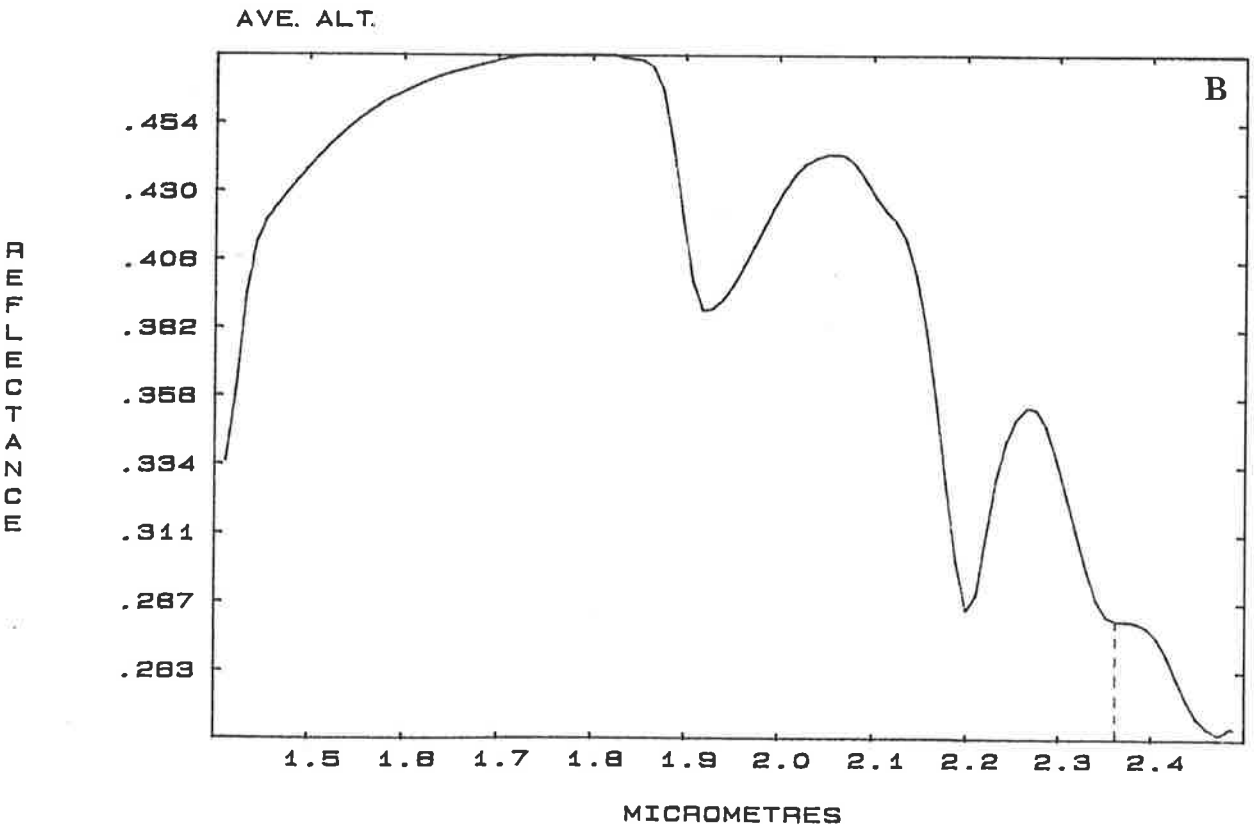
AVE. ALT.
B
REFLECTANCE
.454
.430
.406
.382
.358
.334
.311
.287
.263
1.5 1.6 1.7 1.8 1.9 2.0 2.1 2.2 2.3 2.4
MICROMETRES

Figures 5.11a&b Hull residuals of average altered and unaltered SWIR laboratory reflectance spectra.

Once the background slope has been removed using the hull residual technique, the presence of features near 2.35 and 2.45μm in the average unaltered spectrum become apparent (although they are not as well developed as the corresponding features in the average altered spectrum).

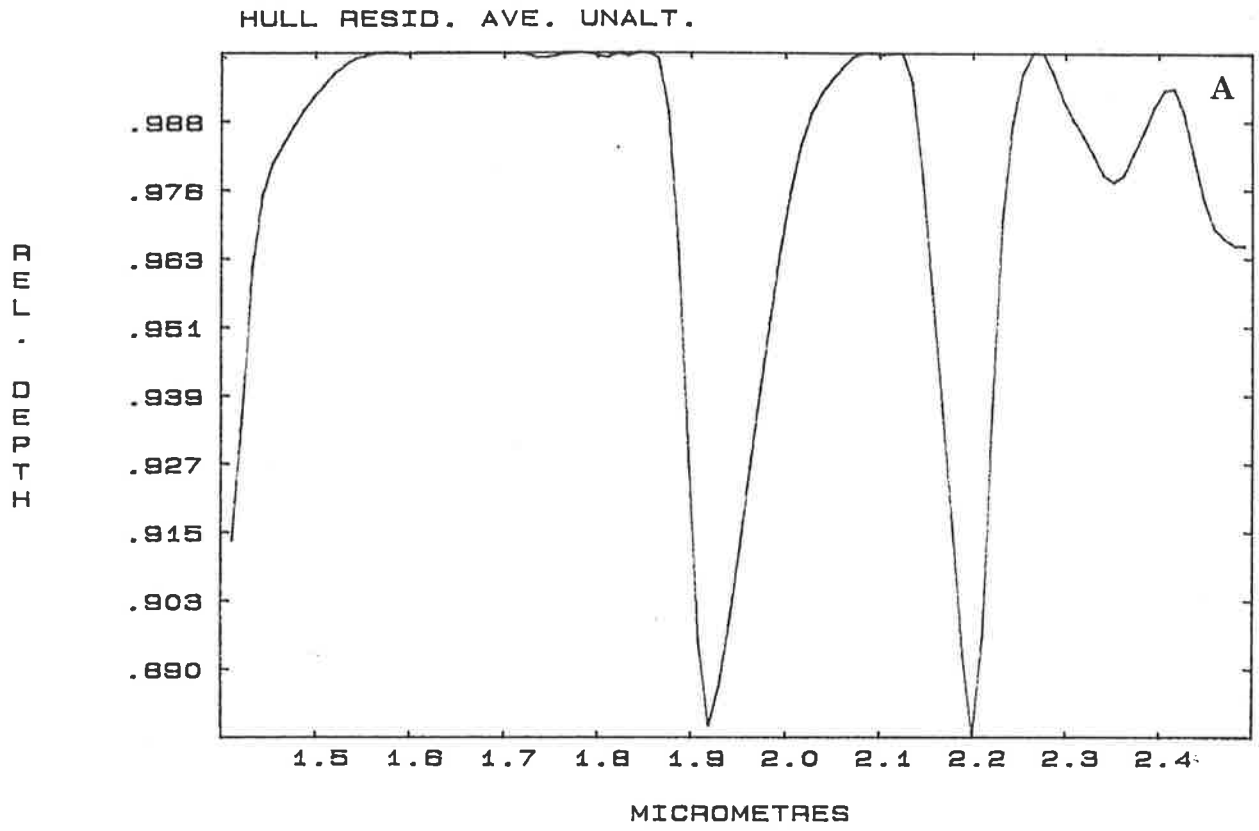
HULL RESID. AVE. UNALT.
A
REL. DEPTH
.988
.976
.963
.951
.939
.927
.915
.903
.890
1.5 1.6 1.7 1.8 1.9 2.0 2.1 2.2 2.3 2.4
MICROMETRES

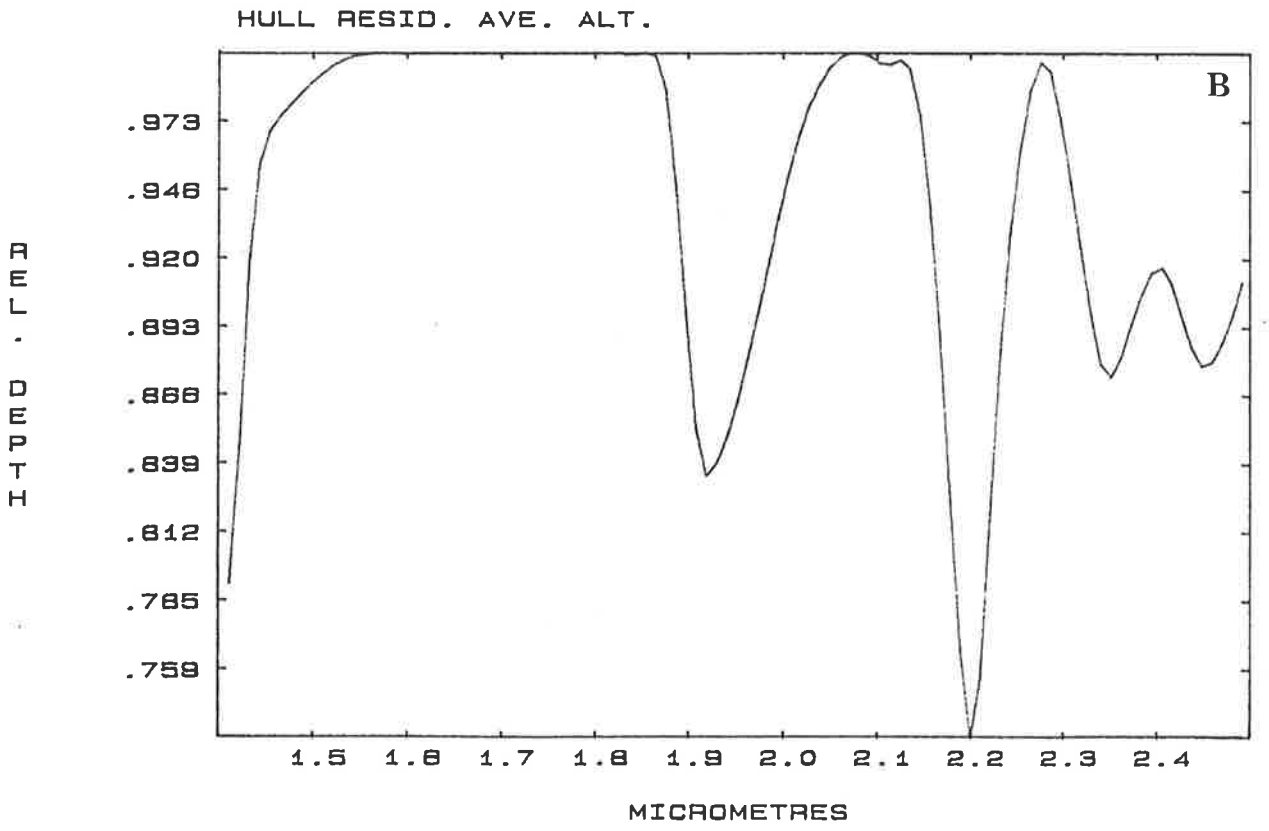
HULL RESID. AVE. ALT.
B
REL. DEPTH
.973
.946
.920
.893
.866
.839
.812
.785
.759
1.5 1.6 1.7 1.8 1.9 2.0 2.1 2.2 2.3 2.4
MICROMETRES

Figures 5.12a-k Mean radiance curves for each Mt Turner flight line.

Note the presence of the 2.2μm feature in every curve (due to atmospheric water absorption), and the varying strength of the shoulder near 2.17μm. This is a result of the influence of mineralogical (lithospheric) absorption (muscovite/sericite and kaolin).

(continued over)

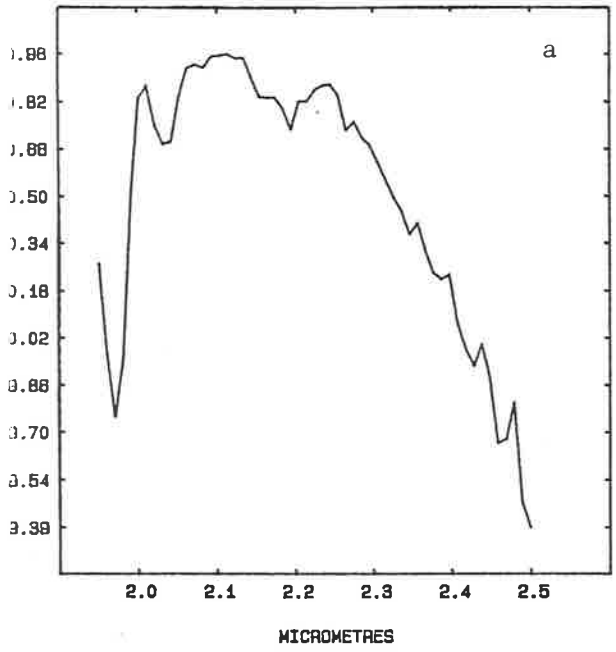

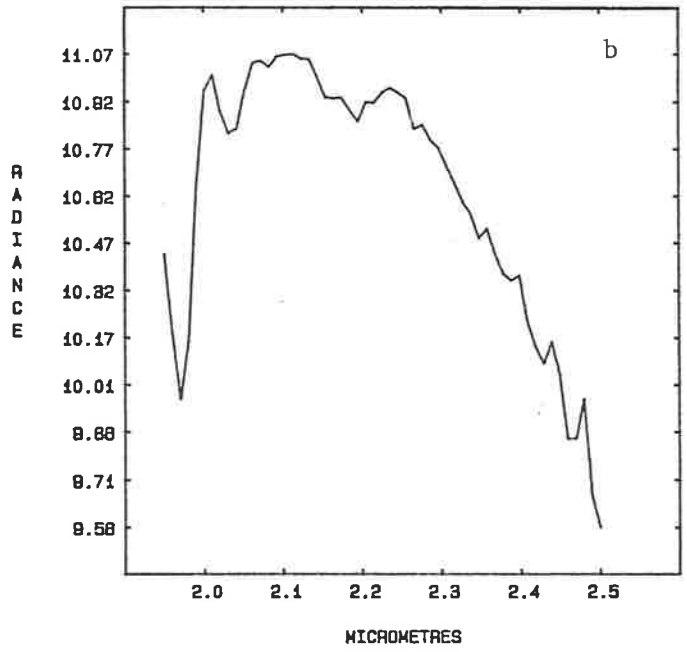

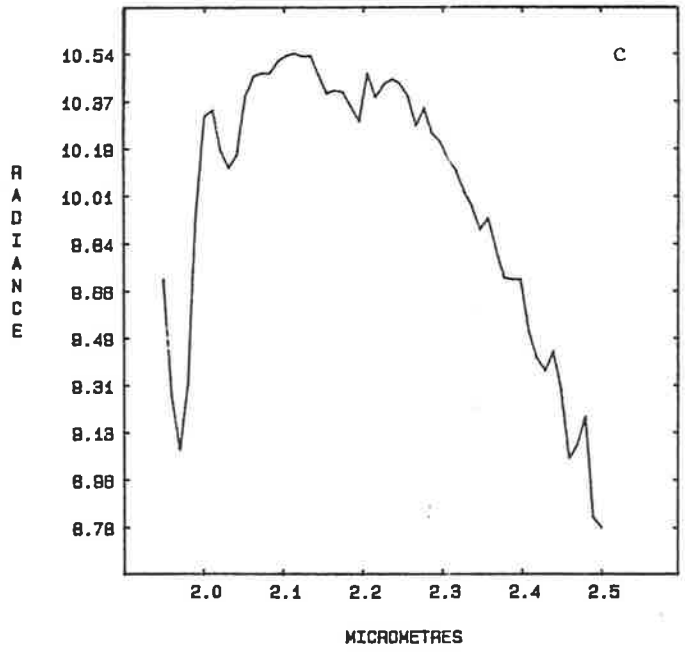

4 D MT4 MEAN

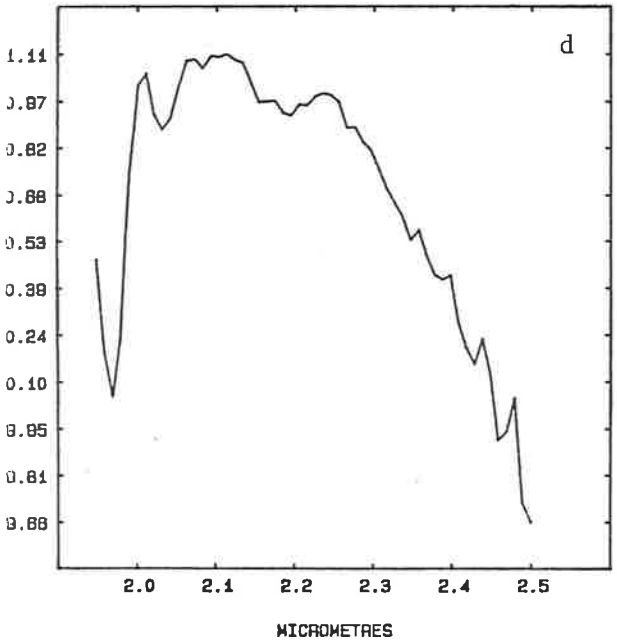

5 E MT5 MEAN

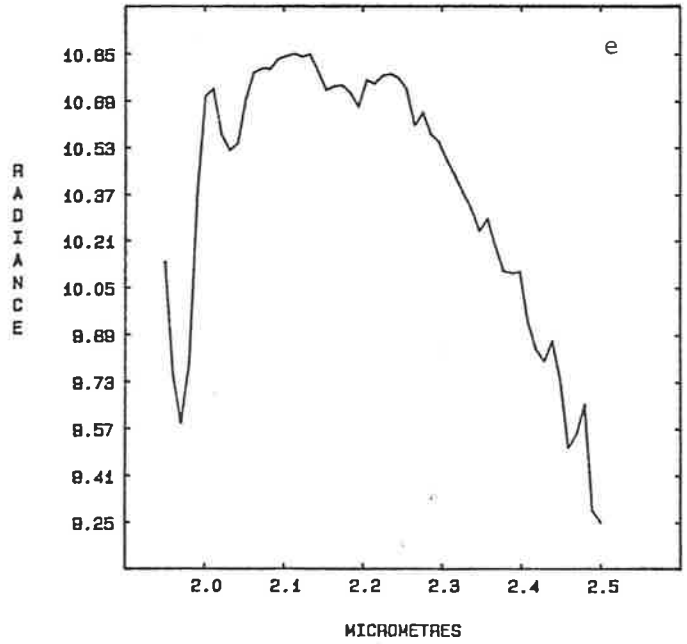

8 F MT8 MEAN

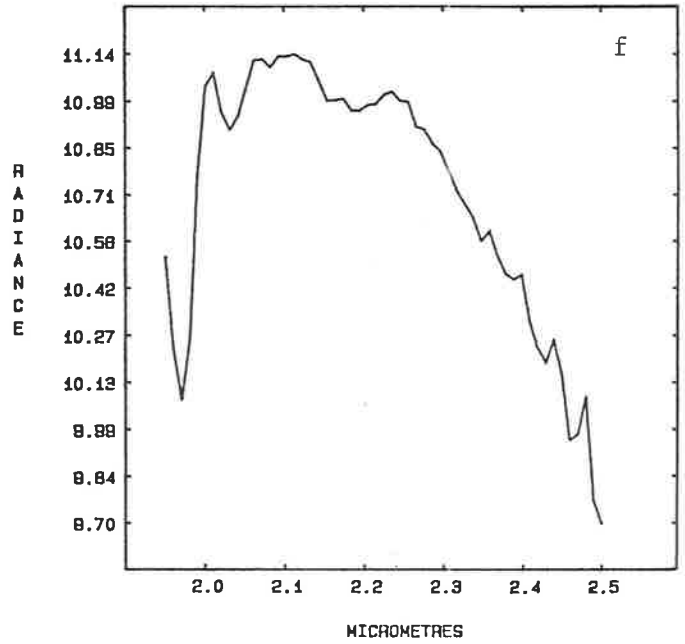

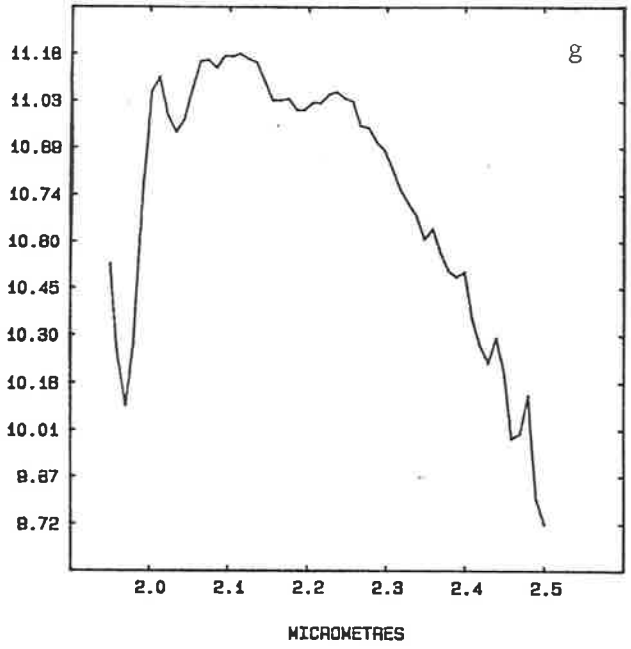
g
11.18
11.03
10.89
10.74
10.60
10.45
10.30
10.16
10.01
9.87
9.72
2.0
2.1
2.2
2.3
2.4
2.5
MICROMETRES

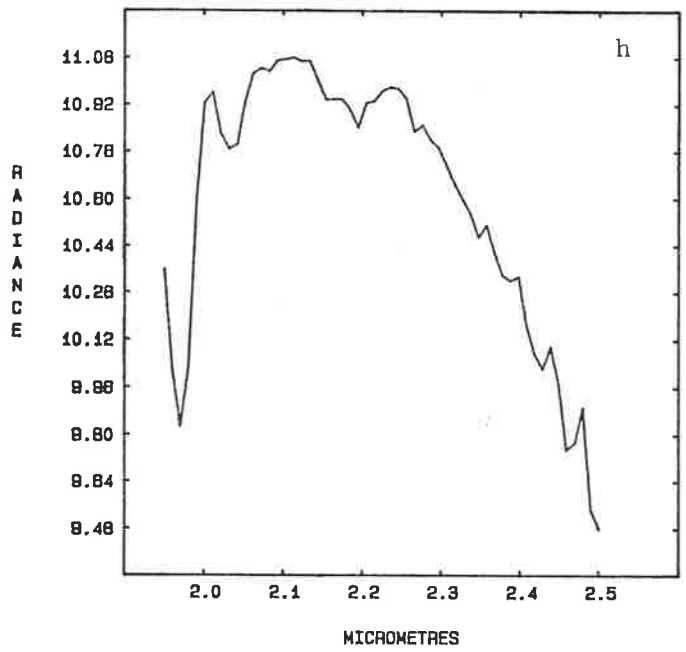
h
RADIANCE
11.08
10.92
10.78
10.60
10.44
10.28
10.12
9.96
9.80
9.64
9.48
2.0
2.1
2.2
2.3
2.4
2.5
MICROMETRES

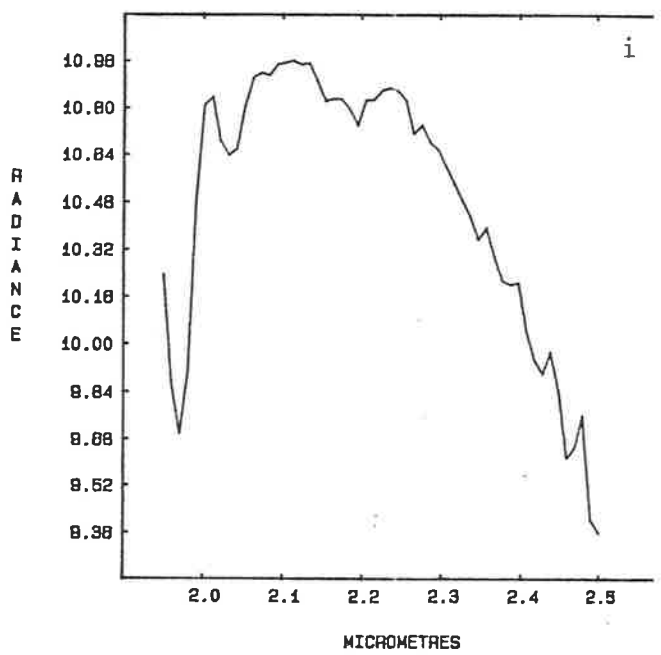
i
RADIANCE
10.96
10.80
10.64
10.48
10.32
10.16
10.00
9.84
9.68
9.52
9.36
2.0
2.1
2.2
2.3
2.4
2.5
MICROMETRES

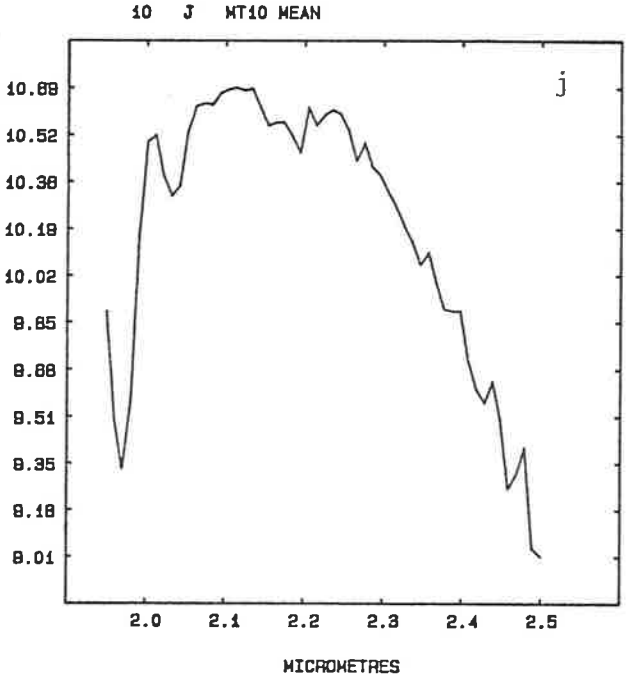
10 J MT10 MEAN
j
10.69
10.52
10.36
10.19
10.02
9.85
9.68
9.51
9.35
9.18
9.01
2.0
2.1
2.2
2.3
2.4
2.5
MICROMETRES

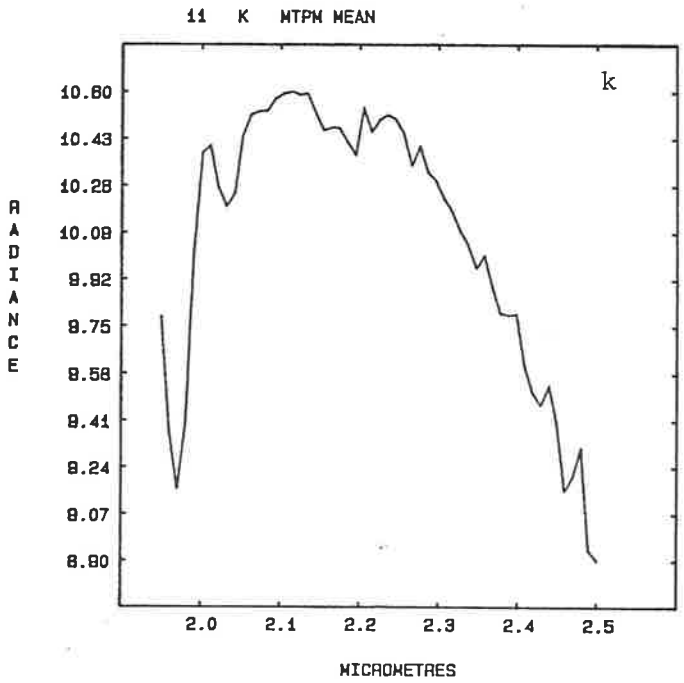
11 K MTPM MEAN
k
RADIANCE
10.60
10.43
10.28
10.09
9.92
9.75
9.58
9.41
9.24
9.07
8.90
2.0
2.1
2.2
2.3
2.4
2.5
MICROMETRES

Figure 5.13 Radiance of a 100% reflector at sea level, calculated using the LOWTRAN model.

The major features present in this spectrum are due to the presence of CO_2 and H_2O in the atmosphere.

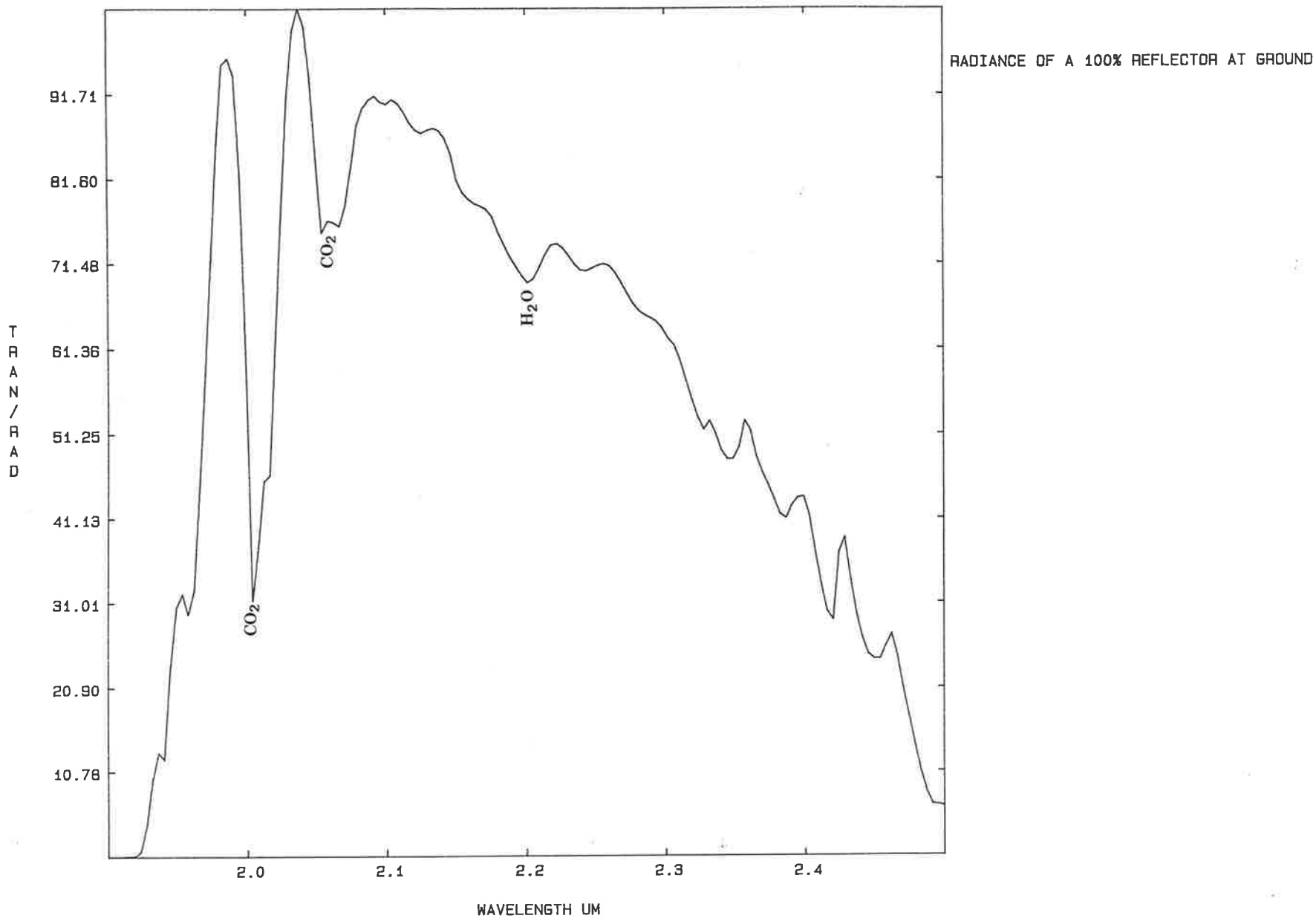
RADIANCE OF A 100% REFLECTOR AT GROUND
TRAN/RAD
91.71
81.60
71.48
61.36
51.25
41.13
31.01
20.90
10.78
CO_2
CO_2
H_2O
2.0
2.1
2.2
2.3
2.4
WAVELENGTH UM

Figures 5.14a&b Radiance curves from U.S. surveys (after Collins et al., 1981).

Note the depth of absorption features at both 2.2μm and 2.3μm. These are much stronger than any mineralogical effects detected at these wavelengths with the same instrument in Australia.

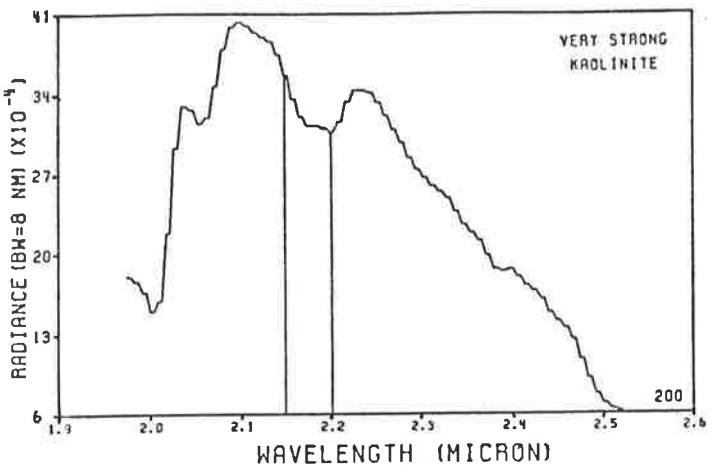
VERY STRONG
KAOLINITE
200
RADIANCE (BW=8 NM) (X10⁻⁴)
WAVELENGTH (MICRON)

a

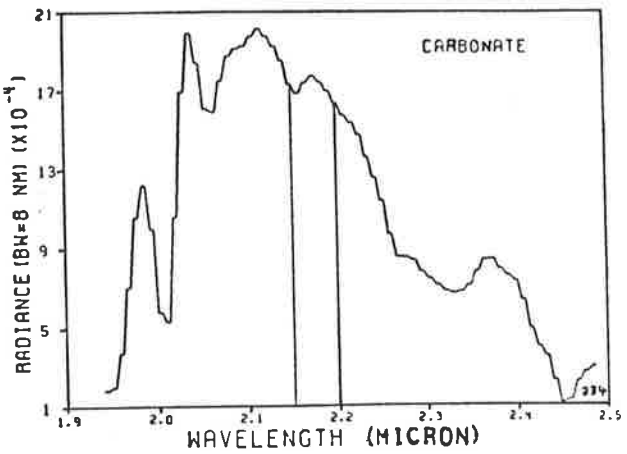
CARBONATE
RADIANCE (BW=8 NM) (X10⁻⁴)
WAVELENGTH (MICRON)

b

Figure 5.15 Log residuals of all Mt Turner flight lines in image format, with overlay showing major spectral types.

For each flight line there are six columns of data. From left to right, they are VNIR (0.4 μm to 1.0 μm) log residuals, VNIR Albedo, SWIR log residuals (1.95 μm to 2.5 μm), SWIR Albedo, a vegetation index derived from VNIR data, and coded geology. VNIR data are labelled Reticon Log Residuals and SWIR data are labelled Pbs Log Residuals.

The overlay shows typical examples of Types A, B and C spectra for line MT9 (blocks labelled B1 and B2 show vaying strengths of the same Type spectrum). Note that MT9 was flown from south to north. The log residual image data are arranged in order of inceasing pixel number, from top to bottom, so the top of the MT9 image data is south, bottom is north. For flight directions of other lines, see overlay B to Fig. 5.2.

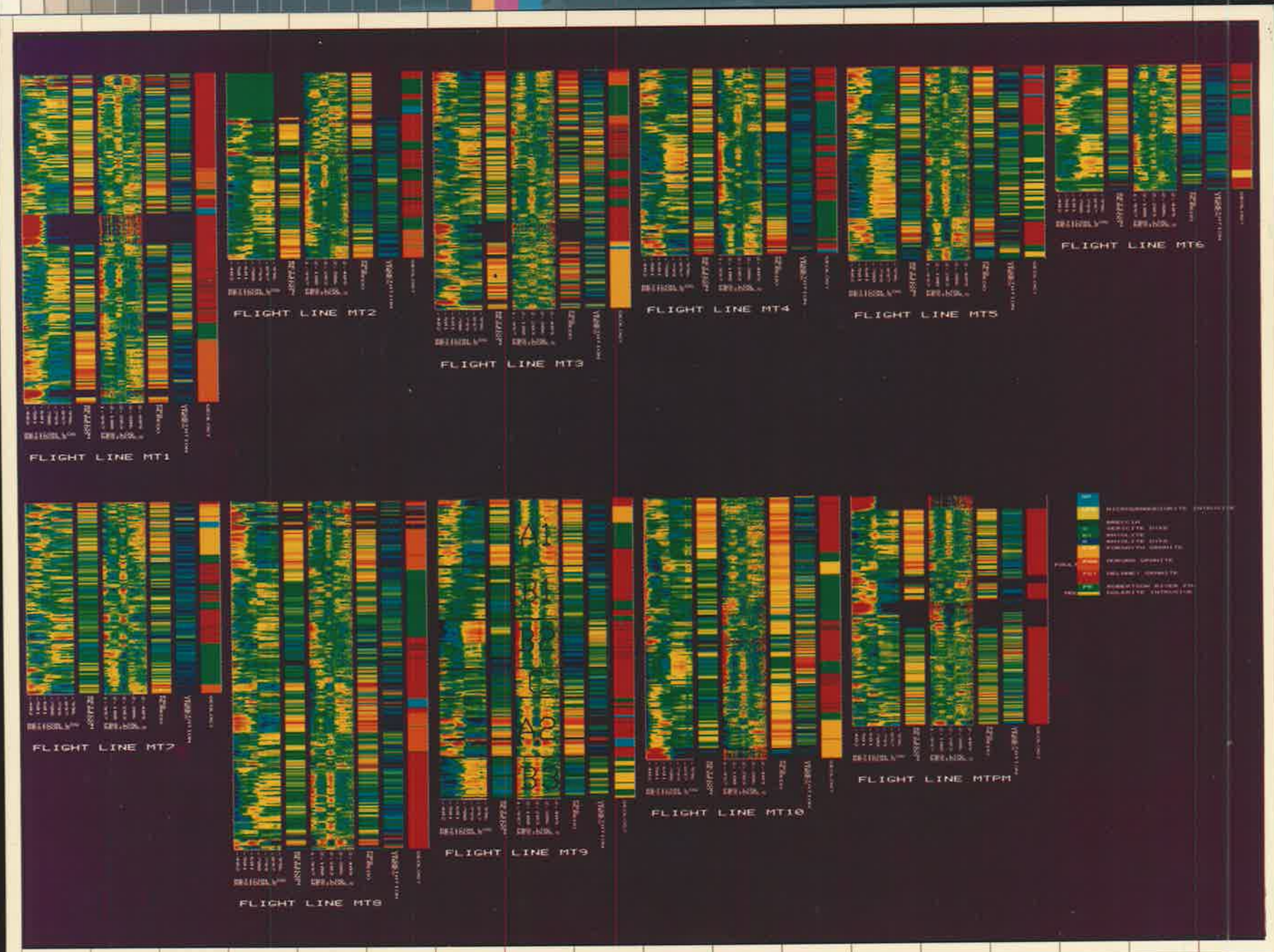
FLIGHT LINE MT1
FLIGHT LINE MT2
FLIGHT LINE MT3
FLIGHT LINE MT4
FLIGHT LINE MT5
FLIGHT LINE MT6
FLIGHT LINE MT7
FLIGHT LINE MT8
FLIGHT LINE MT9
FLIGHT LINE MT10
FLIGHT LINE MTPM

Figure 5.16 Classification of spectrometer data based on visual examination of log residuals in image format, overlain on the geology of Mt Turner.

The nature of the surface (e.g. bare soil, rock, or vegetation), rather than variations in the mineralogy, appears to be the major factor determining the category into which each spectral 'block' falls.

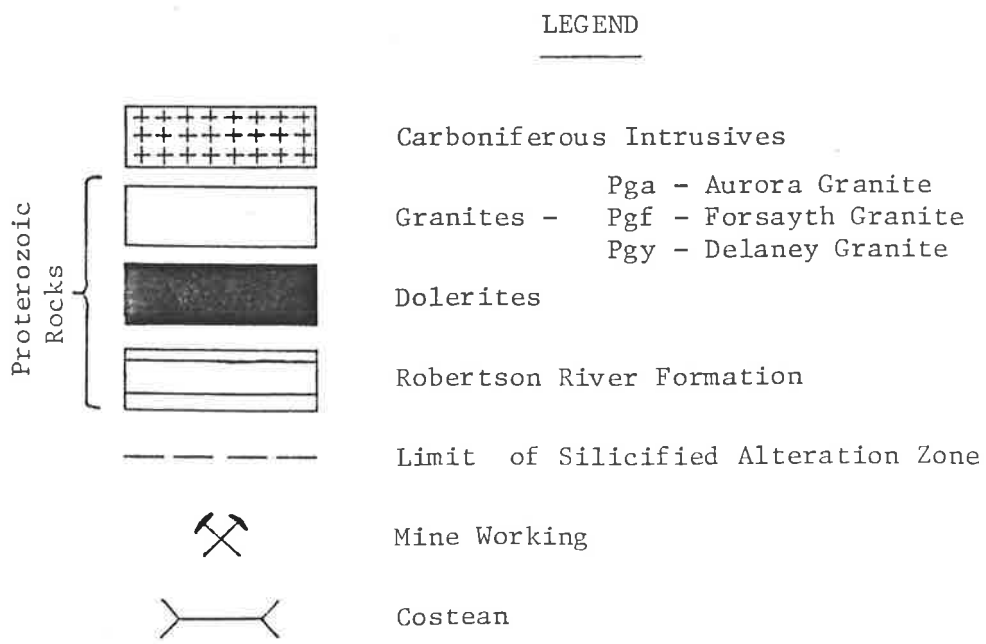

MOUNT TURNER GEOLOGY

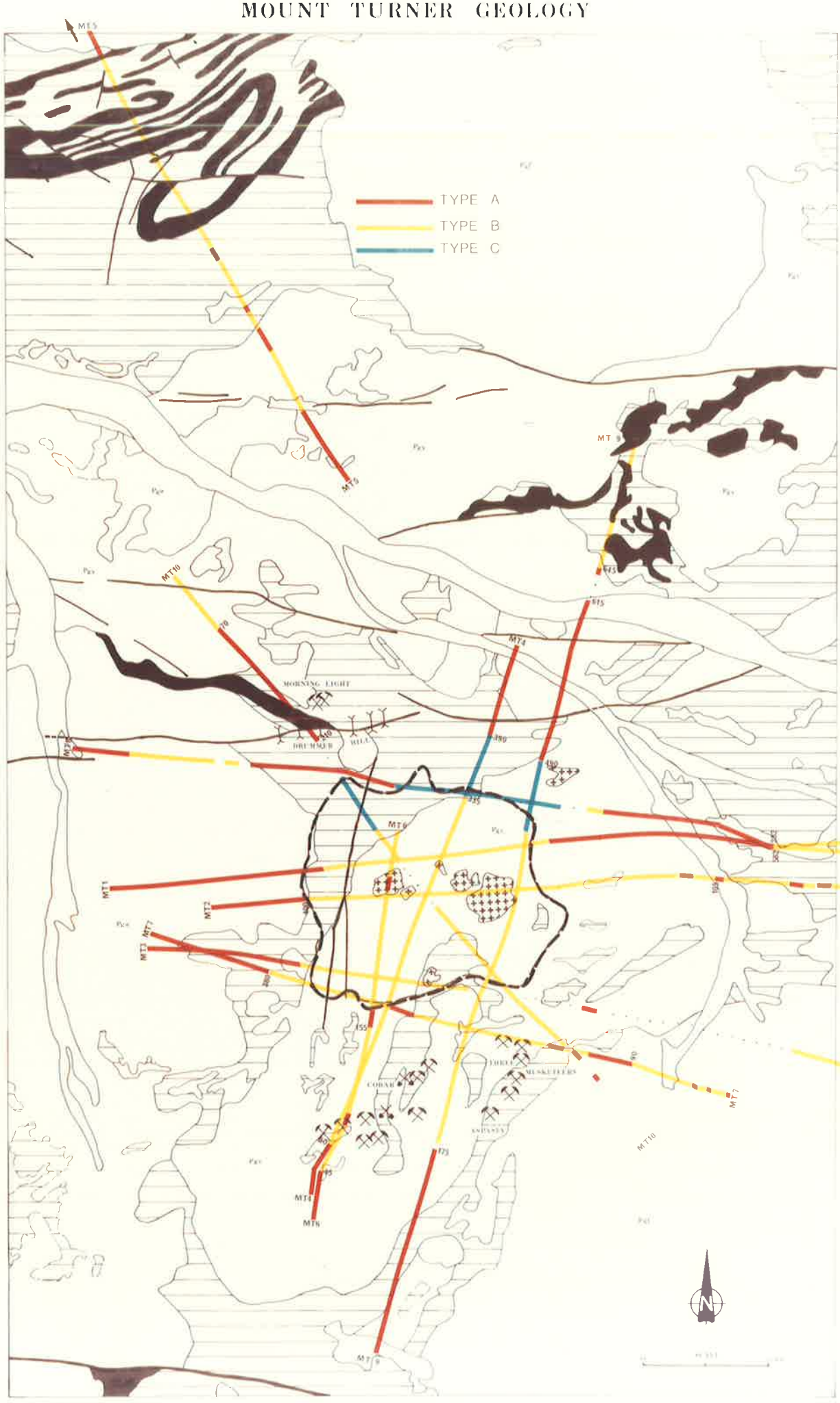

Figures 5.17a-f Spectral 'standards' derived from plots of log residual spectra.

Standard 1 is included as an offset used in the classification procedure. All other spectra have been produced by averaging 'blocks' from flight line MT4, and discarding very close matches.

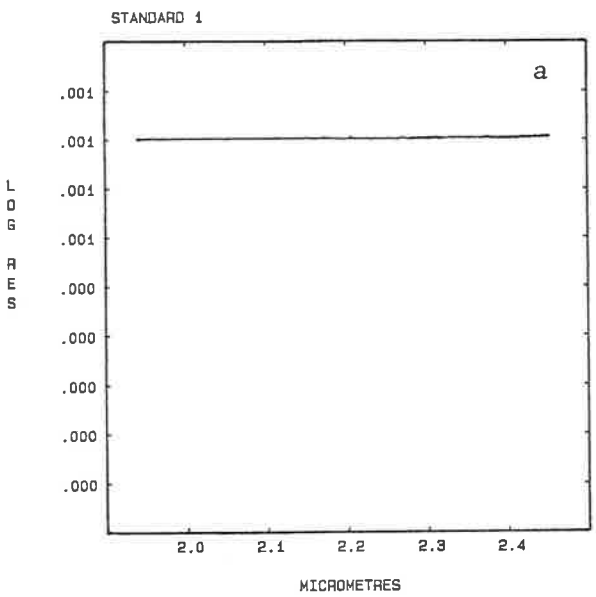
STANDARD 1
a
LOG RES.
.001
.001
.001
.001
.000
.000
.000
.000
2.0
2.1
2.2
2.3
2.4
MICROMETRES

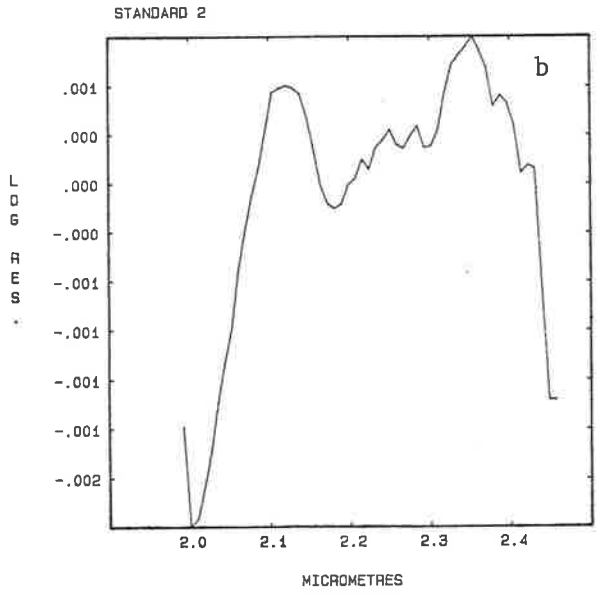
STANDARD 2
b
LOG RES.
.001
.000
.000
-.000
-.001
-.001
-.001
-.002
2.0
2.1
2.2
2.3
2.4
MICROMETRES

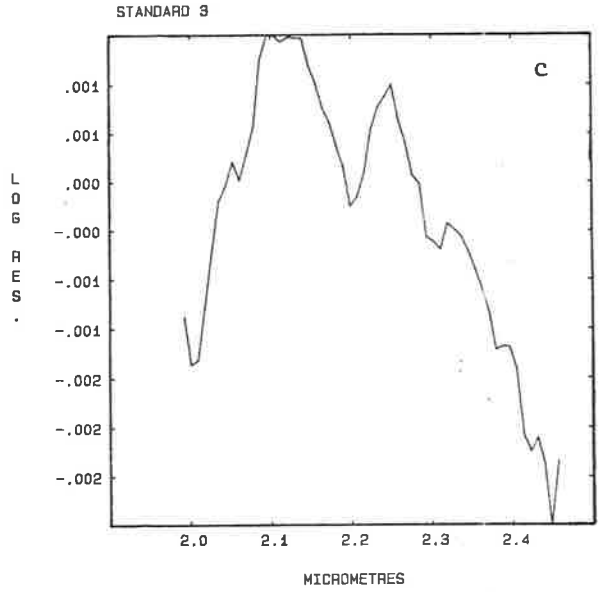
STANDARD 3
c
LOG RES.
.001
.001
.000
-.000
-.001
-.001
-.002
-.002
-.002
2.0
2.1
2.2
2.3
2.4
MICROMETRES

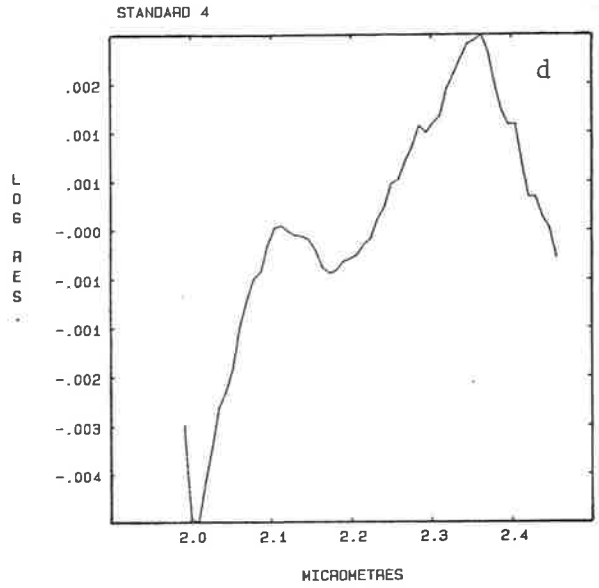
STANDARD 4
d
LOG RES.
.002
.001
.001
-.000
-.001
-.001
-.002
-.003
-.004
2.0
2.1
2.2
2.3
2.4
MICROMETRES

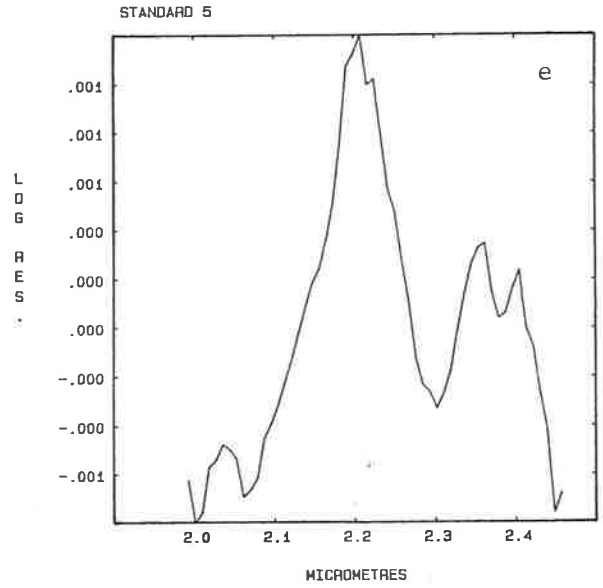
STANDARD 5
e
LOG RES.
.001
.001
.001
.000
.000
-.000
-.000
-.001
2.0
2.1
2.2
2.3
2.4
MICROMETRES

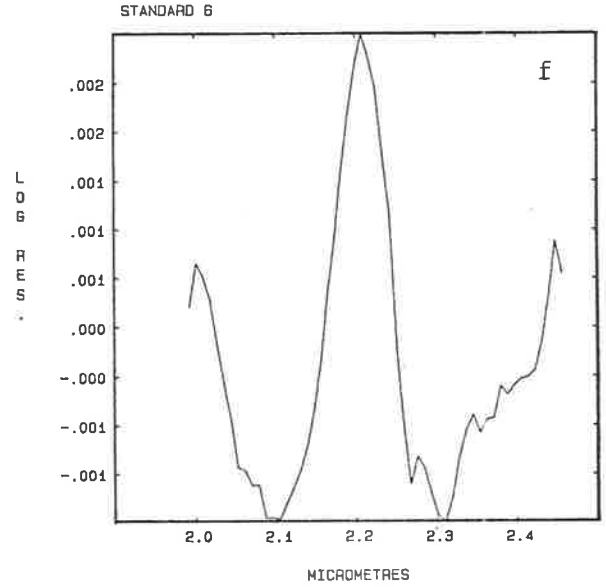
STANDARD 6
f
LOG RES.
.002
.002
.001
.001
.001
.000
-.000
-.001
-.001
2.0
2.1
2.2
2.3
2.4
MICROMETRES

Figures 5.17g-l Spectral 'standards' derived from plots of log residual spectra.

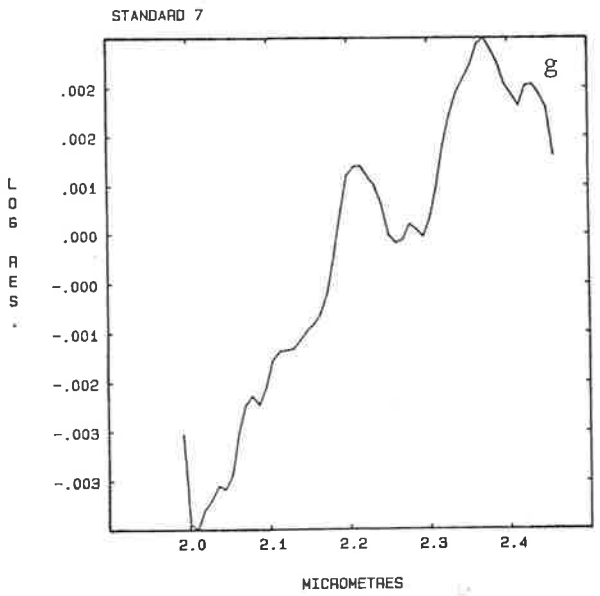
STANDARD 7
g
LOG RES.
.002
.002
.001
.000
-.000
-.001
-.002
-.003
-.003
2.0
2.1
2.2
2.3
2.4
MICROMETRES

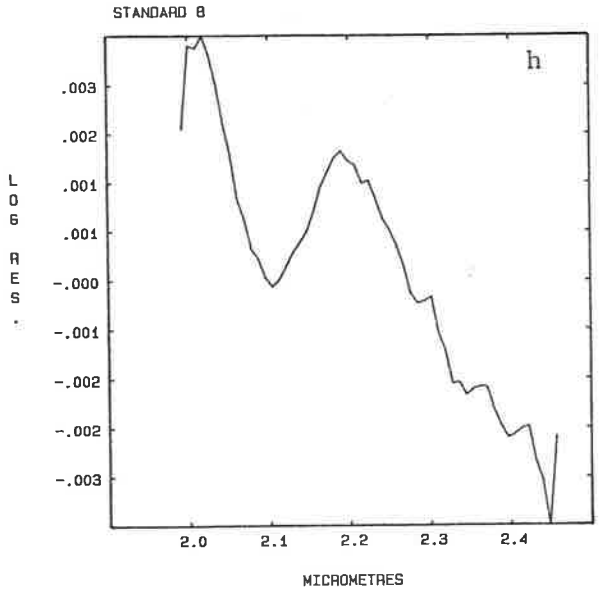
STANDARD 8
h
LOG RES.
.003
.002
.001
.001
-.000
-.001
-.002
-.002
-.003
2.0
2.1
2.2
2.3
2.4
MICROMETRES

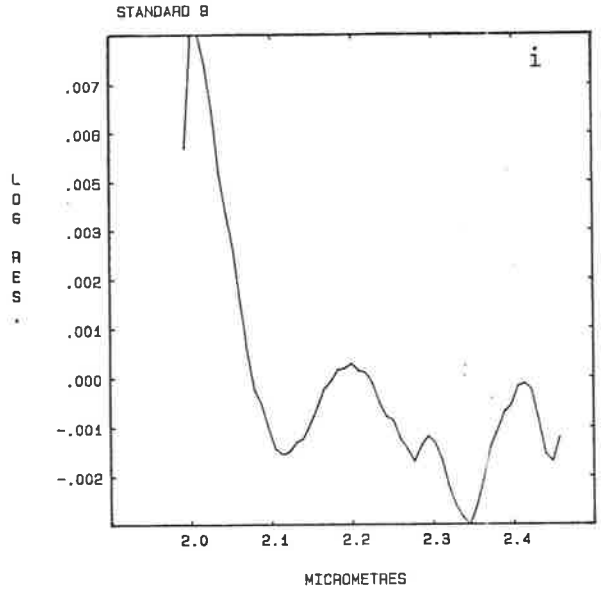
STANDARD 9
i
LOG RES.
.007
.006
.005
.003
.002
.001
.000
-.001
-.002
2.0
2.1
2.2
2.3
2.4
MICROMETRES

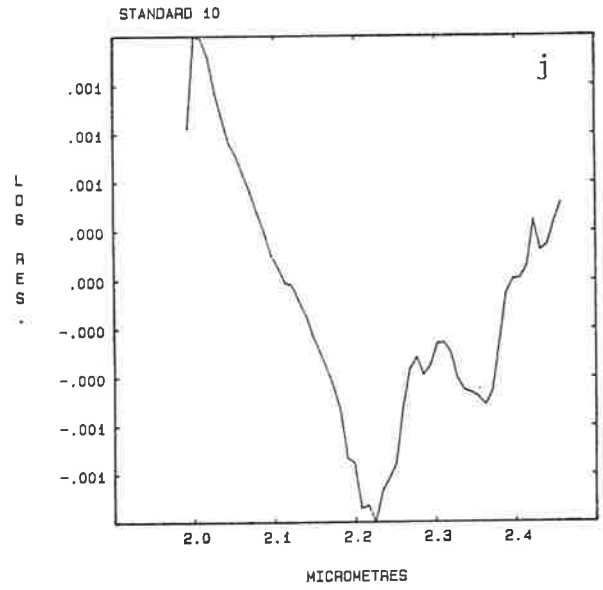
STANDARD 10
j
LOG RES.
.001
.001
.001
.000
.000
-.000
-.000
-.001
-.001
2.0
2.1
2.2
2.3
2.4
MICROMETRES

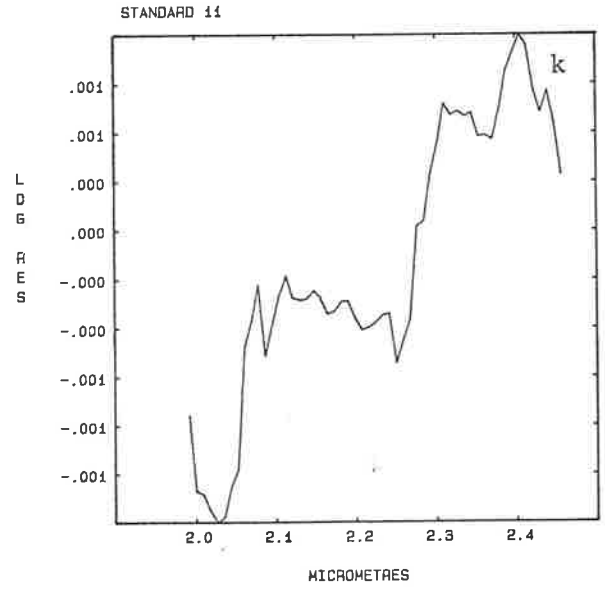
STANDARD 11
k
LOG RES
.001
.001
.000
.000
-.000
-.000
-.001
-.001
-.001
2.0
2.1
2.2
2.3
2.4
MICROMETRES

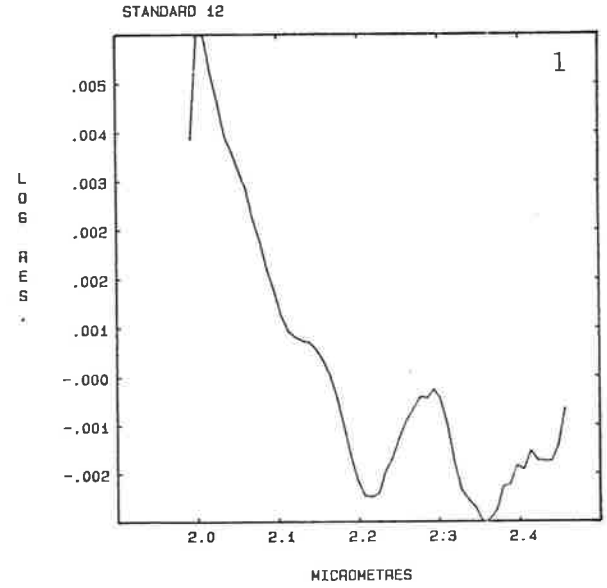
STANDARD 12
l
LOG RES.
.005
.004
.003
.002
.002
.001
-.000
-.001
-.002
2.0
2.1
2.2
2:3
2.4
MICROMETRES

Figures 5.17m&n Spectral 'standards' derived from plots of log residual spectra.

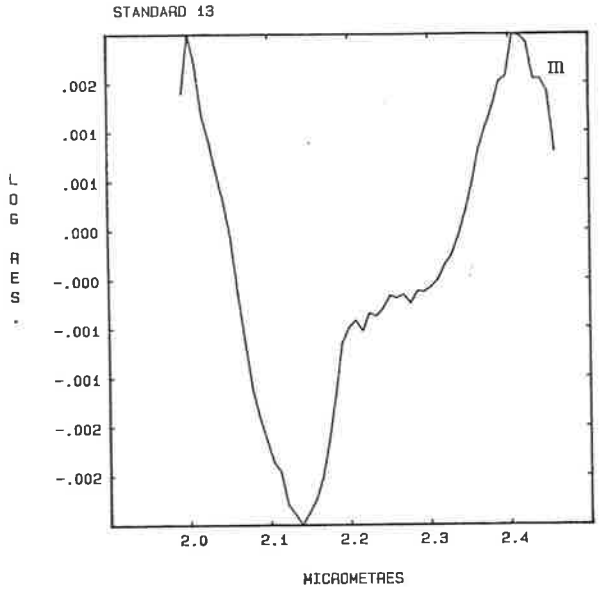
STANDARD 13
m
.002
.001
.001
.000
-.000
-.001
-.001
-.002
-.002
LOG RES.
2.0
2.1
2.2
2.3
2.4
MICROMETRES

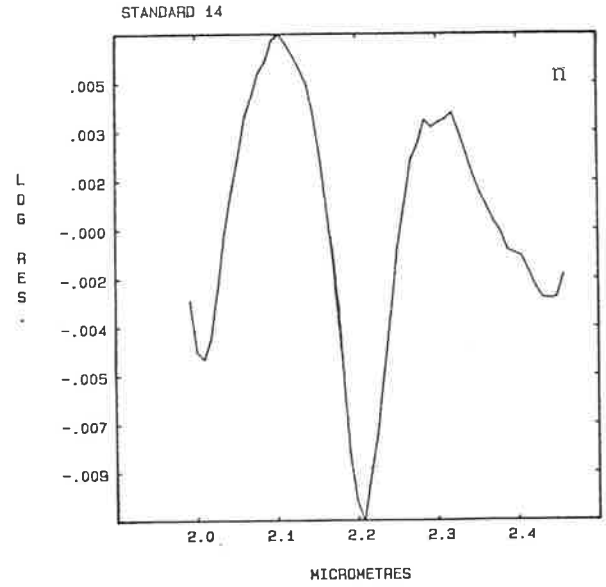
STANDARD 14
m
.005
.003
.002
-.000
-.002
-.004
-.005
-.007
-.009
LOG RES.
2.0
2.1
2.2
2.3
2.4
MICROMETRES

Figure 5.18 Output of portion of the least-squares classification of flight line MT8.

Solid vertical lines coincide with boundaries easily visible on Fig. 5.15. Dashed vertical lines represent boundaries which have been defined using the classification output itself.

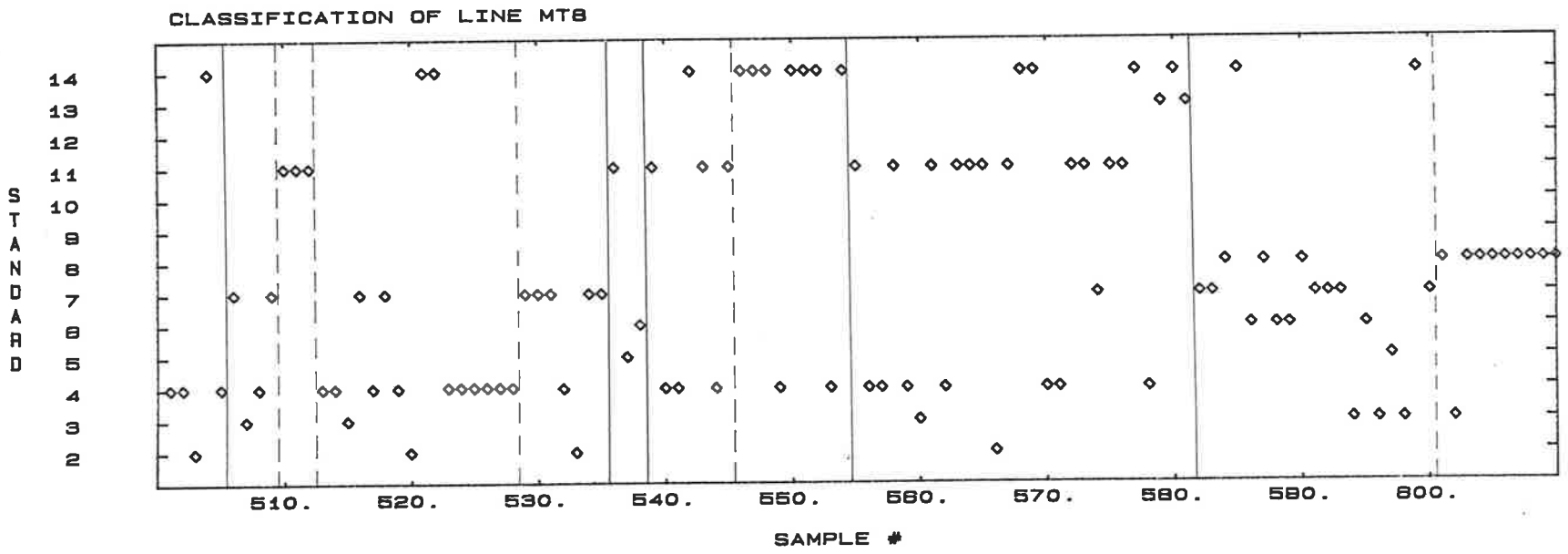
CLASSIFICATION OF LINE MT8
STANDARD
14
13
12
11
10
9
8
7
6
5
4
3
2
510.
520.
530.
540.
550.
560.
570.
580.
590.
600.
SAMPLE #

Figure 5.19 Least-squares classification of log residual spectra, overlain on the geology map of Mt Turner.

Note that there are differences between this classification and Fig. 5.16. Mineralogical variations appear to have more of an influence on the result in this case. Although the technique is not perfect, and has resulted in a number of misclassifications, areas of sericitic alteration have generally been discriminated successfully.

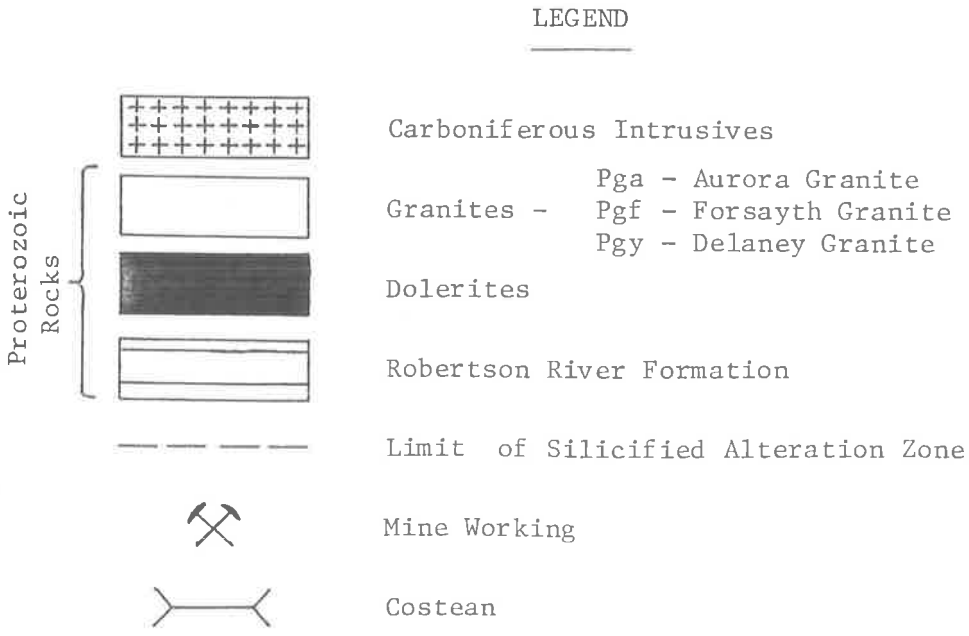

MOUNT TURNER GEOLOGY

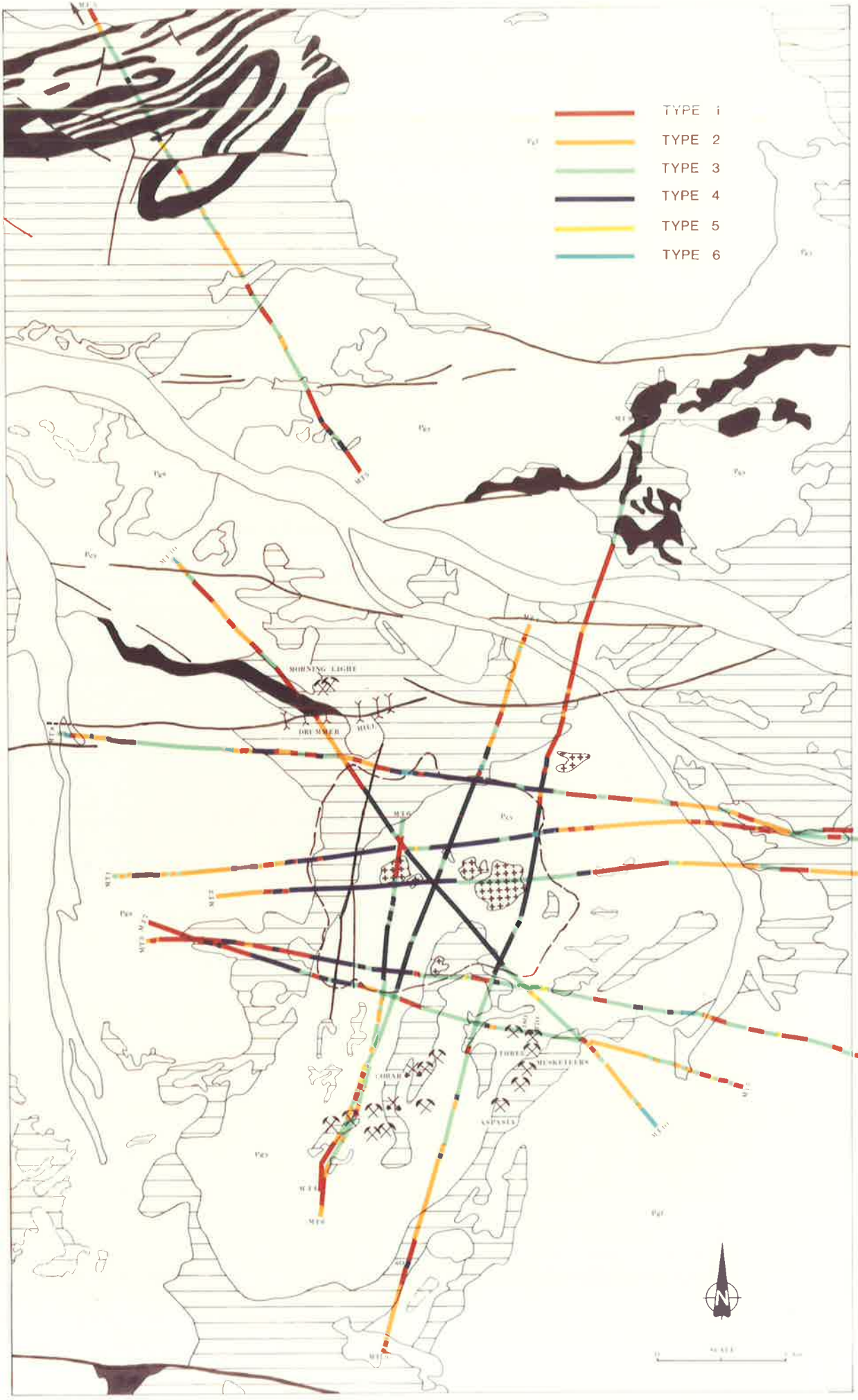

Figures 5.20a&b SWIR laboratory reflectance spectra of propylitically altered samples collected south of Mt Turner.

Both spectra shown have weak absorption features in the 2.3μm region. However, these features are not developed strongly enough to allow identification of the mineralogy. This is probably a contributing factor in the failure of the classification to discriminate propylitic alteration from dry vegetation.

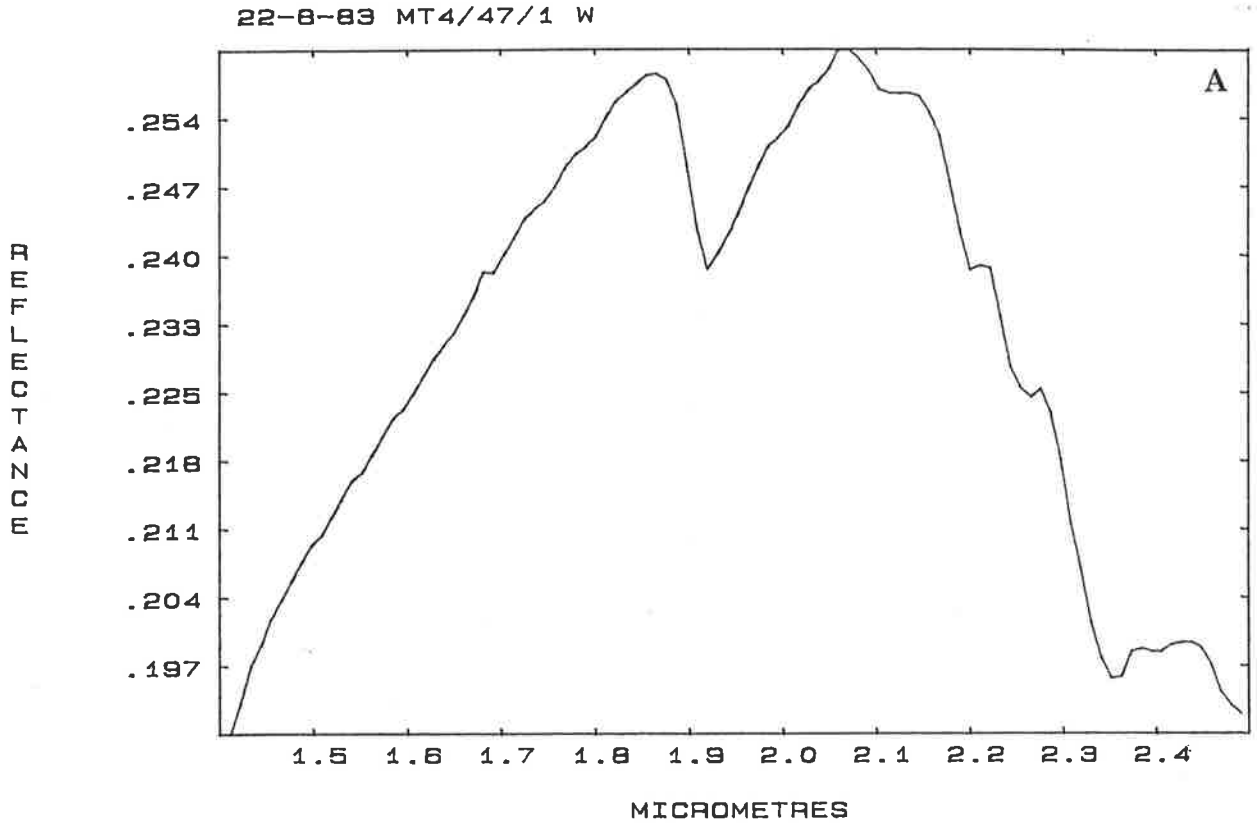
22-8-83 MT4/47/1 W
A
REFLECTANCE
.254
.247
.240
.233
.225
.218
.211
.204
.197
1.5 1.6 1.7 1.8 1.9 2.0 2.1 2.2 2.3 2.4
MICROMETRES

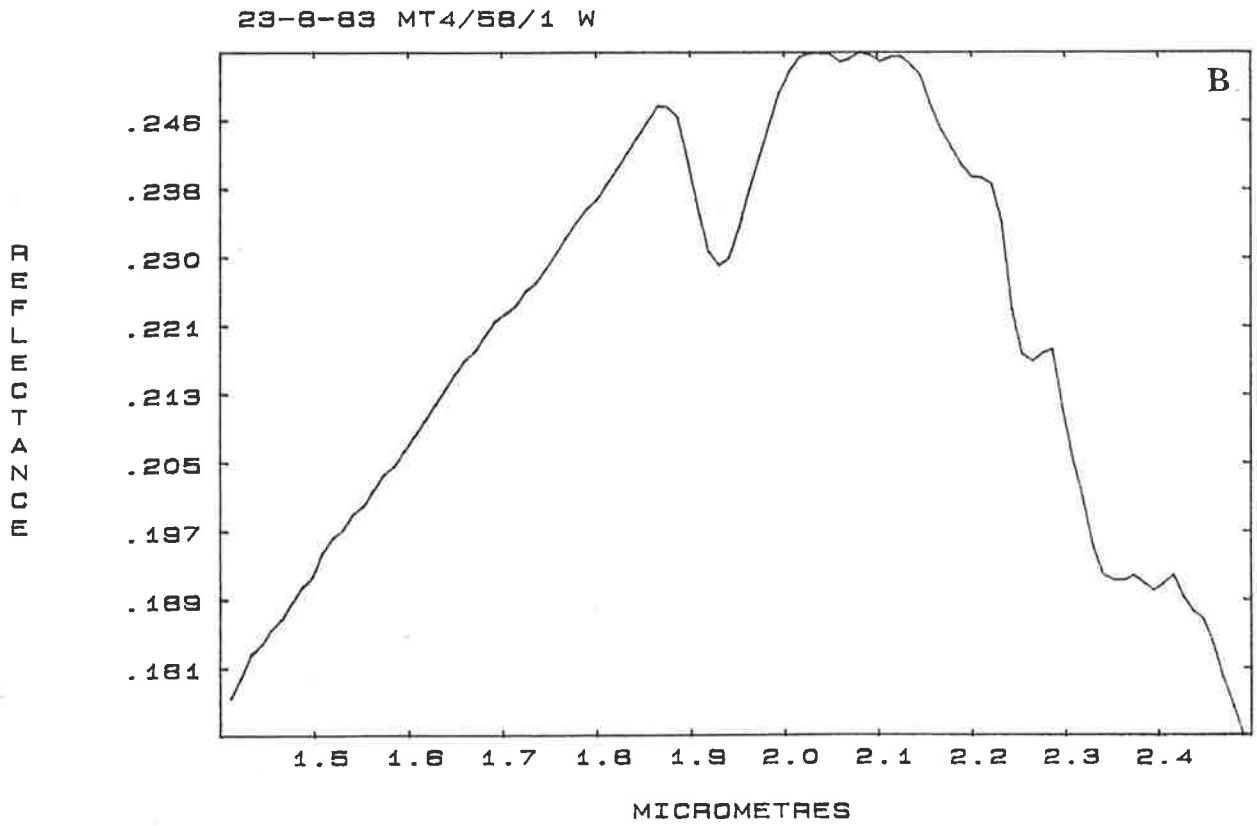
23-8-83 MT4/58/1 W
B
REFLECTANCE
.246
.238
.230
.221
.213
.205
.197
.189
.181
1.5 1.6 1.7 1.8 1.9 2.0 2.1 2.2 2.3 2.4
MICROMETRES

Figures 5.21a&b Airborne SWIR log residual and laboratory reflectance spectra of kaolin.

The kaolin spectra depicted here show much better definition of absorption features than those from other areas covered at Mt Turner.

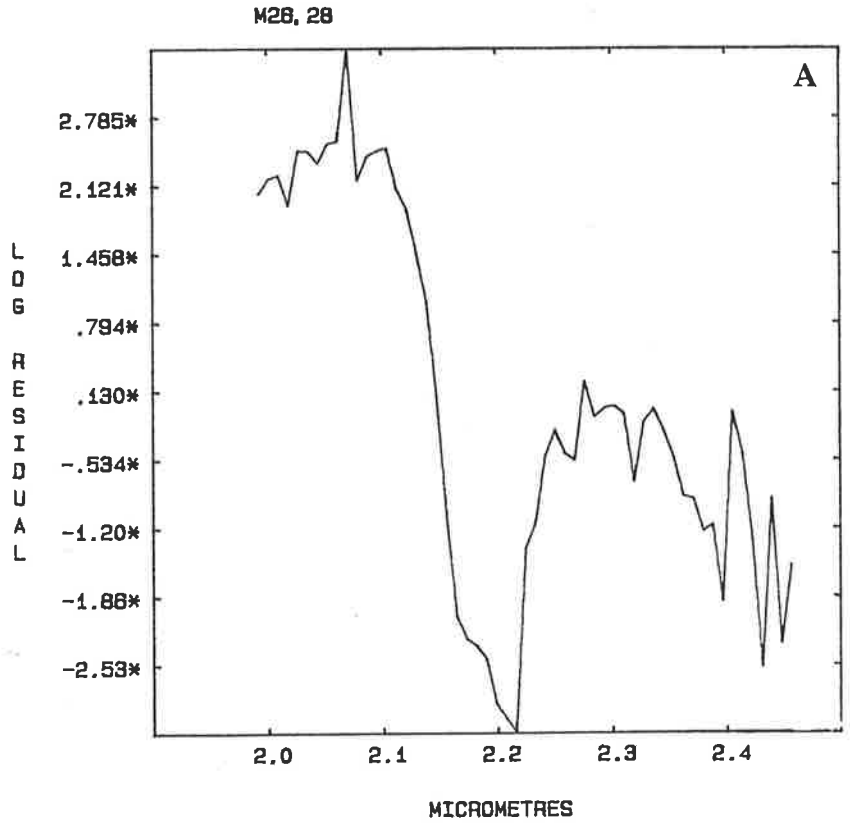
M28, 28
A
2.785*
2.121*
1.458*
.794*
.130*
-.534*
-1.20*
-1.88*
-2.53*
LOG RESIDUAL
2.0
2.1
2.2
2.3
2.4
MICROMETRES

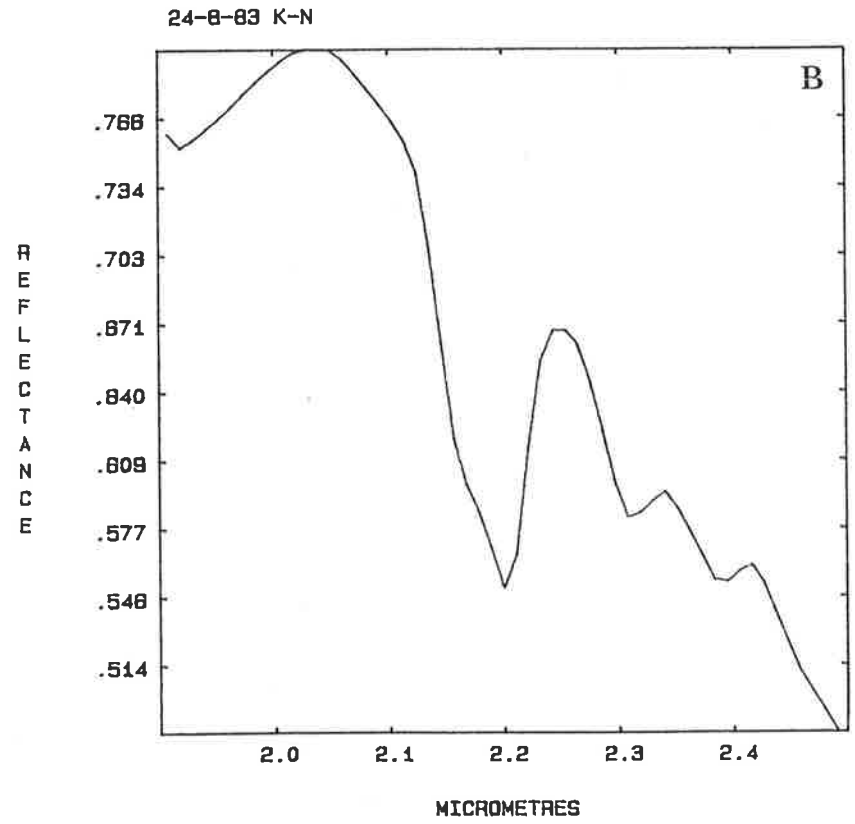
24-8-83 K-N
B
.766
.734
.703
.671
.640
.609
.577
.546
.514
REFLECTANCE
2.0
2.1
2.2
2.3
2.4
MICROMETRES

Figure 5.22 Airborne SWIR log residual spectrum of chlorite/amphibole? mixture from line MT5.

The airborne spectrum was collected over an outcrop of amphibolite on flight line MT5. The sharp feature at 2.26μm is indicative of chlorite, while the noisy minimum near 2.4μm may indicate the presence of amphibole. The absorption feature near 2.3μm is likely to be the result of the combined influence of both minerals.

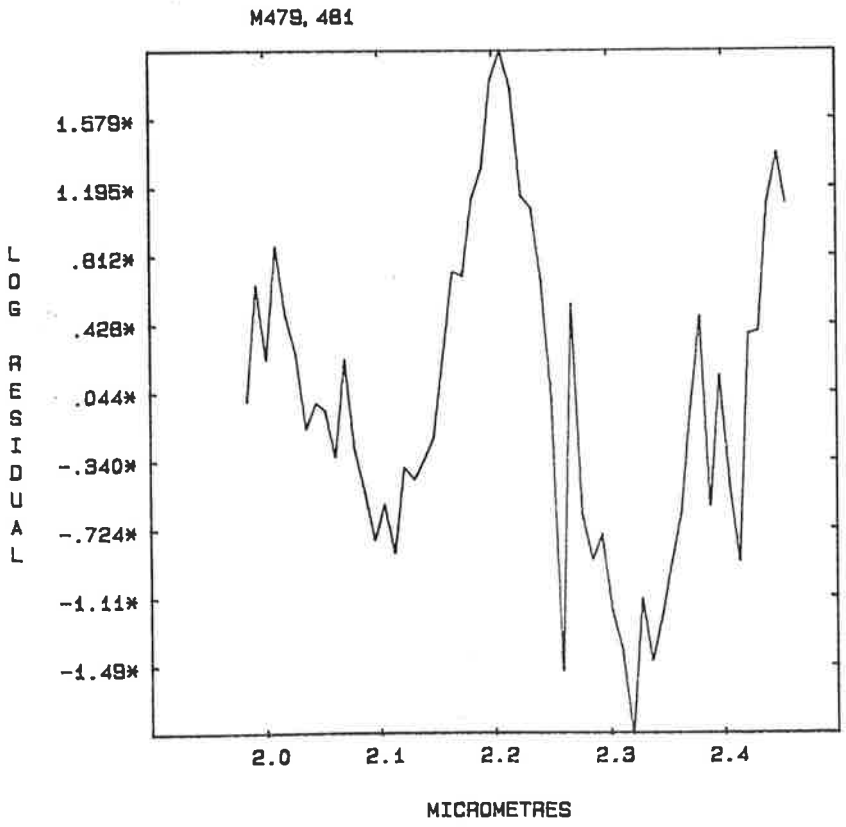
M479, 481
1.579*
1.195*
.812*
.428*
.044*
-.340*
-.724*
-1.11*
-1.49*
LOG RESIDUAL
2.0
2.1
2.2
2.3
2.4
MICROMETRES

Figures 5.23a&b Tchebychev coefficient ratio and simulated narrow-band ratio plots for line MT9.

The dashed vertical lines are boundaries that have been determined from the classification scheme (Fig. 5.19). Boundaries of the major sericitic alteration zone are shown by the arrows.

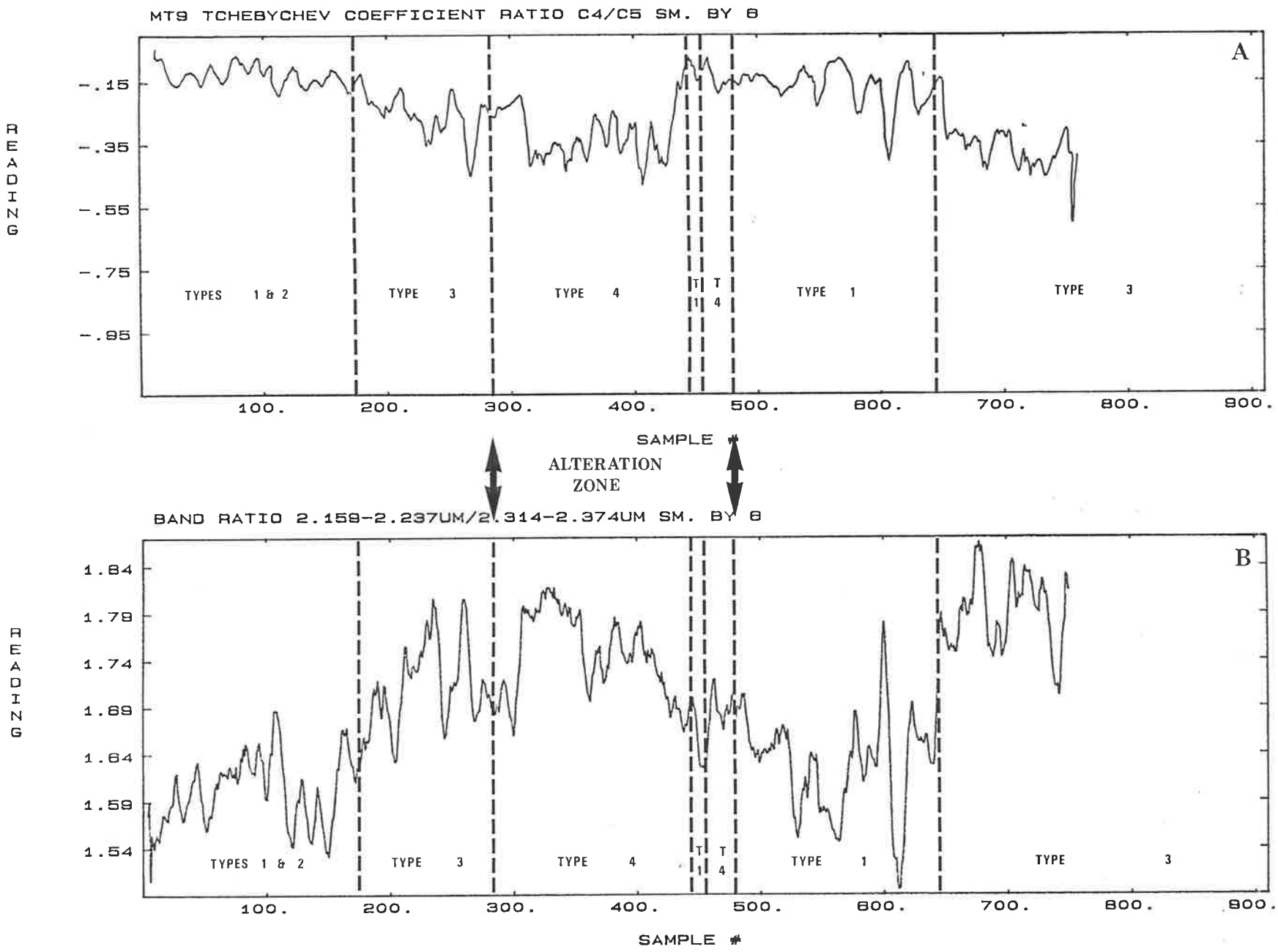
MT9 TCHEBYCHEV COEFFICIENT RATIO C4/C5 SM. BY 8
A
READING
-.15
-.35
-.55
-.75
-.95
TYPES 1 & 2
TYPE 3
TYPE 4
T 1
T 4
TYPE 1
TYPE 3
100.
200.
300.
400.
500.
600.
700.
800.
900.
SAMPLE #
ALTERATION ZONE
BAND RATIO 2.158-2.237UM/2.314-2.374UM SM. BY 8
B
READING
1.84
1.79
1.74
1.69
1.64
1.59
1.54
TYPES 1 & 2
TYPE 3
TYPE 4
T 1
T 4
TYPE 1
TYPE 3
100.
200.
300.
400.
500.
600.
700.
800.
900.
SAMPLE #

Figure 5.24 Log mean of all SWIR laboratory reflectance spectra from Mt Turner.

The mean spectrum of all field samples has been calculated using spectra of both weathered and fresh surfaces. A sampling bias towards altered samples has resulted in stronger 2.35 and 2.45μm absorption features than would be expected for a similar spectrum derived from the airborne data.

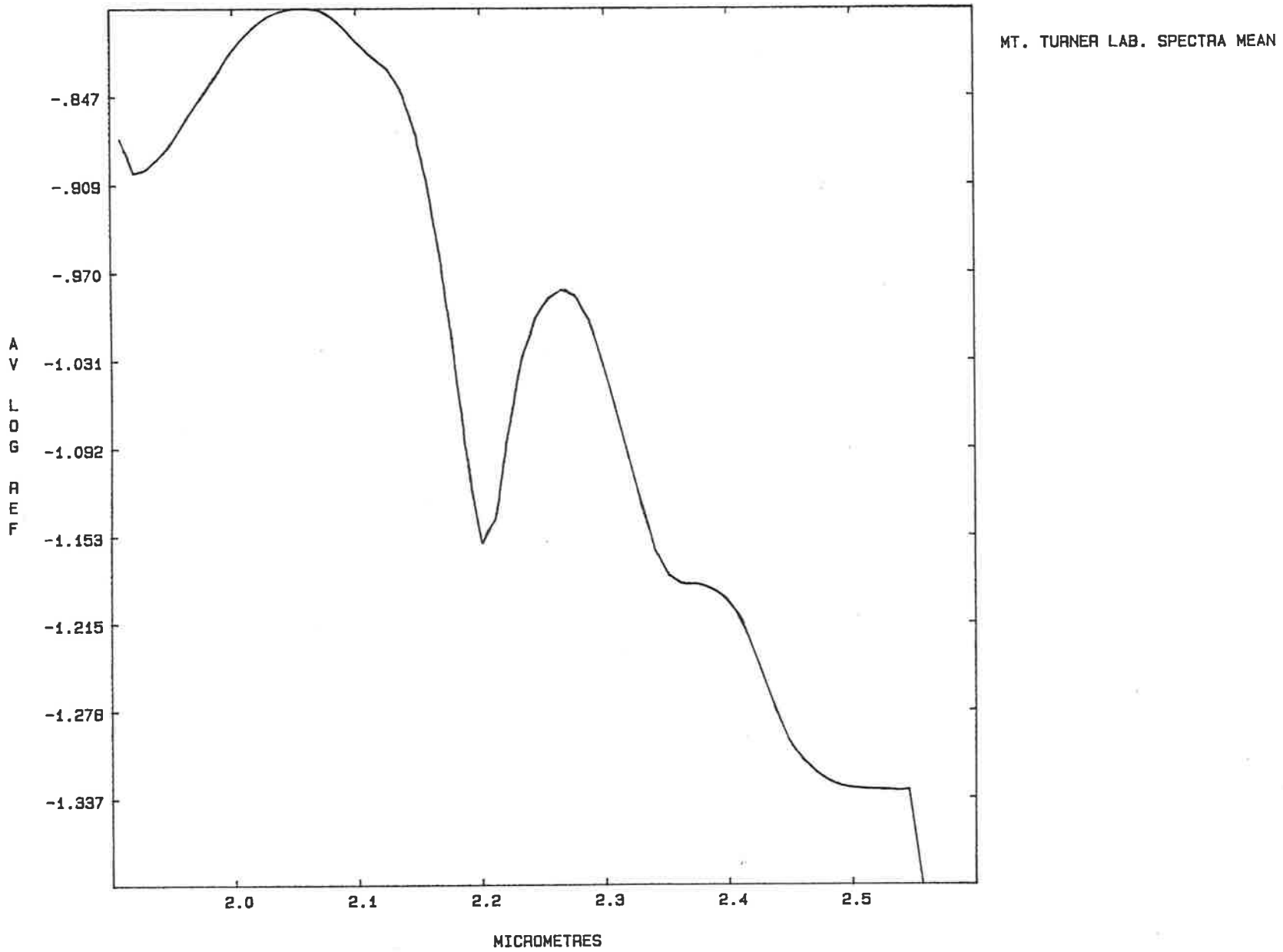
MT. TURNER LAB. SPECTRA MEAN
-.847
-.909
-.970
-1.031
-1.092
-1.153
-1.215
-1.278
-1.337
AVLOG REF
2.0
2.1
2.2
2.3
2.4
2.5
MICROMETRES

Figures 5.25a-f Selected SWIR laboratory reflectance spectra and their 'log residuals'.

These plots illustrate the difficulty of separating the effects of dry vegetation from propylitic alteration. Similarly-shaped 'log residuals' (Figs. 5.25d&f) have resulted from the spectra of these two very different materials.

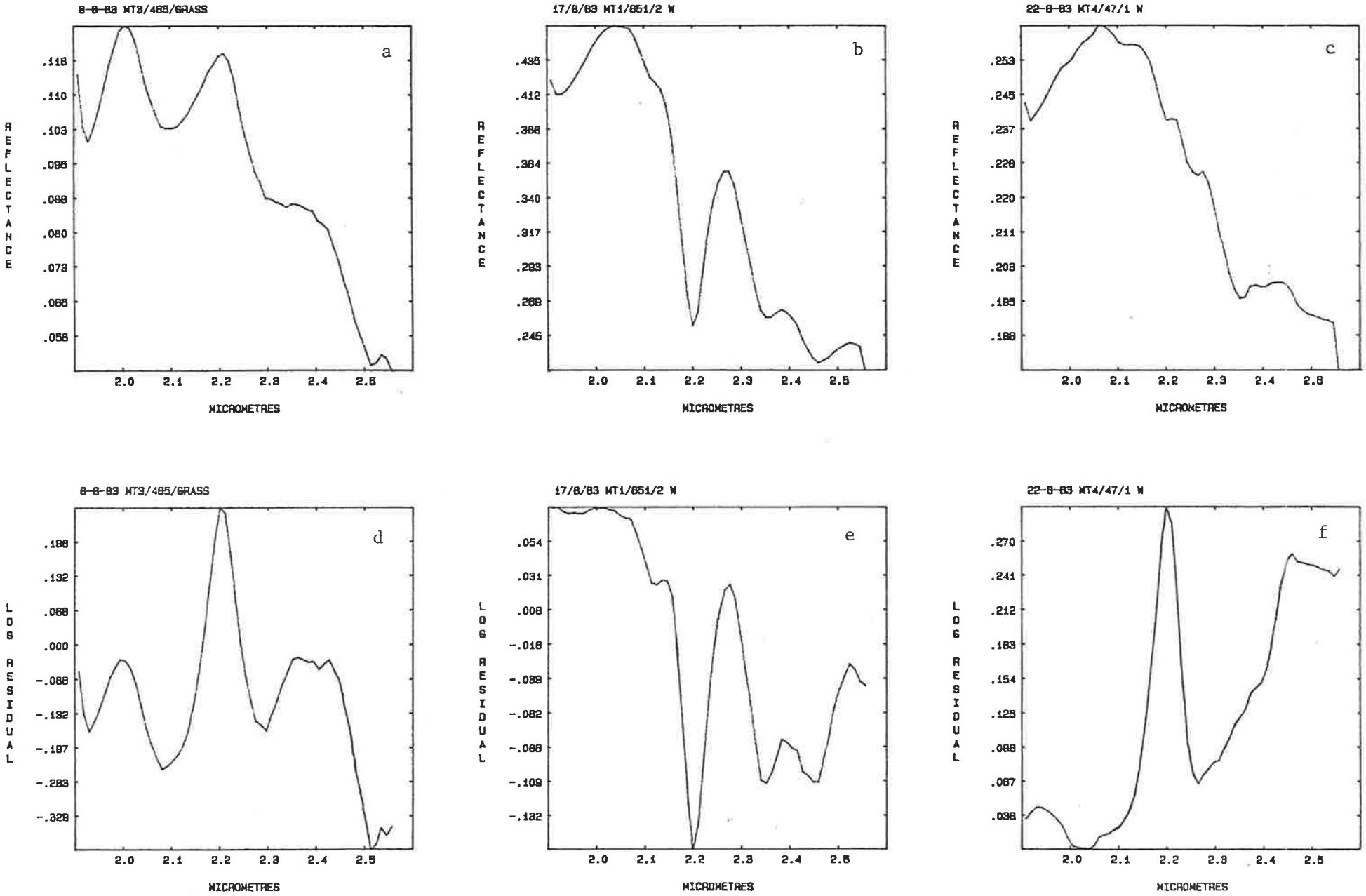
8-8-83 MT3/485/GRASS
a
REFLECTANCE
.118
.110
.103
.095
.088
.080
.073
.065
.058
2.0 2.1 2.2 2.3 2.4 2.5
MICROMETRES
17/8/83 MT1/851/2 W
b
REFLECTANCE
.495
.412
.388
.364
.340
.317
.293
.269
.245
2.0 2.1 2.2 2.3 2.4 2.5
MICROMETRES
22-8-83 MT4/47/1 W
c
REFLECTANCE
.253
.245
.237
.228
.220
.211
.203
.195
.186
2.0 2.1 2.2 2.3 2.4 2.5
MICROMETRES
8-8-83 MT3/485/GRASS
d
LOG RESIDUAL
.196
.132
.068
.000
-.068
-.132
-.197
-.263
-.329
2.0 2.1 2.2 2.3 2.4 2.5
MICROMETRES
17/8/83 MT1/851/2 W
e
LOG RESIDUAL
.054
.031
.008
-.018
-.039
-.062
-.086
-.109
-.132
2.0 2.1 2.2 2.3 2.4 2.5
MICROMETRES
22-8-83 MT4/47/1 W
f
LOG RESIDUAL
.270
.241
.212
.183
.154
.125
.096
.067
.038
2.0 2.1 2.2 2.3 2.4 2.5
MICROMETRES

Figures 5.26a-d 'Log residual' spectra calculated from various mixtures of SWIR laboratory reflectance spectra.

Figures 5.26a&b are synthetic 'log residual' spectra of 1:1 mixtures of vegetation with the average muscovitic, and the average sericitic, spectra respectively.

Figures 5.26c&d are the equivalent synthetic 'log residuals' for 1:1.5 mixtures.

Note that both the sericite + vegetation log residuals have a 2.35μm feature, and minima at 2.2μm. Corresponding muscovite + vegetation log residuals still have positive 2.2μm features (maxima) because they do not absorb strongly enough to overcome the effect of mixing with vegetation.

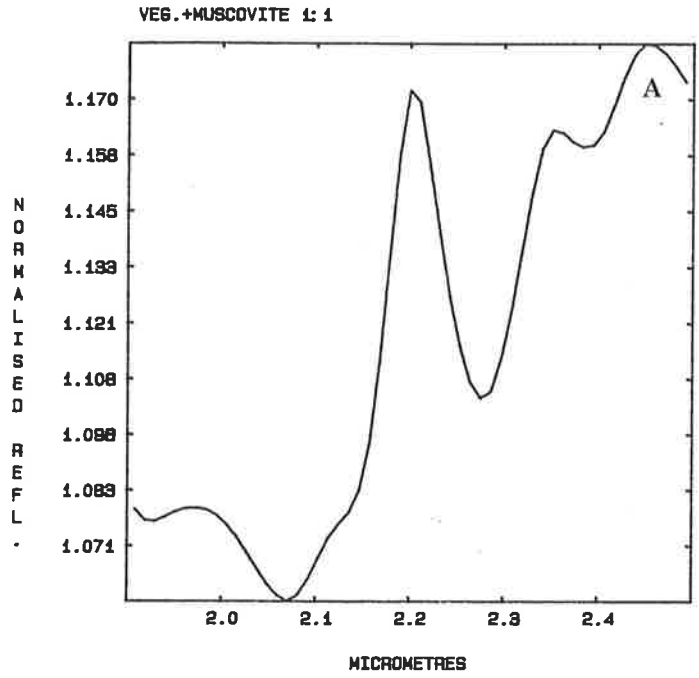
VEG.+MUSCOVITE 1: 1
A
1.170
1.158
1.145
1.133
1.121
1.108
1.096
1.083
1.071
NORMALISED REFL.
2.0
2.1
2.2
2.3
2.4
MICROMETRES

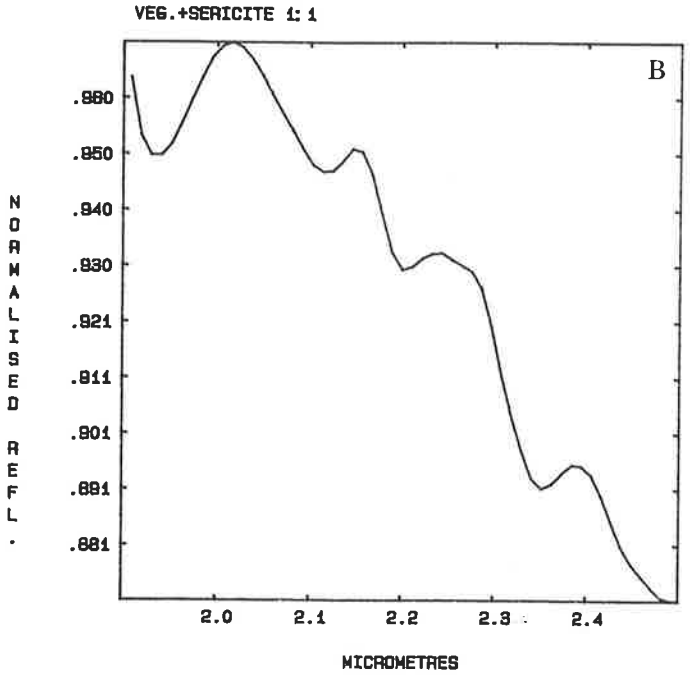
VEG.+SERICITE 1: 1
B
.960
.950
.940
.930
.921
.911
.901
.891
.881
NORMALISED REFL.
2.0
2.1
2.2
2.3
2.4
MICROMETRES

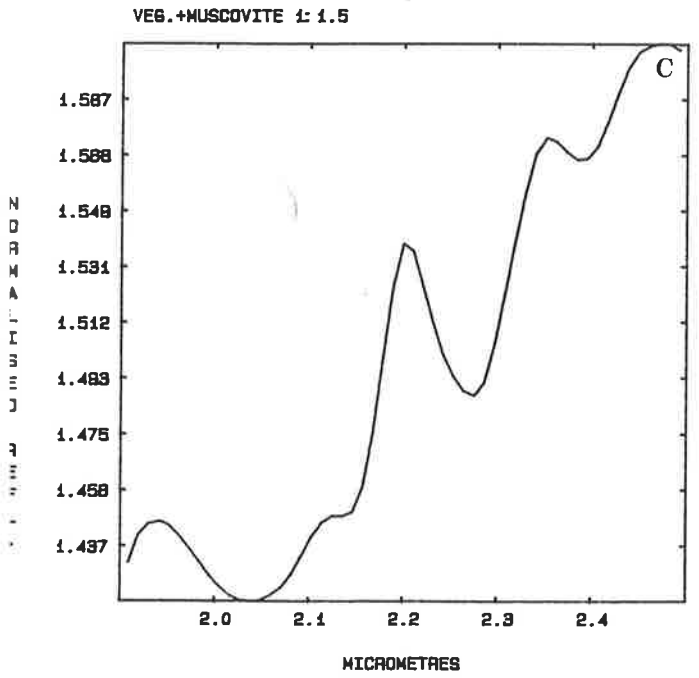
VEG.+MUSCOVITE 1: 1.5
C
1.587
1.568
1.549
1.531
1.512
1.493
1.475
1.456
1.437
NORMALISED REFL.
2.0
2.1
2.2
2.3
2.4
MICROMETRES

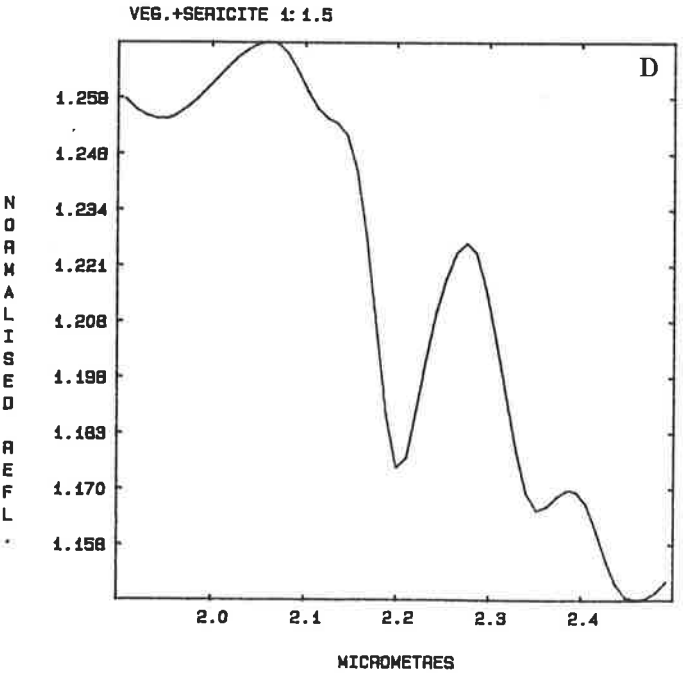
VEG.+SERICITE 1: 1.5
D
1.259
1.246
1.234
1.221
1.208
1.196
1.183
1.170
1.158
NORMALISED REFL.
2.0
2.1
2.2
2.3
2.4
MICROMETRES

Figures 5.27a&b Airborne SWIR log residual and laboratory reflectance spectra of talc-rich soil from line MT8.

Figure 5.27a is the airborne spectrum of a talc-rich soil (flight line MT8, samples 447-450).

Figure 5.27b is the laboratory spectrum of a representative field sample from pixel 448 on line MT8.

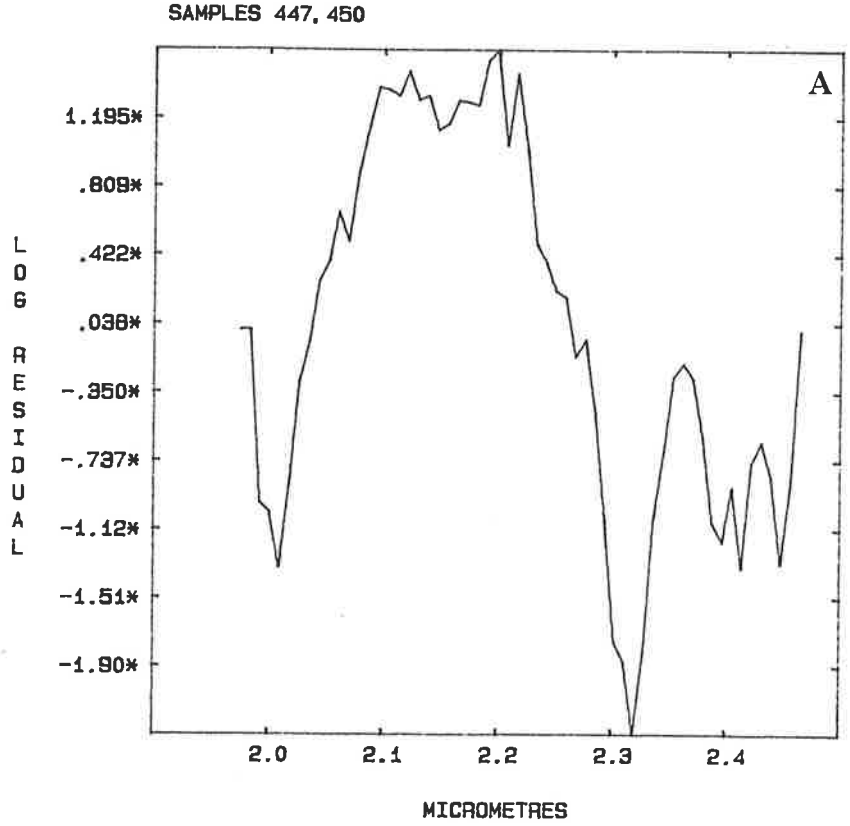
SAMPLES 447, 450
A
1.195*
.809*
.422*
.038*
-.350*
-.737*
-1.12*
-1.51*
-1.90*
LOG RESIDUAL
2.0
2.1
2.2
2.3
2.4
MICROMETRES

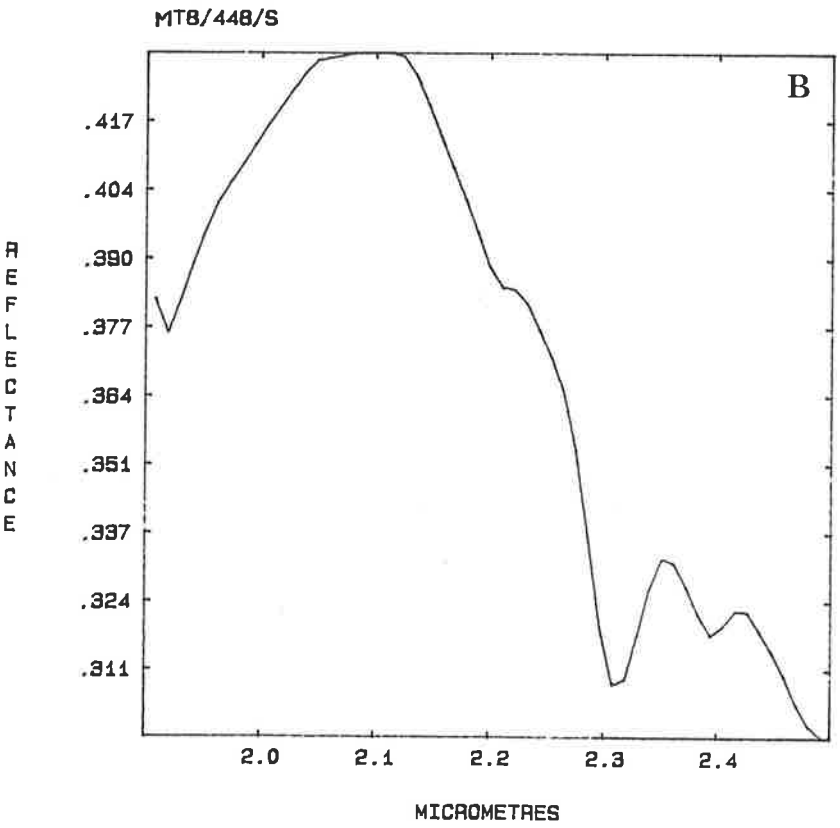
MT8/448/S
B
.417
.404
.390
.377
.364
.351
.337
.324
.311
REFLECTANCE
2.0
2.1
2.2
2.3
2.4
MICROMETRES

Figure 5.28 Airborne SWIR log residual spectrum of line MT10, pixels 347-349.

This spectrum is extremely noisy, and there is no sign of any absorption feature that could be attributed to the presence of topaz.

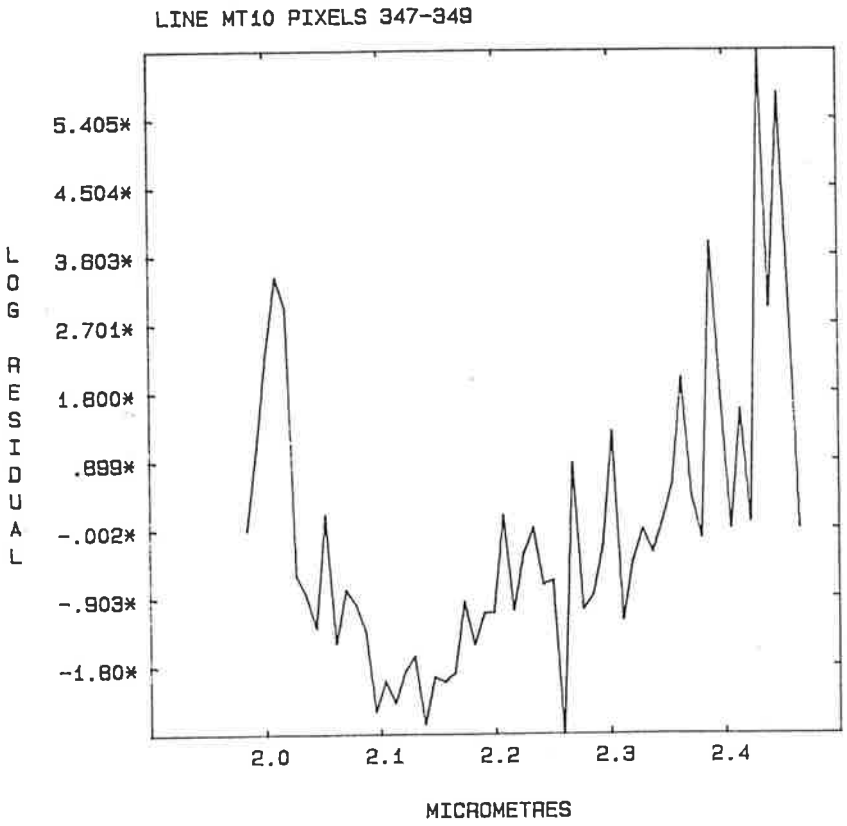
LINE MT10 PIXELS 347-349
5.405*
4.504*
3.603*
2.701*
1.800*
.899*
-.002*
-.903*
-1.80*
LOG RESIDUAL
2.0
2.1
2.2
2.3
2.4
MICROMETRES

Figures 5.29a&b SWIR laboratory reflectance spectra of weathered and fresh surfaces of topaz-rich sample.

Figure 5.29a is the laboratory spectrum of a weathered surface of a rock containing between 5% and 20% topaz.

Figure 5.29b is the laboratory spectrum of a fresh surface of the same sample. Note that sericite-type features are present in the spectrum as well as the sharp 2.1μm absorption due to topaz.

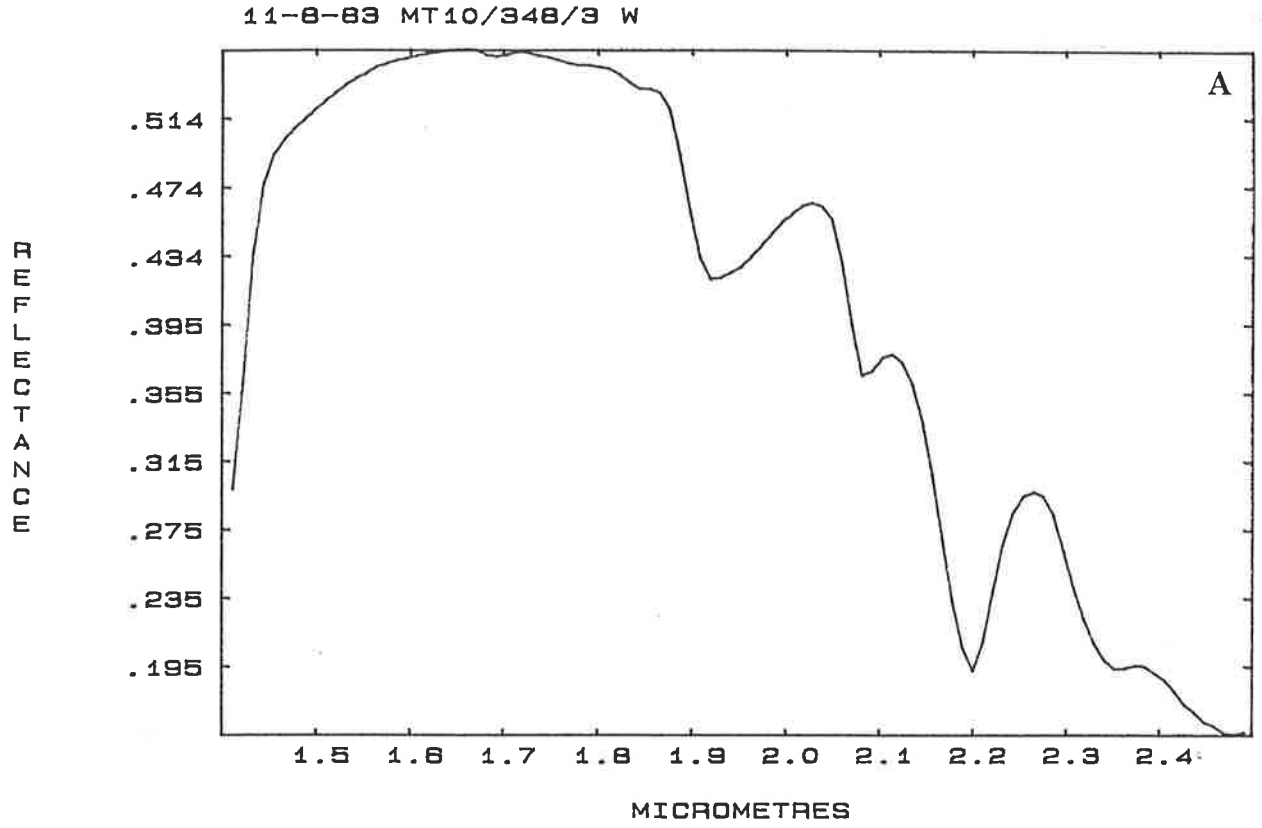
11-8-83 MT10/348/3 W
A
.514
.474
.434
.395
.355
.315
.275
.235
.195
REFLECTANCE
1.5 1.6 1.7 1.8 1.9 2.0 2.1 2.2 2.3 2.4
MICROMETRES

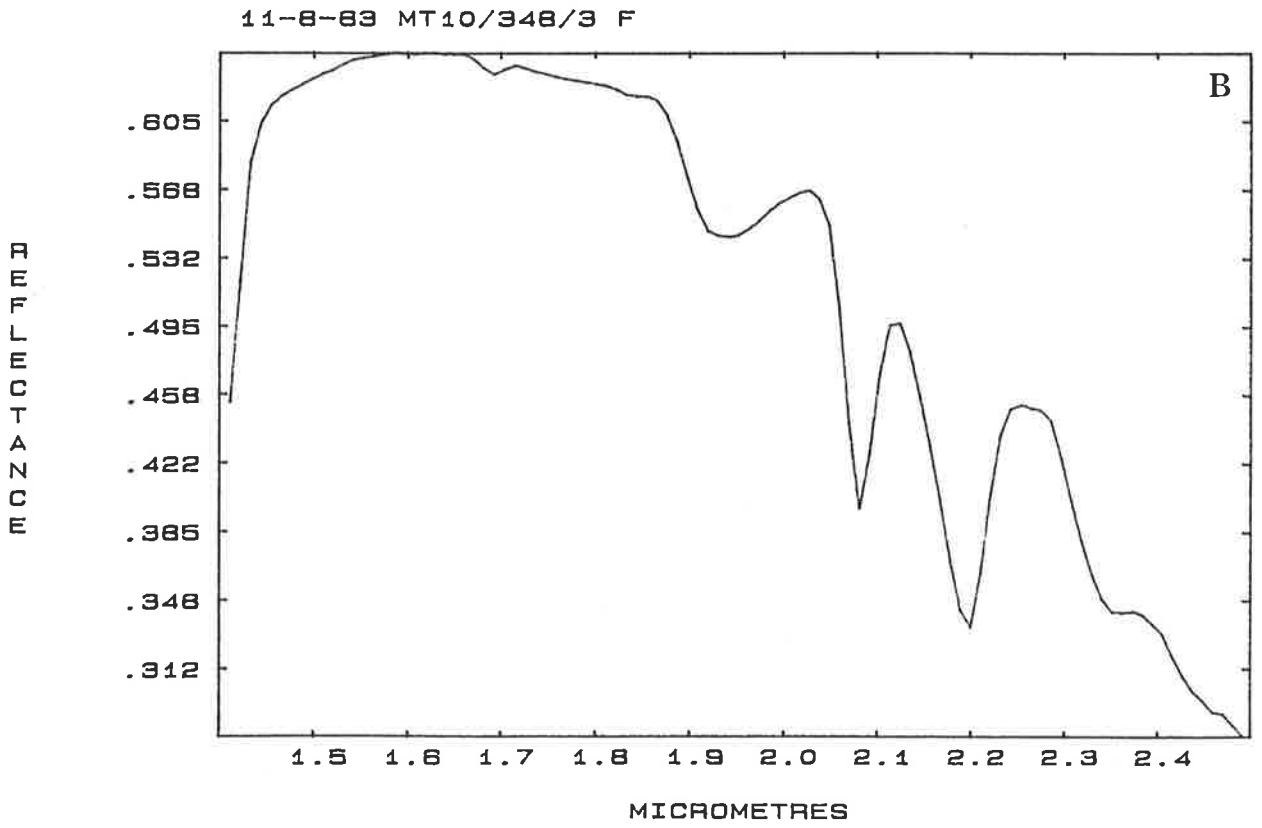
11-8-83 MT10/348/3 F
B
.605
.568
.532
.495
.458
.422
.385
.348
.312
REFLECTANCE
1.5 1.6 1.7 1.8 1.9 2.0 2.1 2.2 2.3 2.4
MICROMETRES

Figure 5.30 Field spectra of altered and unaltered rocks from Silver Bell, Arizona (after Abrams and Brown, 1985).

Note that absorption features at all wavelengths are either much weaker, or entirely absent, in unaltered equivalents of the altered rocks. Spectra were acquired *in situ* using the Jet Propulsion Laboratory's Portable Field Reflectance Spectrometer (PFRS).

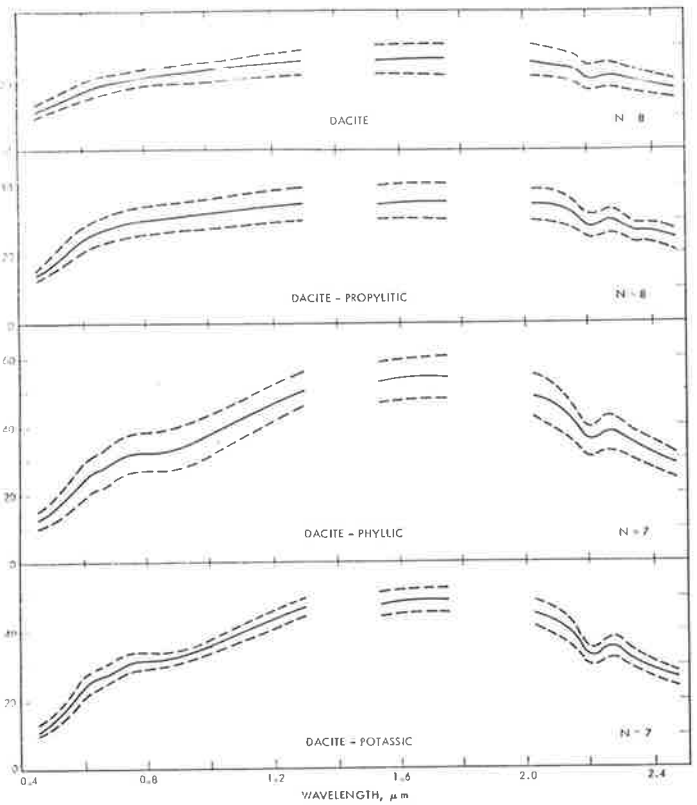
DACITE
N = 8
DACITE - PROPYLITIC
N = 8
DACITE - PHYLLIC
N = 7
DACITE - POTASSIC
N = 7
WAVELENGTH, μm

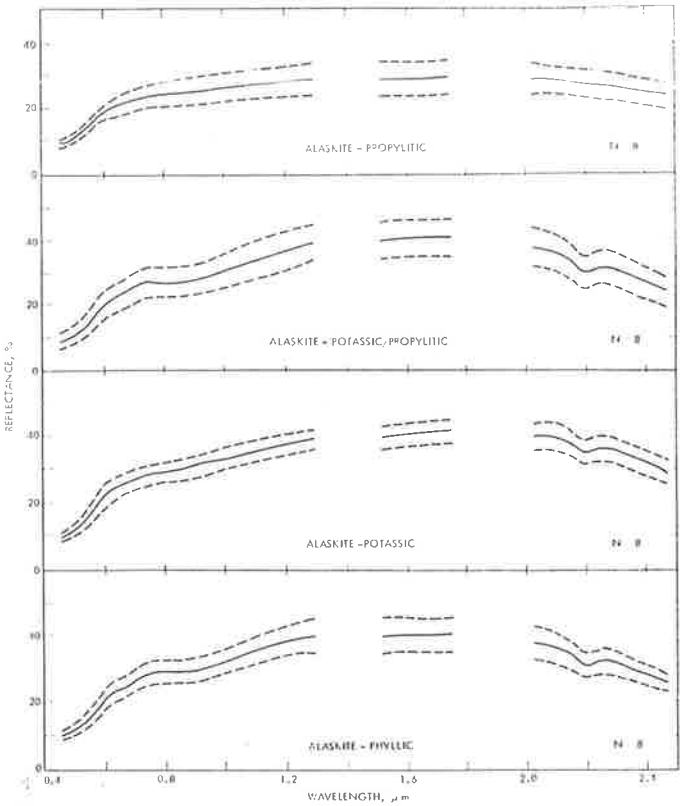
ALASKITE - PROPYLITIC
ALASKITE - POTASSIC/PROPYLITIC
N = 8
ALASKITE -POTASSIC
N = 8
ALASKITE - PHYLLIC
N = 8
REFLECTANCE, %
WAVELENGTH, μm

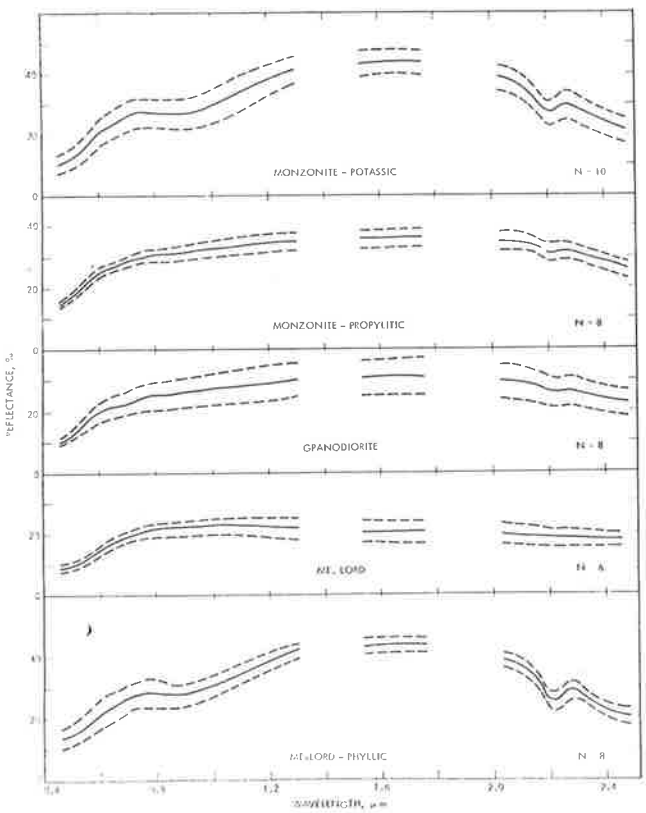
MONZONITE - POTASSIC
N = 10
MONZONITE - PROPYLITIC
N = 8
GRANODIORITE
N = 8
MELORD
N = 6
MELORD - PHYLLIC
N = 8
REFLECTANCE, %

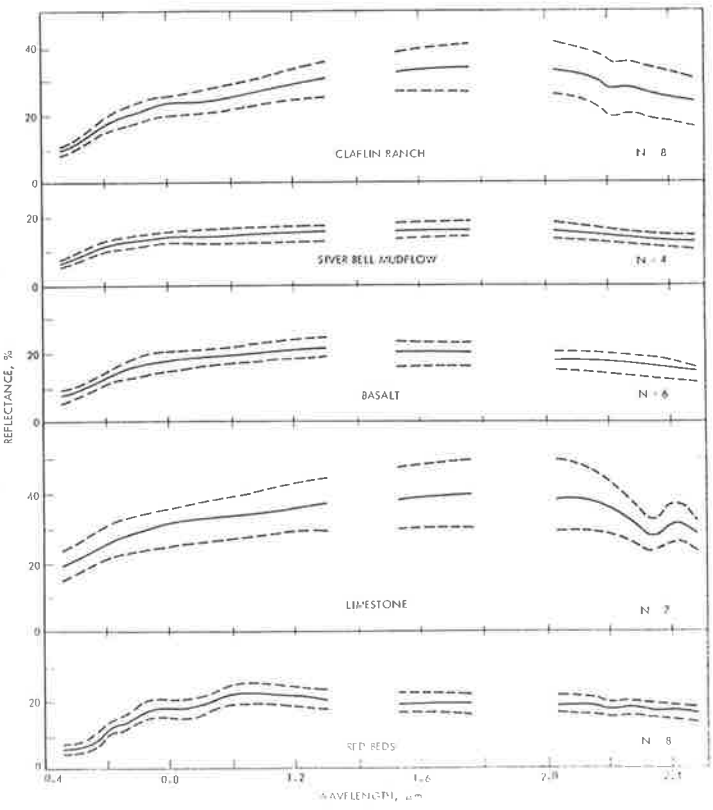
CLAFLIN RANCH
N = 8
SILVER BELL MUDFLOW
N = 4
BASALT
N = 6
LIMESTONE
N = 7
RED BEDS
N = 8
REFLECTANCE, %

Figure 6.1 Kambalda area geology and flight line locations (modified after Gresham and Loftus-Hills, 1981).

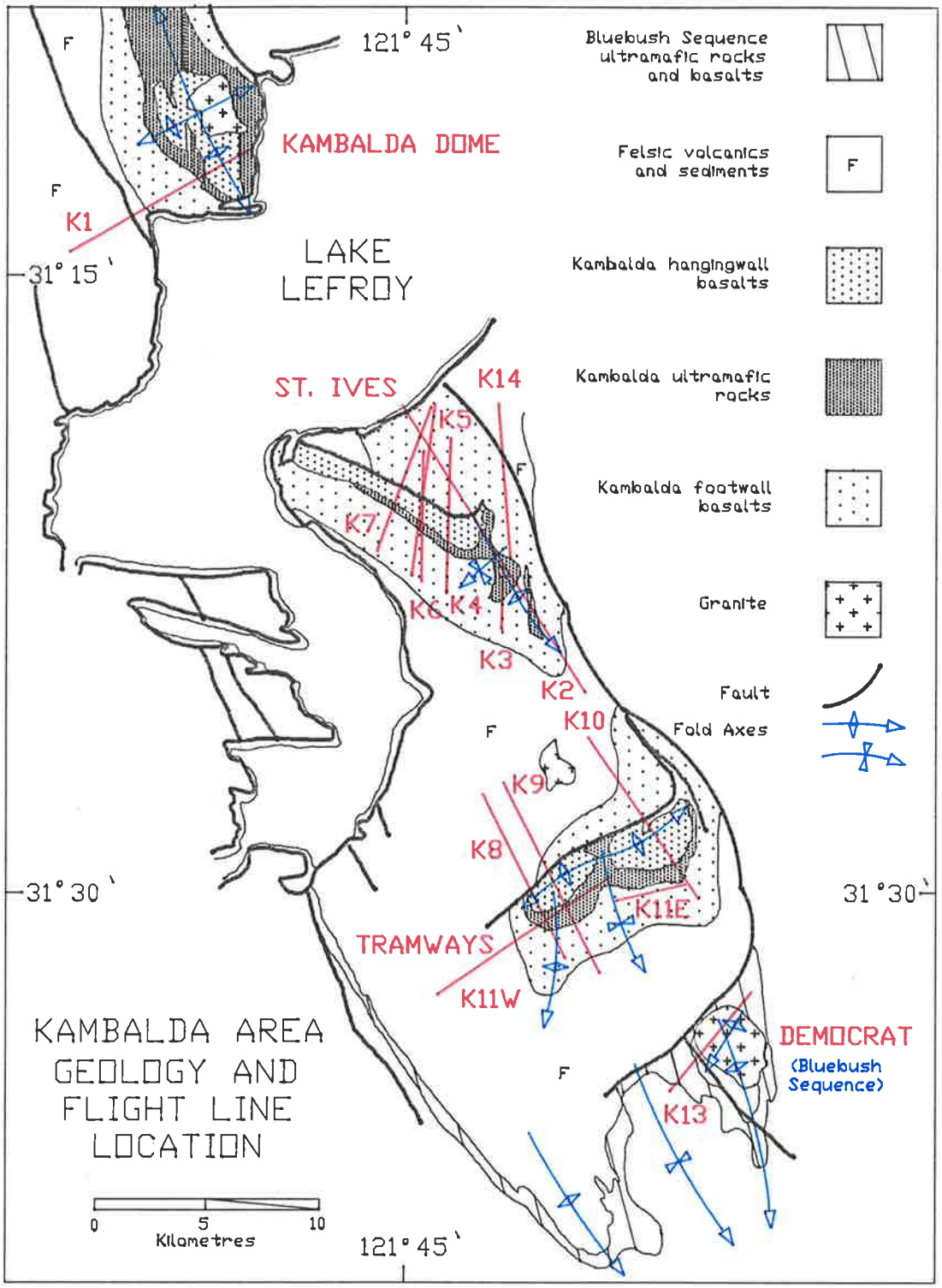
121° 45'
31° 15'
31° 30'
KAMBALDA DOME
LAKE LEFROY
ST. IVES
TRAMWAYS
DEMOCRAT
(Bluebush Sequence)
K1
K2
K3
K4
K5
K6
K7
K8
K9
K10
K11E
K11W
K13
K14
F
Bluebush Sequence ultramafic rocks and basalts
Felsic volcanics and sediments
Kambalda hangingwall basalts
Kambalda ultramafic rocks
Kambalda footwall basalts
Granite
Fault
Fold Axes
KAMBALDA AREA GEOLOGY AND FLIGHT LINE LOCATION
0
5
10
Kilometres

Figures 6.2a-c Photograph and SWIR laboratory reflectance spectra of weathered and fresh surfaces of a basalt sample from Kambalda.

Figure 6.2a is a hand specimen of basalt with weathering rind.

Figure 6.2b is the spectrum of the weathered surface of the sample shown in Fig. 6.2a. Spectral features are those of amphibole and chlorite (responsible for the position of the major feature).

Figure 6.2c is the spectrum of the "fresh" surface of sample shown in Fig. 6.2a. Note the similarity to the 'weathered' spectrum. The 2.0μm feature in this spectrum is due to chlorite.

A

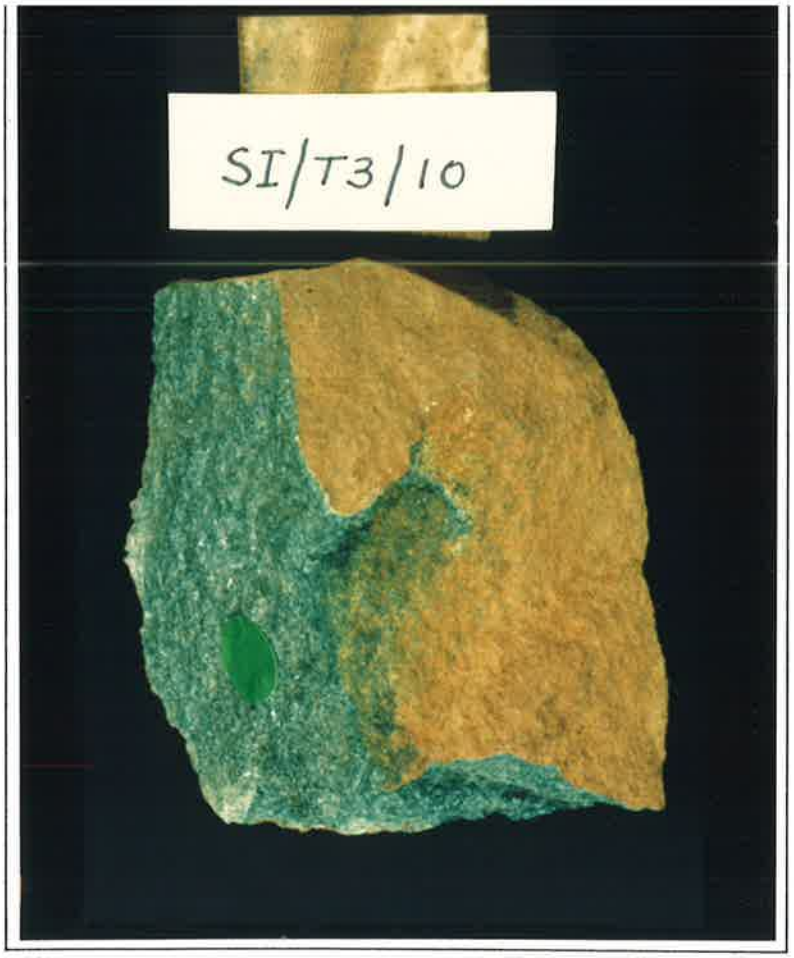
SI/T3/10

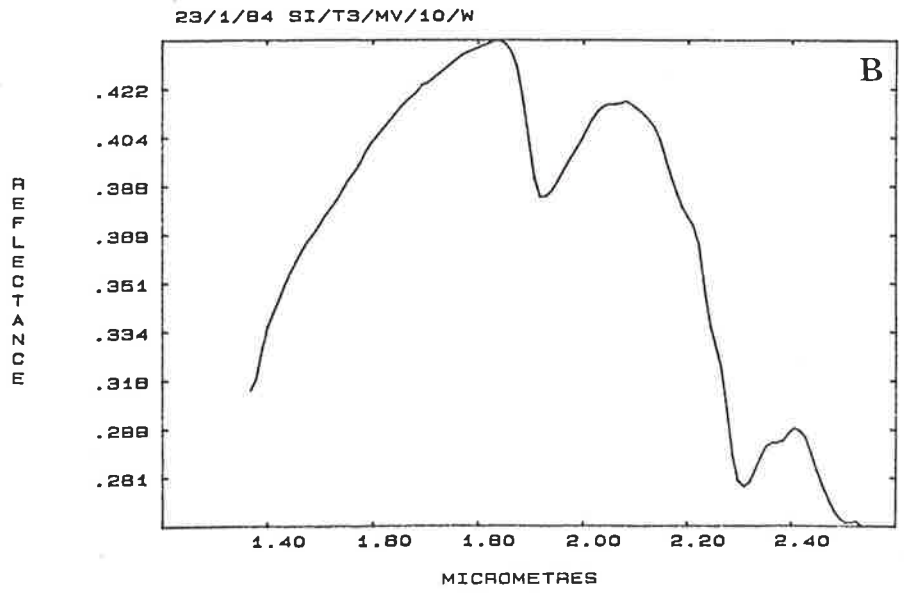
23/1/84 SI/T3/MV/10/W
B
REFLECTANCE
.422
.404
.388
.369
.351
.334
.318
.288
.281
1.40
1.60
1.80
2.00
2.20
2.40
MICROMETRES

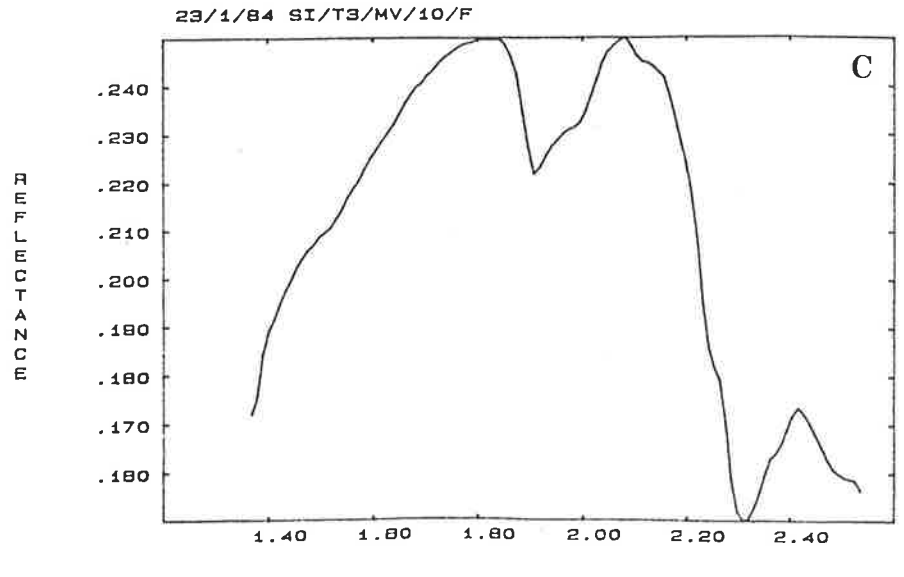
23/1/84 SI/T3/MV/10/F
C
REFLECTANCE
.240
.230
.220
.210
.200
.190
.180
.170
.180
1.40
1.60
1.80
2.00
2.20
2.40

Figures 6.3a&b Photograph and SWIR laboratory reflectance spectrum of a lichen-covered soil from Kambalda.

Figure 6.3a shows the lichen 'crust' and, to the left, the soil beneath the lichen.

Figure 6.3b is the spectrum of soil-lichen showing kaolin absorption features. Familiar 2.1 and 2.3μm absorption features typical of dry vegetation are caused by the lichen. Fine kaolin on the surface is also contributing to the spectrum with a 2.17 and 2.208μm doublet.

A

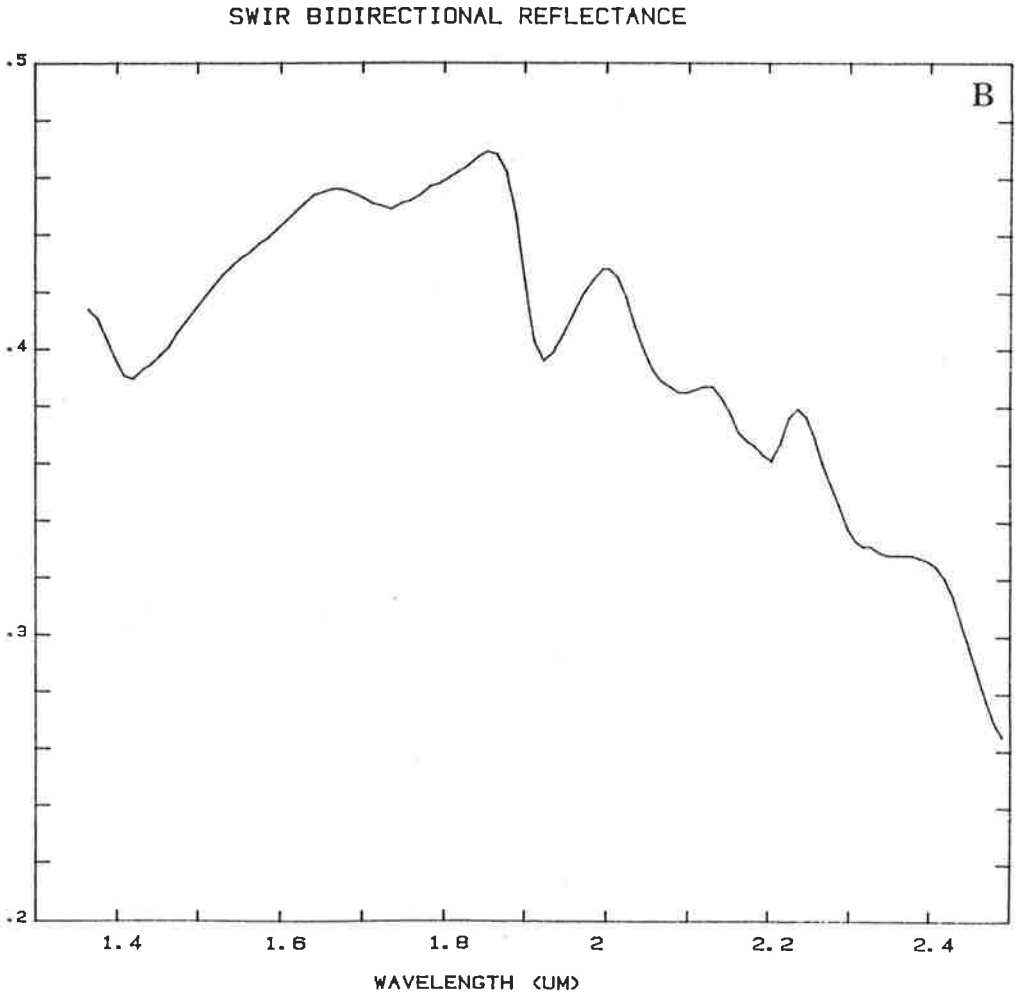
SWIR BIDIRECTIONAL REFLECTANCE
.5
.4
.3
.2
1.4
1.6
1.8
2
2.2
2.4
WAVELENGTH (UM)

B

Figure 6.4 Flat SWIR laboratory reflectance spectrum from Kambalda.

The dark colour of the sample, and a lack of strongly absorbing minerals results in a flat, noisy spectrum.

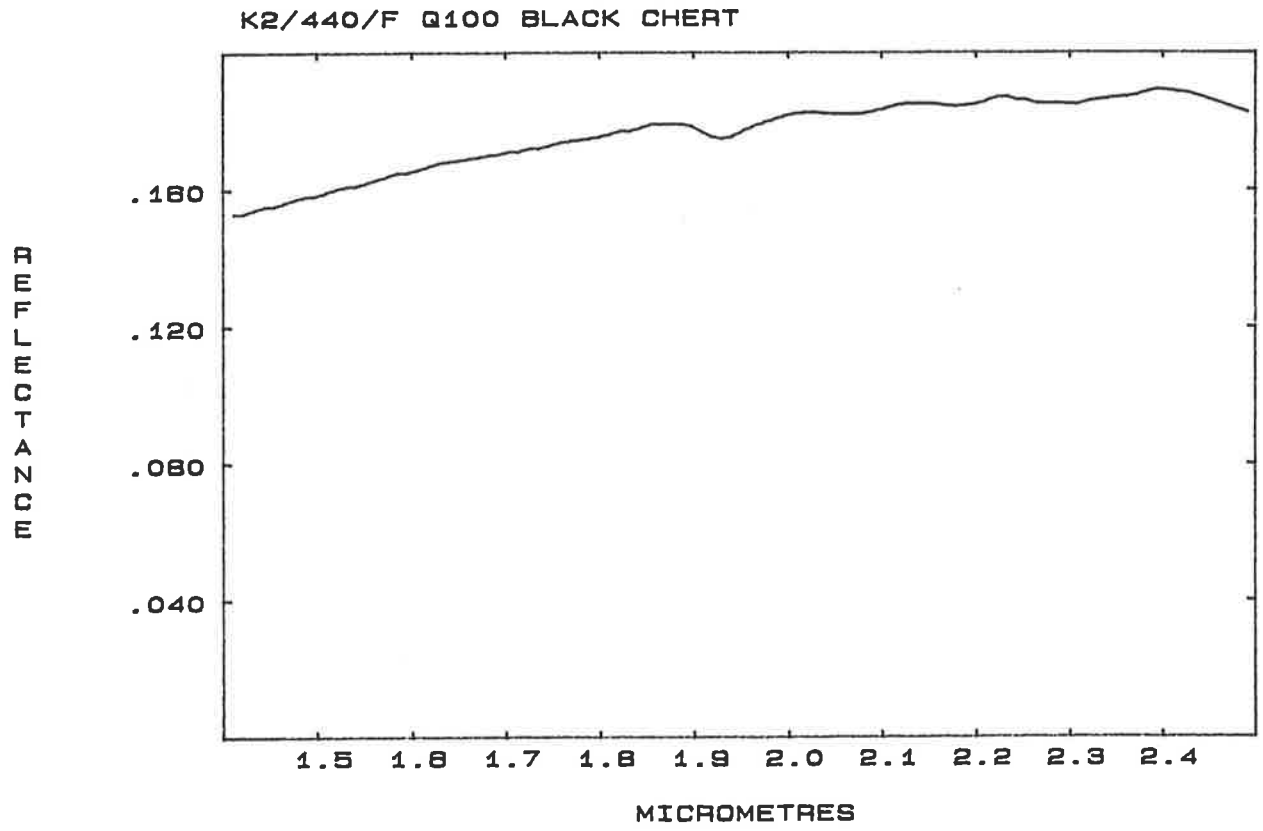
K2/440/F Q100 BLACK CHERT
REFLECTANCE
.160
.120
.080
.040
1.5
1.6
1.7
1.8
1.9
2.0
2.1
2.2
2.3
2.4
MICROMETRES

Figures 6.5a-c SWIR laboratory reflectance spectra of samples with varying quartz content from Kambalda.

Figure 6.5a has moderate 1.9μm (water) absorption, while Figs. 6.5b&c have strong and very strong 1.9μm (water) absorption features, respectively.The strength of these features is correlated with the percentage of quartz in the samples (see plot titles).

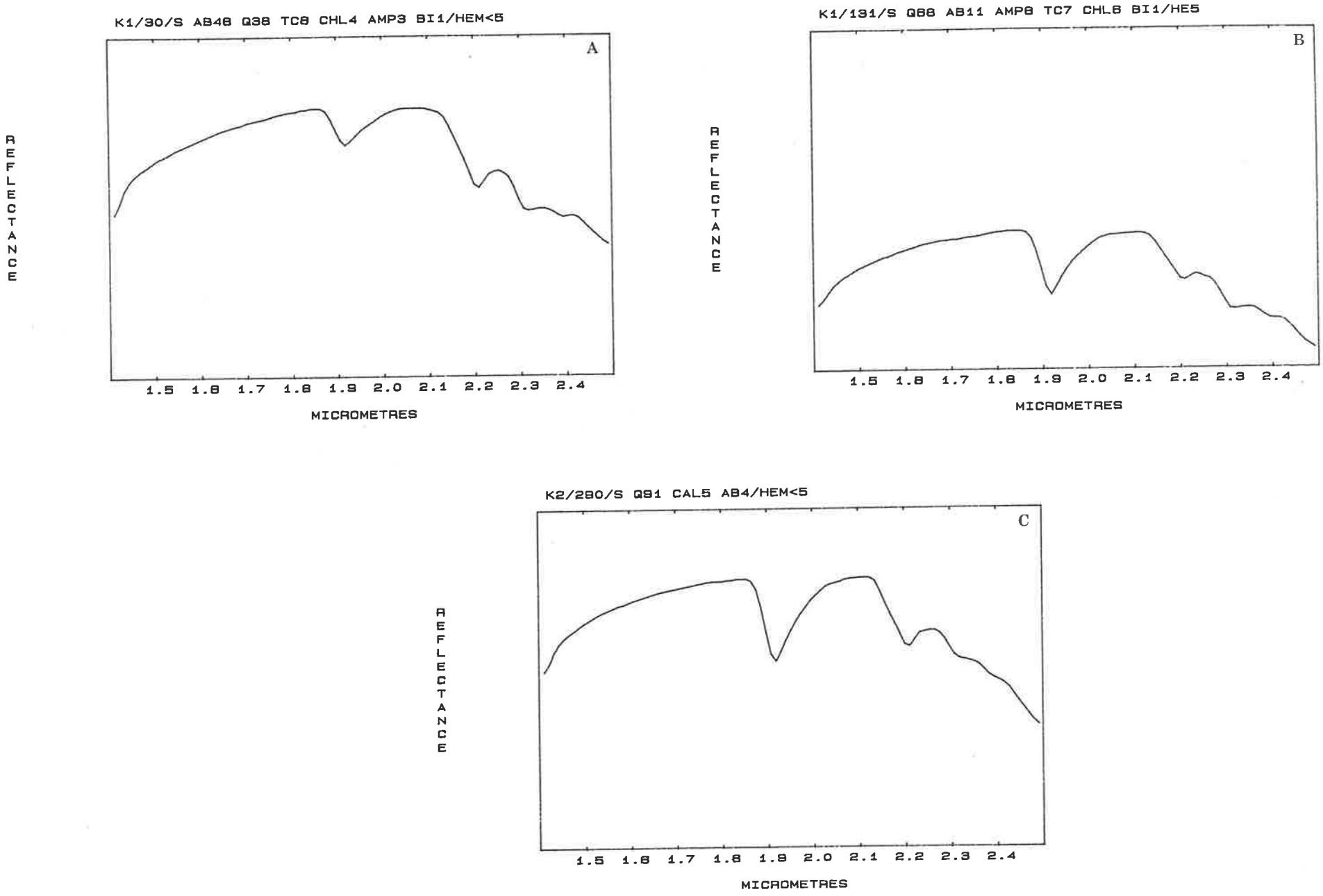
K1/30/S AB48 Q38 TC8 CHL4 AMP3 BI1/HEM<5
A
REFLECTANCE
1.5 1.6 1.7 1.8 1.9 2.0 2.1 2.2 2.3 2.4
MICROMETRES
K1/131/S Q68 AB11 AMP8 TC7 CHL6 BI1/HE5
B
REFLECTANCE
1.5 1.6 1.7 1.8 1.9 2.0 2.1 2.2 2.3 2.4
MICROMETRES
K2/290/S Q91 CAL5 AB4/HEM<5
C
REFLECTANCE
1.5 1.6 1.7 1.8 1.9 2.0 2.1 2.2 2.3 2.4
MICROMETRES

Figures 6.6a&b SWIR laboratory reflectance spectra of kaolin-bearing samples from Kambalda.

Kaolin's 2.17μm absorption feature is generally only well developed where kaolin crystallinity is high. At Kambalda, the 2.17μm feature usually only causes an asymmetry in the major absorption feature. There are many cases at Kambalda where weak 2.2μm absorption features appear in the spectrum, but no mineral which absorbs in that region is detected by XRD. Where 2.2μm features are strongest, the characteristic kaolin shape is seen. Figure 6.6a depicts one example of a stronger kaolin spectrum, while Fig. 6.6b depicts a spectrum where the mineralogy cannot be accurately determined, but is likely to be kaolin.

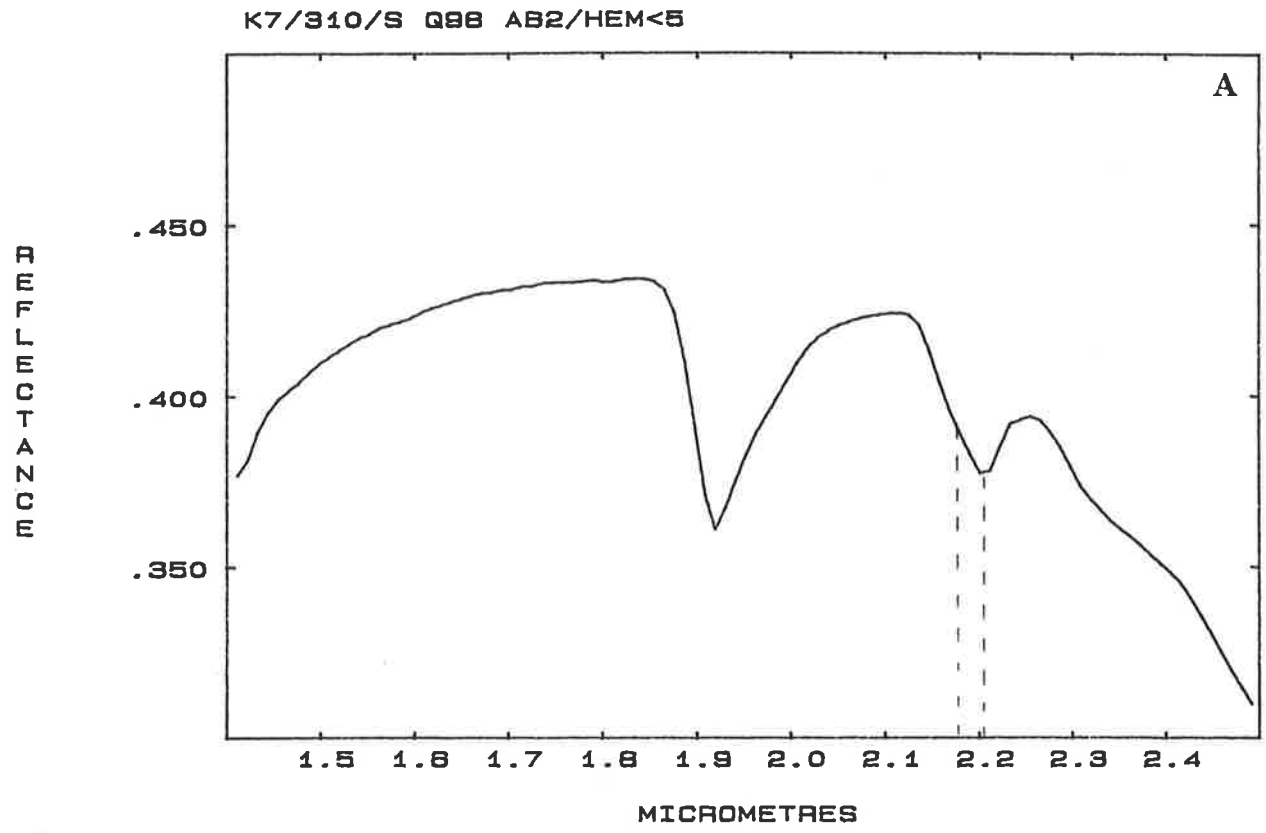
K7/310/S Q98 AB2/HEM<5
A
.450
.400
.350
REFLECTANCE
1.5 1.6 1.7 1.8 1.9 2.0 2.1 2.2 2.3 2.4
MICROMETRES

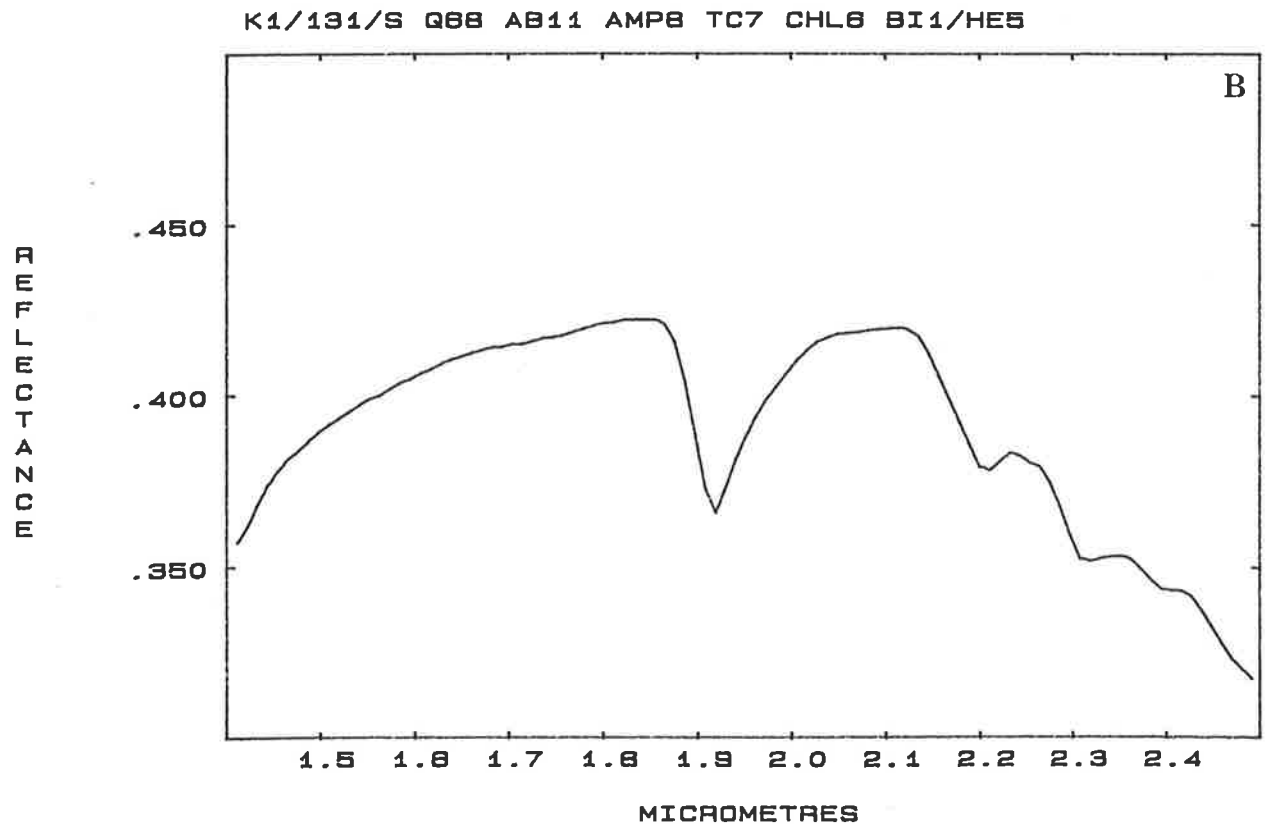
K1/131/S Q88 AB11 AMP8 TC7 CHL6 BI1/HE5
B
.450
.400
.350
REFLECTANCE
1.5 1.6 1.7 1.8 1.9 2.0 2.1 2.2 2.3 2.4
MICROMETRES

Figures 6.7a&b SWIR laboratory reflectance spectra of intact and powdered calcrete nodules from Kambalda.

Figure 6.7a depicts the spectrum of calcrete nodules showing kaolin spectral features. The failure of XRD analysis to detect kaolin is attributed to its poorly crystalline form. Al-OH bonds are still present, however, and this is sufficient to produce the observed absorption features.

Figure 6.7b is the spectrum of the same calcrete in powdered form, showing kaolin and calcite absorption features. The presence of calcite features in the crushed sample suggests that their absence in Fig. 6.7a is a surface phenomenon.

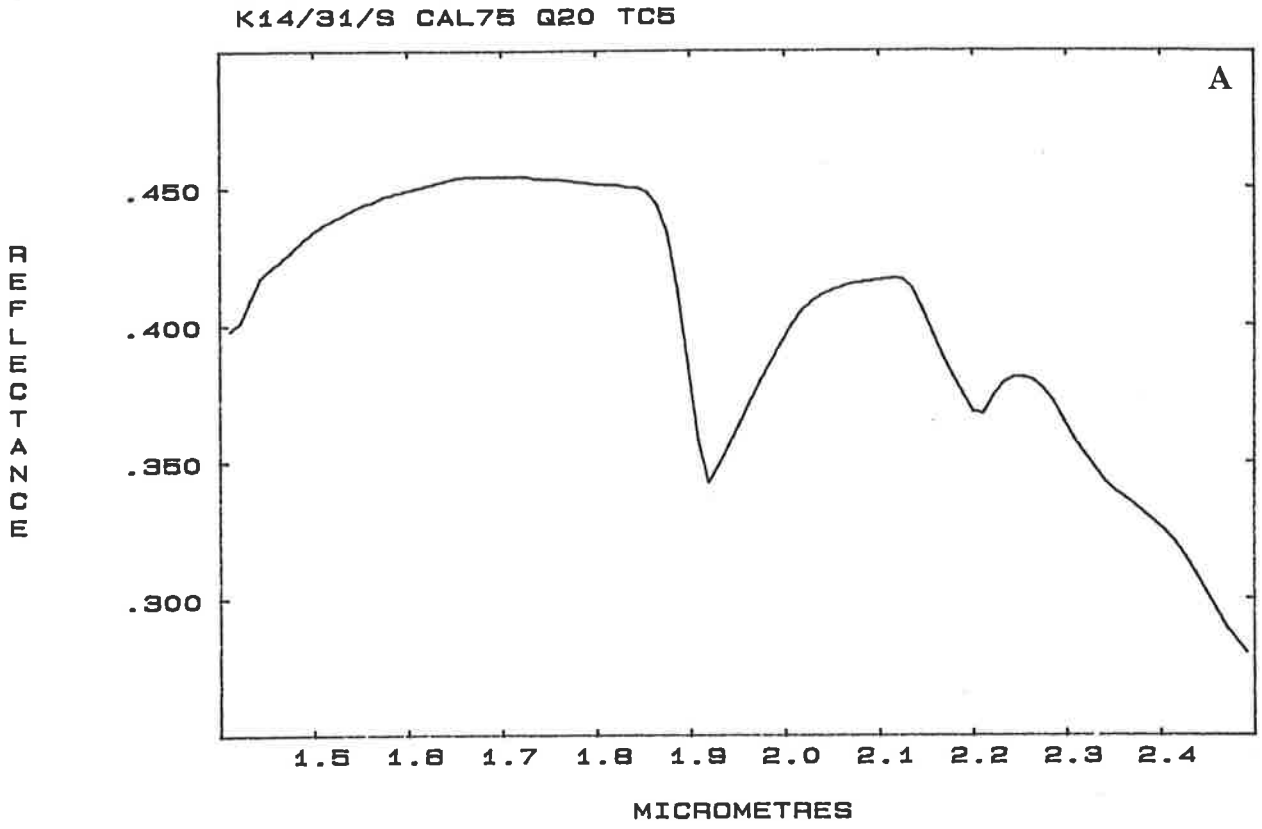
K14/31/S CAL75 Q20 TC5
A
REFLECTANCE
.450
.400
.350
.300
1.5 1.6 1.7 1.8 1.9 2.0 2.1 2.2 2.3 2.4
MICROMETRES

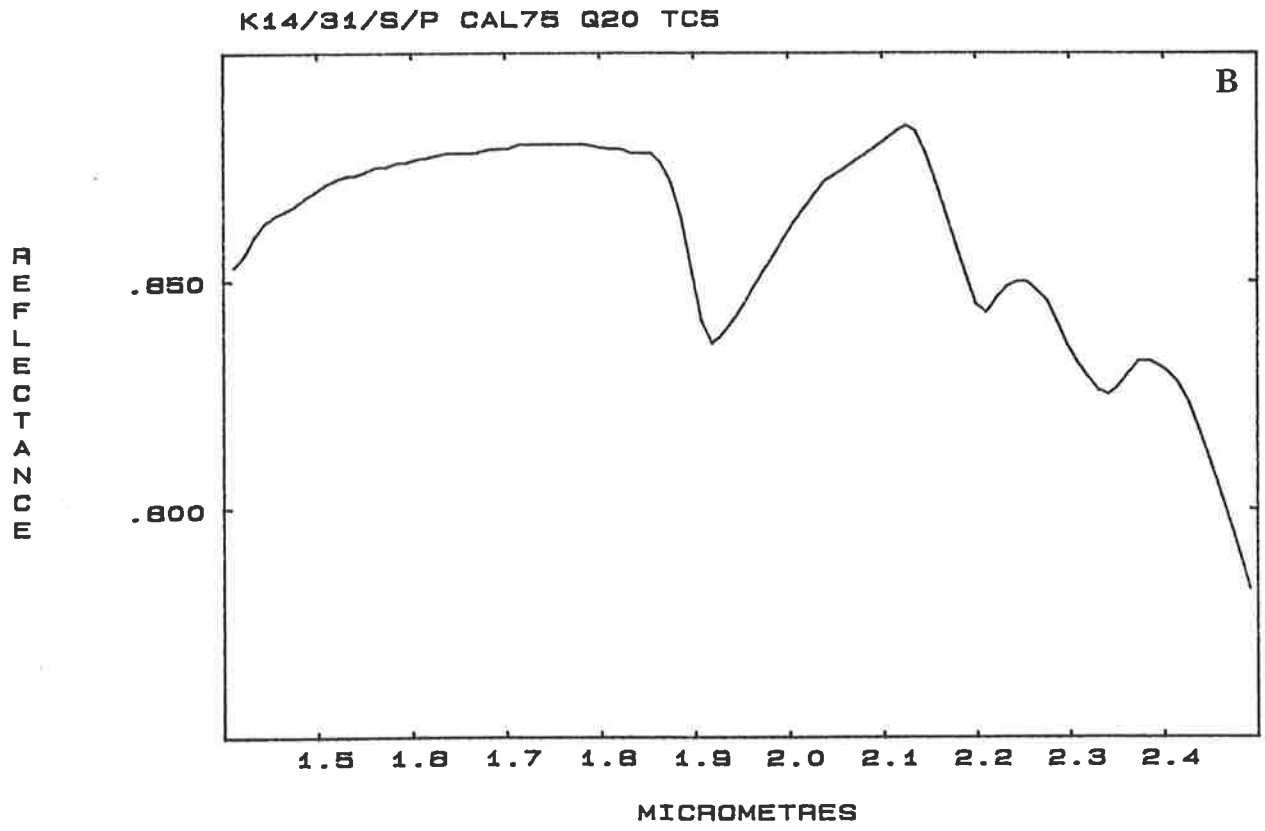
K14/31/S/P CAL75 Q20 TC5
B
REFLECTANCE
.850
.800
1.5 1.6 1.7 1.8 1.9 2.0 2.1 2.2 2.3 2.4
MICROMETRES

Figures 6.8a-c SWIR laboratory reflectance spectra of talc-bearing samples from Kambalda.

Talc absorption features can be detected even at low percentages (depending on the other minerals present and their percentages). Expansion of the y-axis scales would make the absorption features in Figs. 6.8b&c look stronger, but they are all presented at the same scale for comparison of their relative strengths.

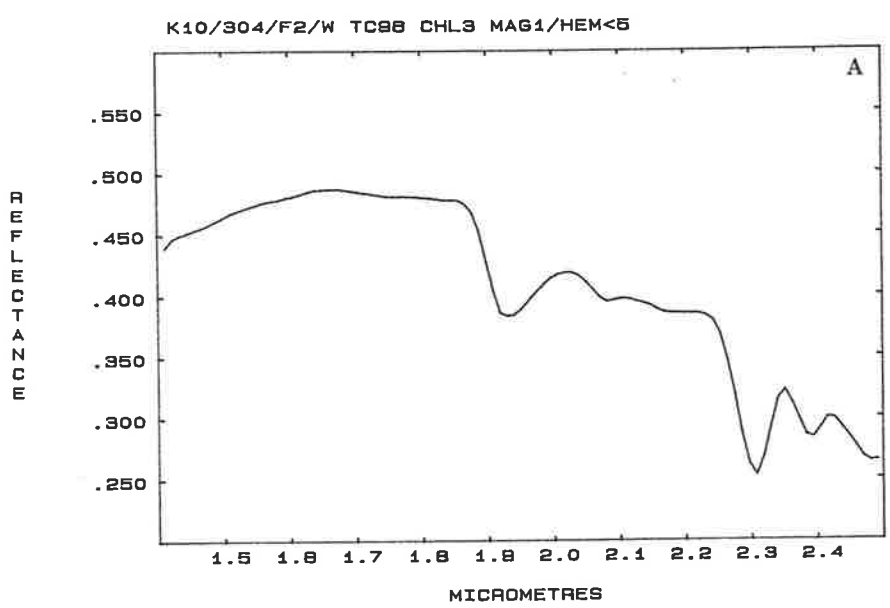
K10/304/F2/W TC98 CHL3 MAG1/HEM<5
A
REFLECTANCE
.550
.500
.450
.400
.350
.300
.250
1.5 1.6 1.7 1.8 1.9 2.0 2.1 2.2 2.3 2.4
MICROMETRES

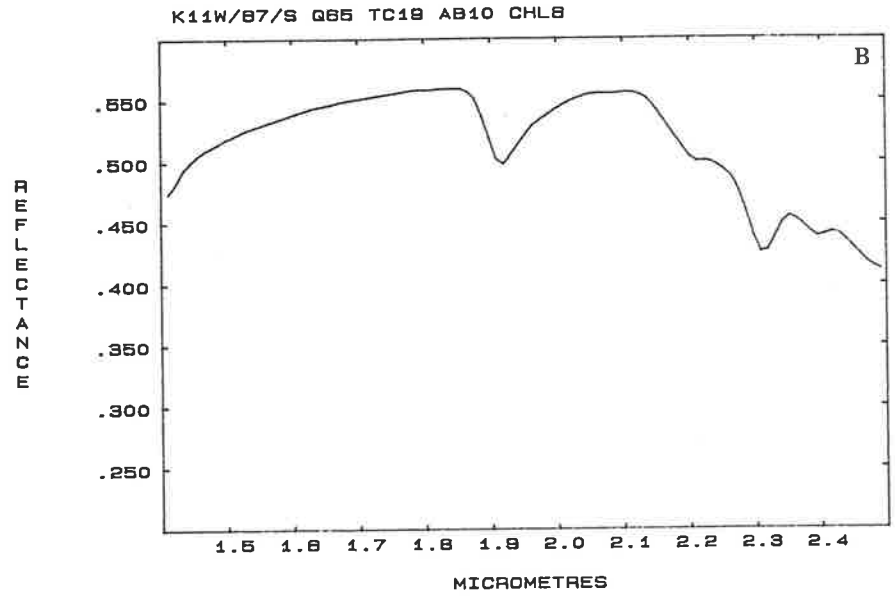
K11W/87/S Q65 TC19 AB10 CHL8
B
REFLECTANCE
.550
.500
.450
.400
.350
.300
.250
1.5 1.6 1.7 1.8 1.9 2.0 2.1 2.2 2.3 2.4
MICROMETRES

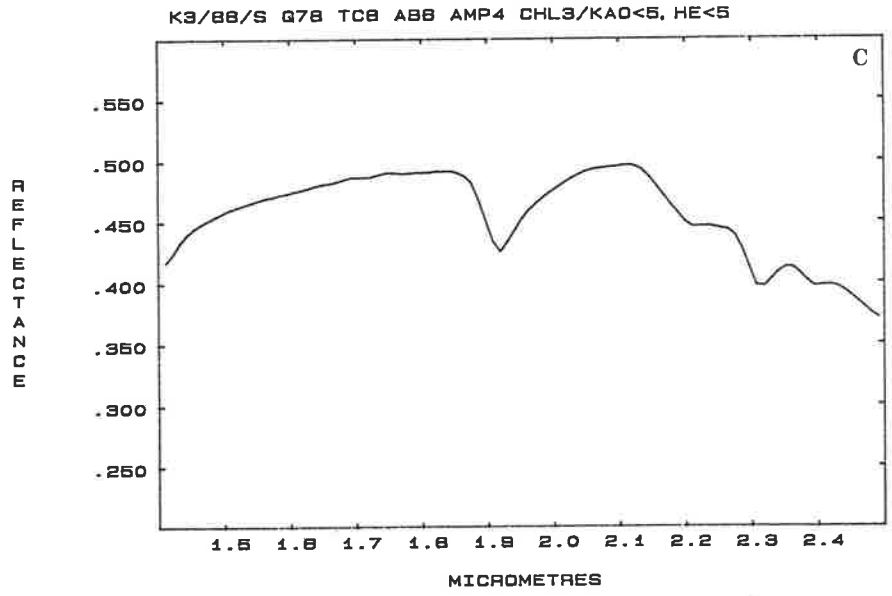
K3/88/S Q78 TC8 AB8 AMP4 CHL3/KAO<5, HE<5
C
REFLECTANCE
.550
.500
.450
.400
.350
.300
.250
1.5 1.6 1.7 1.8 1.9 2.0 2.1 2.2 2.3 2.4
MICROMETRES

Figures 6.9a&b SWIR laboratory reflectance spectra of chlorite- and amphibole-bearing samples from Kambalda.

The chlorite spectrum (Fig. 6.9a) has a more pronounced background curve than talc. Diagnostic absorption features are at 2.0μm (causing the asymmetry of the 1.9μm water absorption feature), 2.26 and 2.34μm.

Like chlorite, amphibole (Fig 6.9b) has a pronounced background curve. The asymmetry of the 1.9μm water absorption feature in this spectrum is caused by the presence of 7% chlorite. Amphibole's absorption features are at 2.32μm and a shoulder near 2.4μm, but in this case the spectrum shows a minimum at 2.33μm. This may be due to the influence of chlorite, which tends to absorb at wavelengths slightly longer than amphibole.

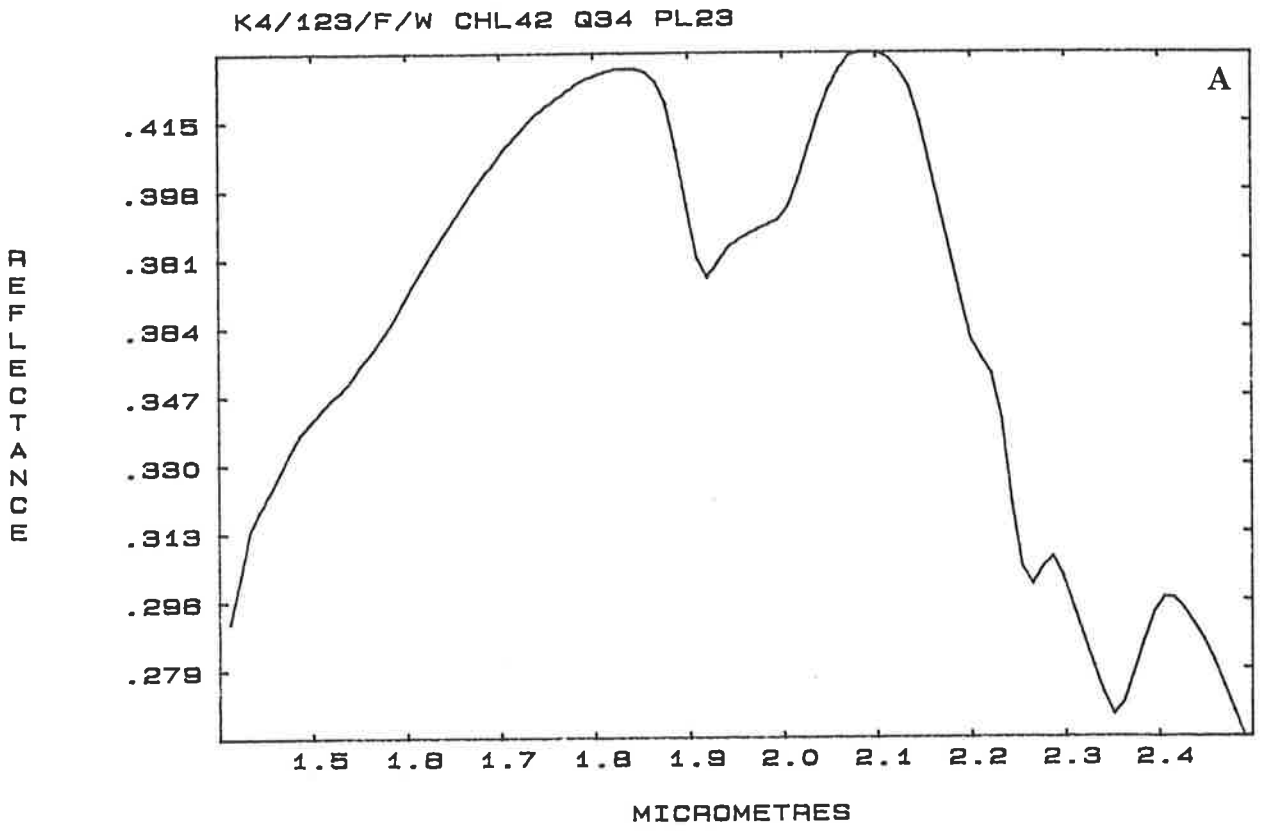
K4/123/F/W CHL42 Q34 PL23
A
.415
.398
.381
.364
.347
.330
.313
.296
.279
REFLECTANCE
1.5 1.6 1.7 1.8 1.9 2.0 2.1 2.2 2.3 2.4
MICROMETRES

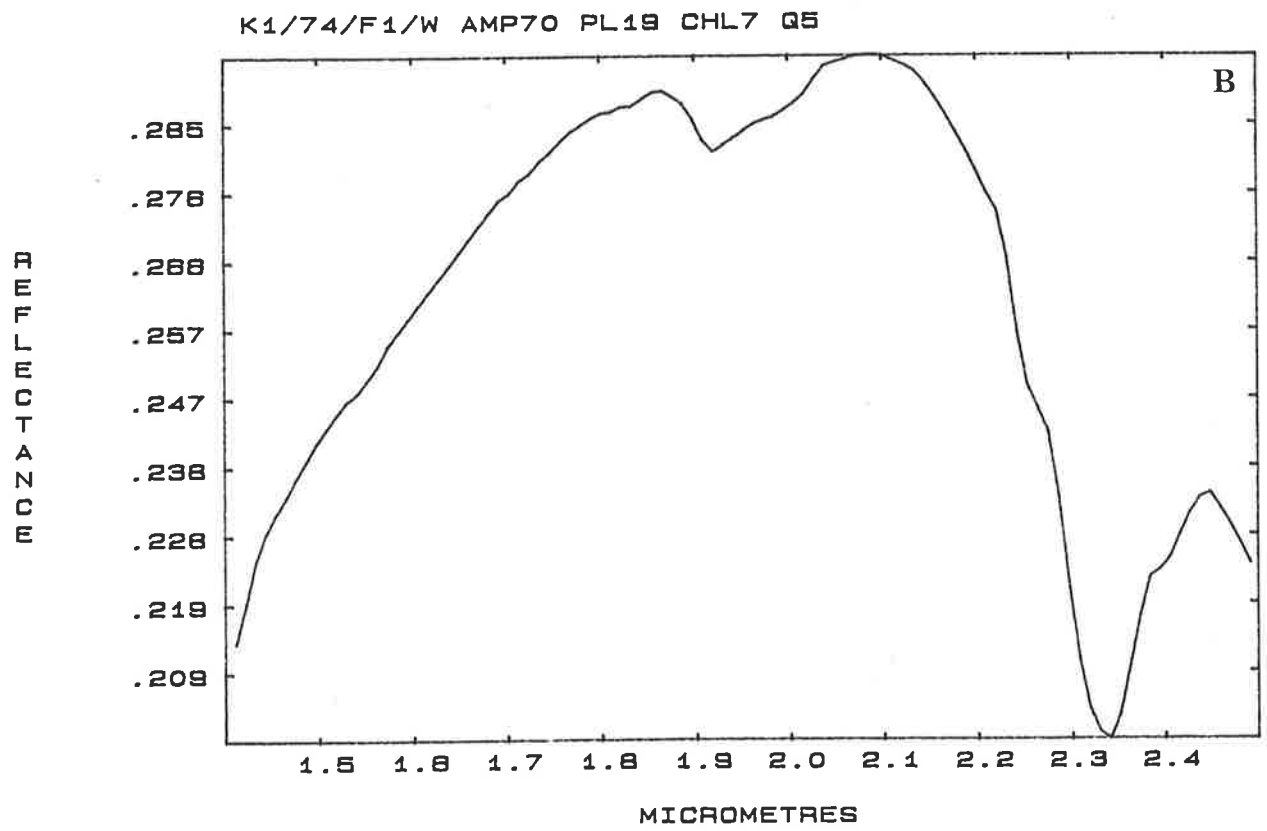
K1/74/F1/W AMP70 PL19 CHL7 Q5
B
.285
.276
.268
.257
.247
.238
.228
.219
.209
REFLECTANCE
1.5 1.6 1.7 1.8 1.9 2.0 2.1 2.2 2.3 2.4
MICROMETRES

Figures 6.10a-d SWIR laboratory reflectance spectra of typical mixtures from Kambalda.

The spectra shown in Figs. 6.10a&b, of an amphibole-chlorite-talc rock and a talc-chlorite rock, respectively, show that talc dominates the spectrum, even though (in the case of Fig. 6.10a) it forms the smallest proportion of the rock. Any contribution by amphibole to both spectra is swamped by the talc, but chlorite still produces an absorption feature at 2.0μm.

Figure 6.10c is the spectrum of an amphibole-chlorite rock powder. Most rocks containing almost equal amounts of amphibole and chlorite tend to have spectra dominated by chlorite, if their natural surfaces are measured. In some cases, powdered samples of the same material will produce spectra with slightly different characteristics. This spectrum appears to be dominated by effects due to amphibole.

Figure 6.10d is the spectrum of an amphibole-chlorite-epidote rock. The shape of this spectrum's major absorption feature is similar to those of both amphibole and epidote. The wavelength at which it occurs is 2.34μm, which is longer than normal for amphibole, suggesting a contribution from epidote. The 2.0μm absorption feature is due to chlorite, which may also be influencing the position of the major feature.

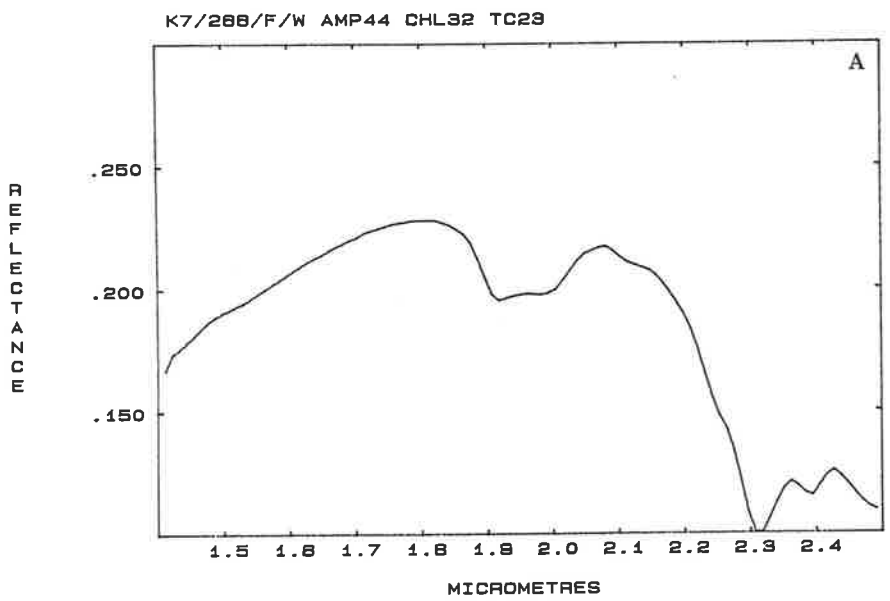
K7/288/F/W AMP44 CHL32 TC23
A
.250
.200
.150
REFLECTANCE
1.5 1.6 1.7 1.8 1.9 2.0 2.1 2.2 2.3 2.4
MICROMETRES

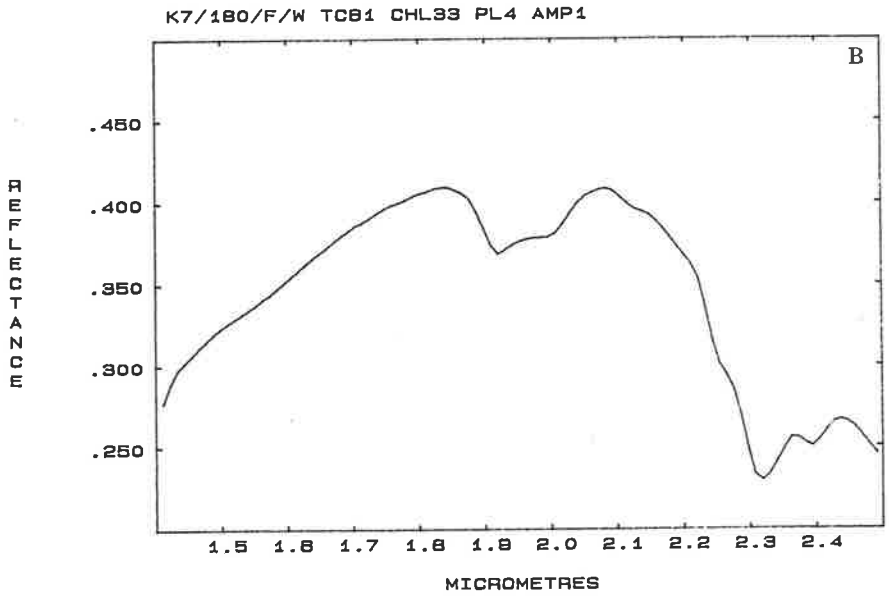
K7/180/F/W TC81 CHL33 PL4 AMP1
B
.450
.400
.350
.300
.250
REFLECTANCE
1.5 1.6 1.7 1.8 1.9 2.0 2.1 2.2 2.3 2.4
MICROMETRES

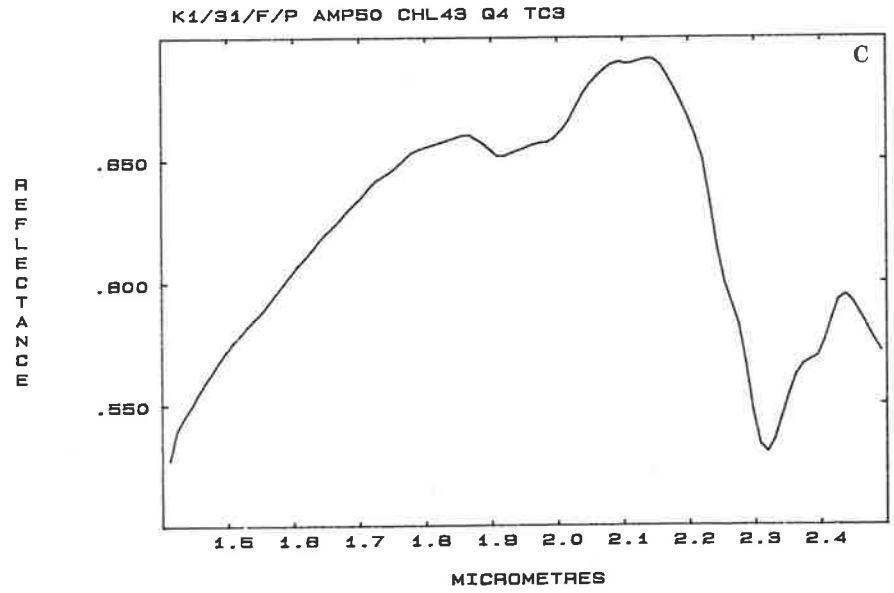
K1/31/F/P AMP50 CHL43 Q4 TC3
C
.850
.800
.550
REFLECTANCE
1.5 1.6 1.7 1.8 1.9 2.0 2.1 2.2 2.3 2.4
MICROMETRES

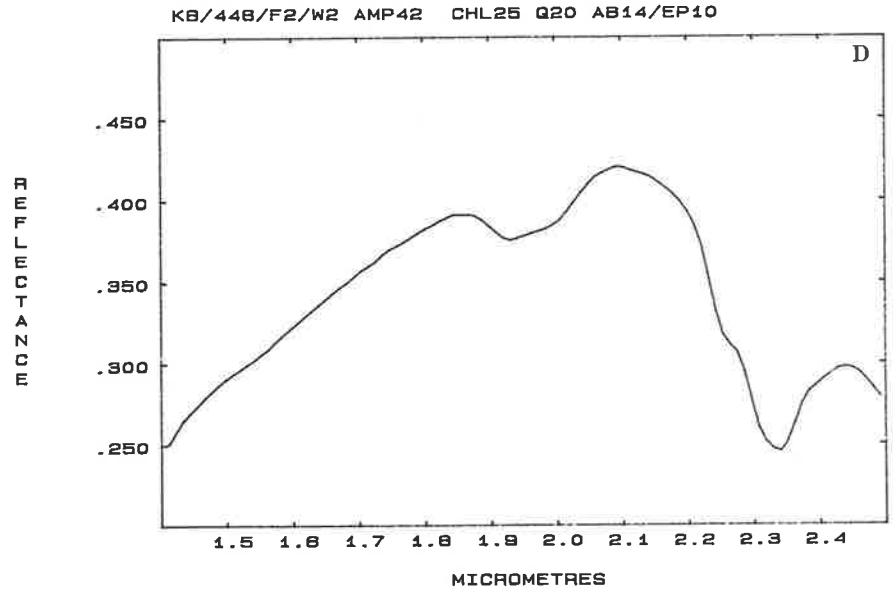
K8/448/F2/W2 AMP42 CHL25 Q20 AB14/EP10
D
.450
.400
.350
.300
.250
REFLECTANCE
1.5 1.6 1.7 1.8 1.9 2.0 2.1 2.2 2.3 2.4
MICROMETRES

Figures 6.11a&b SWIR laboratory reflectance spectra of materials exhibiting weak absorption features from Kambalda.

There are numerous examples of weak absorption features from Kambalda. Most of these cannot be interpreted confidently. Figure 6.11a is one example that shows weak features in both the 2.2 and 2.3μm regions. Figure 6.11b, on the other hand, exhibits a broad, weak absorption feature only in the 2.3μm region. This could be attributed to the 'mafic' mineralogy of Archaean basalts, except that XRD shows that diopside is present and the most likely cause of the absorption. Diopside is found only in Proterozoic dykes at Kambalda (D. Quick, pers. comm., 1984). This example underlines the importance of ground-truth work and supporting laboratory data.

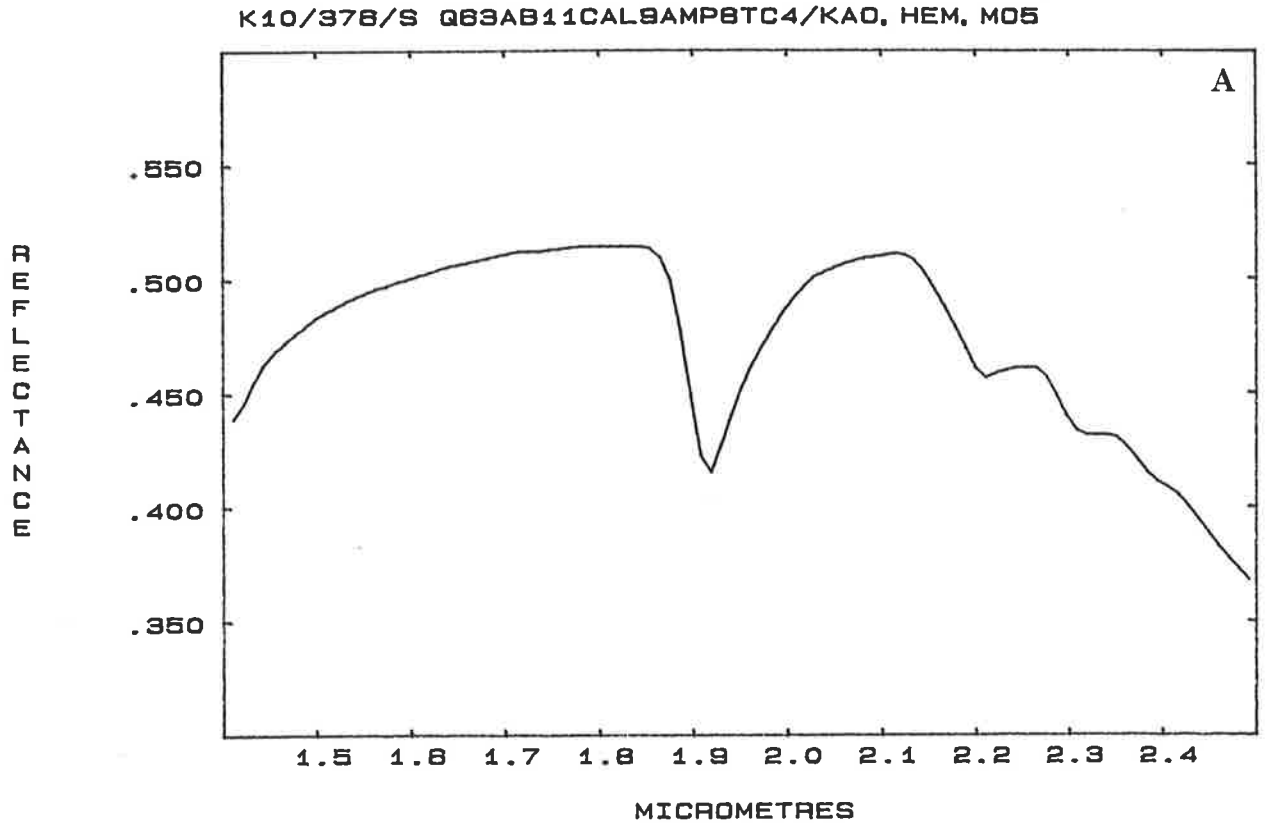
K10/378/S Q63AB11CAL9AMP8TC4/KAO, HEM, M05
A
REFLECTANCE
.550
.500
.450
.400
.350
1.5 1.6 1.7 1.8 1.9 2.0 2.1 2.2 2.3 2.4
MICROMETRES

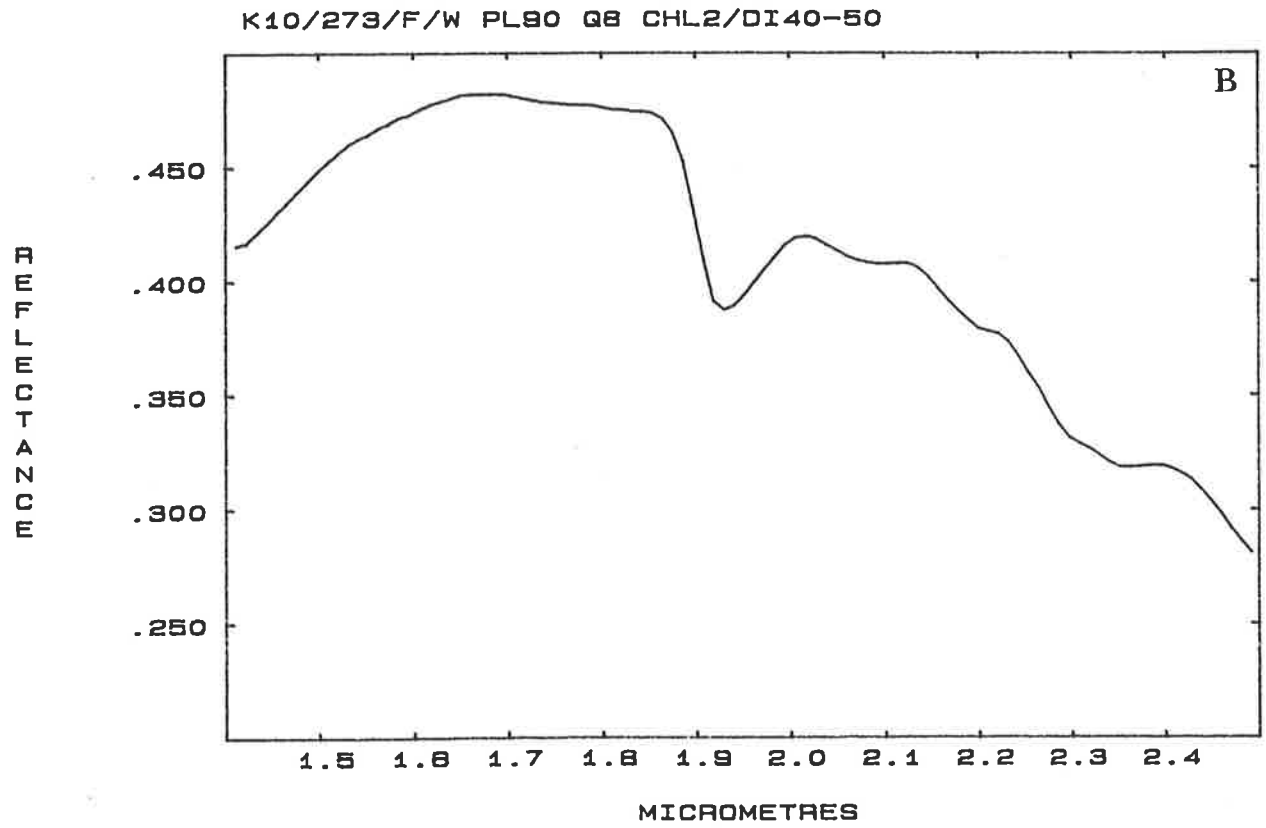
K10/273/F/W PL90 Q8 CHL2/DI40-50
B
REFLECTANCE
.450
.400
.350
.300
.250
1.5 1.6 1.7 1.8 1.9 2.0 2.1 2.2 2.3 2.4
MICROMETRES

Figure 6.12 SWIR airborne log residual spectra of two chlorite-bearing areas at Kambalda.

Note particularly that the positions of the 2.26μm absorption features vary. This is difficult to explain other than by variation of the chlorites' composition. However, any variation in the position of the 2.34μm minimum could be explained by the presence of other minerals absorbing at slightly different wavelengths (e.g. talc, amphibole, or epidote).

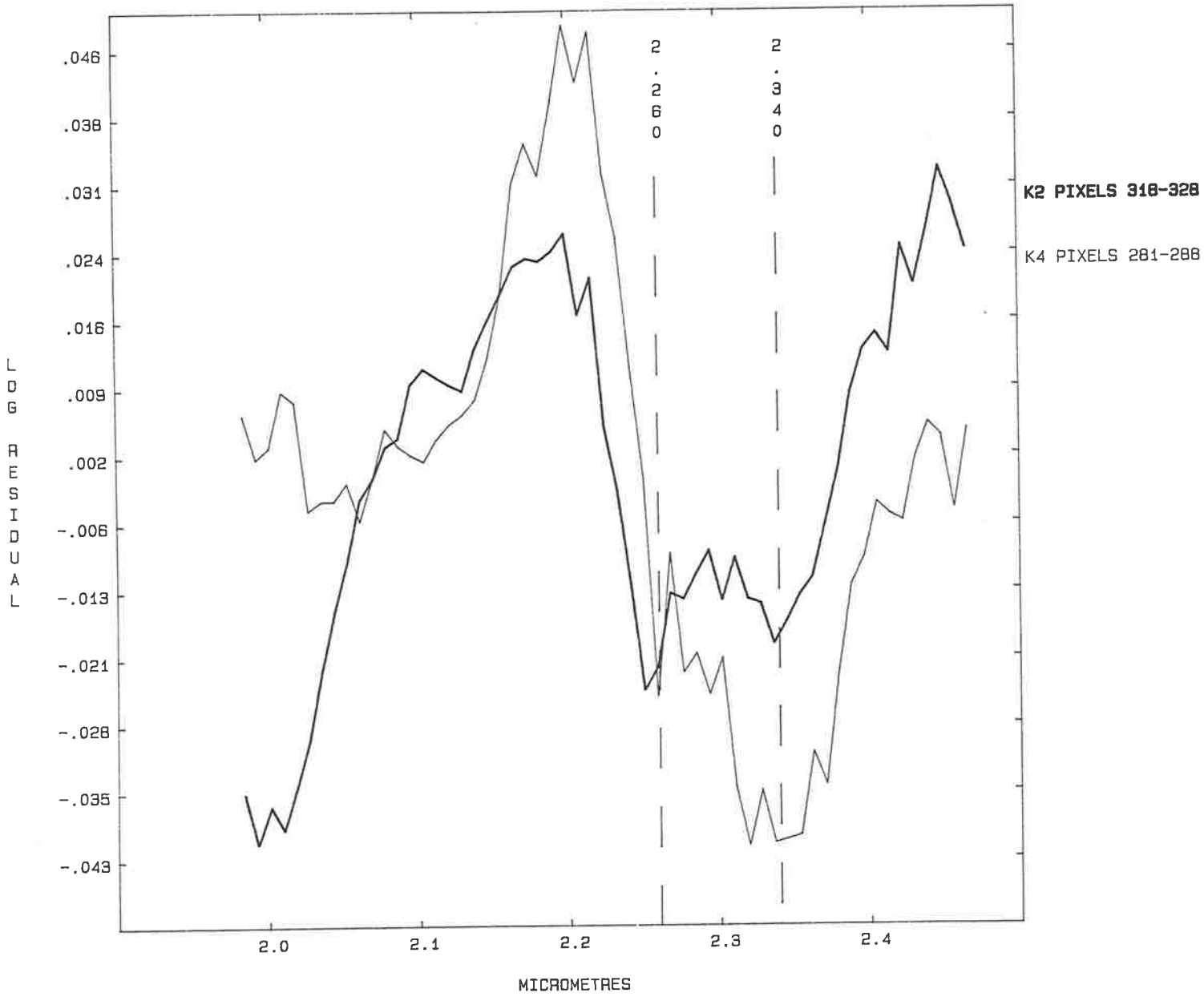
.046
.038
.031
.024
.016
.009
.002
-.006
-.013
-.021
-.028
-.035
-.043
LOG RESIDUAL
2.260
2.340
2.0
2.1
2.2
2.3
2.4
MICROMETRES
K2 PIXELS 318-328
K4 PIXELS 281-288

Figures 6.13a-f SWIR airborne mean radiance spectra of Kambalda flight lines.

Note the similarity of all flight line means, and the absence of any recognisable mineralogical absorption features (in particular at 2.3μm).

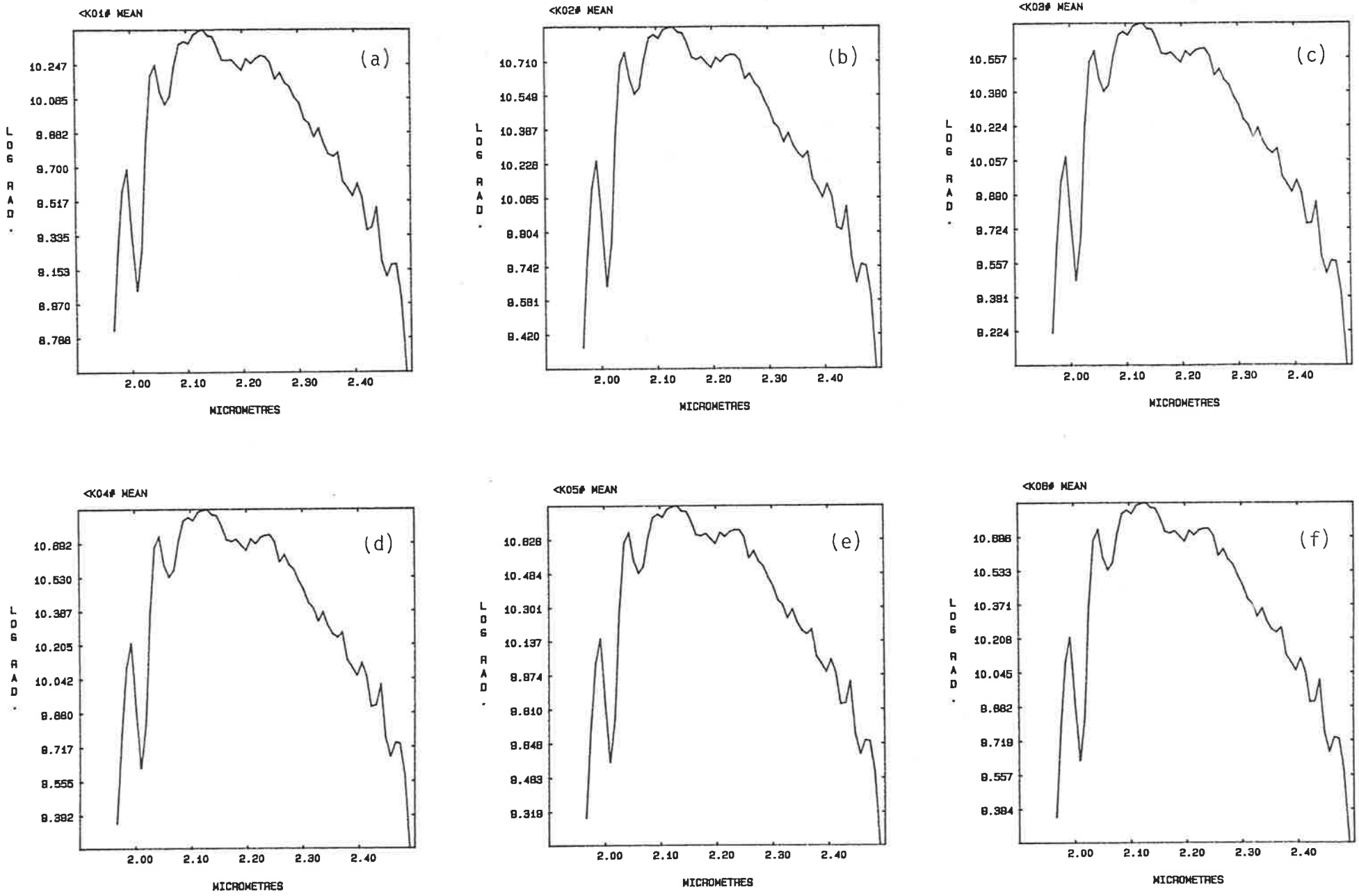
<K01# MEAN
(a)
10.247
10.085
9.882
9.700
9.517
9.335
9.153
8.970
8.788
LOG RAD.
2.00
2.10
2.20
2.30
2.40
MICROMETRES
<K02# MEAN
(b)
10.710
10.549
10.387
10.228
10.065
9.904
9.742
9.581
9.420
LOG RAD.
2.00
2.10
2.20
2.30
2.40
MICROMETRES
<K03# MEAN
(c)
10.557
10.380
10.224
10.057
9.890
9.724
9.557
9.391
9.224
LOG RAD.
2.00
2.10
2.20
2.30
2.40
MICROMETRES
<K04# MEAN
(d)
10.892
10.530
10.387
10.205
10.042
9.880
9.717
9.555
9.392
LOG RAD.
2.00
2.10
2.20
2.30
2.40
MICROMETRES
<K05# MEAN
(e)
10.828
10.484
10.301
10.137
9.974
9.810
9.648
9.483
9.318
LOG RAD.
2.00
2.10
2.20
2.30
2.40
MICROMETRES
<K06# MEAN
(f)
10.696
10.533
10.371
10.208
10.045
9.882
9.719
9.557
9.394
LOG RAD.
2.00
2.10
2.20
2.30
2.40
MICROMETRES

Figures 6.13g-l SWIR airborne mean radiance spectra of Kambalda flight lines.

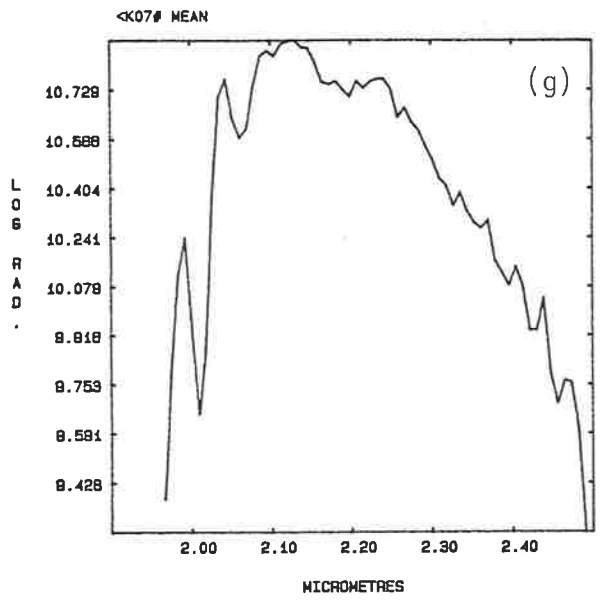
<K07# MEAN
(g)
LOG RAD.
10.729
10.588
10.404
10.241
10.078
9.918
9.753
9.591
9.428
2.00
2.10
2.20
2.30
2.40
MICROMETRES

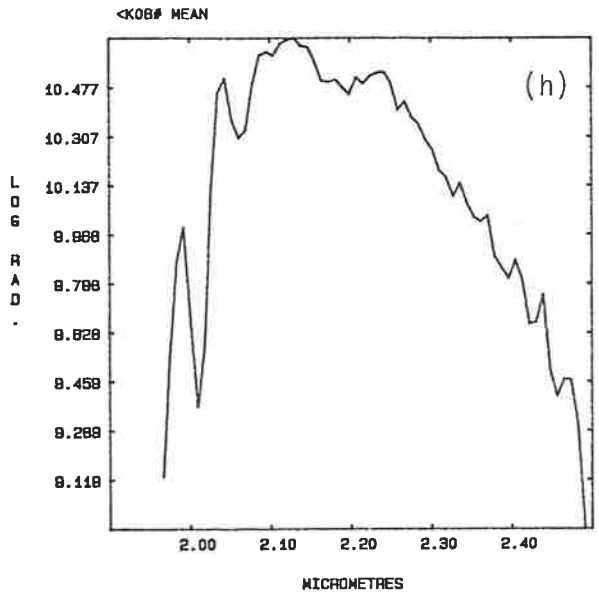
<K08# MEAN
(h)
LOG RAD.
10.477
10.307
10.137
9.968
9.798
9.628
9.459
9.289
9.118
2.00
2.10
2.20
2.30
2.40
MICROMETRES

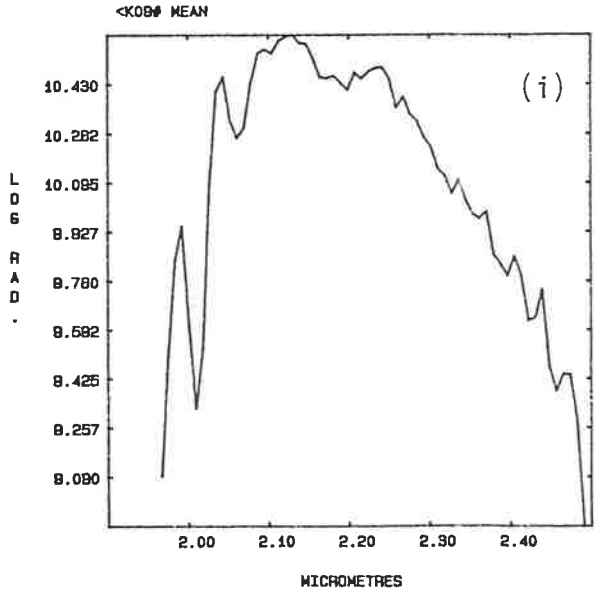
<K09# MEAN
(i)
LOG RAD.
10.430
10.262
10.095
9.927
9.760
9.592
9.425
9.257
9.090
2.00
2.10
2.20
2.30
2.40
MICROMETRES

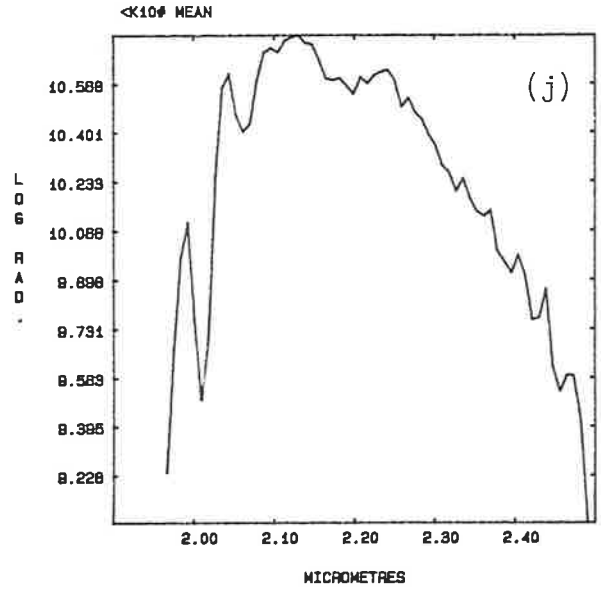
<K10# MEAN
(j)
LOG RAD.
10.588
10.401
10.239
10.088
9.898
9.731
9.569
9.395
9.228
2.00
2.10
2.20
2.30
2.40
MICROMETRES

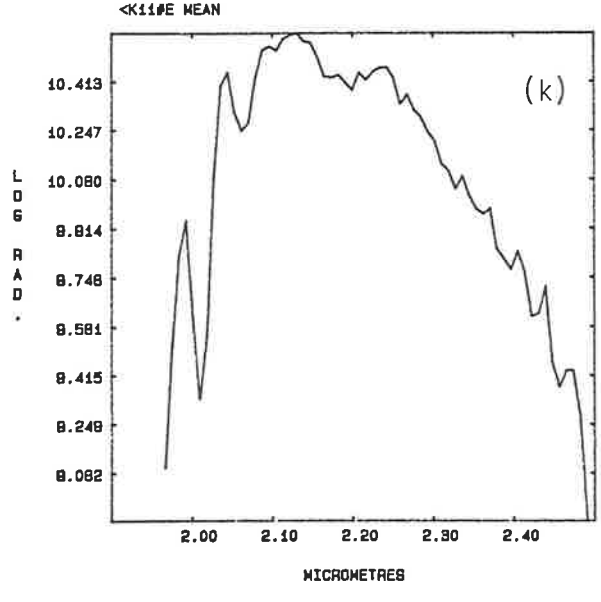
<K11#E MEAN
(k)
LOG RAD.
10.413
10.247
10.080
9.914
9.748
9.581
9.415
9.248
9.082
2.00
2.10
2.20
2.30
2.40
MICROMETRES

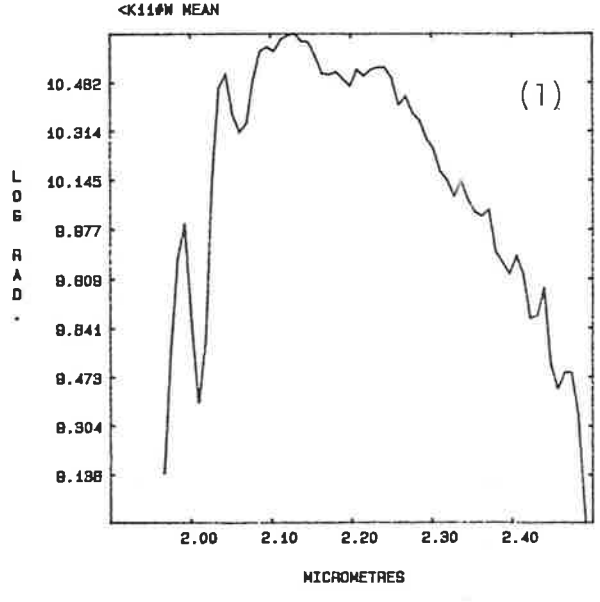
<K11#W MEAN
(l)
LOG RAD.
10.482
10.314
10.145
9.977
9.809
9.641
9.473
9.304
9.138
2.00
2.10
2.20
2.30
2.40
MICROMETRES

Figures 6.13m&n SWIR airborne mean radiance spectra of Kambalda flight lines.

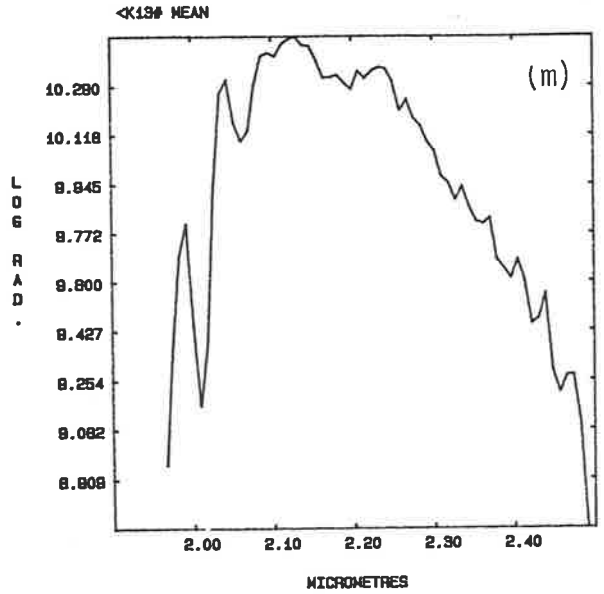
<K13# MEAN
(m)
10.290
10.118
9.945
9.772
9.600
9.427
9.254
9.082
8.909
LOG RAD.
2.00
2.10
2.20
2.30
2.40
MICROMETRES

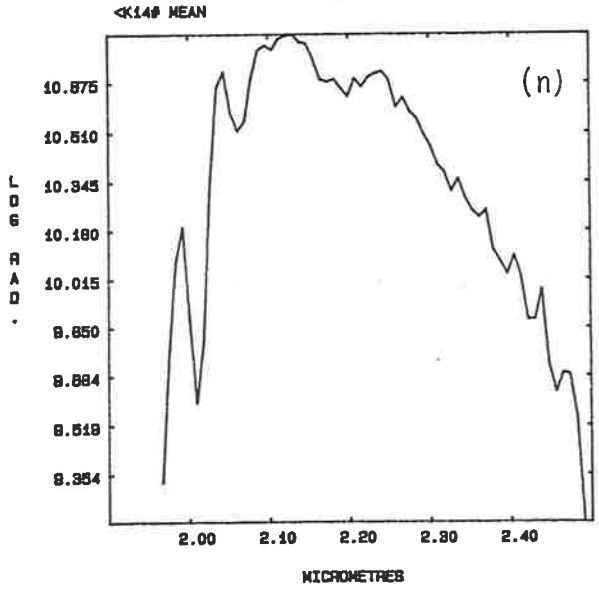
<K14# MEAN
(n)
10.675
10.510
10.345
10.180
10.015
9.850
9.684
9.519
9.354
LOG RAD.
2.00
2.10
2.20
2.30
2.40
MICROMETRES

Figures 6.14a-d Two SWIR airborne radiance spectra and their corresponding log residuals from Kambalda.

Figures 6.14a&b are averaged airborne radiance data over a spectrally flat area, and a talc-bearing area, respectively. Note the apparent absence of mineralogical features.

Figures 6.14c&d are the equivalent averaged log residual spectra. The spectrally flat area has no obvious absorption features, but the talc-bearing zone exhibits a strong talc log-residual signature.

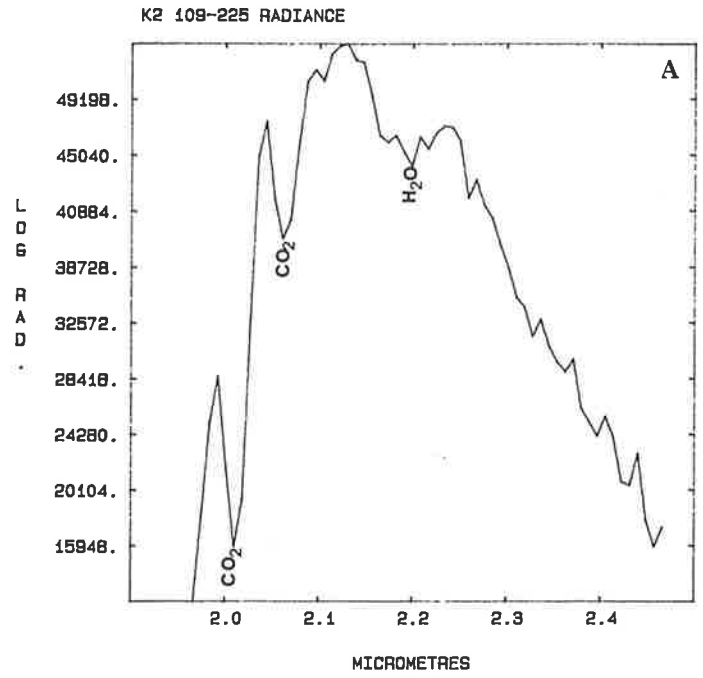
K2 109-225 RADIANCE
A
49198.
45040.
40884.
38728.
32572.
28418.
24280.
20104.
15948.
LOG RAD.
CO_2
CO_2
H_2O
2.0
2.1
2.2
2.3
2.4
MICROMETRES

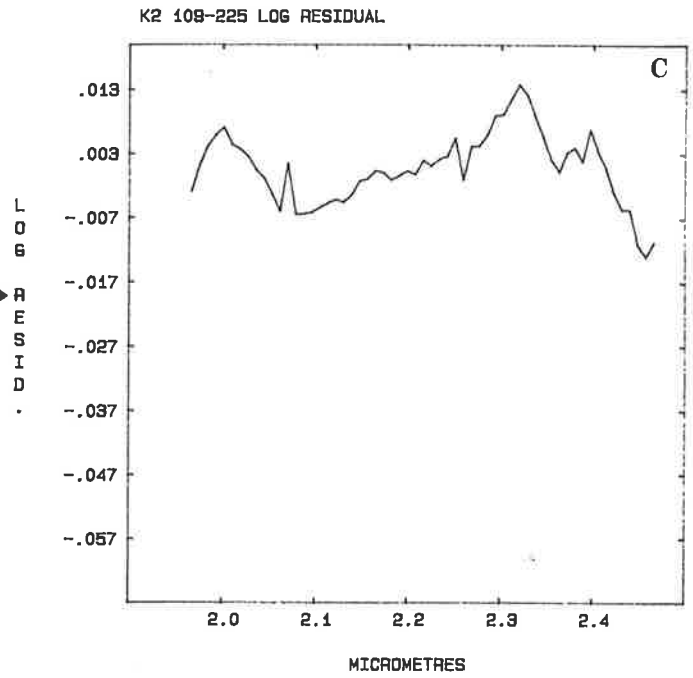
K2 109-225 LOG RESIDUAL
C
.013
.003
-.007
-.017
-.027
-.037
-.047
-.057
LOG RESID.
2.0
2.1
2.2
2.3
2.4
MICROMETRES

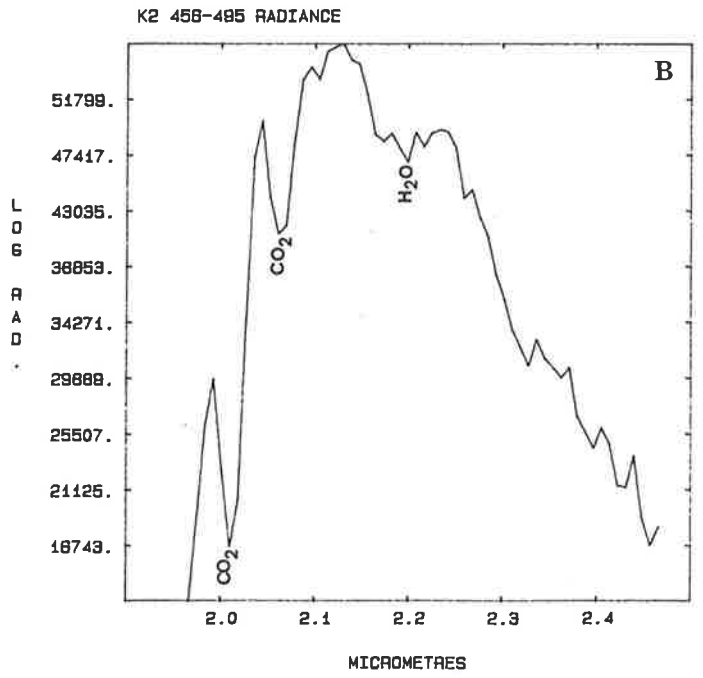
K2 458-485 RADIANCE
B
51799.
47417.
43035.
38653.
34271.
29889.
25507.
21125.
16743.
LOG RAD.
CO_2
CO_2
H_2O
2.0
2.1
2.2
2.3
2.4
MICROMETRES

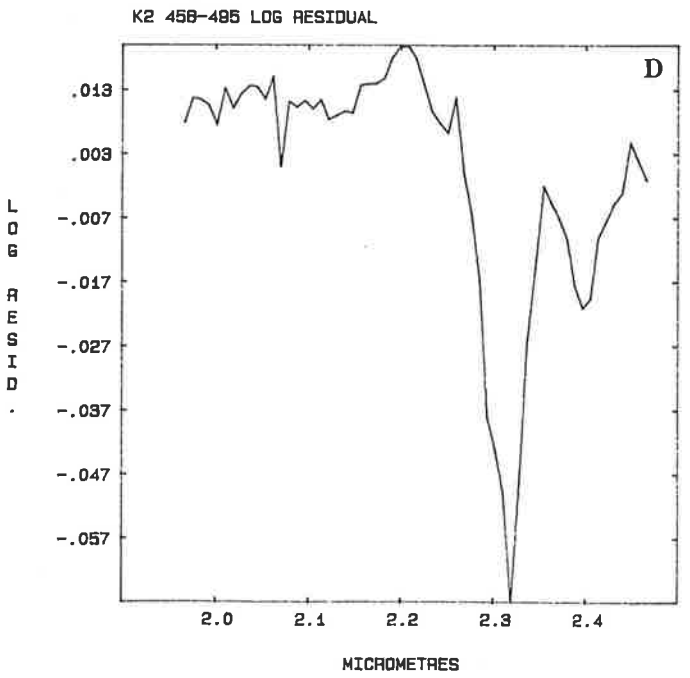
K2 458-485 LOG RESIDUAL
D
.013
.003
-.007
-.017
-.027
-.037
-.047
-.057
LOG RESID.
2.0
2.1
2.2
2.3
2.4
MICROMETRES

Figures 6.15a&b Airborne log residual spectra (line K2) - image format.

The log residual data have been put into an image format and density sliced. Dark blue colours represent the lowest log residual values (deepest absorption features), the mid-green colours (see vertical strips at extremities of some of the columns of data) represent zero values, and deep red colours represent the highest log residual values. The four columns of data are, from left to right, VNIR log residuals, VNIR albedo, SWIR log residuals and SWIR albedo.

The block boundaries (horizontal lines) have been drawn after visual examination of the image. Each block has been numbered, and average log residual spectra for each block have been plotted and interpreted (see Appendix IX).

The data fall naturally into a number of 'bands' defined by the wavelength limits of the absorption features. The vertical lines outline these bands. Wavelengths of the band boundaries are ;

VNIR	1	0.327μm (start)
	2	0.635μm
	3	0.784μm
	4	1.012μm (end)
SWIR	5	1.954μm (start)
	6	2.147μm
	7	2.216μm
	8	2.302μm
	9	2.328μm
	10	2.353μm
	11	2.422μm
	12	2.500μm (end)

A

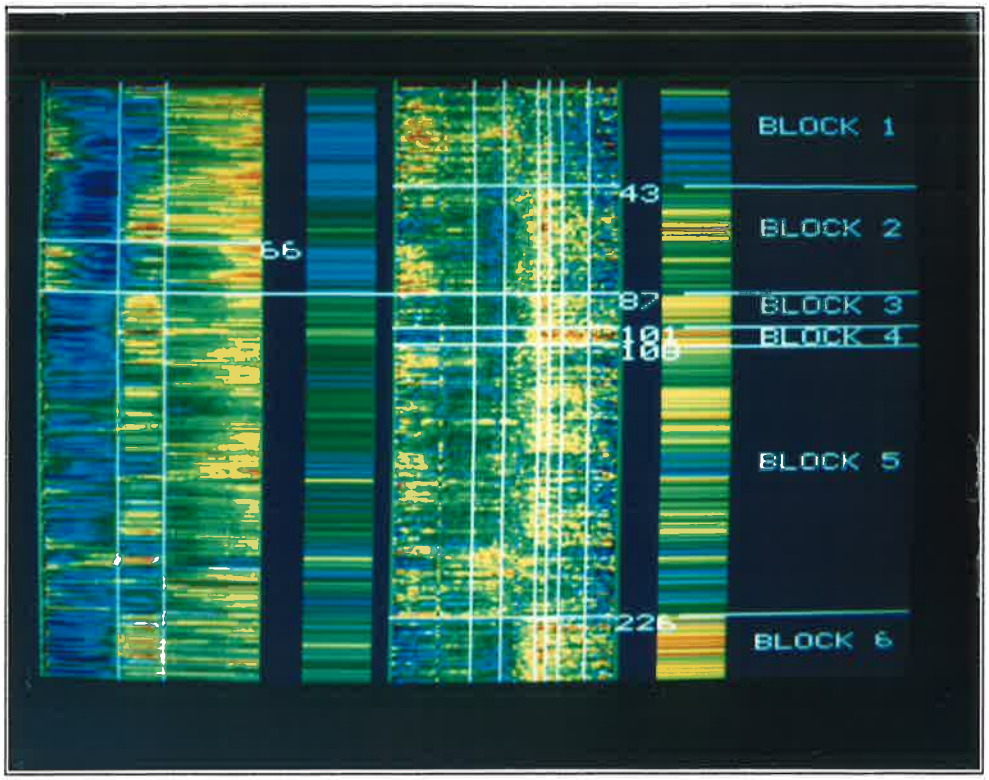
BLOCK 1
43
BLOCK 2
66
87
BLOCK 3
101
BLOCK 4
108
BLOCK 5
226
BLOCK 6

B

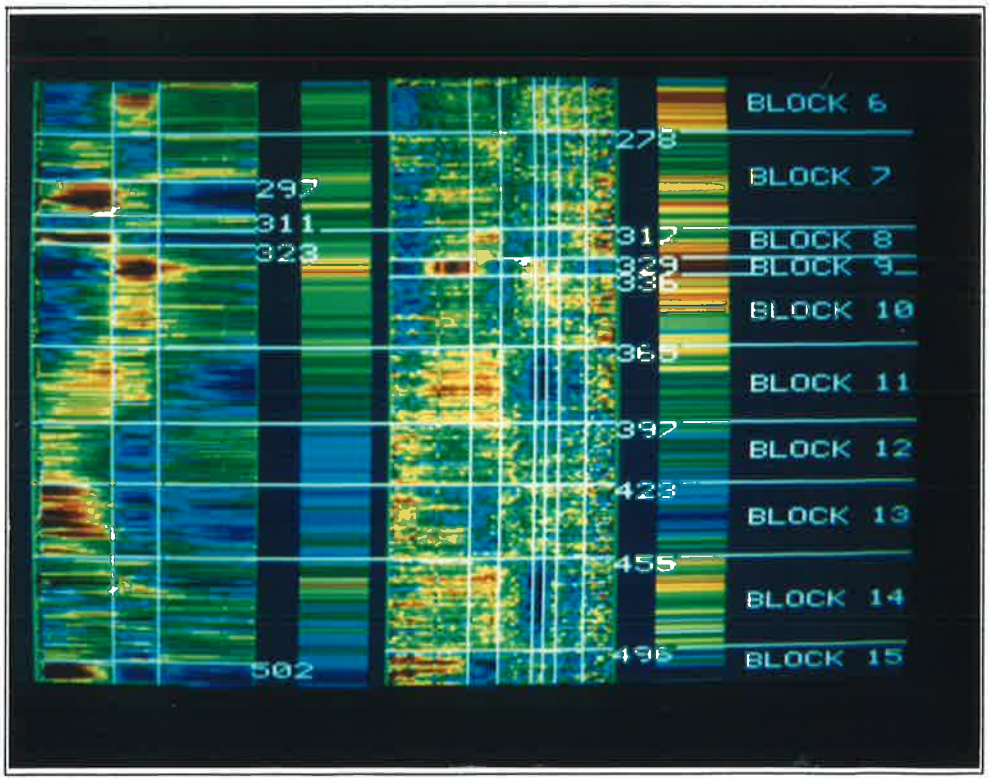
BLOCK 6
278
BLOCK 7
297
311
323
317
329
BLOCK 8
BLOCK 9
336
BLOCK 10
365
BLOCK 11
397
BLOCK 12
423
BLOCK 13
455
BLOCK 14
496
BLOCK 15
502

Figures 6.15c&d Airborne log residual spectra (line K2) - image format.

Blocks 15 to 26.

C

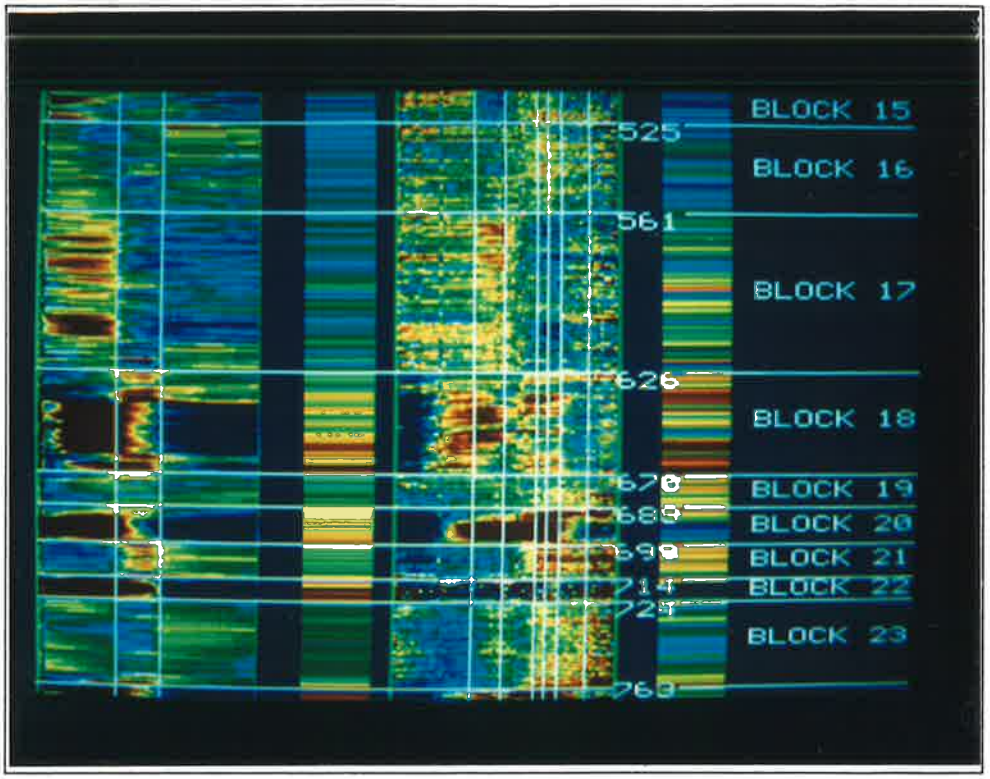
BLOCK 15
525
BLOCK 16
561
BLOCK 17
626
BLOCK 18
670
BLOCK 19
688
BLOCK 20
699
BLOCK 21
714
BLOCK 22
724
BLOCK 23
768

D

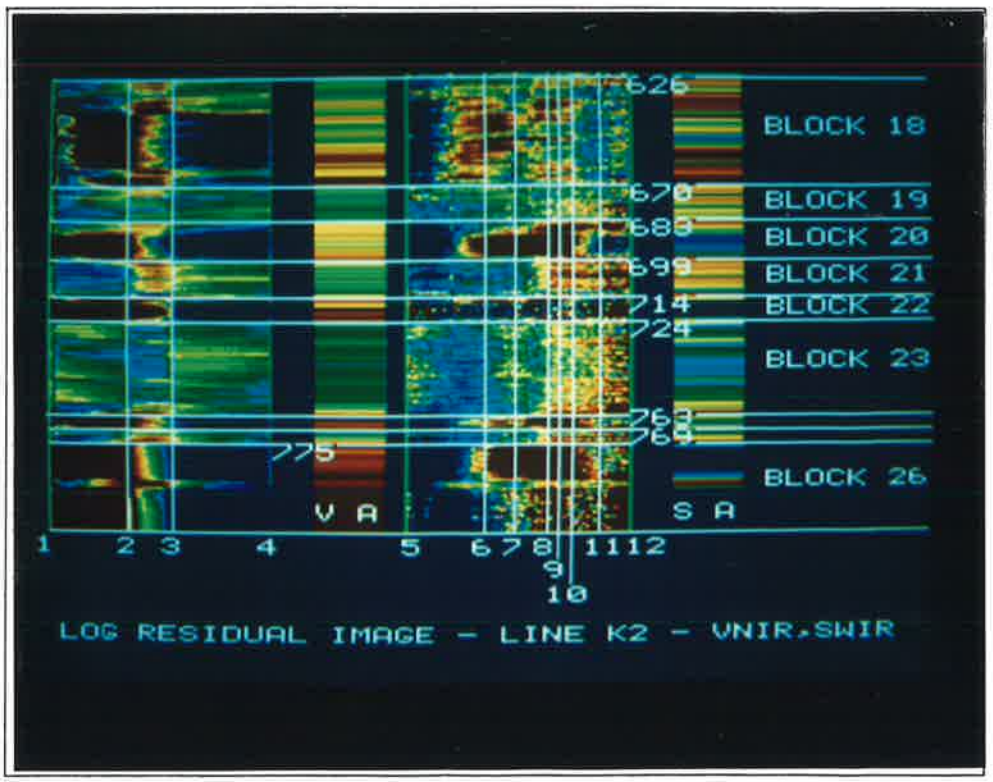
626
BLOCK 18
670
BLOCK 19
688
BLOCK 20
699
BLOCK 21
714
BLOCK 22
724
BLOCK 23
763
768
775
BLOCK 26
V A
S A
1 2 3 4 5 6 7 8 9 10 11 12
LOG RESIDUAL IMAGE - LINE K2 - VNIR.SWIR

Figures 6.16a&b SWIR laboratory reflectance spectrum and airborne log residual spectrum of halite from Kambalda.

Figure 6.16a is the average airborne log residual spectrum over a portion of Lake Lefroy. It exhibits a weak local minimum at 2.25μm (similar to a feature documented by Hunt et al., 1972), which may be related to the moisture content of the halite.

Figure 6.16b is the laboratory spectrum of a (dry) halite sample from Lake Lefroy. It has no absorption features near 2.25μm.

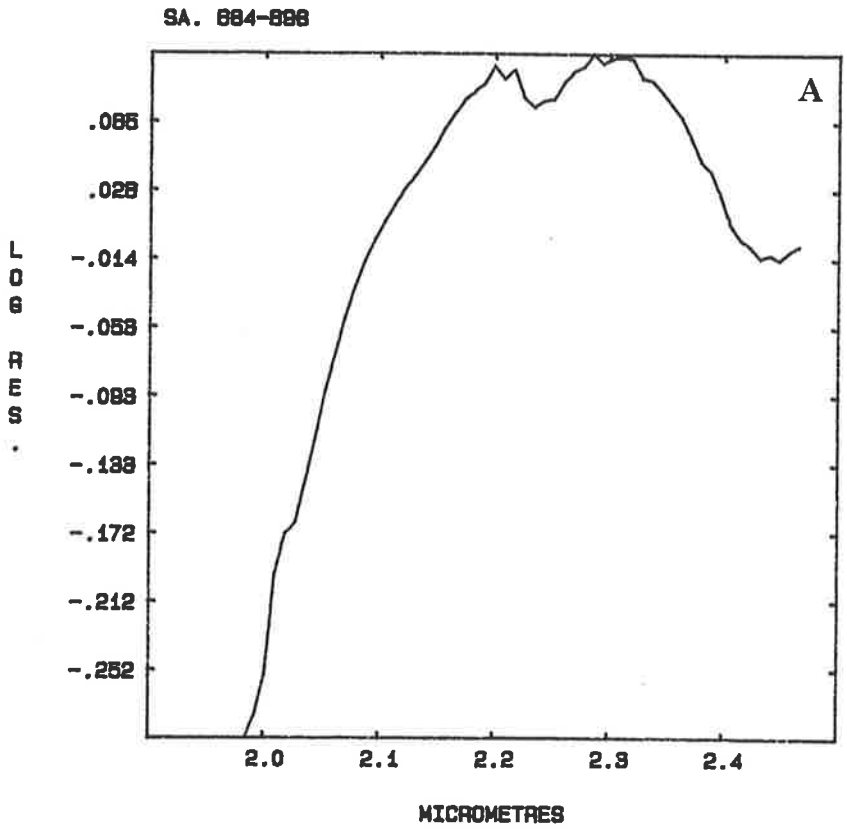
SA. 884-888
A
.086
.028
-.014
-.058
-.088
-.138
-.172
-.212
-.252
LOG RES.
2.0
2.1
2.2
2.3
2.4
MICROMETRES

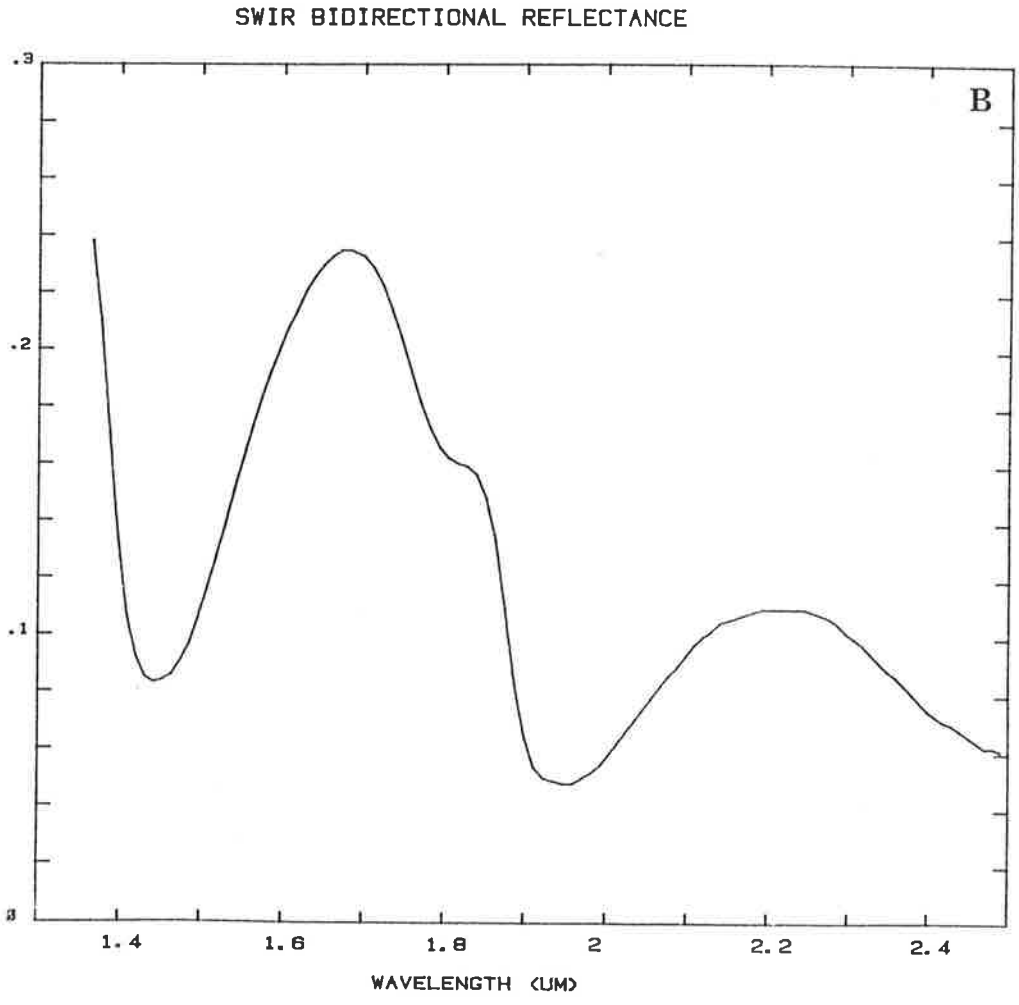
SWIR BIDIRECTIONAL REFLECTANCE
B
.3
.2
.1
0
1.4
1.6
1.8
2
2.2
2.4
WAVELENGTH (UM)

Figure 6.17 SWIR airborne log residual spectrum of a kaolinitic laterite at Kambalda.

Although somewhat noisy, the characteristic 2.17 and 2.208μm absorption minima of kaolin are well developed in this spectrum.

Figure 6.18 Airborne SWIR log residual spectrum of a talc-bearing soil at Kambalda.

This spectrum exhibits all of the characteristic features of talc, with minor features at 2.26, 2.30 (shoulder), 2.39 and 2.47μm, and with the sharp and deep major absorption feature at 2.32μm. Compare to the 2.2μm absorption of kaolin in Fig. 6.17 above.

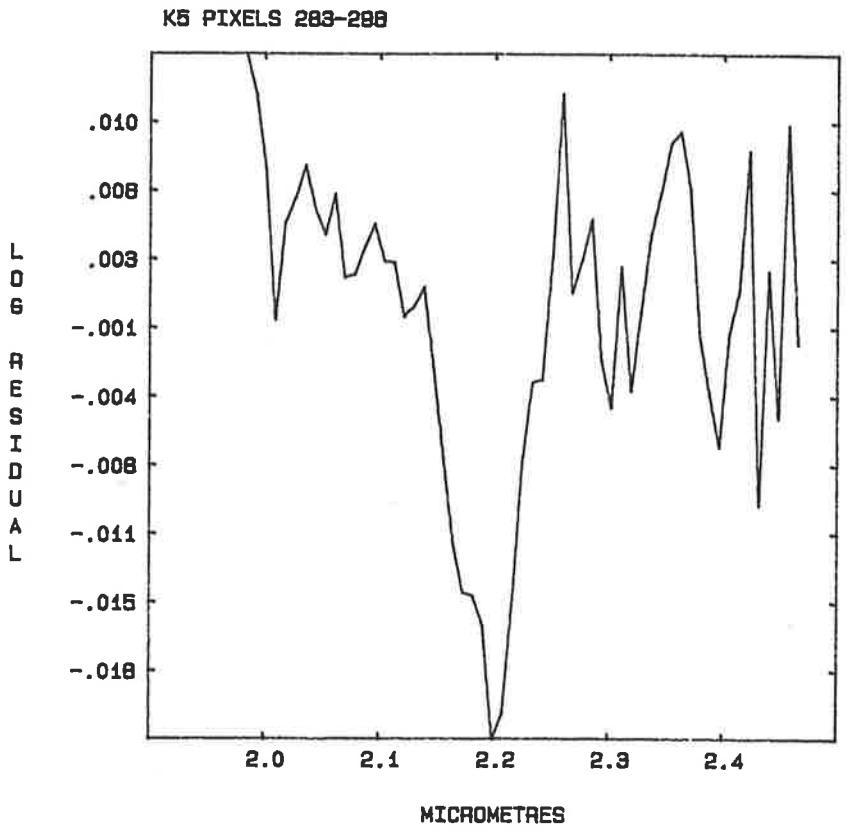
K5 PIXELS 283-288
.010
.008
.003
-.001
-.004
-.008
-.011
-.015
-.018
LOG RESIDUAL
2.0
2.1
2.2
2.3
2.4
MICROMETRES

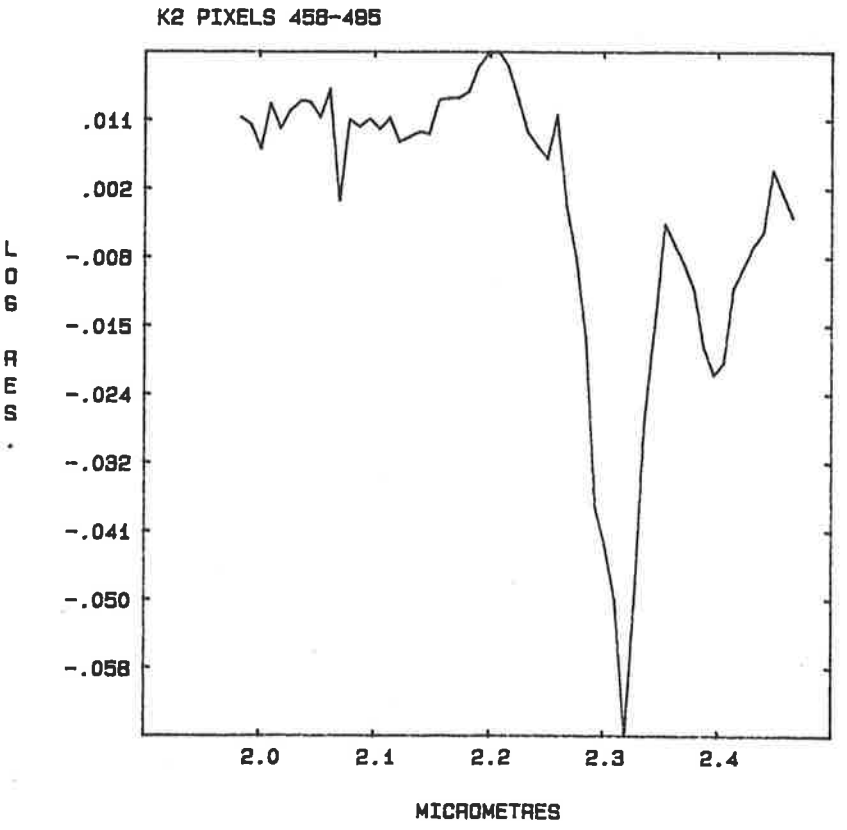
K2 PIXELS 458-495
.011
.002
-.008
-.015
-.024
-.032
-.041
-.050
-.058
LOG RES.
2.0
2.1
2.2
2.3
2.4
MICROMETRES

Figures 6.19a&b Photograph and airborne log residual spectrum of a talc-bearing portion of line K9.

Figure 6.19a shows the absence of outcrop or substantial float. Note also that soil lichen (right side of photo) and saltbush (just visible top and left) will contribute to the airborne spectrum. The author estimates that no more than 50% of each pixel in this area is composed of bare, talc-rich soil. XRD analysis shows that the talc content of the bare areas is approximately 20%. Therefore, it can be inferred that an effective talc concentration of only 10% has produced the log residual spectrum shown in Fig. 6.19b.

A

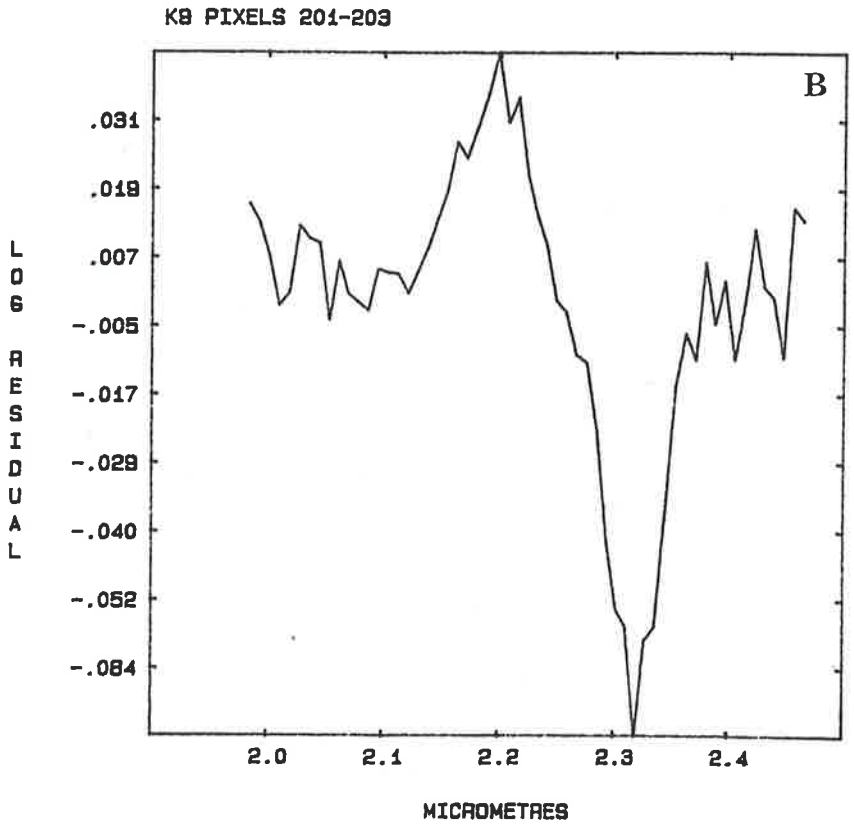
K8 PIXELS 201-203
B
.031
.019
.007
-.005
-.017
-.029
-.040
-.052
-.064
LOG RESIDUAL
2.0
2.1
2.2
2.3
2.4
MICROMETRES

Figure 6.20 Interpreted and factual geology of the St Ives area, with overlay showing mineralogy interpreted from airborne spectral data.

KEY

- ● Kaolin
- □ Chlorite
- ■ Chlorite/amphibole
- ▲ Amphibole/epidote
- △ Amphibole/chlorite
- ☆ Talc
- ★ Talc/chlorite
- ? Uncertain

35mm photo centres are marked for each flight line, and every hundredth pixel is numbered.

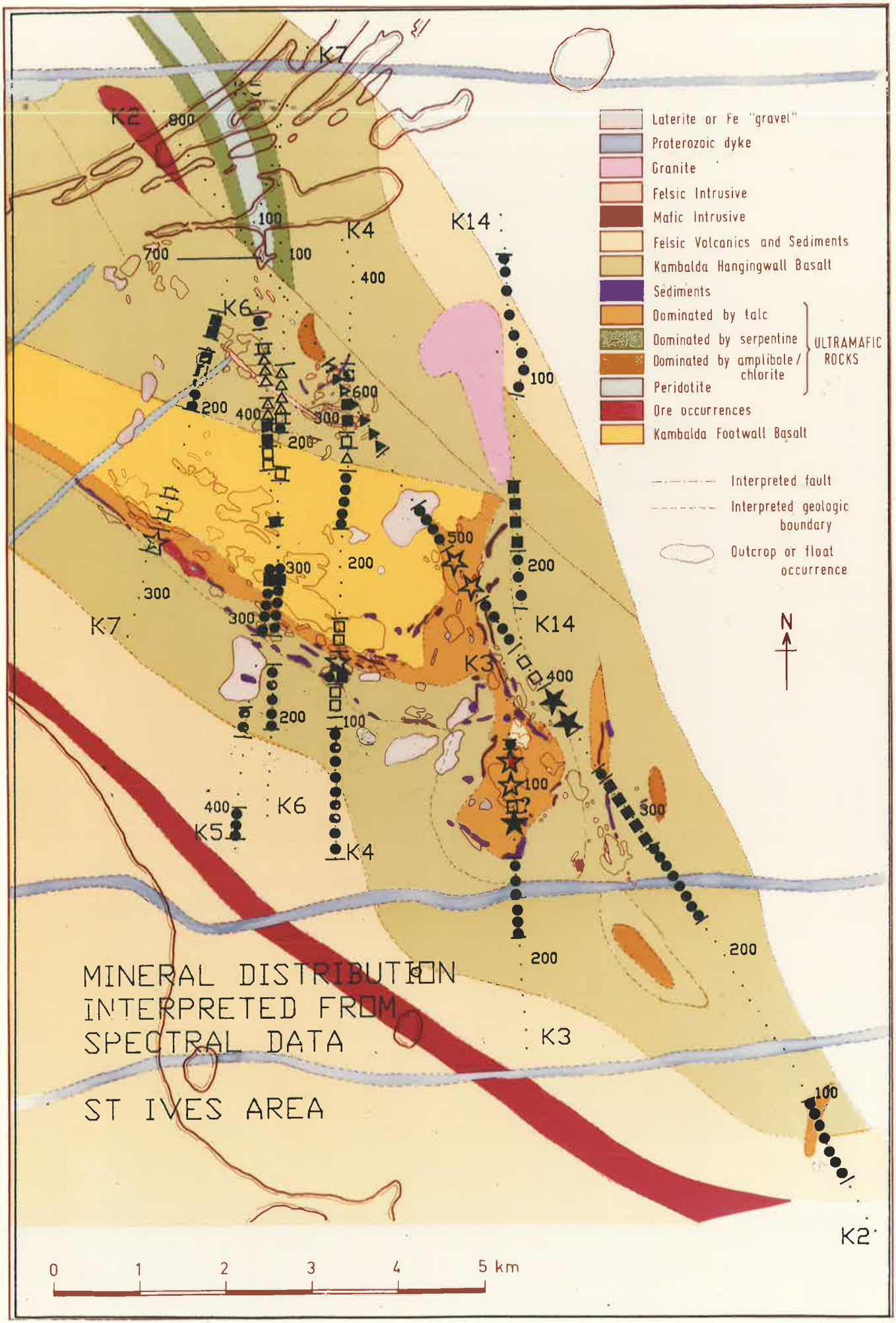
Laterite or Fe "gravel"
Proterozoic dyke
Granite
Felsic Intrusive
Mafic Intrusive
Felsic Volcanics and Sediments
Kambalda Hangingwall Basalt
Sediments
Dominated by talc
Dominated by serpentine
Dominated by amplibole / chlorite
Peridotite
ULTRAMAFIC ROCKS
Ore occurrences
Kambalda Footwall Basalt
Interpreted fault
Interpreted geologic boundary
Outcrop or float occurrence
N
K2
K4
K5
K6
K7
K14
K3
MINERAL DISTRIBUTION
INTERPRETED FROM
SPECTRAL DATA
ST IVES AREA
0
1
2
3
4
5 km

Figure 6.21 Interpreted and factual geology of the Tramways area, with overlay showing mineralogy interpreted from airborne spectral data.

KEY

● Kaolin

□ Chlorite

■ Chlorite/amphibole

▲ Amphibole/epidote

△ Amphibole/chlorite

☆ Talc

★ Talc/chlorite

? Uncertain

35mm photo centres are marked for each flight line, and every hundredth pixel is numbered.

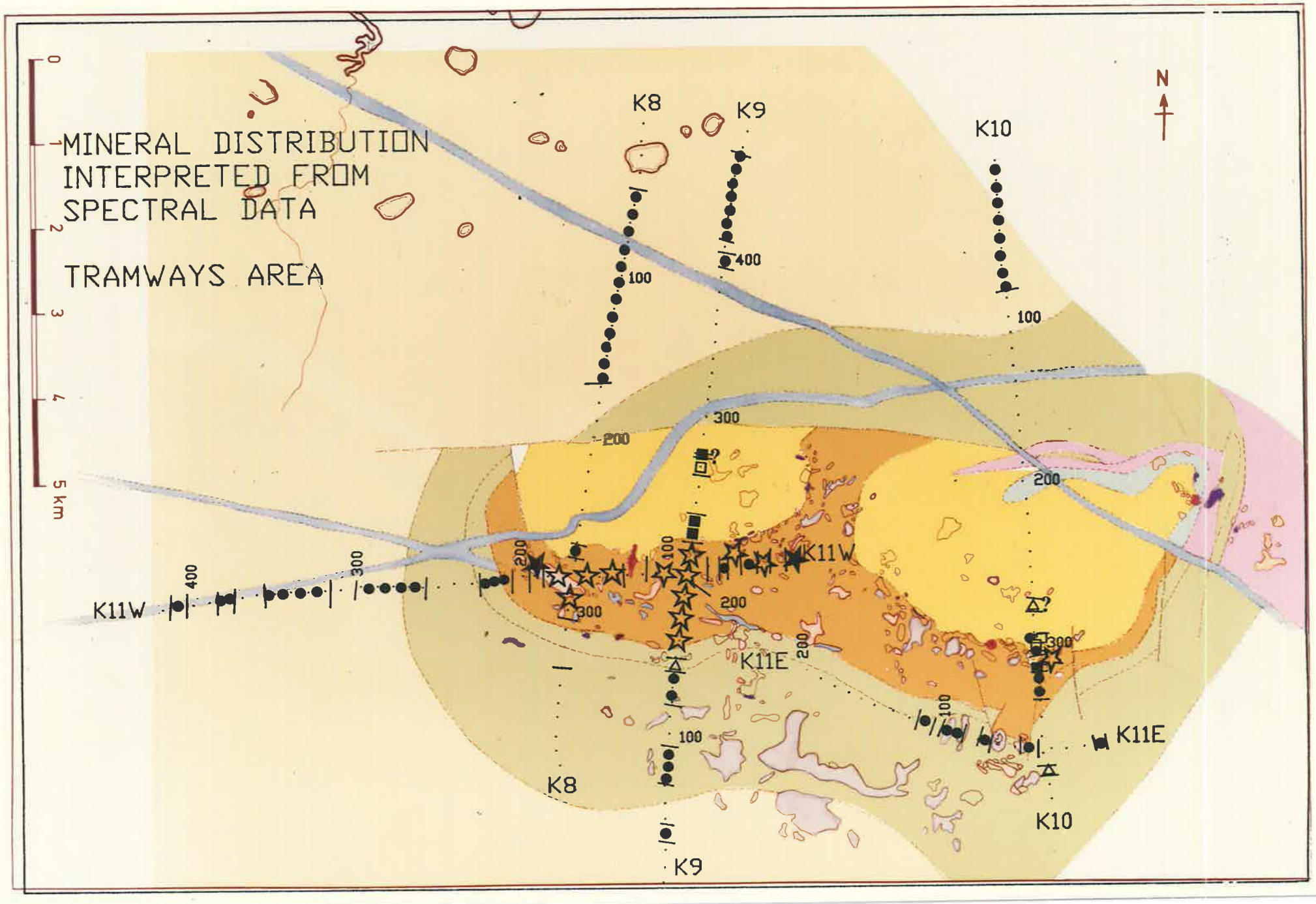
MINERAL DISTRIBUTION
INTERPRETED FROM
SPECTRAL DATA
TRAMWAYS AREA
0
1
2
3
4
5 km
N
K8
K9
K10
K11W
K11E
100
200
300
400

Figures 6.22a&b Geology and interpretation of mineralogy from airborne data for the Kambalda Dome and Democrat areas.

Figure 6.22a is the Kambalda Dome interpretation, and Fig. 6.22b that for Democrat. For both diagrams the spectral interpretation appears in the top line, mapped geology in the middle, and an estimate of the amount of outcrop or float in the bottom line.

KEY

SPECTRA	SL	Salt Lake
	Tc	Talc
	C	Chlorite
	A	Amphibole
	E	Epidote
	K	Kaolin
	KV	Combined Kaolin/Vegetation
	BG	Background
GEOLOGY	PO	Porphyry (felsic)
	UM	Ultramafic
	FWB	Footwall Basalt
	HWB	Hangingwall Basalt
	AI	Acid Intrusive
	B	Basalt
	MI	Mafic Intrusive
	TT	Trotting Track
OUTCROP	DG	Disturbed Ground
	HF	Heavy Float
	90	% float

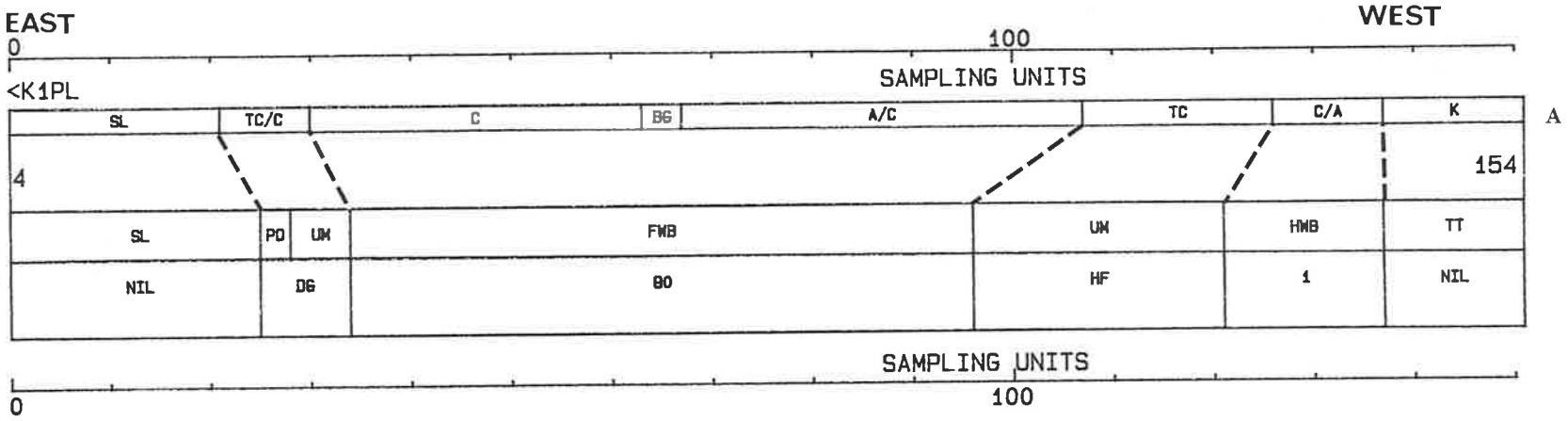
EAST
WEST
0
100
SAMPLING UNITS
<K1PL
SL
TC/C
C
BG
A/C
TC
C/A
K
A
4
154
SL
PO
UM
FWB
UM
HWB
TT
NIL
DG
80
HF
1
NIL
SAMPLING UNITS
0
100

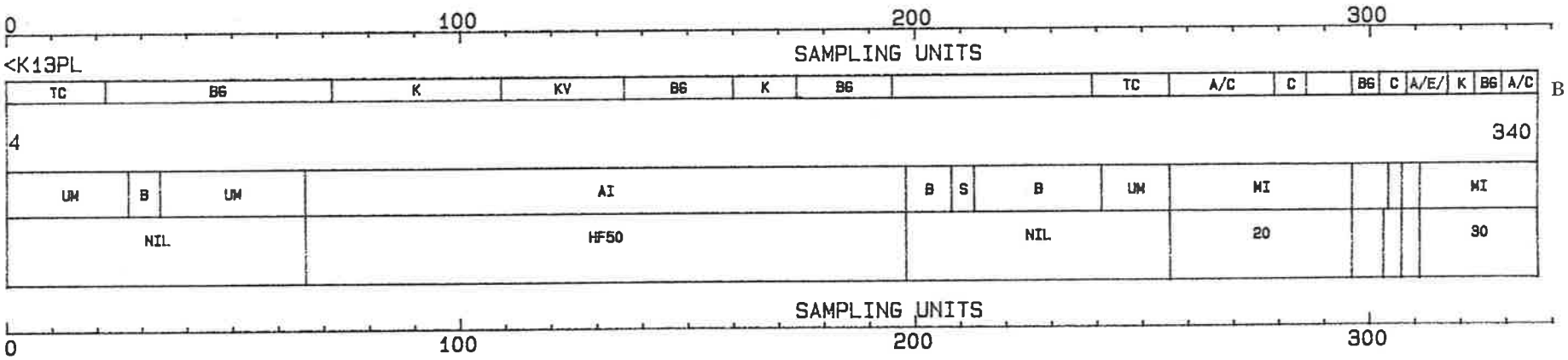
0
100
200
300
SAMPLING UNITS
<K13PL
TC
BG
K
KV
BG
K
BG
TC
A/C
C
BG
C
A/E/
K
BG
A/C
B
4
340
UM
B
UM
AI
B
S
B
UM
MI
MI
NIL
HF50
NIL
20
30
SAMPLING UNITS
0
100
200
300

Figures 6.23a&b Variation of simulated narrow-band ratios derived from radiance data along flight line K2.

Figure 6.23a depicts the variation of a simulated narrow-band ratio (2.3018 to 2.3276μm/2.2158 to 2.3018μm) derived from radiance data.

Figure 6.23b depicts a similar, but narrower ratio (2.3018 to 2.3276μm/2.3276 to 2.3534μm).

The areas within vertical dashed lines have been interpreted (from second-order effects) as containing the minerals shown.

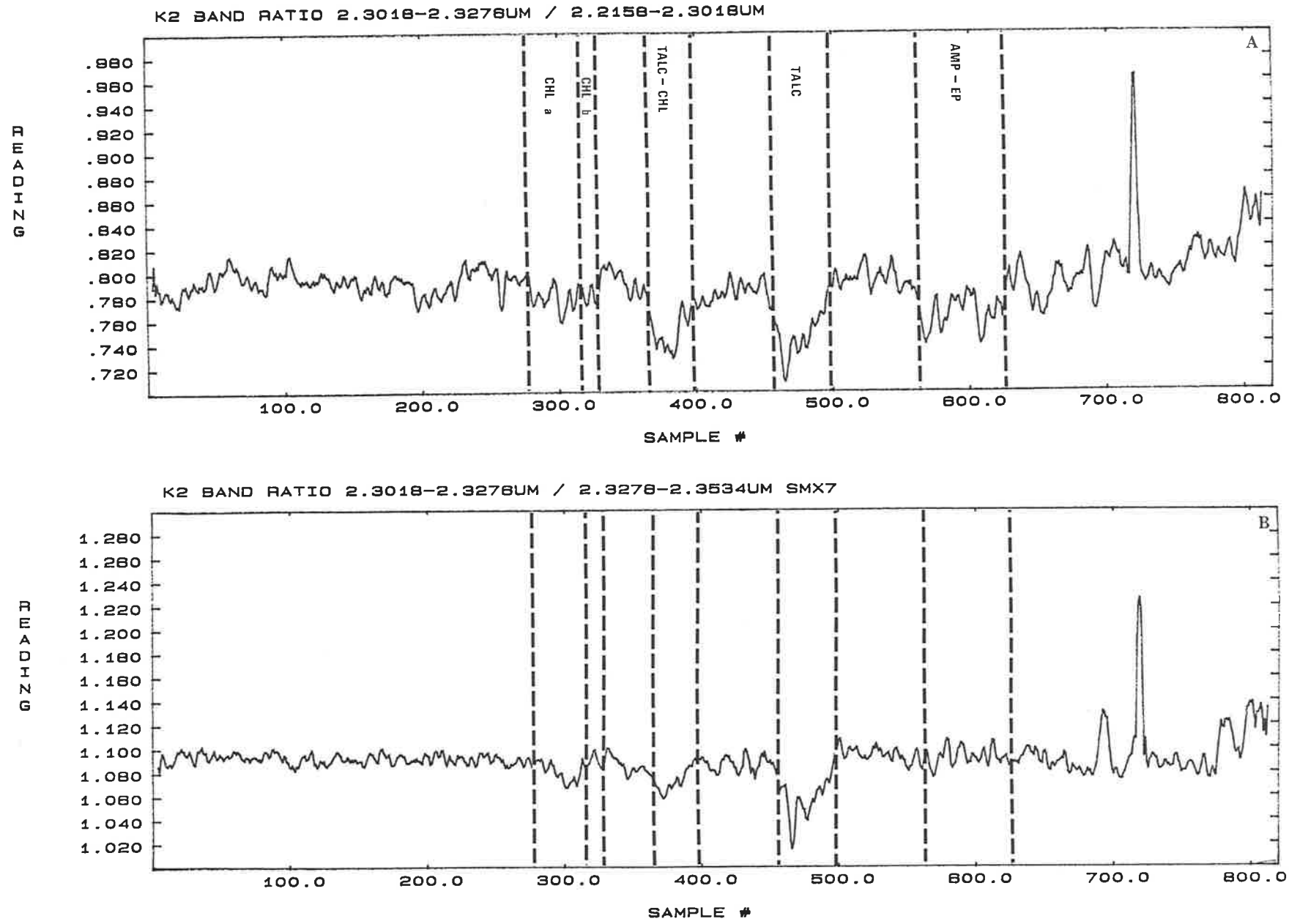
K2 BAND RATIO 2.3018-2.3276UM / 2.2158-2.3018UM
A
READING
.980
.960
.940
.920
.900
.880
.860
.840
.820
.800
.780
.760
.740
.720
CHL a
CHL b
TALC - CHL
TALC
AMP - EP
100.0
200.0
300.0
400.0
500.0
600.0
700.0
800.0
SAMPLE #
K2 BAND RATIO 2.3018-2.3276UM / 2.3278-2.3534UM SMX7
B
READING
1.280
1.260
1.240
1.220
1.200
1.180
1.160
1.140
1.120
1.100
1.080
1.060
1.040
1.020
100.0
200.0
300.0
400.0
500.0
600.0
700.0
800.0
SAMPLE #

Figures 6.24a&b Variation of a simulated narrow-band derived from log residual data, and of a simulated broad-band (TM) ratio, along flight line K2.

Figure 6.24a plots the value of simulated narrow-band reflectance data (2.3018 to 2.3276μm) derived from log residual values.

Figure 6.24b has been created from radiance data using two broad bands - 2.08 to 2.35μm (equivalent to TM band) and 1.958 to 2.08μm. The bands have then been ratioed to produce a result similar to the 1.6μm/2.2μm ratio commonly used in analysis of TM data. Note the lack of well-defined minima in the critical areas.

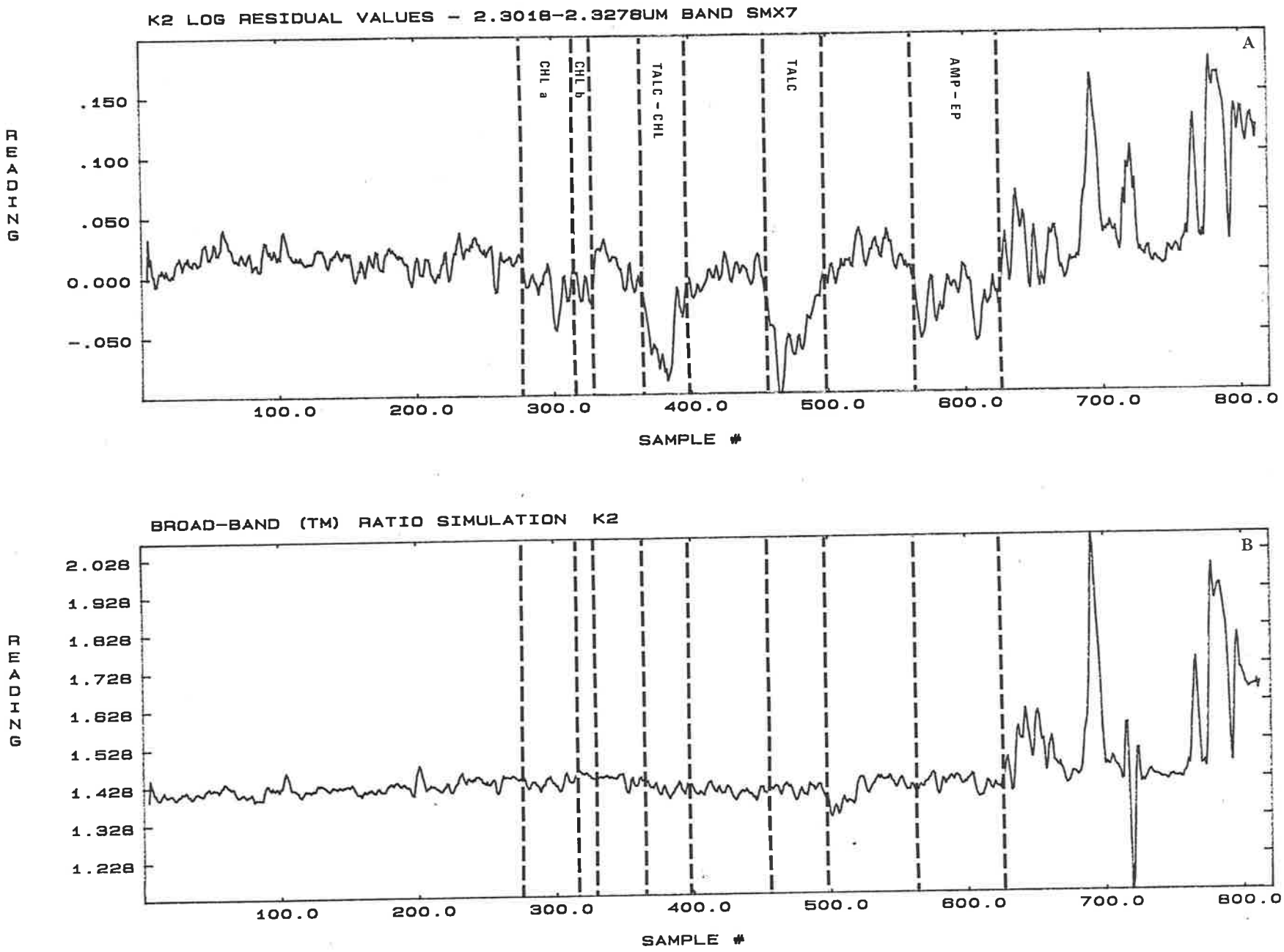
K2 LOG RESIDUAL VALUES - 2.3018-2.3278UM BAND SMX7
A
CHL a
CHL b
TALC-CHL
TALC
AMP-EP
READING
.150
.100
.050
0.000
-.050
100.0
200.0
300.0
400.0
500.0
600.0
700.0
800.0
SAMPLE #
BROAD-BAND (TM) RATIO SIMULATION K2
B
READING
2.028
1.928
1.828
1.728
1.628
1.528
1.428
1.328
1.228
100.0
200.0
300.0
400.0
500.0
600.0
700.0
800.0
SAMPLE #

Figure 7.1 Geologic map of the Hamersley Basin showing the distribution of its major components (modified after Smith et al., 1982).

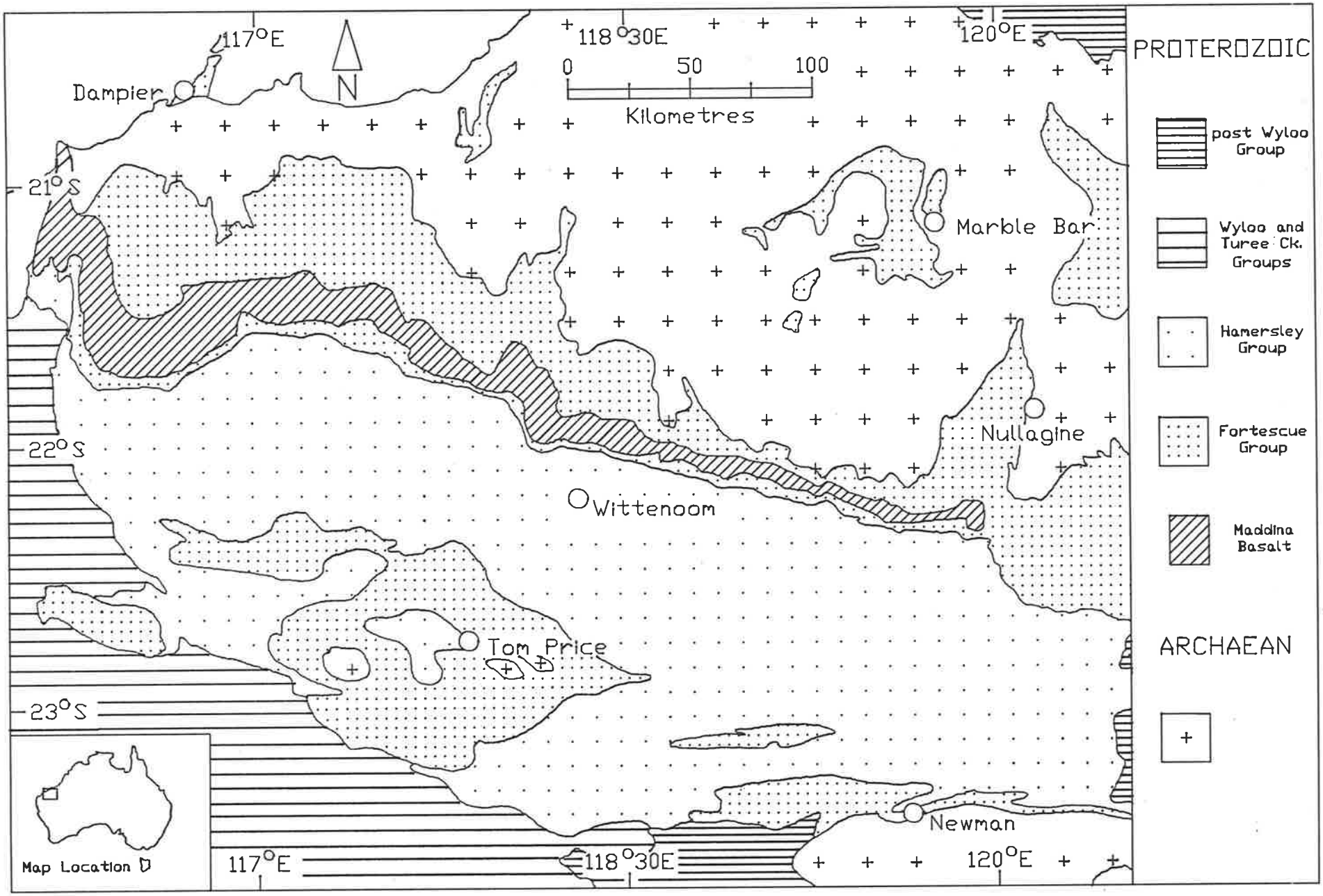
117°E
118°30E
120°E
N
0
50
100
Kilometres
Dampier
21°S
22°S
23°S
Marble Bar
Nullagine
Wittenoom
Tom Price
Newman
Map Location
PROTEROZOIC
post Wyloo Group
Wyloo and Turee Ck. Groups
Hamersley Group
Fortescue Group
Maddina Basalt
ARCHAEAN

Figure 7.2 Typical profile through hydrothermally altered basic lava (after Smith et al., 1978).

Flows average about 50m in thickness. The altered flow-top lithologies are dominantly amygdaloidal, greenish-grey, and heterogeneous on an outcrop scale. Fresh material from the central layers is grey, fine-grained and uniform.

Figure 7.3 Plot of total Fe, as FeO, for two metasomatically altered lava flows in the Hamersley Basin (after Smith et al., 1982).

Analyses of samples from massive portions of flows C and E form a cluster of points of relatively uniform composition. Flow-top compositions vary widely, interpreted as being due to metasomatic alteration.

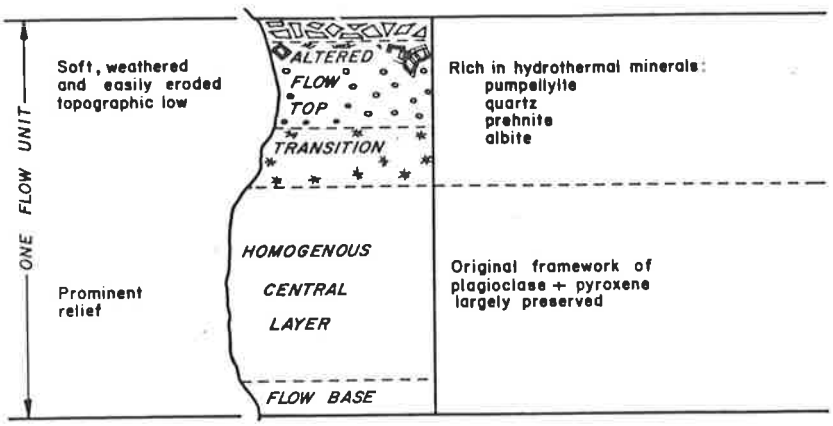
ONE FLOW UNIT
Soft, weathered and easily eroded topographic low
Prominent relief
ALTERED
FLOW TOP
TRANSITION
HOMOGENOUS CENTRAL LAYER
FLOW BASE
Rich in hydrothermal minerals:
pumpellyite
quartz
prehnite
albite
Original framework of plagioclase + pyroxene largely preserved

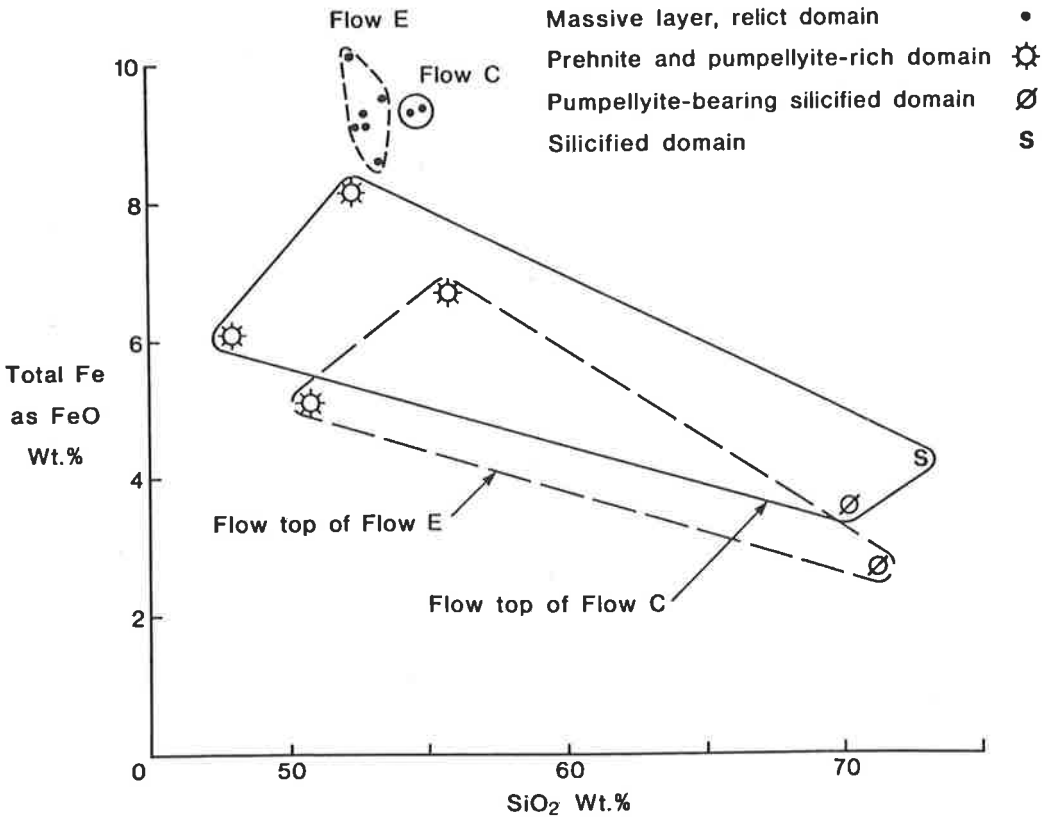
Flow E
Flow C
Massive layer, relict domain
Prehnite and pumpellyite-rich domain
Pumpellyite-bearing silicified domain
Silicified domain
S
Flow top of Flow E
Flow top of Flow C
Total Fe as FeO Wt.%
10
8
6
4
2
0
50
60
70
SiO2 Wt.%

Figure 7.4 Metamorphic zone boundaries and sample locations (modified after Smith et al., 1982).

Z-I samples come from the Maddina Basalt (see magnified inset). Other samples are from scattered locations, but mainly in the vicinity of Tom Price.

METAMORPHIC ZONES AND SAMPLE LOCATIONS

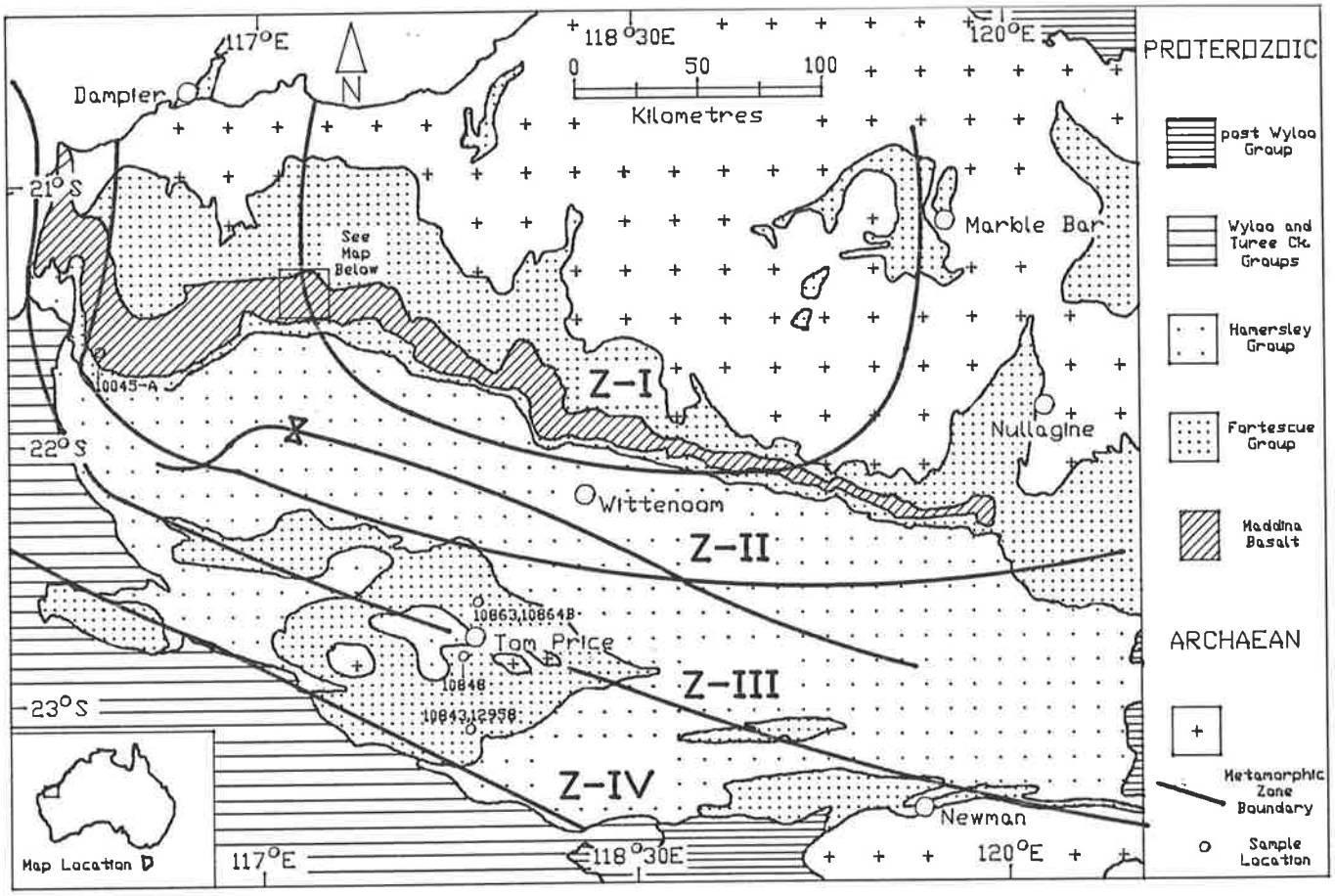

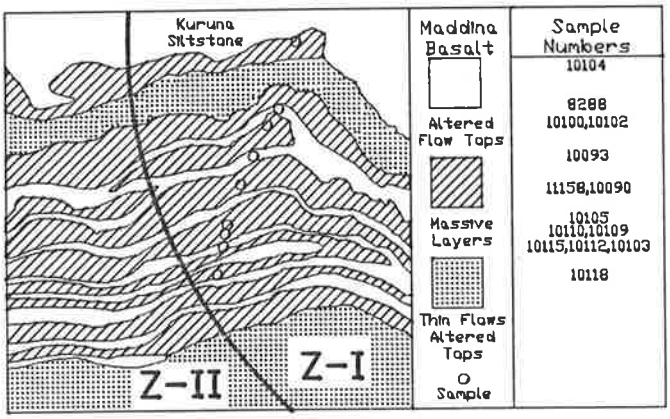

Figures 7.5a-c VNIR laboratory reflectance spectra of typical samples from Z-I of the Fortescue Group - weathered surfaces.

Most weathered surface spectra of Z-I rocks have the characteristics of haematite, with a single, broad absorption feature near .86μm. Note that sample 10112 is from an altered flow top, and sample 10090 is from the massive, central portion of a flow. The single goethitic spectrum (10112W2, Fig. 7.5c) was measured on a different part of the same sample as Fig. 7.5a.

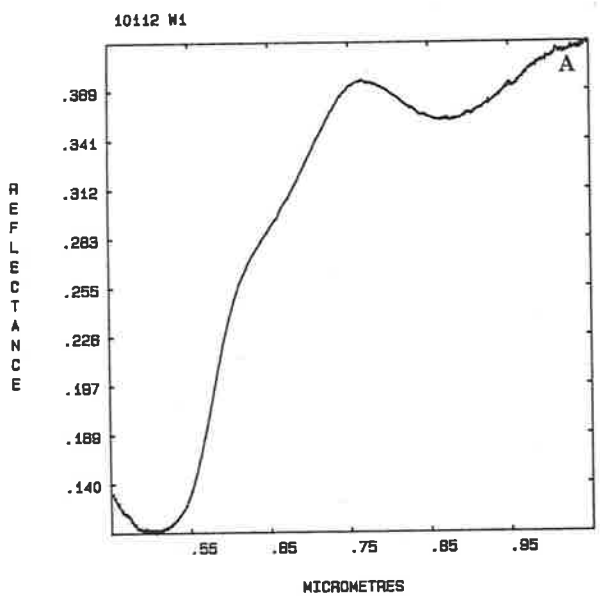
10112 W1
A
.389
.341
.312
.283
.255
.226
.197
.169
.140
REFLECTANCE
.55
.65
.75
.85
.95
MICROMETRES

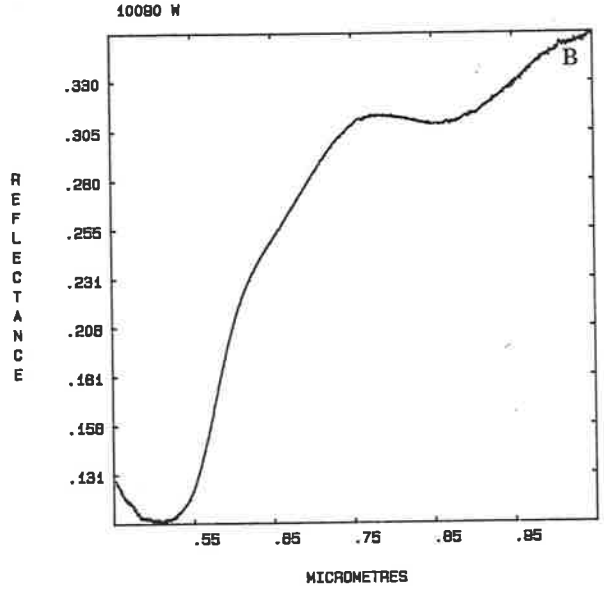
10090 W
B
.330
.305
.280
.255
.231
.208
.181
.158
.131
REFLECTANCE
.55
.65
.75
.85
.95
MICROMETRES

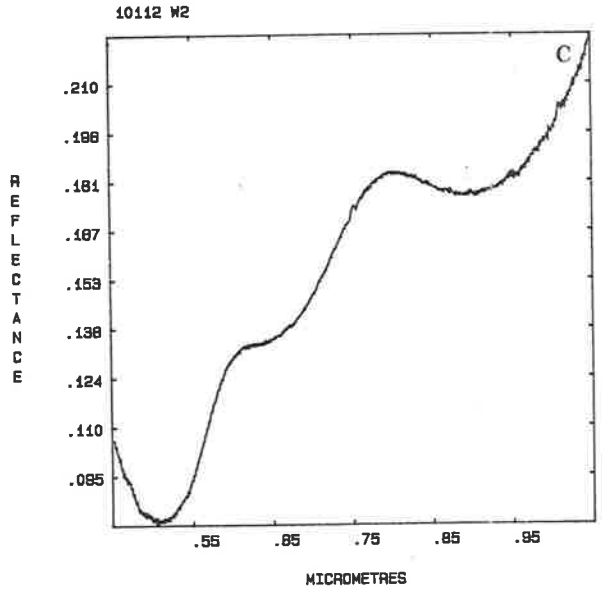
10112 W2
C
.210
.198
.181
.167
.153
.138
.124
.110
.095
REFLECTANCE
.55
.65
.75
.85
.95
MICROMETRES

Figures 7.6a&b VNIR laboratory reflectance spectra of typical samples from higher-grade areas of the Fortescue Group - weathered surfaces.

Figure 7.6a shows the spectrum of a sample from the massive part of a Z-IV flow. Note the similarity to Figs. 7.5a&b.

Figure 7.6b is the spectrum of another Z-IV sample. The lack of absorption features in this case is attributed to lower surficial iron, probably because of less severe weathering.

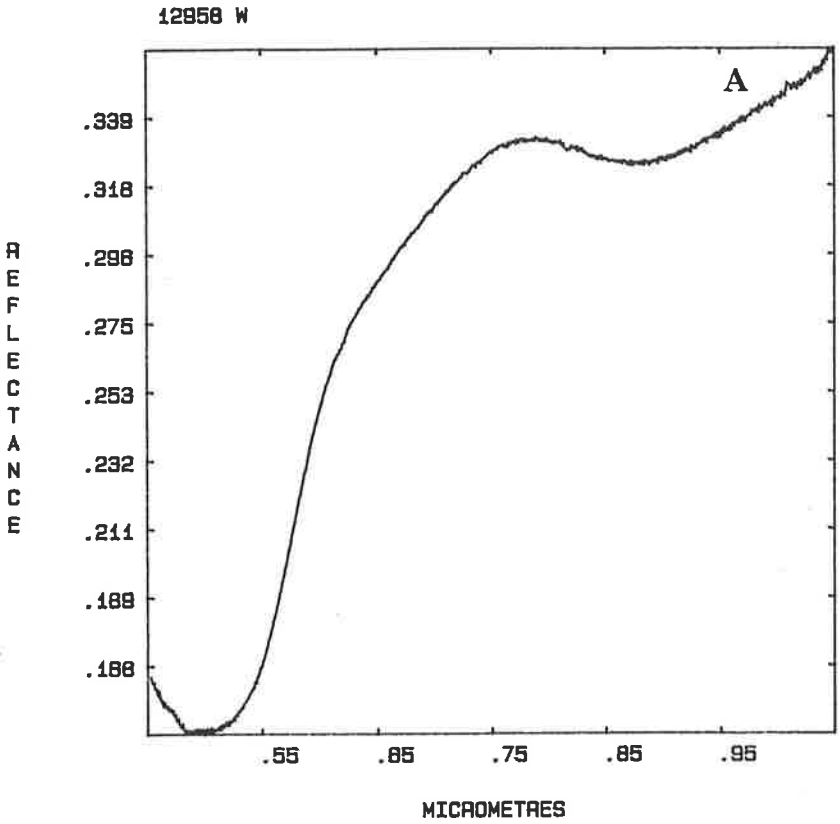
12958 W
A
.339
.318
.298
.275
.253
.232
.211
.189
.168
REFLECTANCE
.55
.65
.75
.85
.95
MICROMETRES

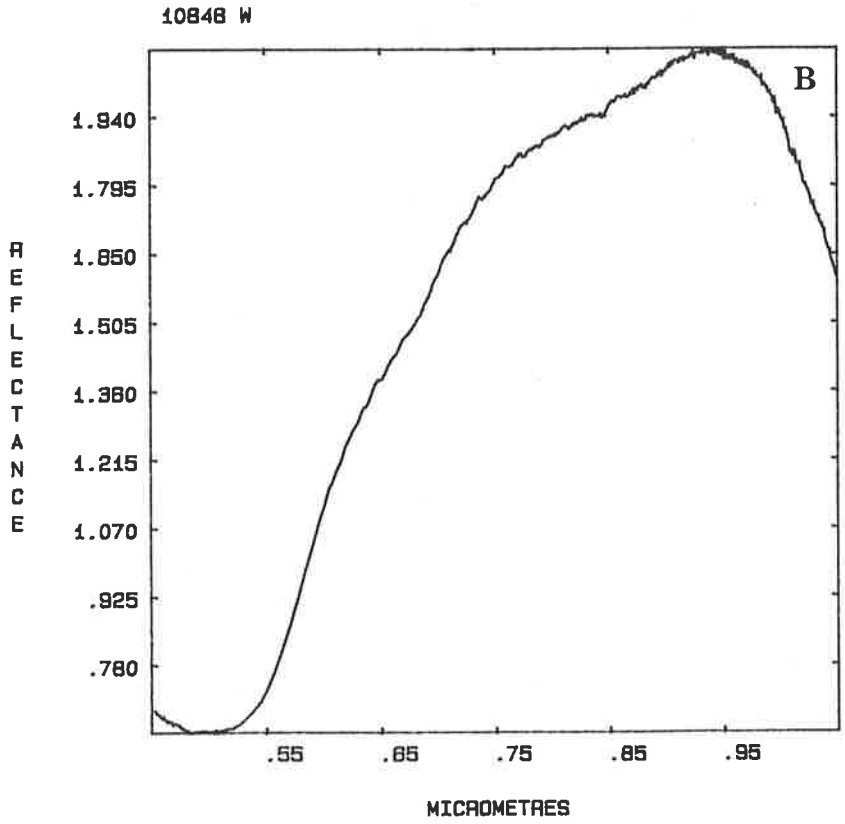
10848 W
B
1.940
1.795
1.650
1.505
1.360
1.215
1.070
.925
.780
REFLECTANCE
.55
.65
.75
.85
.95
MICROMETRES

Figures 7.7a-c VNIR laboratory reflectance spectra of typical samples from the Fortescue Group - fresh surfaces, and the spectrum of Fe^{2+} (after Burns, 1970).

Figures 7.7a&b are spectra of Z-I samples from the transition and from a massive, unaltered layer, respectively.

The absorption spectrum shown in Fig. 7.7c is of the aqueous Fe^{2+} ion in a solution of iron (II) ammonium sulphate, and is inverted relative to the reflectance spectra. Nevertheless, the same overall shape can be seen in all plots. Differences can be attributed to the crystal fields influencing absorption frequencies in the reflectance spectra.

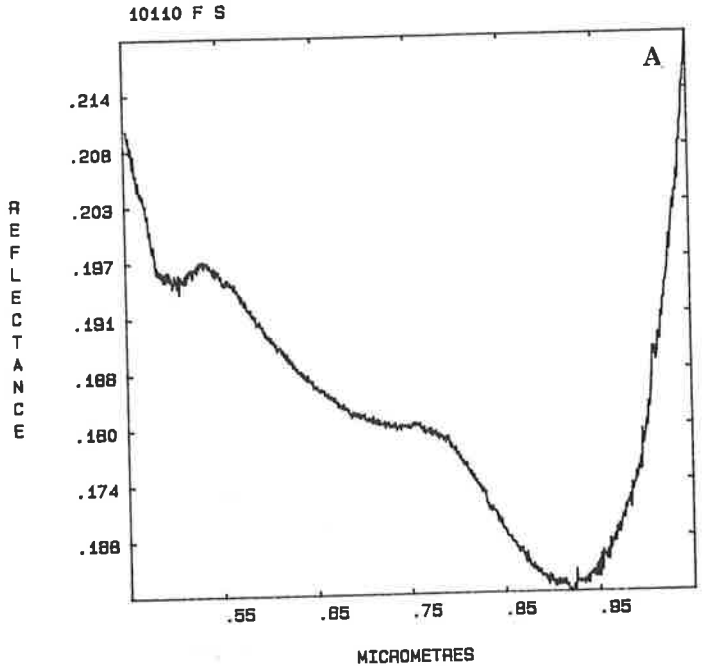
10110 F S
A
.214
.208
.203
.197
.191
.186
.180
.174
.168
.55
.65
.75
.85
.95
MICROMETRES
REFLECTANCE

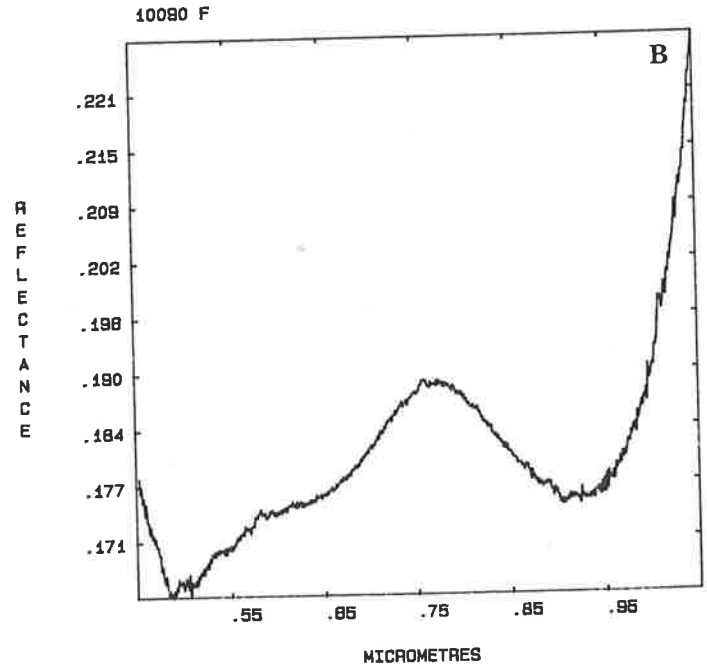
10090 F
B
.221
.215
.209
.202
.196
.190
.184
.177
.171
.55
.65
.75
.85
.95
MICROMETRES
REFLECTANCE

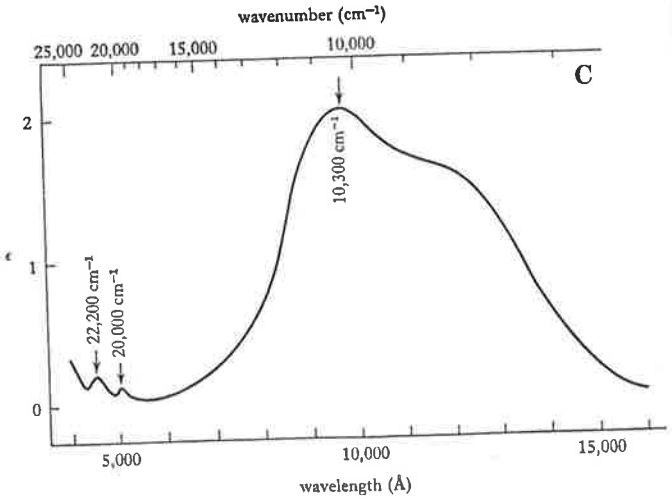
wavenumber (cm⁻¹)
25,000 20,000 15,000 10,000
C
2
1
0
10,300 cm⁻¹
22,200 cm⁻¹
20,000 cm⁻¹
5,000
10,000
15,000
wavelength (Å)

Figures 7.8a-c VNIR laboratory reflectance spectra of pumpellyite- and epidote-bearing samples from the Fortescue Group - fresh surfaces, and the polarised absorption spectrum of epidote (after Burns, 1970).

Figures 7.8a&b are spectra of an epidote-bearing rock and a pumpellyite-bearing rock, respectively.

Figure 7.8c comprises polarised absorption spectra of epidote (dots, α spectrum, dashes β spectrum, solid line γ spectrum). Inset is the absorption spectrum of Fe^{3+} in ferric ammonium sulphate solution. Although inverted relative to the reflectance spectra, a number of similarities are evident.

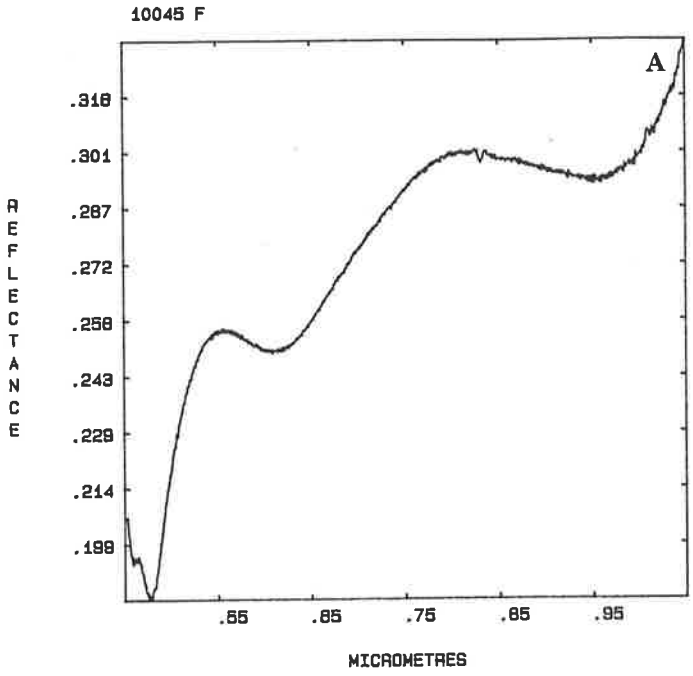
10045 F
A
.318
.301
.287
.272
.258
.243
.229
.214
.198
REFLECTANCE
.55
.65
.75
.85
.95
MICROMETRES

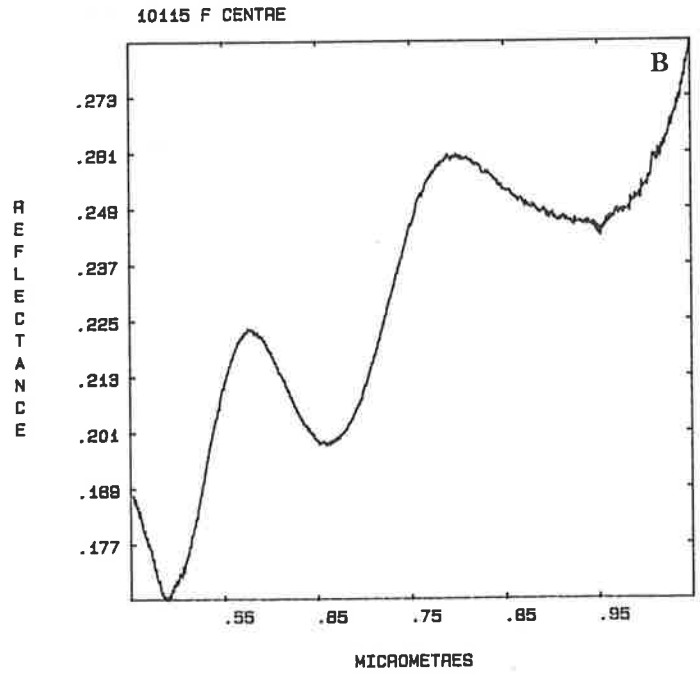
10115 F CENTRE
B
.273
.261
.249
.237
.225
.213
.201
.189
.177
REFLECTANCE
.55
.65
.75
.85
.95
MICROMETRES

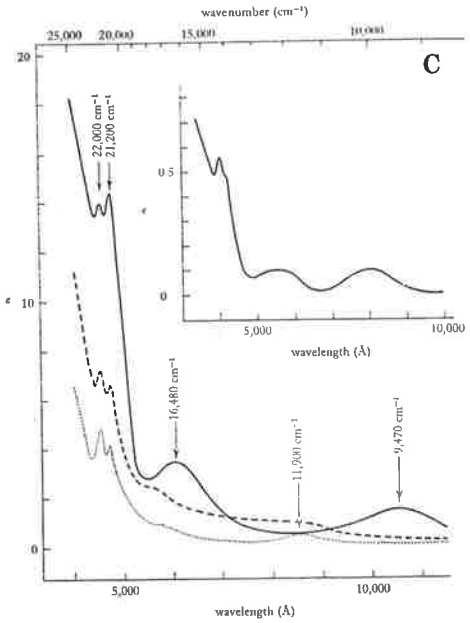
wavenumber (cm⁻¹)
25,000
20,000
15,000
10,000
C
22,000 cm⁻¹
21,200 cm⁻¹
16,480 cm⁻¹
11,900 cm⁻¹
9,470 cm⁻¹
wavelength (Å)
5,000
10,000

Figure 7.9 SWIR laboratory reflectance spectrum of pumpellyite compared to radiance of a 100% reflector at sea level.

The pumpellyite spectrum is shown as the dark line, while the radiance spectrum is the faint line. The radiance plot contains the theoretical atmospheric absorption features present in a spectrum measured at sea-level.

The comparison shows that all except the 1.8μm absorption feature should be detectable in a remote sensing mode.

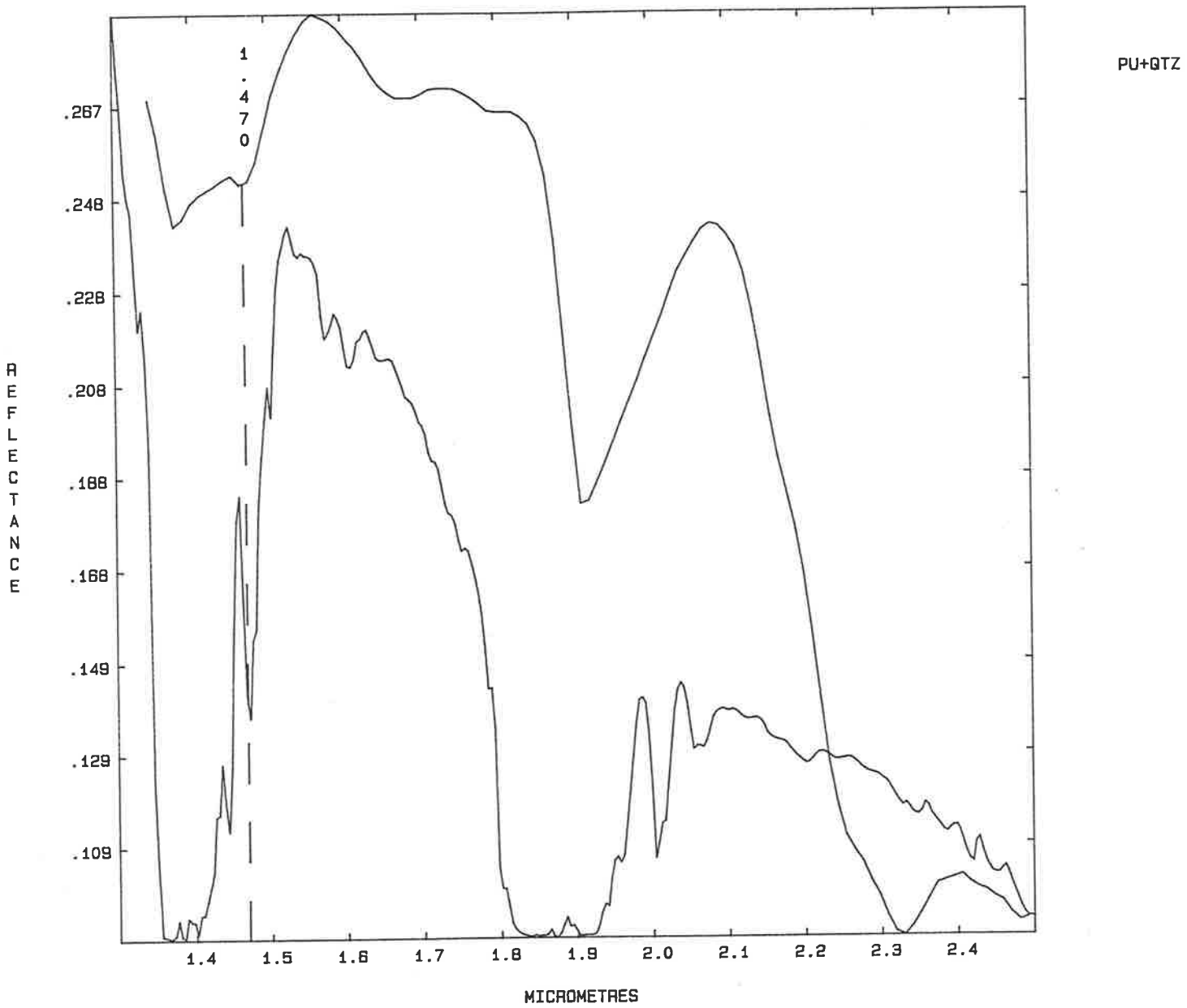
1.470
.267
.248
.228
.208
.188
.168
.149
.129
.109
REFLECTANCE
1.4
1.5
1.6
1.7
1.8
1.9
2.0
2.1
2.2
2.3
2.4
MICROMETRES
PU+QTZ

Figures 7.10a-d SWIR laboratory reflectance spectra of typical altered samples from the Fortescue Group - weathered surfaces.

Samples depicted in Figs. 7.10a-c are from Z-I, that in Fig 7.10d is from Z-II. Fig. 7.10a depicts a pumpellyite spectrum. Almost all of the features in Fig. 7.9 can be seen here.

Figure 7.10b exhibits only some of the pumpellyite features. In particular, the 1.47μm absorption feature is diagnostic. The 2.3μm absorption is due to a mixture of pumpellyite and chlorite, and is not recognisable as either.

Figure 7.10c shows a weak 2.2μm absorption feature (probably kaolin). Although the mineralogy of this sample is pumpellyite + quartz, in this case the surface weathering rind is too thick to allow diagnostic spectral features to be seen.

Despite being the spectrum of a weathered surface, Fig. 7.10d shows all of the characteristics of epidote (see Hunt et al., 1973a, p.91). The feature at 2.32μm is particularly strong. Epidote is a resistant mineral, and presumably persists in the weathered surface rind.

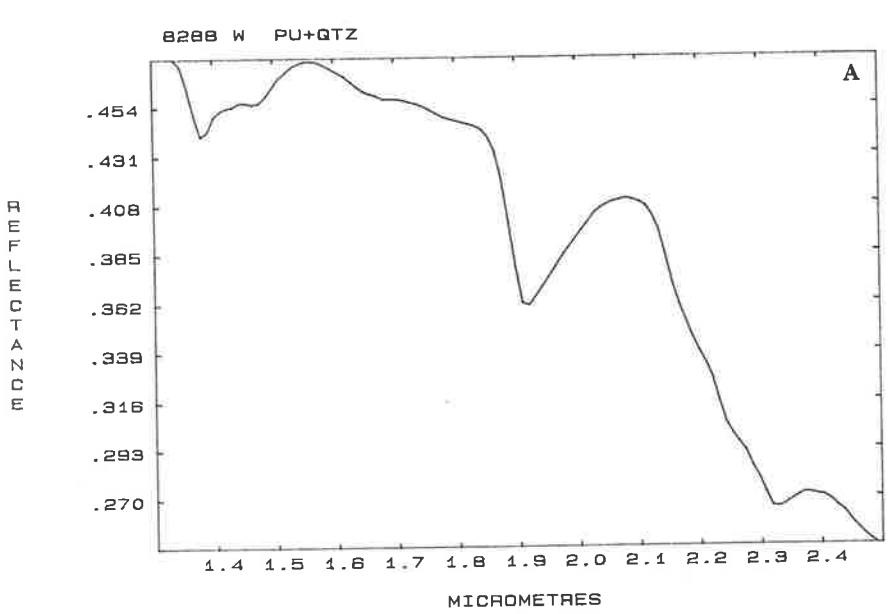
8288 W PU+QTZ
A
REFLECTANCE
.454
.431
.408
.385
.362
.339
.316
.293
.270
1.4 1.5 1.6 1.7 1.8 1.9 2.0 2.1 2.2 2.3 2.4
MICROMETRES

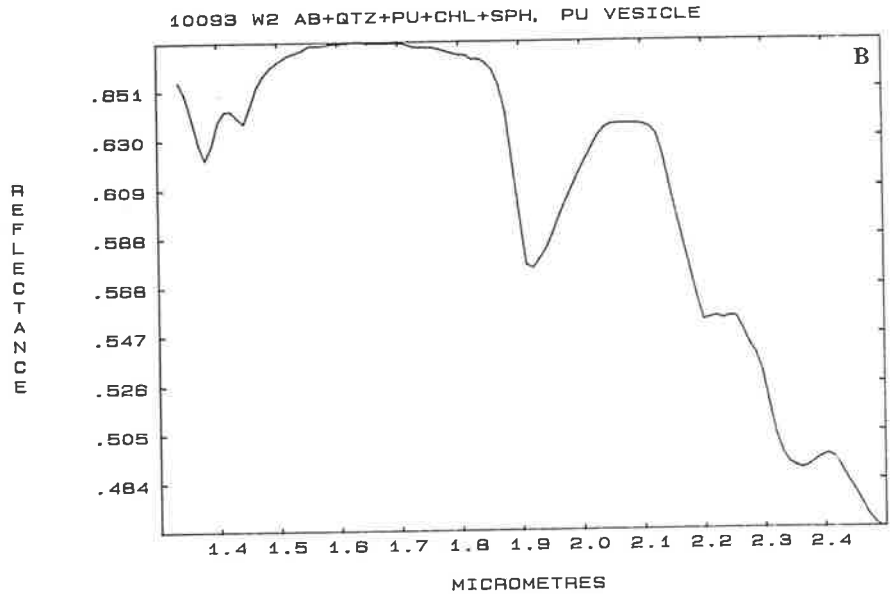
10093 W2 AB+QTZ+PU+CHL+SPH. PU VESICLE
B
REFLECTANCE
.851
.630
.609
.588
.568
.547
.526
.505
.484
1.4 1.5 1.6 1.7 1.8 1.9 2.0 2.1 2.2 2.3 2.4
MICROMETRES

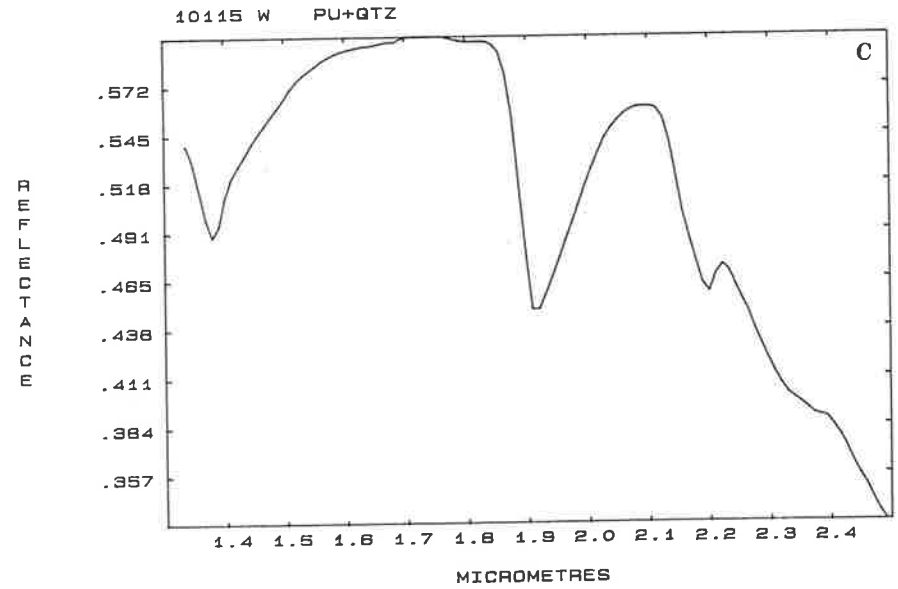
10115 W PU+QTZ
C
REFLECTANCE
.572
.545
.518
.491
.465
.438
.411
.384
.357
1.4 1.5 1.6 1.7 1.8 1.9 2.0 2.1 2.2 2.3 2.4
MICROMETRES

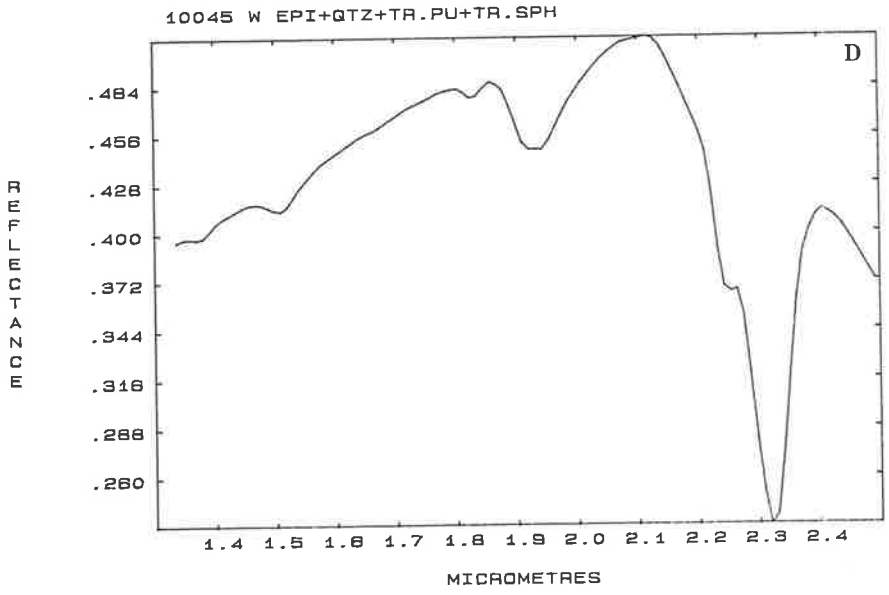
10045 W EPI+QTZ+TR.PU+TR.SPH
D
REFLECTANCE
.484
.456
.428
.400
.372
.344
.316
.288
.260
1.4 1.5 1.6 1.7 1.8 1.9 2.0 2.1 2.2 2.3 2.4
MICROMETRES

Figures 7.11a&b SWIR laboratory reflectance spectra of typical metadomain samples from Z-I of the Fortescue Group - weathered surfaces.

Both spectra have 2.2μm absorption features, probably due to kaolin. Figure 7.11b also has a 2.3μm feature due to chlorite, although this identification cannot be made from the spectrum alone.

The similarity of these plots to Fig. 7.10c means that there will be cases where SWIR reflectance spectra will not discriminate altered and unaltered samples.

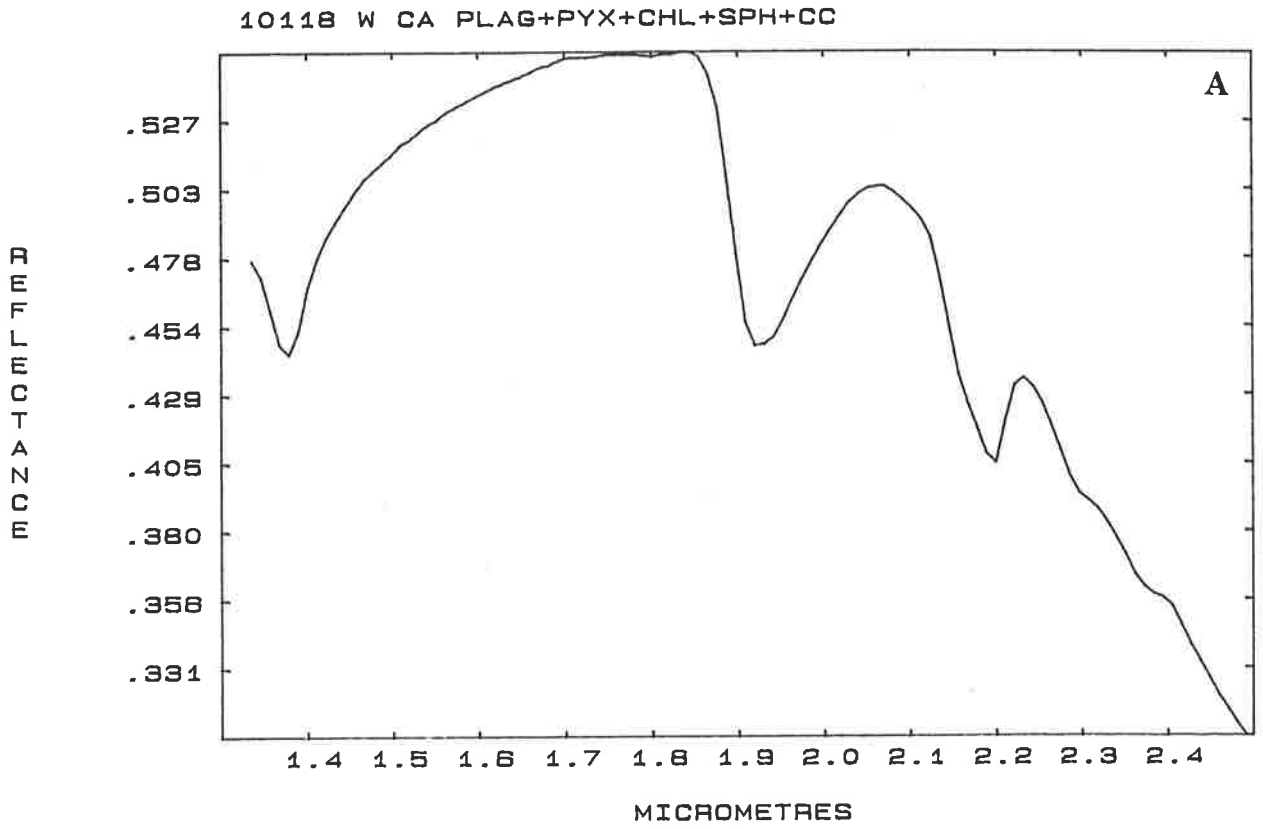
10118 W CA PLAG+PYX+CHL+SPH+CC
A
.527
.503
.478
.454
.429
.405
.380
.358
.331
REFLECTANCE
1.4 1.5 1.6 1.7 1.8 1.9 2.0 2.1 2.2 2.3 2.4
MICROMETRES

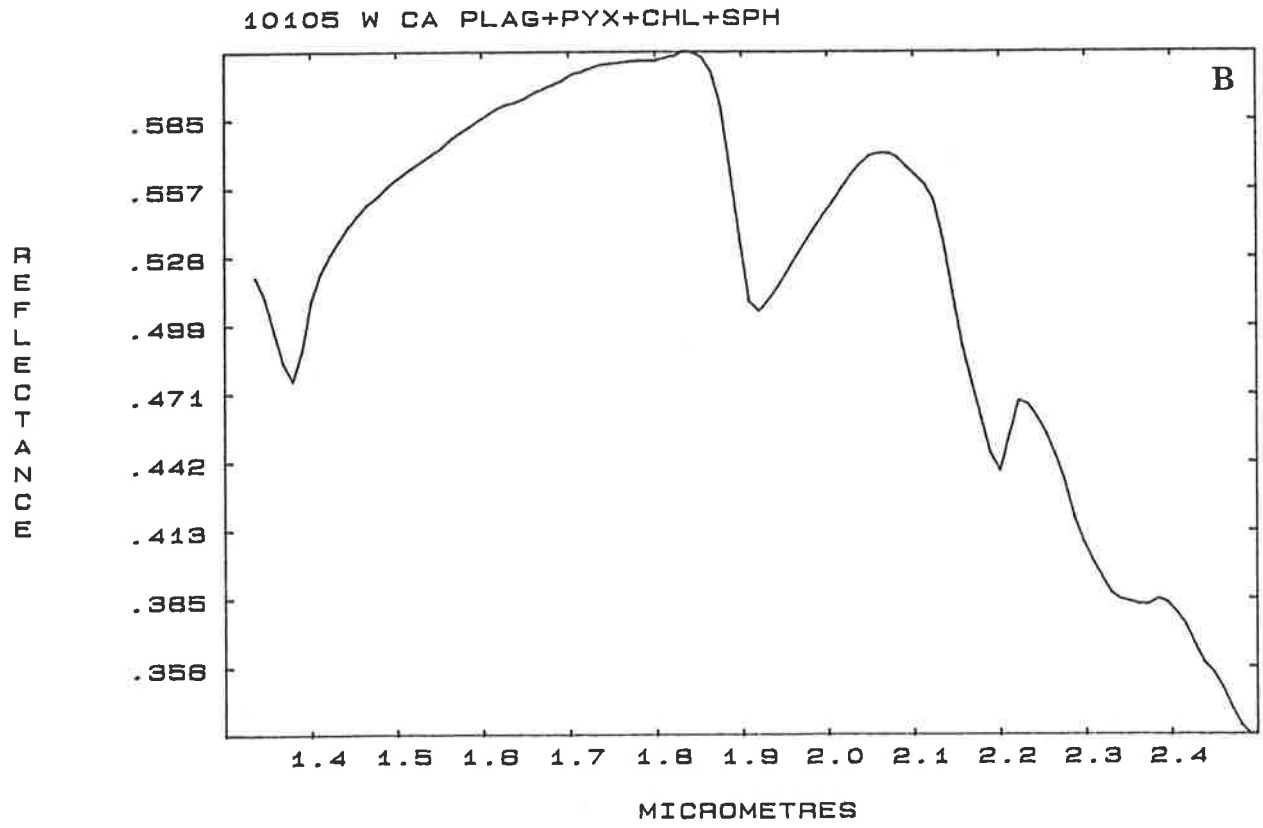
10105 W CA PLAG+PYX+CHL+SPH
B
.585
.557
.528
.499
.471
.442
.413
.385
.356
REFLECTANCE
1.4 1.5 1.6 1.7 1.8 1.9 2.0 2.1 2.2 2.3 2.4
MICROMETRES

Figures 7.12a&b SWIR laboratory reflectance spectra of chlorite- and actinolite-bearing samples from higher-grade areas of the Fortescue Group - weathered surfaces.

Figure 7.12a is the chlorite spectrum. Note the similarity in the 2.3μm region to pumpellyite (Fig. 7.9). However, the lack of an absorption feature at 1.47μm, and the presence of the 2.0μm absorption feature are sufficient to differentiate these two minerals.

Figure 7.12b is an actinolite spectrum. The shape of the 2.3μm feature, and the shoulder at 2.4μm indicate this. A larger number of spectra need to be measured before the feasibility of accurately mapping actinolite in this environment can be determined.

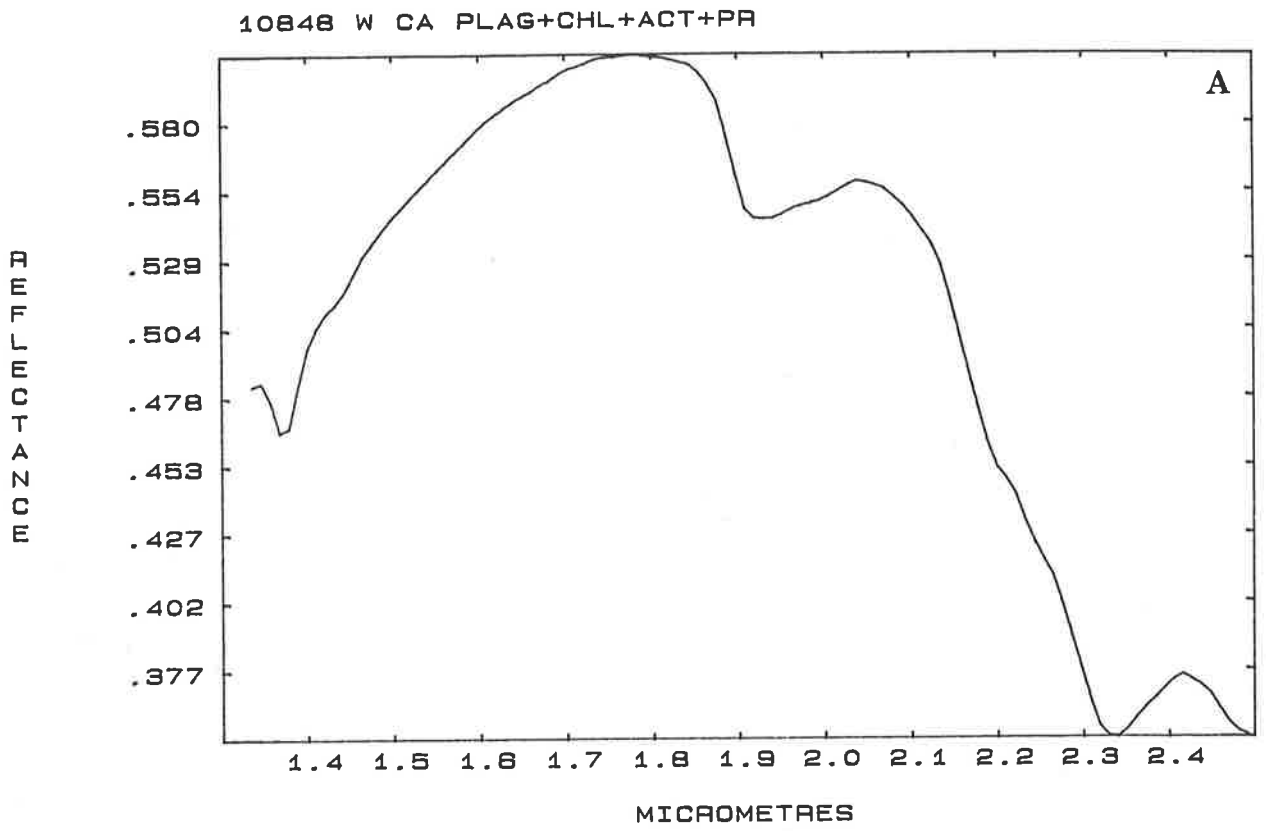
10848 W CA PLAG+CHL+ACT+PR
A
.580
.554
.529
.504
.478
.453
.427
.402
.377
REFLECTANCE
1.4 1.5 1.6 1.7 1.8 1.9 2.0 2.1 2.2 2.3 2.4
MICROMETRES

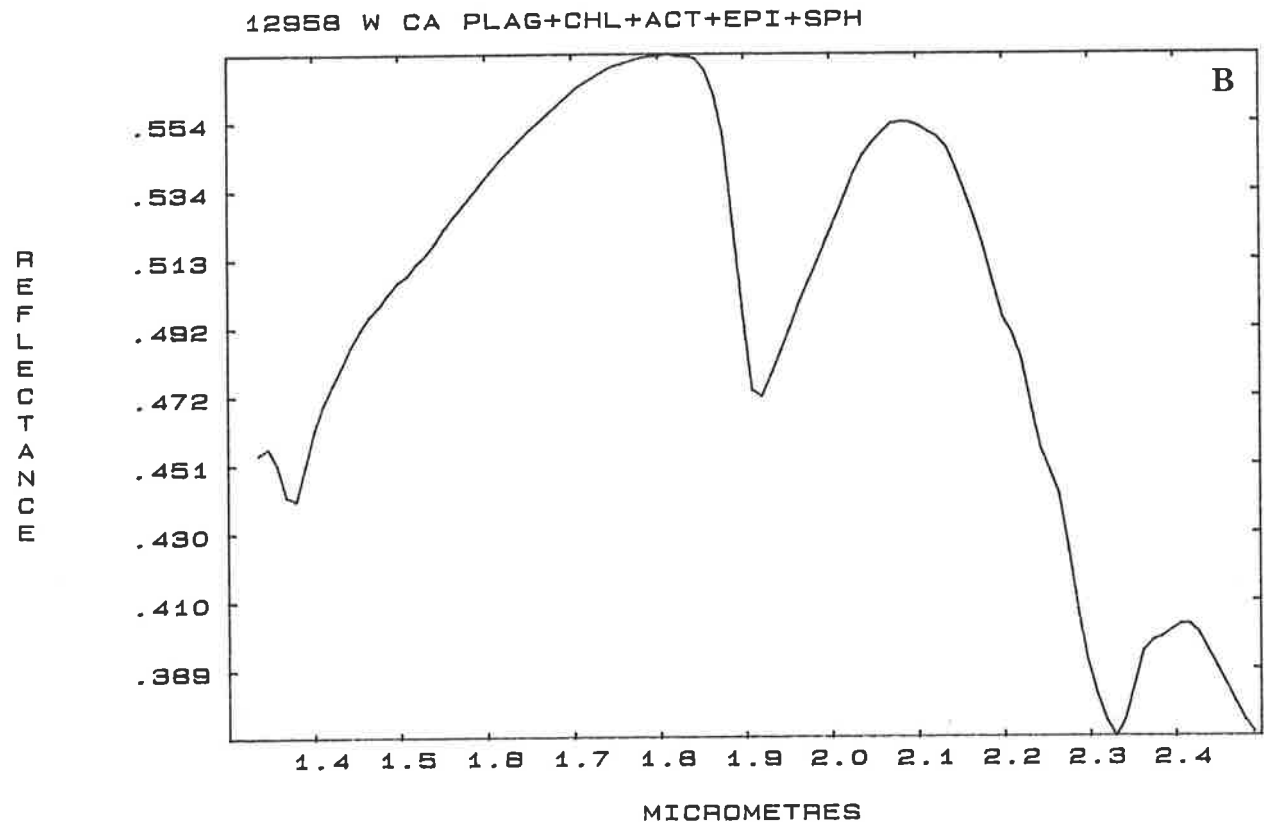
12958 W CA PLAG+CHL+ACT+EPI+SPH
B
.554
.534
.513
.492
.472
.451
.430
.410
.389
REFLECTANCE
1.4 1.5 1.6 1.7 1.8 1.9 2.0 2.1 2.2 2.3 2.4
MICROMETRES

Figure 7.13a&b SWIR laboratory reflectance spectra of chlorite-bearing samples from Z-I of the Fortescue Group - fresh surfaces.

Both spectra have the characteristic chlorite absorption features at 2.0 and 2.26μm.

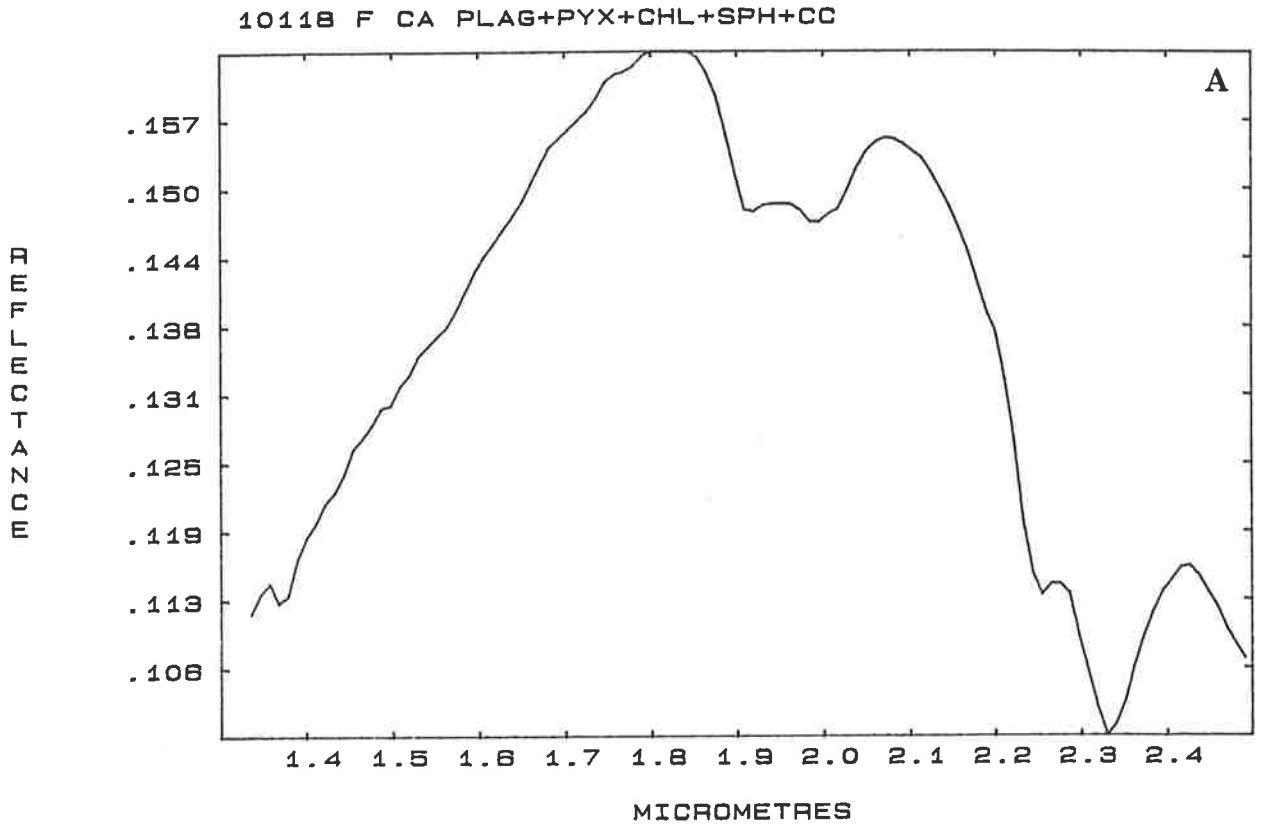
10118 F CA PLAG+PYX+CHL+SPH+CC
A
.157
.150
.144
.138
.131
.125
.119
.113
.108
REFLECTANCE
1.4 1.5 1.6 1.7 1.8 1.9 2.0 2.1 2.2 2.3 2.4
MICROMETRES

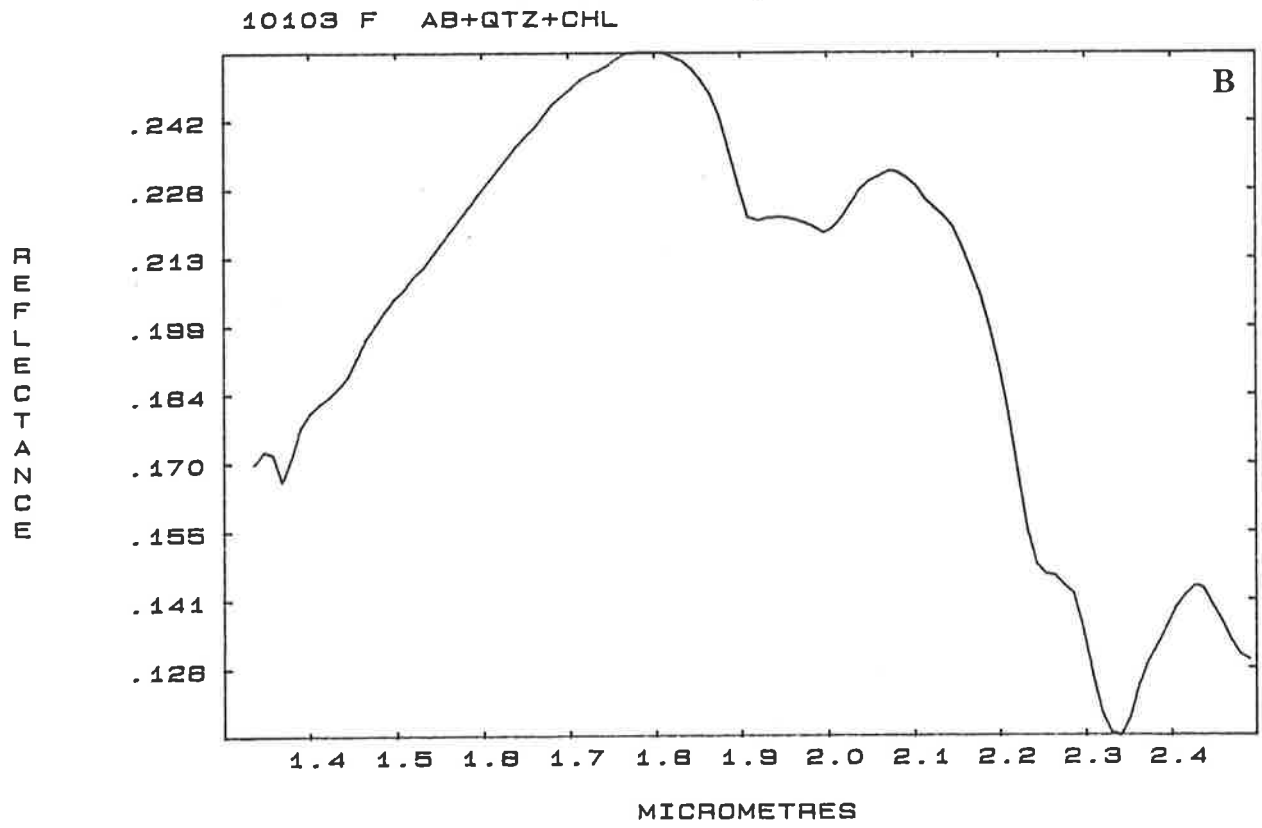
10103 F AB+QTZ+CHL
B
.242
.228
.213
.199
.184
.170
.155
.141
.128
REFLECTANCE
1.4 1.5 1.6 1.7 1.8 1.9 2.0 2.1 2.2 2.3 2.4
MICROMETRES

Figure 7.14a&b SWIR laboratory reflectance spectra of pumpellyite-bearing samples from Z-I of the Fortescue Group - fresh surfaces.

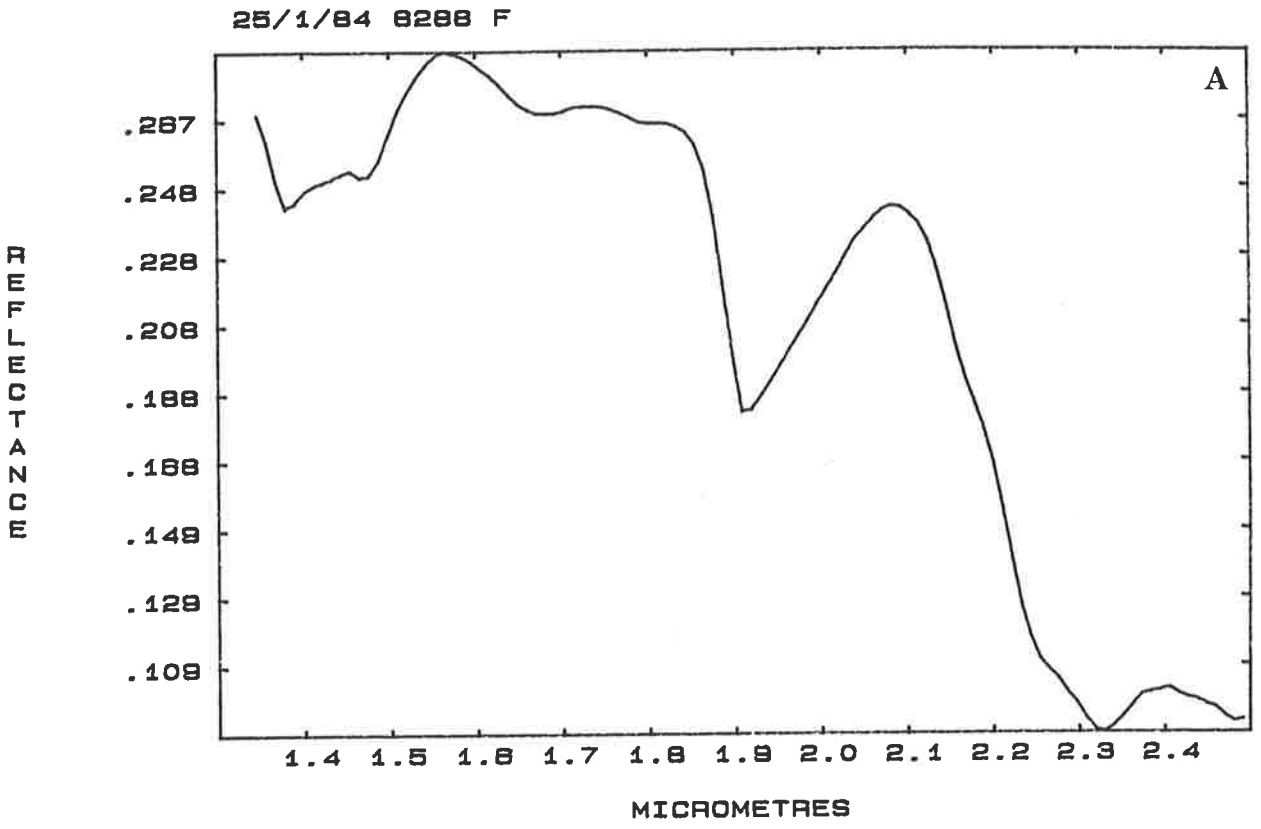
25/1/84 8288 F
A
REFLECTANCE
.287
.248
.228
.208
.188
.168
.149
.129
.109
1.4 1.5 1.6 1.7 1.8 1.9 2.0 2.1 2.2 2.3 2.4
MICROMETRES

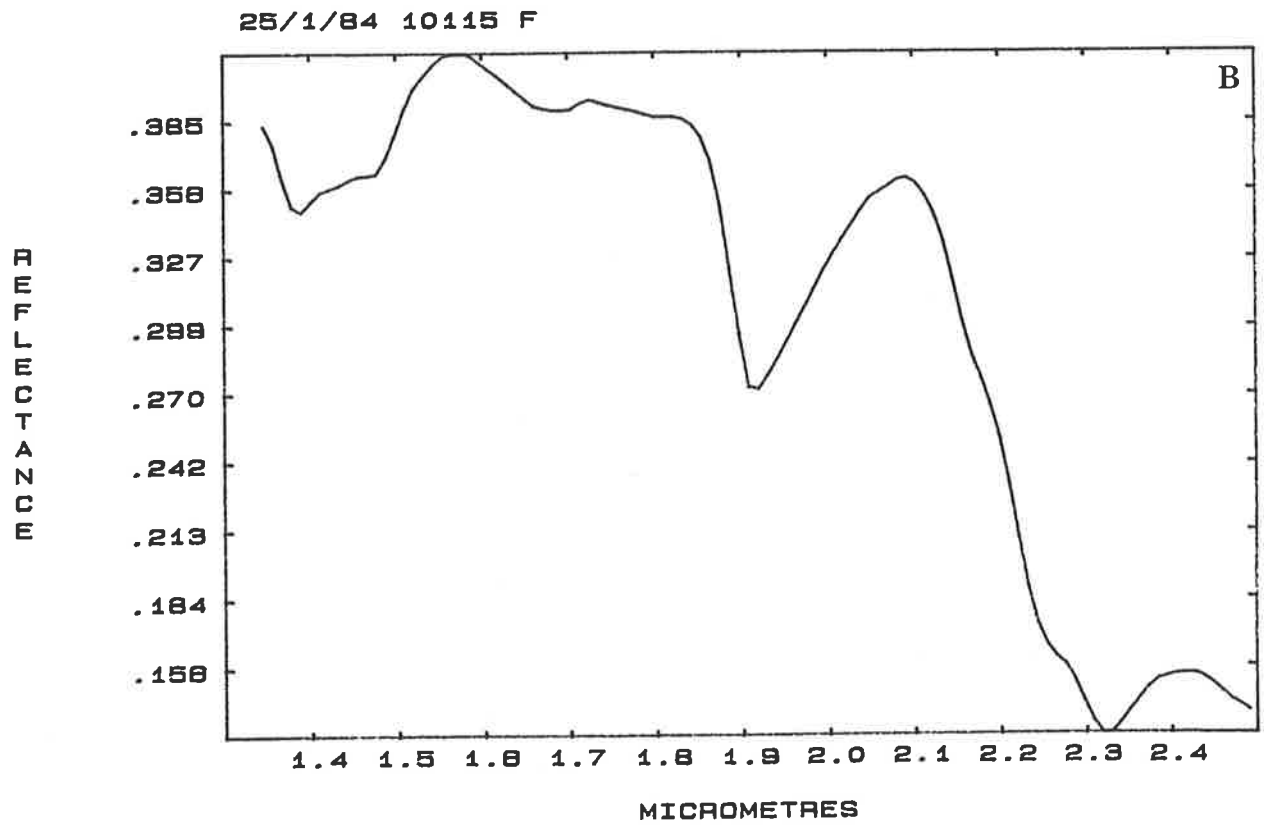
25/1/84 10115 F
B
REFLECTANCE
.385
.358
.327
.298
.270
.242
.213
.184
.158
1.4 1.5 1.6 1.7 1.8 1.9 2.0 2.1 2.2 2.3 2.4
MICROMETRES

Figures 7.15a-c SWIR laboratory reflectance spectra of typical samples from higher-grade areas of the Fortescue Group - fresh surfaces.

The spectra shown in Figs. 7.15a-c are dominated by effects due to epidote, chlorite, and a chlorite/epidote mixture, respectively. Figures 7.15b&c also appear to have a minor influence due to actinolite. Prehnite (which has a 2.3μm feature similar to pumpellyite, but different structure in the 1.4 to 1.6μm region - V. Gardavsky, pers. comm., 1986) may also be influencing the shape of the spectrum in Fig. 7.15b.

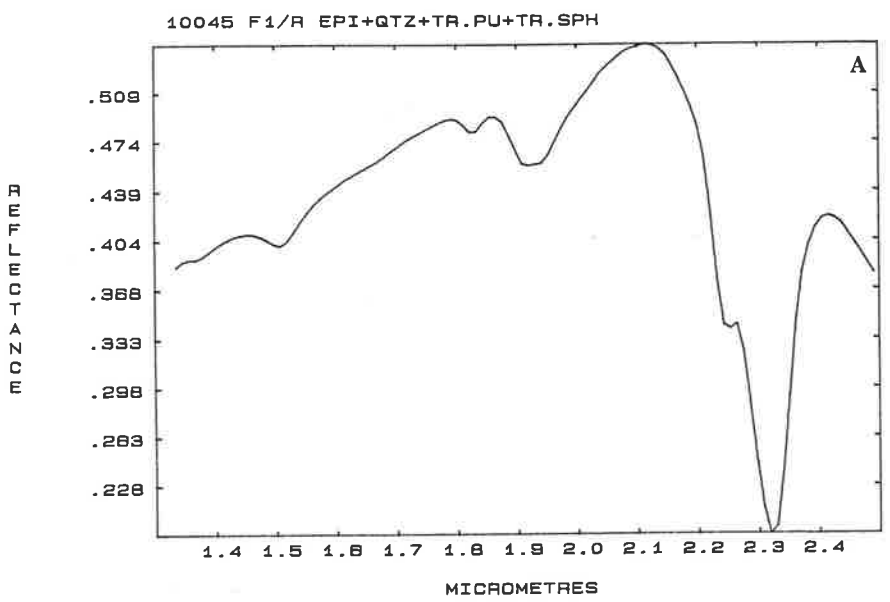
10045 F1/R EPI+QTZ+TR.PU+TR.SPH
A
REFLECTANCE
.509
.474
.439
.404
.368
.333
.298
.263
.228
1.4 1.5 1.6 1.7 1.8 1.9 2.0 2.1 2.2 2.3 2.4
MICROMETRES

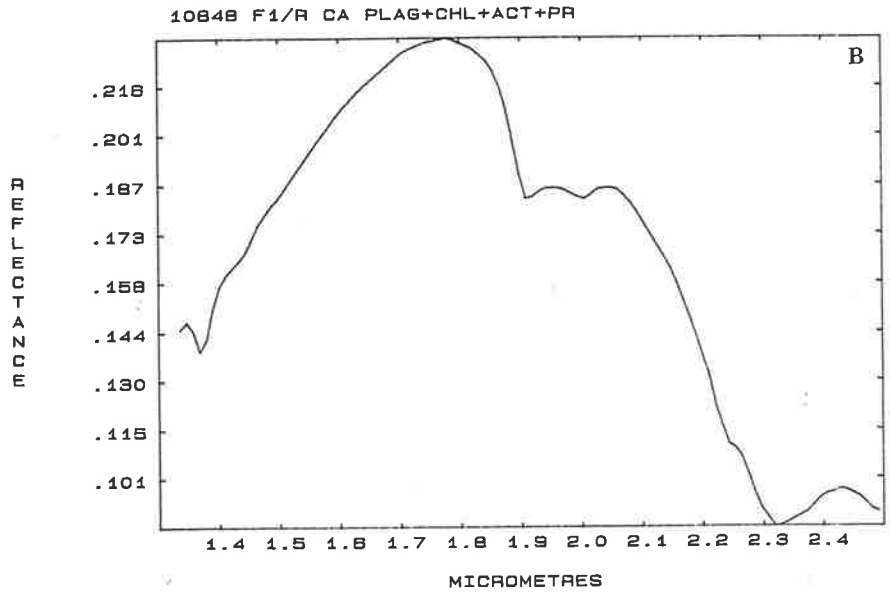
10848 F1/R CA PLAG+CHL+ACT+PR
B
REFLECTANCE
.218
.201
.187
.173
.158
.144
.130
.115
.101
1.4 1.5 1.6 1.7 1.8 1.9 2.0 2.1 2.2 2.3 2.4
MICROMETRES

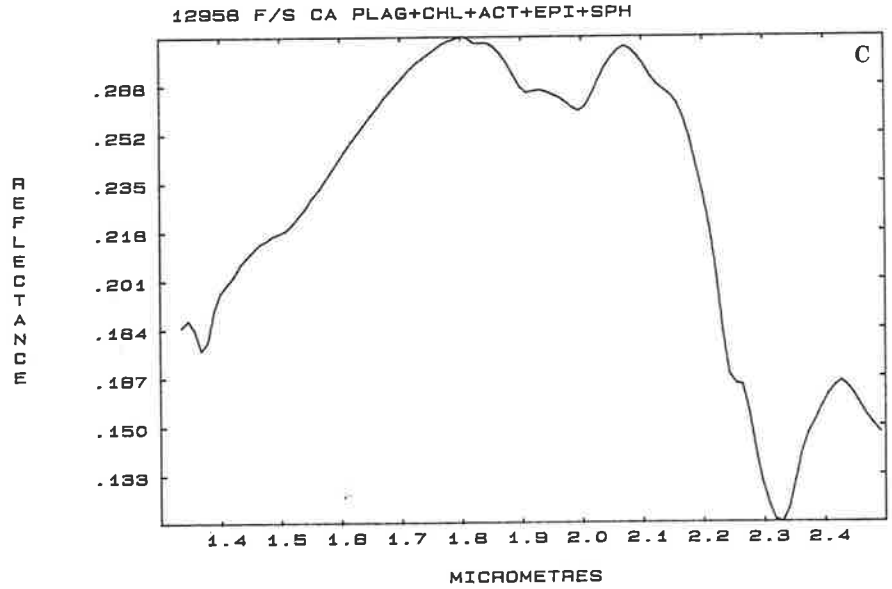
12958 F/S CA PLAG+CHL+ACT+EPI+SPH
C
REFLECTANCE
.288
.252
.235
.218
.201
.184
.187
.150
.133
1.4 1.5 1.6 1.7 1.8 1.9 2.0 2.1 2.2 2.3 2.4
MICROMETRES

Figures 7.16a&b MIR laboratory laser reflectance spectra of typical unaltered and altered samples from the Fortescue Group - weathered surfaces.

Figures 7.16a&b are spectra of Z-I samples, while Figs. 7.16c&d are spectra of Z-II samples. All spectra exhibit the characteristics of haematite (J. Eberhardt, pers. comm., 1984). However, Figs. 7.16b&d (from altered flow tops in Z-I and Z-II, respectively) are both quartz-rich, and show an additional maximum near 9.3μm. The wavelengths used for the ratio to discriminate altered and unaltered samples are marked by the vertical lines.

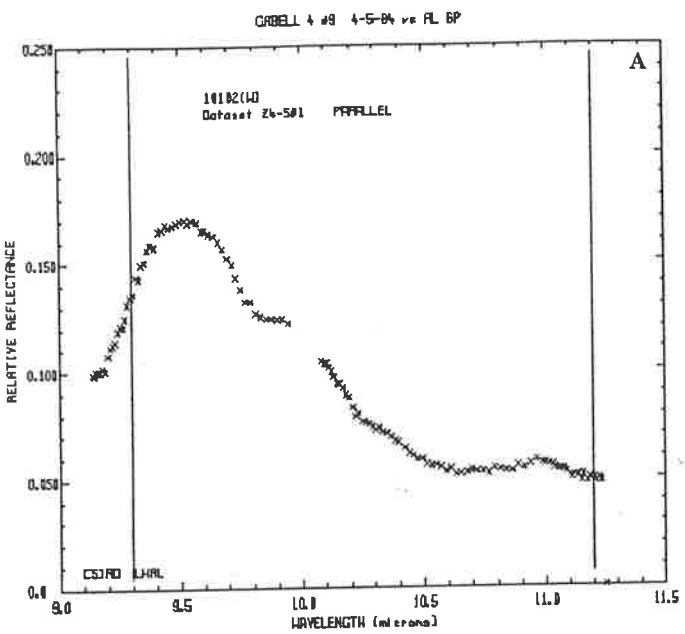
GABELL 4 #9 4-5-84 vs AL 6P
A
10182(W)
Dataset Z4-501 PARALLEL
RELATIVE REFLECTANCE
WAVELENGTH (microns)
CSIRO LHRL

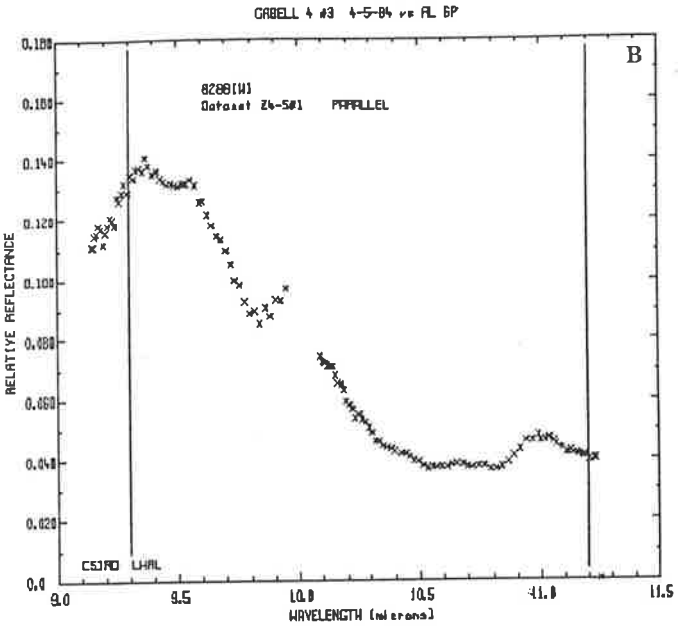
GABELL 4 #3 4-5-84 vs AL 6P
B
8288(W)
Dataset Z4-501 PARALLEL
RELATIVE REFLECTANCE
WAVELENGTH (microns)
CSIRO LHRL

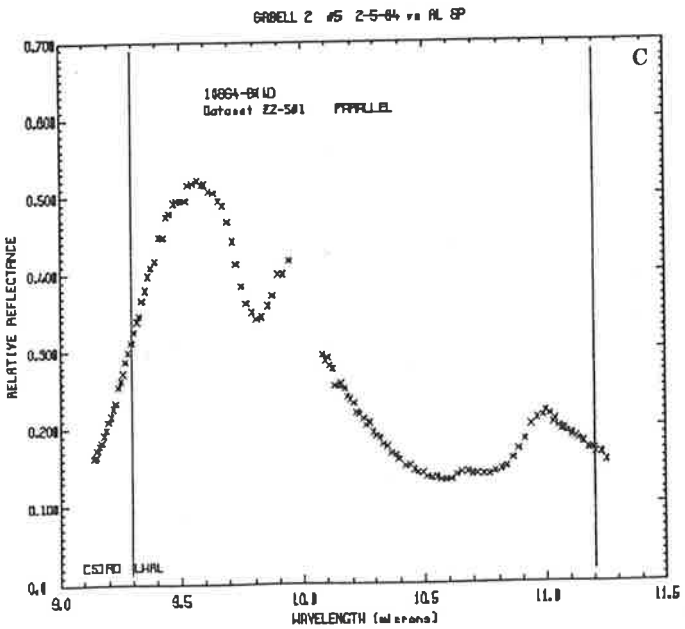
GABELL 2 #5 2-5-84 vs AL 6P
C
10884-6(W)
Dataset Z2-501 PARALLEL
RELATIVE REFLECTANCE
WAVELENGTH (microns)
CSIRO LHRL

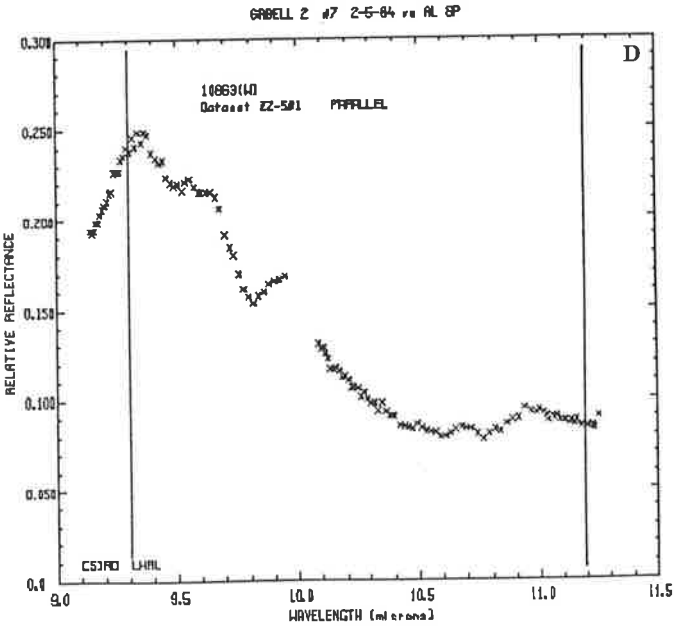
GABELL 2 #7 2-5-84 vs AL 6P
D
10883(W)
Dataset Z2-501 PARALLEL
RELATIVE REFLECTANCE
WAVELENGTH (microns)
CSIRO LHRL

Figure 7.17a&b MIR laboratory laser reflectance spectra of typical unaltered and altered samples from the Fortescue Group - fresh surfaces.

These spectra were measured from the same samples as those in Figs. 7.16a-d. Compare Figs. 7.17a&c to spectra in Figs. 2.12 and 2.13. Most of the unaltered samples from the Fortescue Group have fresh surface spectra of this type. Of the altered samples, Fig. 7.17b exhibits the spectral features of quartz (its mineralogy is pumpellyite + quartz), while Fig. 7.17c has characterisics that can be attributed to both of its major components - quartz and epidote (see Farmer, 1974 for epidote). Note that the reflectance maximum of quartz in Fig. 7.17b is at a shorter, and more commonly observed, wavelength (9.2μm) than in the weathered surface spectra.

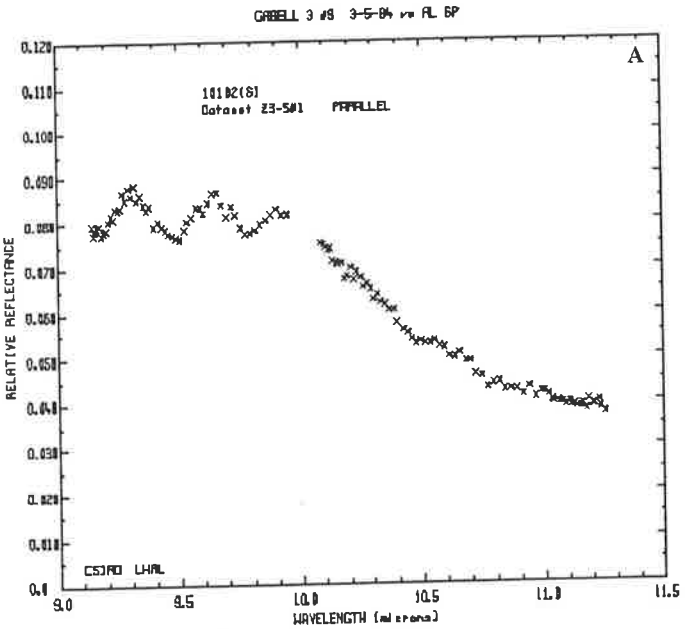
GABELL 3 #8 3-5-84 vs RL BP
A
10182(8)
Dataset Z3-5#1 PARALLEL
RELATIVE REFLECTANCE
WAVELENGTH (millerons)
CSIRO LHRL

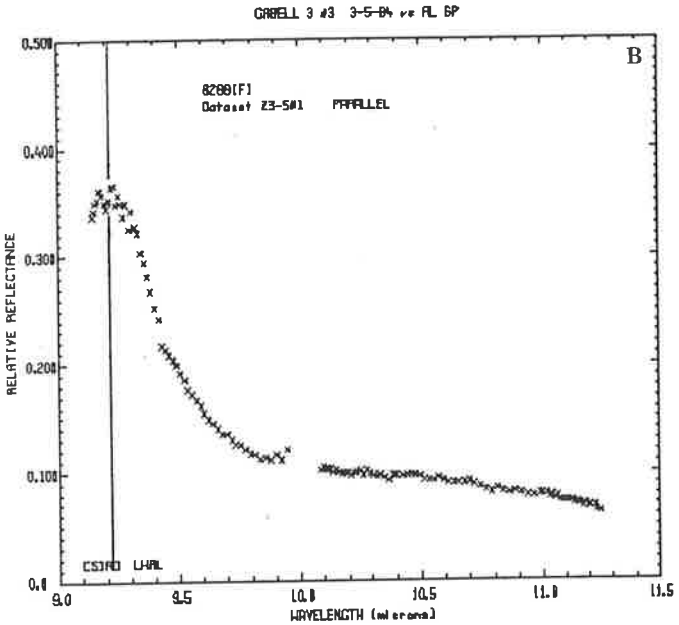
GABELL 3 #3 3-5-84 vs RL BP
B
8288(F)
Dataset Z3-5#1 PARALLEL
RELATIVE REFLECTANCE
WAVELENGTH (millerons)
CSIRO LHRL

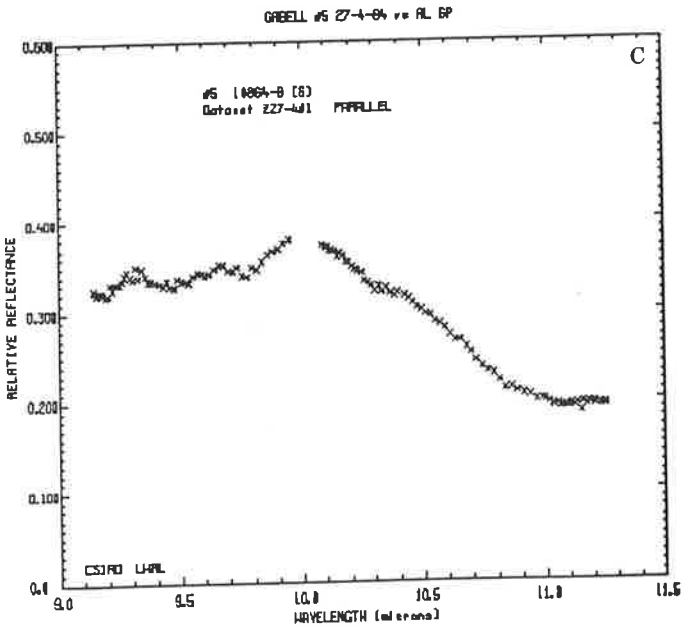
GABELL #6 27-4-84 vs RL BP
C
#6 10864-8 (8)
Dataset Z27-4#1 PARALLEL
RELATIVE REFLECTANCE
WAVELENGTH (millerons)
CSIRO LHRL

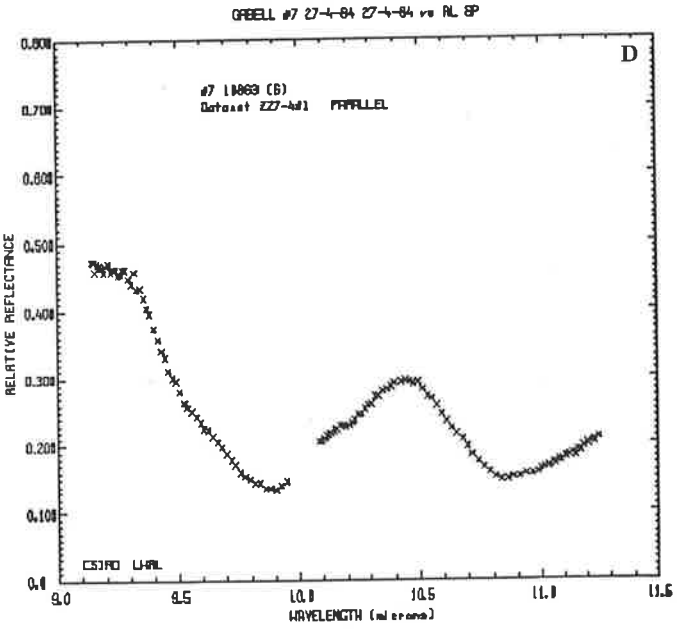
GABELL #7 27-4-84 27-4-84 vs RL BP
D
#7 10863 (8)
Dataset Z27-4#1 PARALLEL
RELATIVE REFLECTANCE
WAVELENGTH (millerons)
CSIRO LHRL

Figure 8.1 Photocopy of a colour aerial photograph of Peak Hill.

Peak Hill township lies immediately to the west of Peak Hill. Scale of the photograph is 1:25,000. Position of Gold Fields' grid (see Figs. 8.12 to 8.18) is shown.


05
27-2-82
3061-3096
PARKES
3086
AAM
1550c

Figure 8.2 Geology of Peak Hill (after Bowman and Richardson, 1978).

Position of Gold Fields' grid is shown.

PEAK HILL GEOLOGY

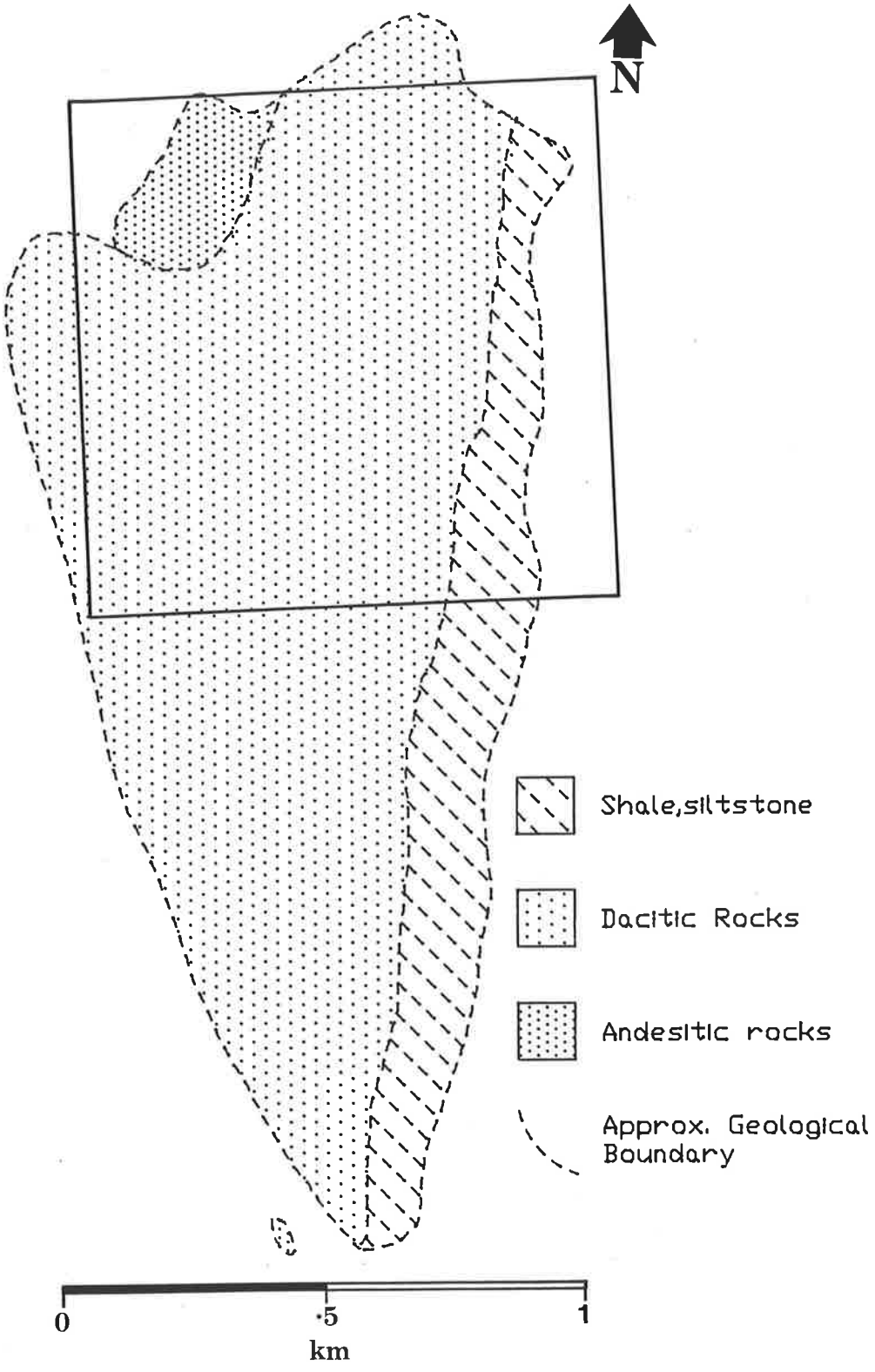

Figures 8.3a-c Representative VNIR laboratory reflectance spectra of core samples from Peak Hill.

The absorption feature in Fig. 8.3a is weak (0.08% depth), and centred at a longer wavelength than is usual for haematite (approx. .87μm) or goethite (approx. .92μm). The sample is from below the base of oxidation, and its spectral features can therefore be attributed to Fe^{2+}.

The spectrum shown in Fig. 8.3b is representative of the majority of core samples collected above the base of oxidation. The position of the major absorption feature (.86μm), and the absence of a shoulder near .65μm, indicate a haematite mineralogy.

Figure 8.3c does not have strong spectral features, but there is some evidence of absorption in the .65μm region, and a feature longer than .9μm. These are characteristics of goethite, although jarosite can also have a similar spectral shape in the VNIR.

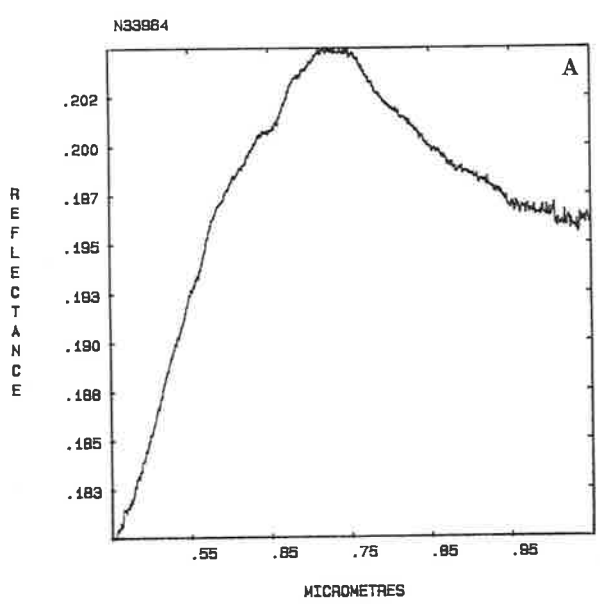
N33984
A
.202
.200
.197
.195
.193
.190
.188
.185
.183
REFLECTANCE
.55
.65
.75
.85
.95
MICROMETRES

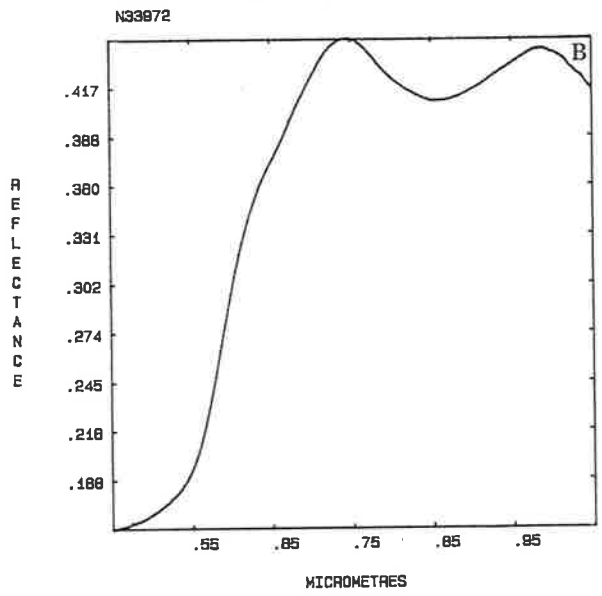
N33972
B
.417
.388
.360
.331
.302
.274
.245
.218
.188
REFLECTANCE
.55
.65
.75
.85
.95
MICROMETRES

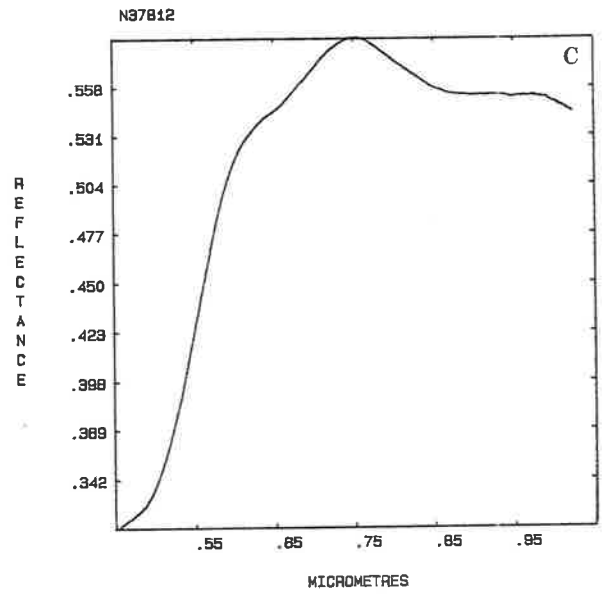
N37812
C
.558
.531
.504
.477
.450
.423
.398
.369
.342
REFLECTANCE
.55
.65
.75
.85
.95
MICROMETRES

Figures 8.4a-c Representative SWIR laboratory reflectance spectra, with strong absorption features, of core samples from Peak Hill.

These plots are good examples of the spectral properties of pyrophyllite, alunite and jarosite. The strong, sharp 2.17μm feature of pyrophyllite (Fig. 8.4a) is diagnostic (see Fig. 2.5), as is the shape of the jarosite spectrum between 2.2 and 2.3μm (compare Figs. 8.4c and Fig. 2.9). Alunite has a doublet near 1.4μm, a unique feature near 1.76μm, and a characteristic shape between 2.17 and 2.2μm (compare Fig. 8.4b to Fig. 2.9).

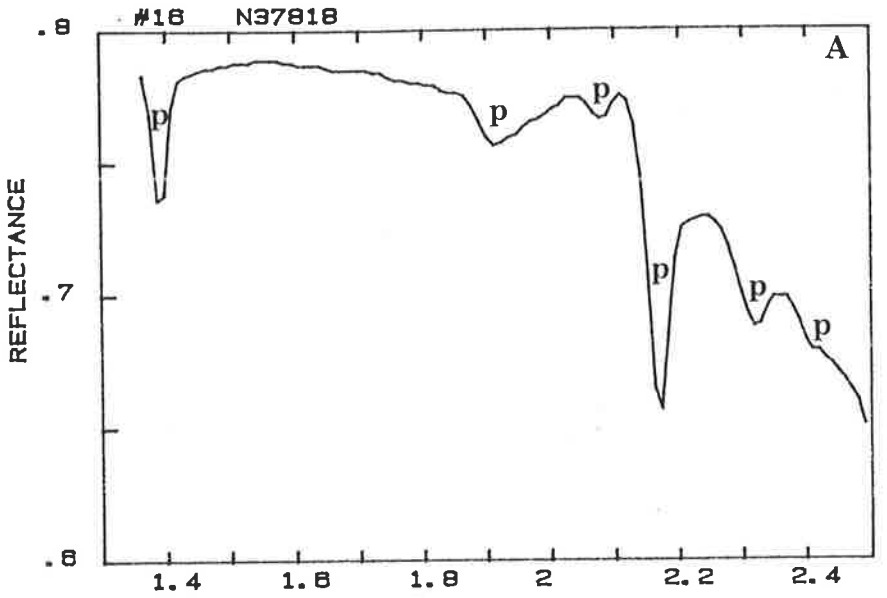
#16 N37818
A
REFLECTANCE
.8
.7
.6
p
p
p
p
p
p
1.4
1.6
1.8
2
2.2
2.4

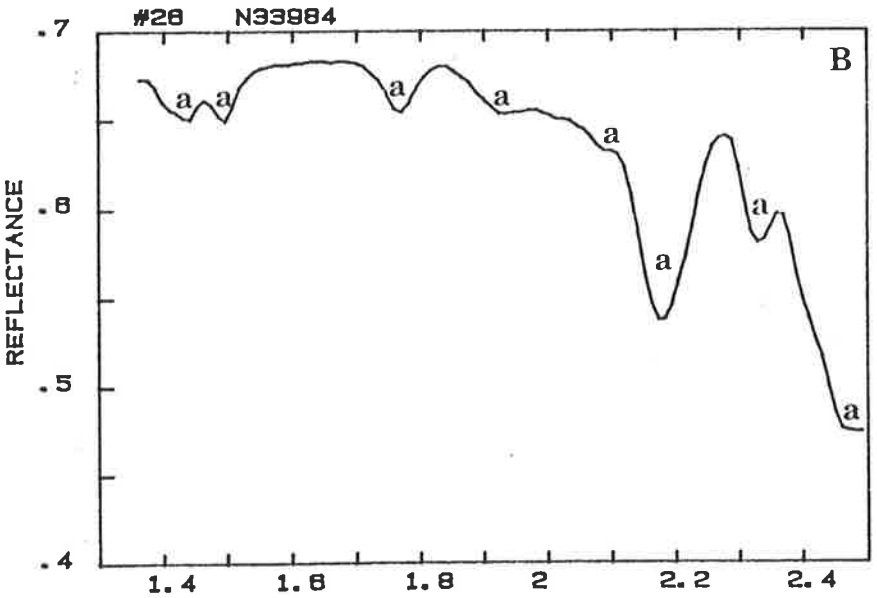
#28 N33984
B
REFLECTANCE
.7
.6
.5
.4
a
a
a
a
a
a
a
a
1.4
1.6
1.8
2
2.2
2.4

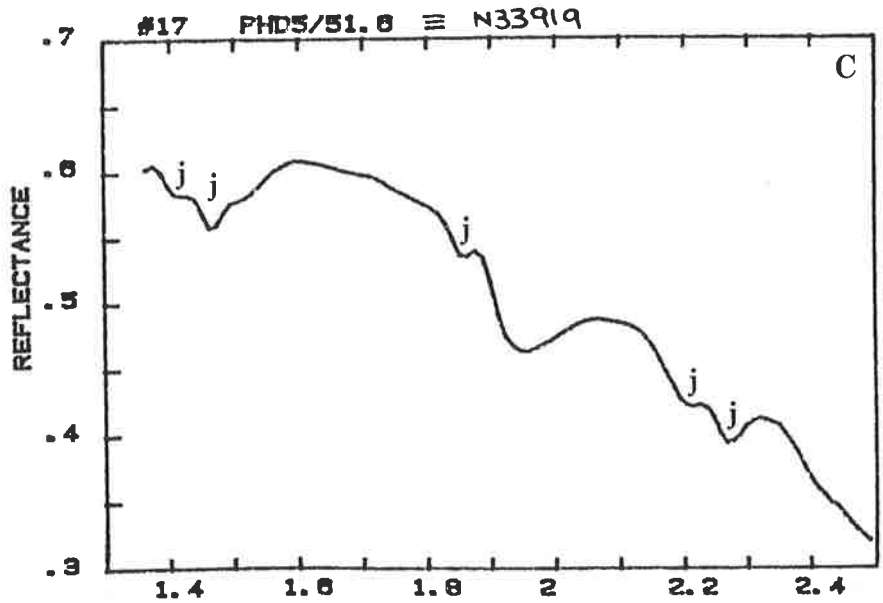
#17 PHD5/51.6 ≡ N33919
C
REFLECTANCE
.7
.6
.5
.4
.3
j
j
j
j
j
1.4
1.6
1.8
2
2.2
2.4

Figures 8.5a&b Representative SWIR laboratory reflectance spectra, with weak absorption features, of core samples from Peak Hill.

Figure 8.5a is a noisy spectrum, with weak absorption features. However, the feature near 2.2μm, with a shoulder at 2.17μm, is reminiscent of kaolinite.

Figure 8.5b appears to have a poorly-developed doublet at 2.17 and 2.2μm. This shape was initially attributed to random noise in the spectrum (note the noise level at other wavelengths), but repeated measurement of the sample resulted in identical structure. These features may therefore represent true spectral absorption. If this is the case, a mixture of pyrophyllite (sharp 2.17μm absorption) and sericite (sharp 2.2μm absorption) could be responsible.

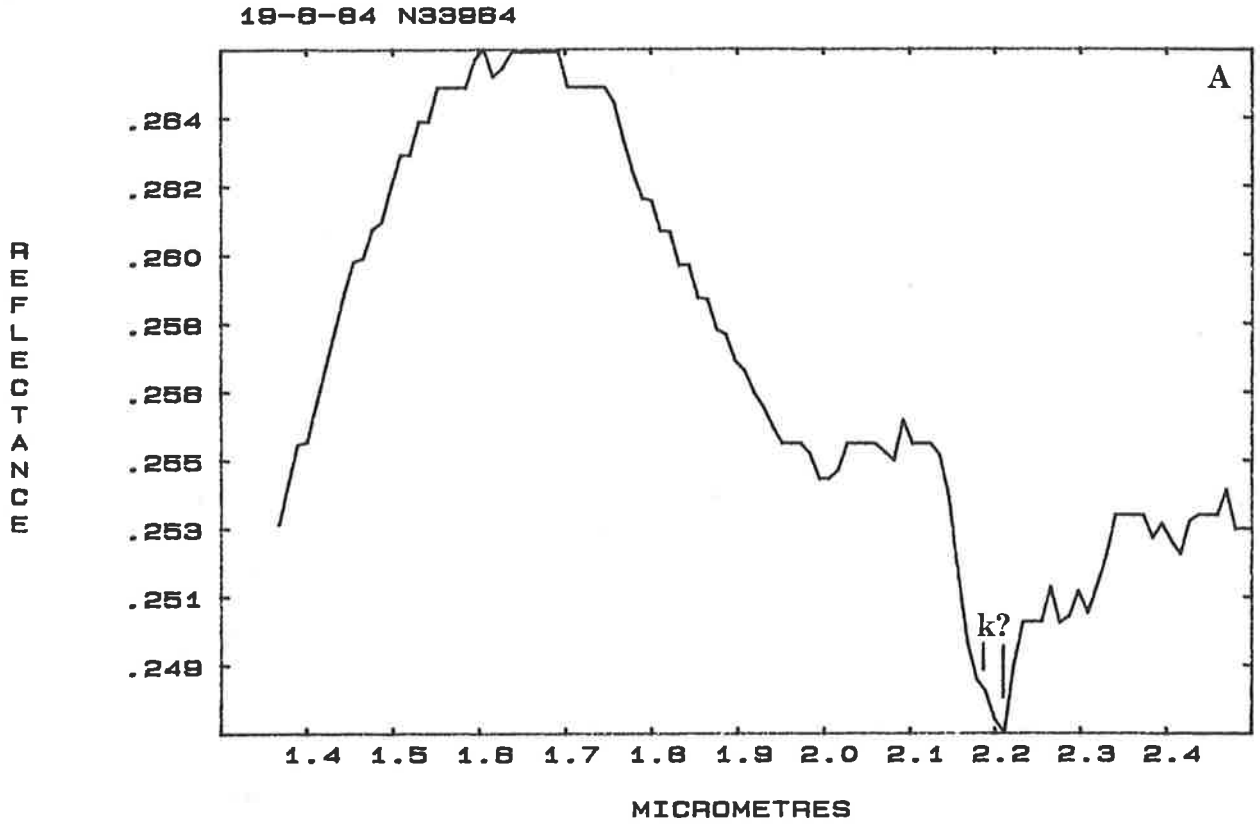
19-8-84 N33864
A
.264
.262
.260
.258
.256
.255
.253
.251
.249
k?
1.4 1.5 1.6 1.7 1.8 1.9 2.0 2.1 2.2 2.3 2.4
MICROMETRES
REFLECTANCE

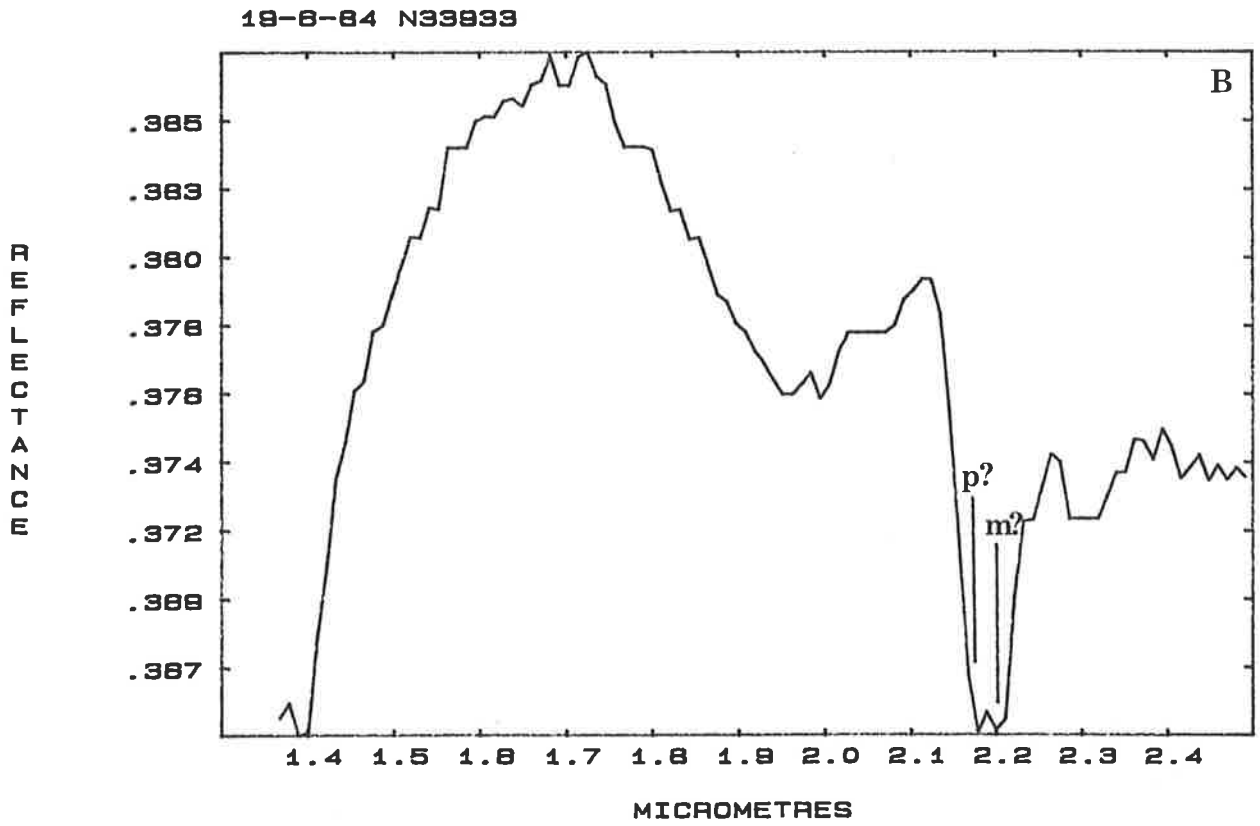
19-8-84 N33833
B
.385
.383
.380
.378
.376
.374
.372
.388
.387
p?
m?
1.4 1.5 1.6 1.7 1.8 1.9 2.0 2.1 2.2 2.3 2.4
MICROMETRES
REFLECTANCE

Figures 8.6a&b SWIR laboratory reflectance spectra of quartz-rich samples from Peak Hill.

Note the unusual, broad shapes of the 1.4 and 1.9μm water absorption features. Similar structure has been noted in a number of quartz samples containing fluid inclusions (J. Huntington, pers. comm., 1985). This information is of little use in a remote-sensing mode, however, because of atmospheric absorption in these regions.

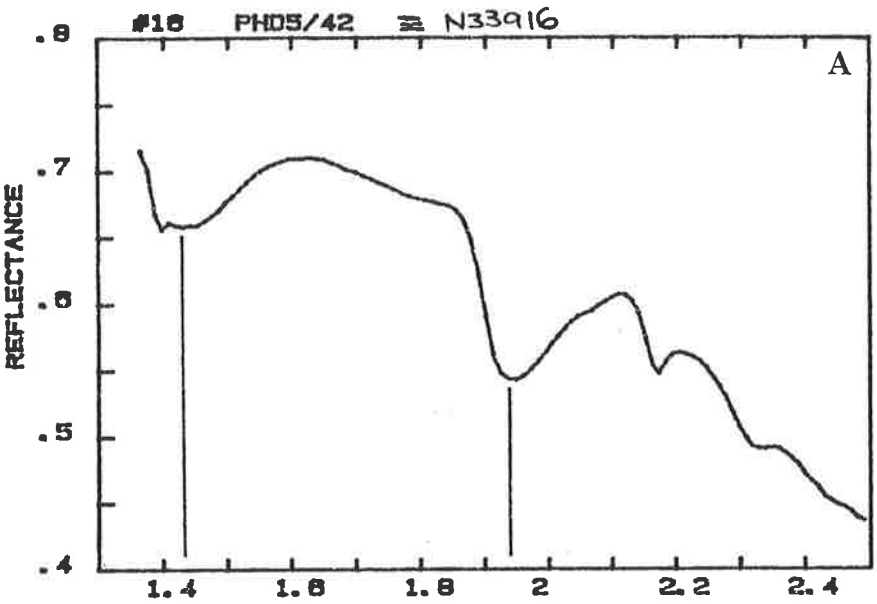
#16 PHD5/42 ≡ N33916
A
REFLECTANCE
.8
.7
.6
.5
.4
1.4
1.6
1.8
2
2.2
2.4

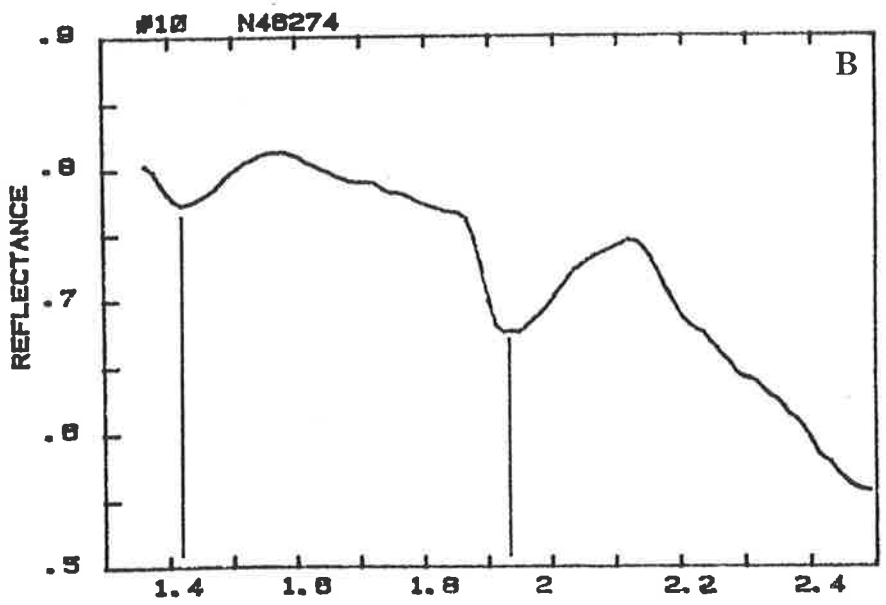
#10 N48274
B
REFLECTANCE
.9
.8
.7
.6
.5
1.4
1.6
1.8
2
2.2
2.4

Figures 8.7a-c Representative VNIR laboratory reflectance spectra of surface samples from Peak Hill.

Figure 8.7a depicts the most common VNIR spectral reflectance curve from Peak Hill surface samples. Like the core samples, the features can be attributed to haematite.

Figure 8.7b has an unusual shape, caused by a significant coating of lichen on the surface of the rock.

Figure 8.7c shows some subtle differences to the majority of the surface samples. Like Fig. 8.3c, absorption at a longer wavelength than haematite, coupled with a .65μm absorption feature, is suggestive of goethite, or perhaps jarosite.

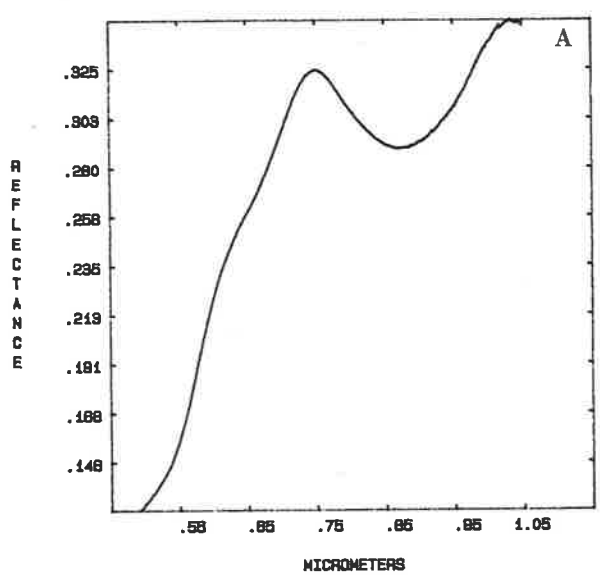
A
REFLECTANCE
.325
.303
.280
.258
.235
.213
.191
.168
.146
.55
.65
.75
.85
.95
1.05
MICROMETERS

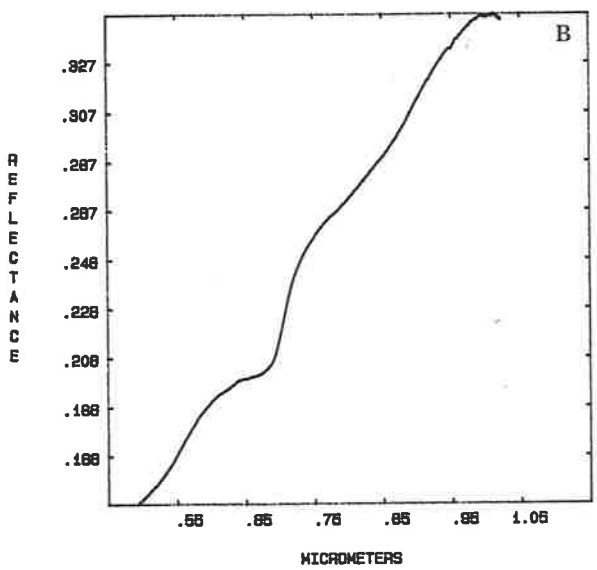
B
REFLECTANCE
.327
.307
.287
.267
.248
.228
.208
.188
.168
.55
.65
.75
.85
.95
1.05
MICROMETERS

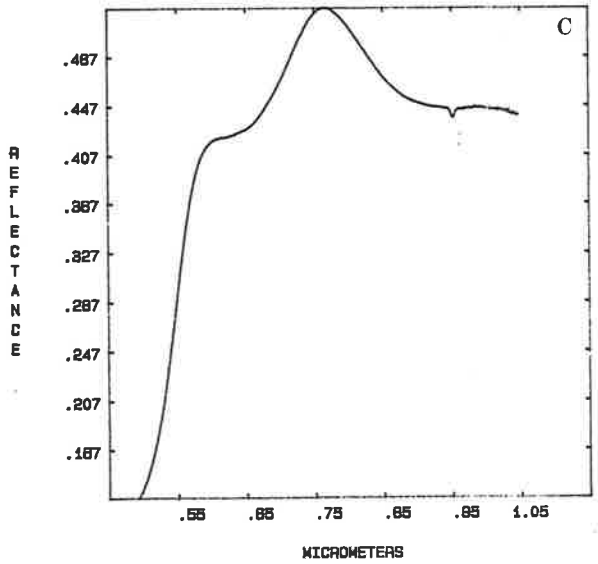
C
REFLECTANCE
.487
.447
.407
.367
.327
.287
.247
.207
.167
.55
.65
.75
.85
.95
1.05
MICROMETERS

Figures 8.8a&b Representative VNIR laboratory reflectance spectra of surface samples from Peak Hill exhibiting .95μm clay absorption features.

Both plots show moderately well-developed .95μm absorption features. Figure 8.8a exhibits the doublet structure (.956 and .965μm) of kaolinite, whilst Fig. 8.8b has a single, sharp feature at .951μm - shorter than most $3\nu_{OH}$ features, but characteristic of pyrophyllite.

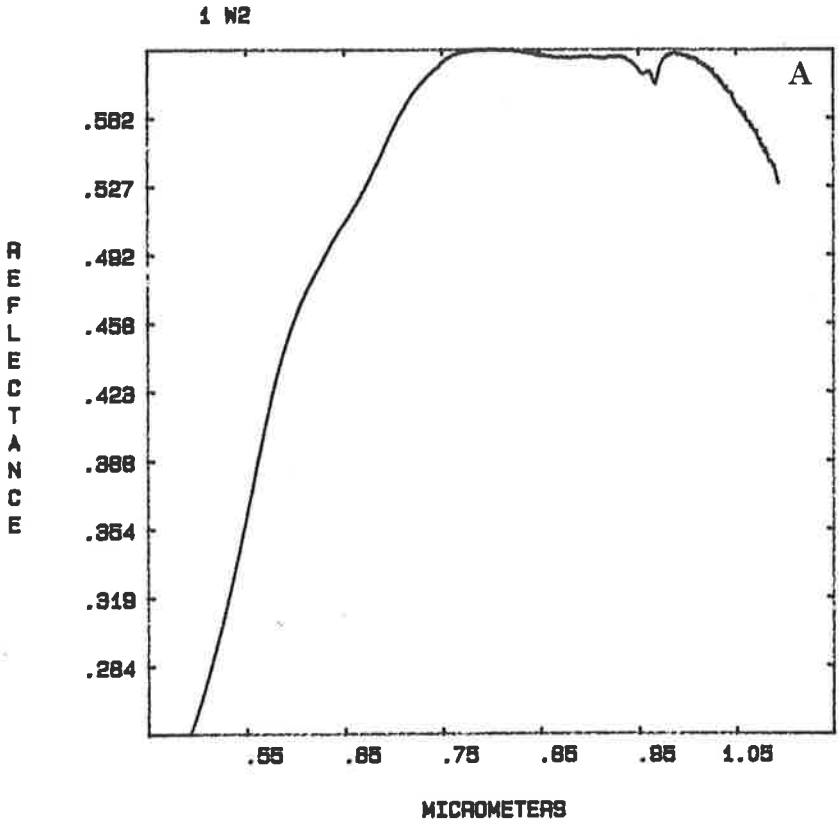
1 W2
A
.582
.527
.492
.458
.423
.388
.354
.319
.284
REFLECTANCE
.55
.65
.75
.85
.95
1.05
MICROMETERS

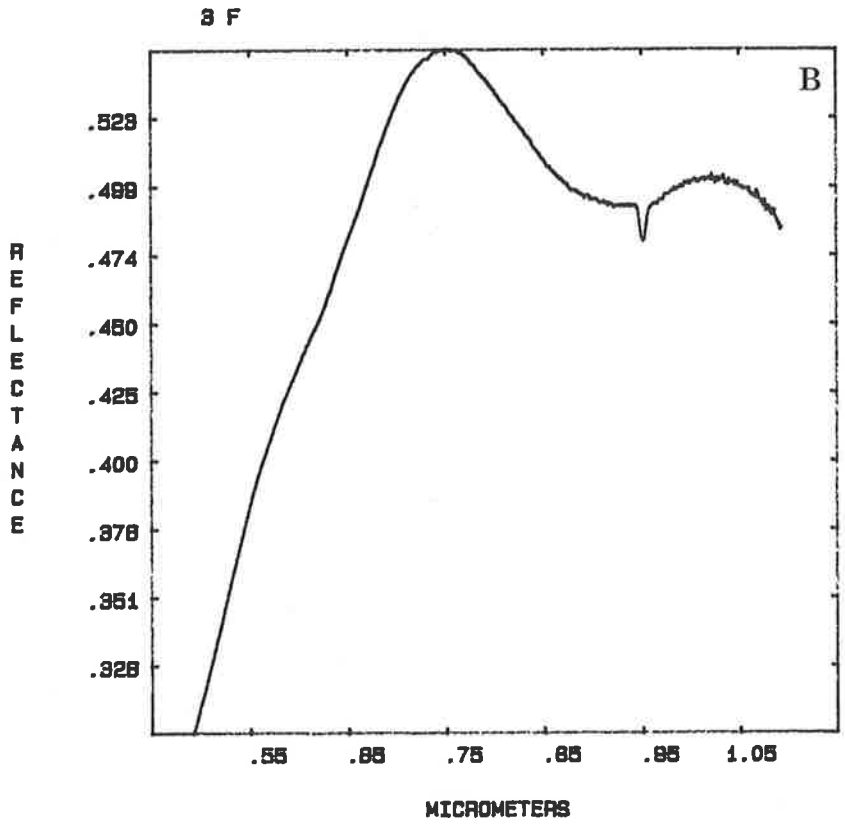
3 F
B
.523
.499
.474
.450
.425
.400
.376
.351
.328
REFLECTANCE
.55
.65
.75
.85
.95
1.05
MICROMETERS

Figures 8.9a&b SWIR laboratory reflectance spectra of pyrophyllite- and kaolinite-bearing samples from Peak Hill.

Both spectra exhibit well-developed spectral features. The pyrophyllite spectrum (Fig. 8.9a) has the unmistakable characteristics also seen in Figs. 2.5 and 8.4a. The kaolinite spectrum (Fig. 8.9b) probably has the strongest features of any Peak Hill sample, yet it is the only one collected outside the alteration zone delineated by Gold Fields. The spectral features may, therefore, be due to intense weathering, rather than to alteration.

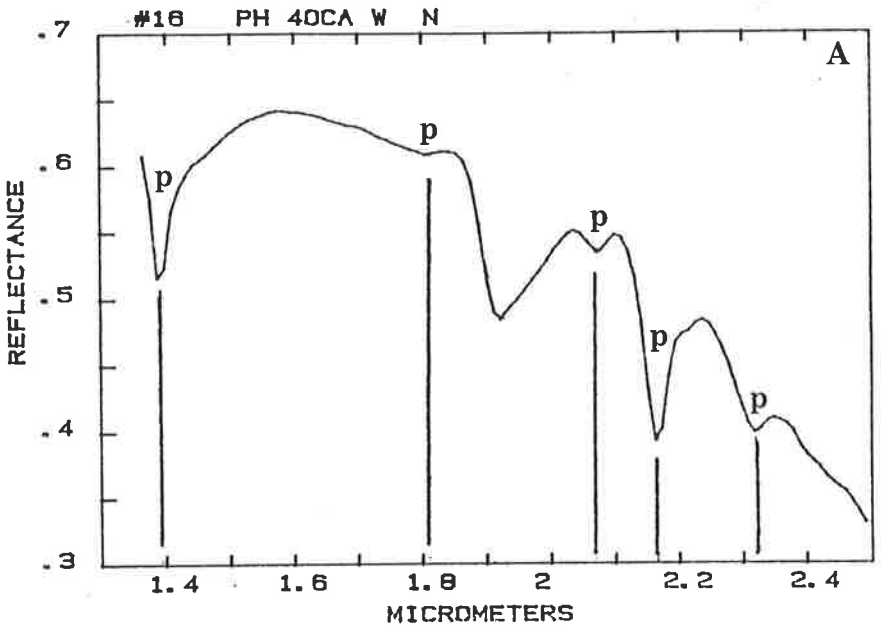
#16 PH 40CA W N
A
REFLECTANCE
.7
.6
.5
.4
.3
p
p
p
p
p
1.4
1.6
1.8
2
2.2
2.4
MICROMETERS

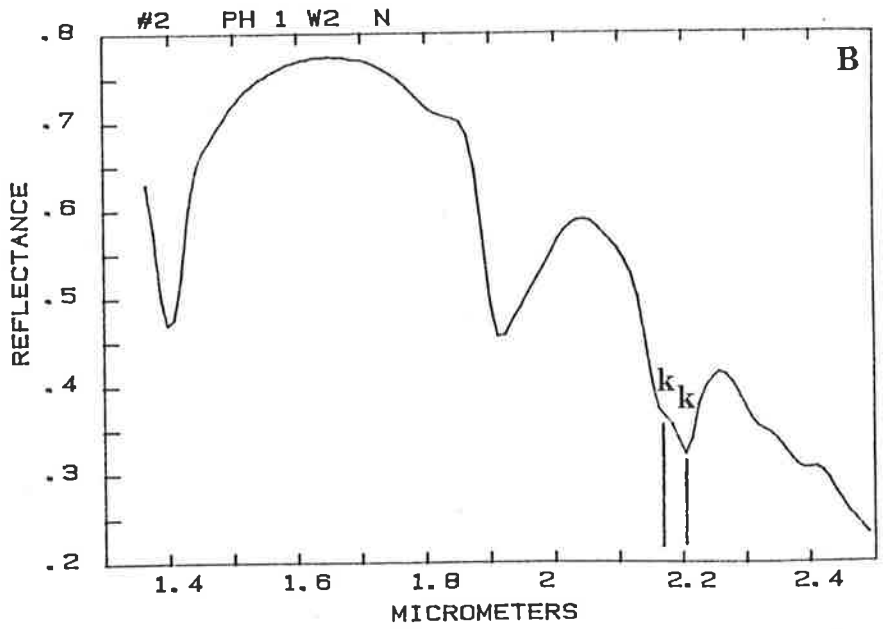
#2 PH 1 W2 N
B
REFLECTANCE
.8
.7
.6
.5
.4
.3
.2
k
k
1.4
1.6
1.8
2
2.2
2.4
MICROMETERS

Figures 8.10a&b Photographs and SWIR laboratory reflectance spectra of muscovite- and jarosite-bearing rocks from Peak Hill.

Figures 8.10a&b show the rock surfaces measured (the black dot indicates the precise centre of measurement), and the resultant spectra of, muscovite- (sericitic) and jarosite-bearing samples, respectively. Both spectra are characteristic (see Fig. 2.5 for muscovite and Fig. 2.9 for jarosite).

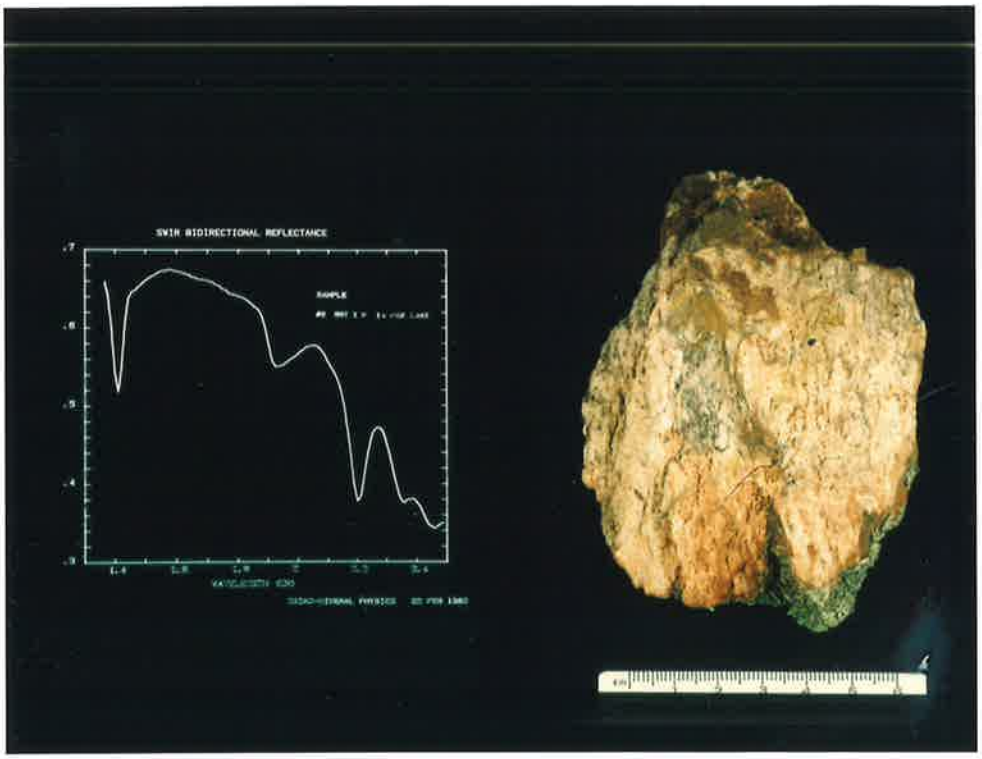
SWIR BIDIRECTIONAL REFLECTANCE
SAMPLE
.7
.6
.5
.4
.3
1.4
1.6
1.8
2
2.2
2.4
WAVELENGTH (UM)
CSIRO-MINERAL PHYSICS

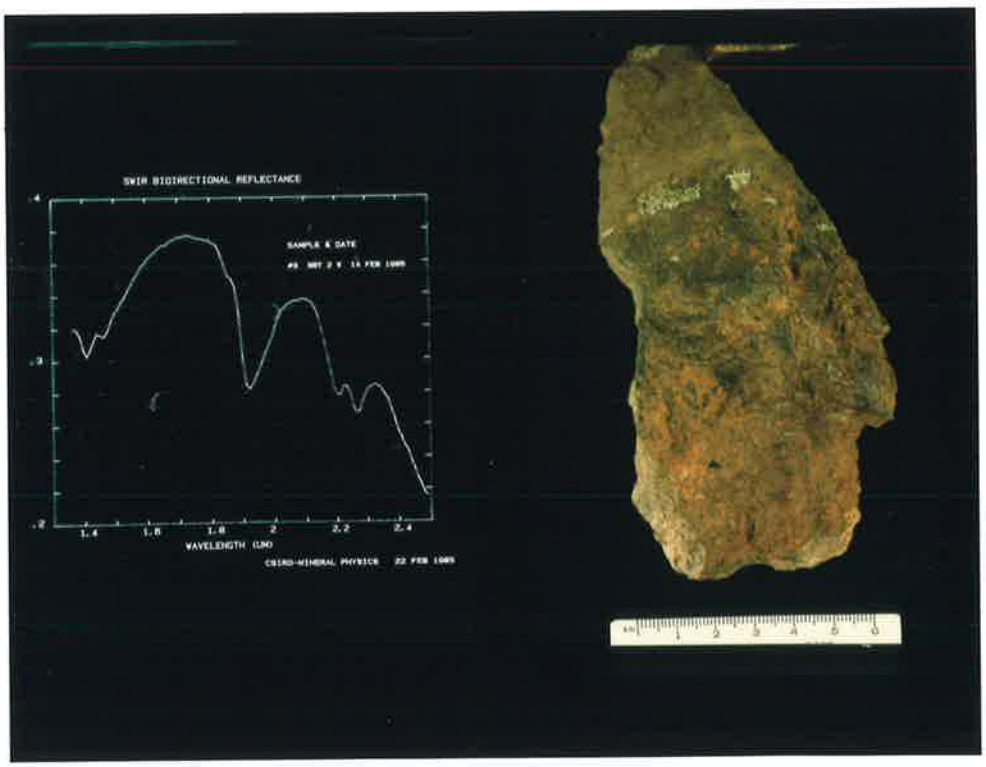
SWIR BIDIRECTIONAL REFLECTANCE
SAMPLE & DATE
.4
.3
.2
1.4
1.6
1.8
2
2.2
2.4
WAVELENGTH (UM)
CSIRO-MINERAL PHYSICS

Figures 8.11a&b Photographs and spectra of weathered and fresh surfaces of rock from Peak Hill with unusual spectral characteristics.

The spectral features of this sample occur in weathered and fresh surfaces, and are both moderately sharp. Both facts point to a mineralogical origin, rather than to lichen. The feature at the shorter wavelength of 2.08μm appears at the same wavelength as that of topaz (see Figs. 5.29a&b), whilst the longer wavelength feature appears at 2.17μm (the same wavelength as pyrophyllite). Neither mineral was reported present from XRD analysis.

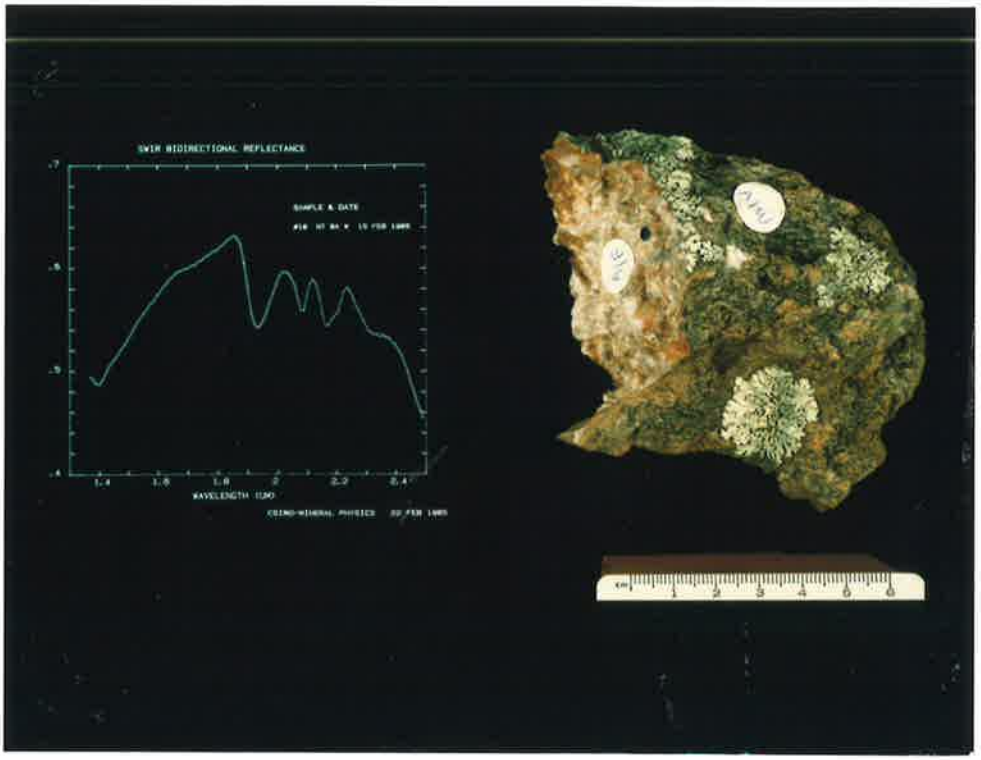
SWIR BIDIRECTIONAL REFLECTANCE
SAMPLE & DATE
.7
.6
.5
.4
1.4
1.6
1.8
2
2.2
2.4
WAVELENGTH (UM)
CSIRO-MINERAL PHYSICS 22 FEB 1985

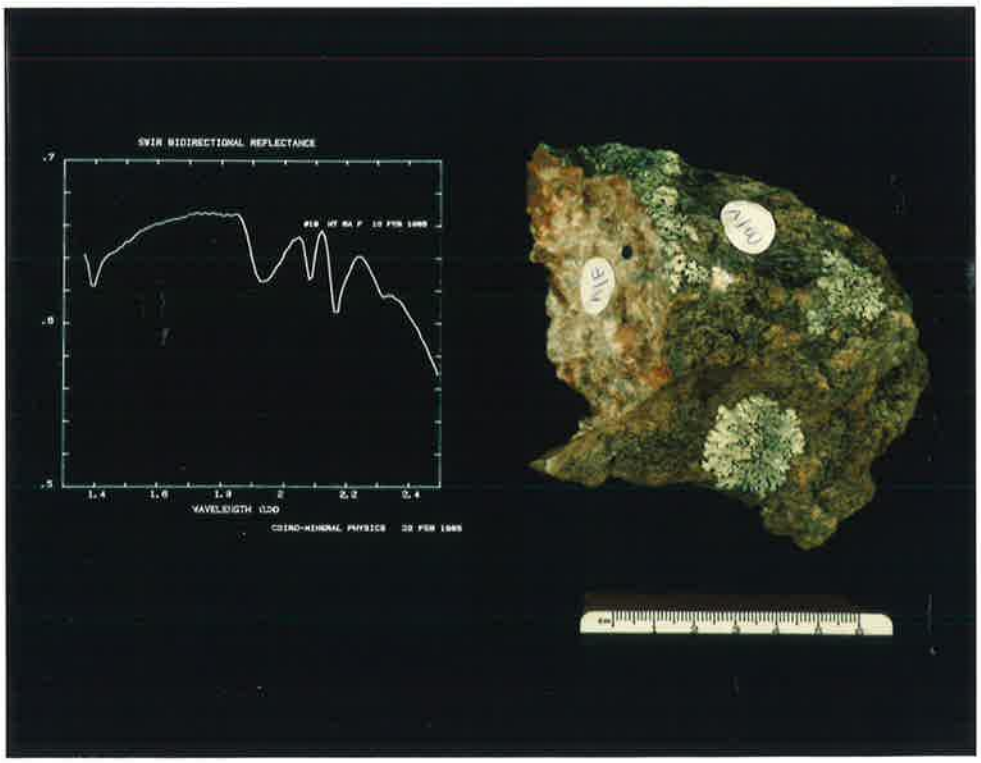
SWIR BIDIRECTIONAL REFLECTANCE
.7
.6
.5
1.4
1.6
1.8
2
2.2
2.4
WAVELEIGTH (UM)
CSIRO-MINERAL PHYSICS 22 FEB 1985

Figure 8.12 Location of samples used in the Peak Hill study.

See Figs. 8.1 and 8.2 for location of the grid. Gold Fields' core samples are shown as circles, surface samples collected by the author are shown as crosses.

PEAK HILL MINERALOGY
SAMPLE LOCATIONS

KEY

O = CORE SAMPLE (XRD)
X = SURFACE SAMPLE (SPECTRA)

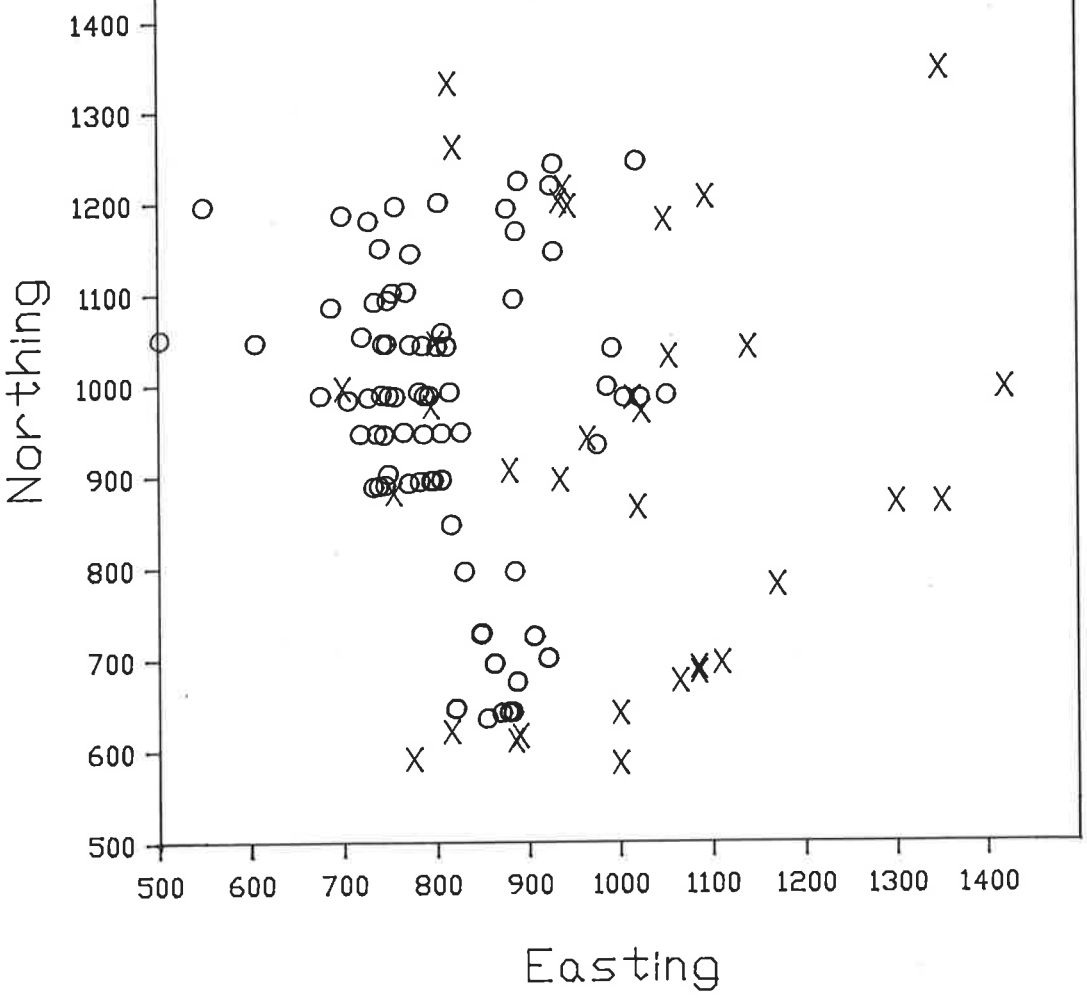

Figure 8.13 Distribution of pyrophyllite at Peak Hill determined from XRD of core samples and interpretation of SWIR laboratory reflectance spectra of surface samples (overlay).

The hatched areas on Figs. 8.14 to 8.18 outline the core samples containing 20% or more of the minerals indicated (as determined by XRD analysis).

Note the good correspondence between the location of the pyrophyllite zone, as determined from XRD of core, with that determined from the spectra of surface samples (overlay).

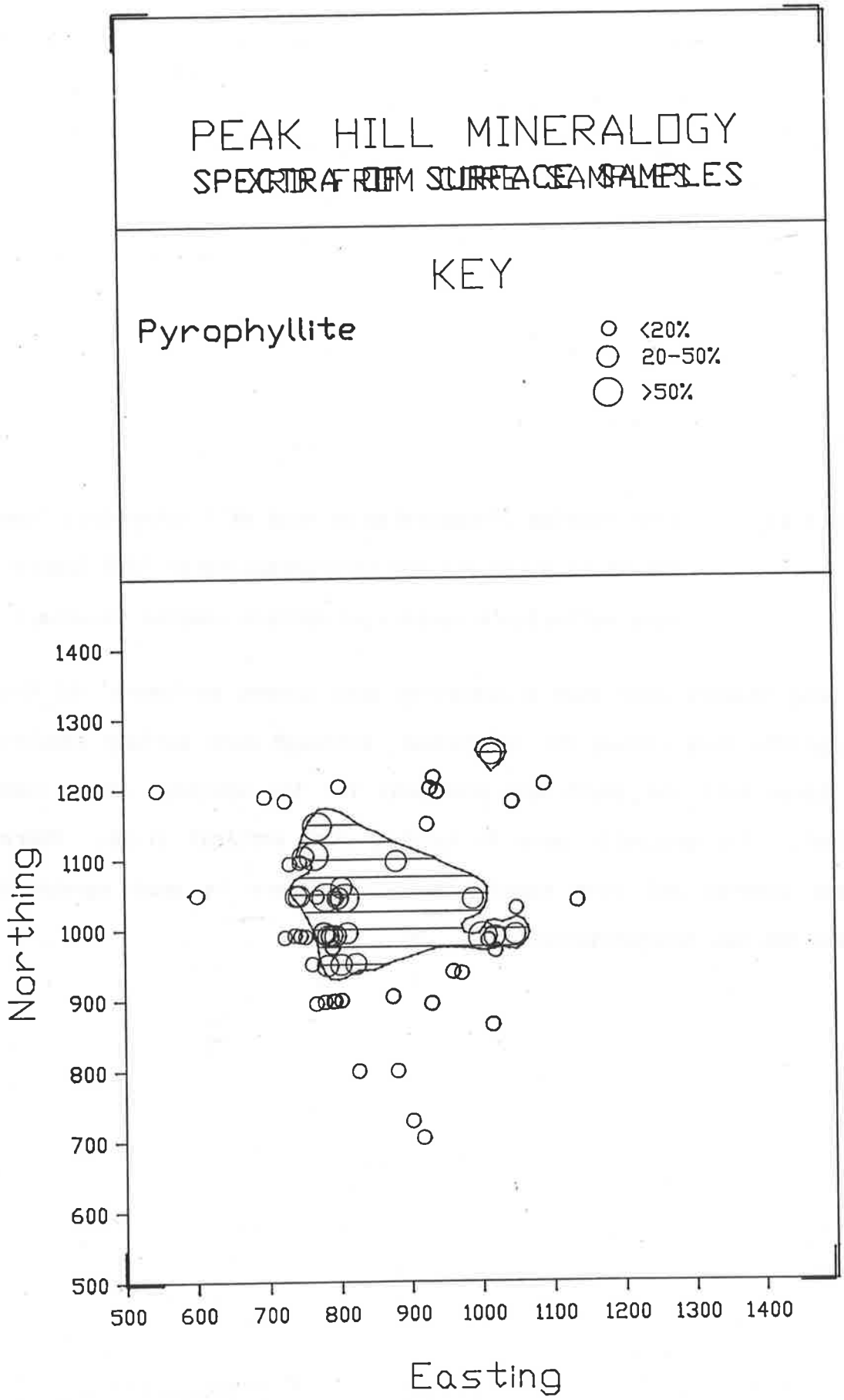
PEAK HILL MINERALOGY
SPECTRA FROM SURFACE SAMPLES
KEY
Pyrophyllite
<20%
20-50%
>50%
1400
1300
1200
1100
1000
900
800
700
600
500
Northing
500
600
700
800
900
1000
1100
1200
1300
1400
Easting

Figure 8.14 Distribution of muscovite at Peak Hill determined from XRD of core samples and interpretation of SWIR laboratory reflectance spectra of surface samples (overlay).

Both studies show that a muscovite zone occurs peripheral to the pyrophyllite zone (shown for reference), although more surface samples were taken from the south and southeast for the spectral study (see overlay). The muscovite zone is hatched with vertical lines. Where surface samples and core samples coincide, there is good agreement between the two interpretations.

PEAK HILL MINERALOGY

SPECTRA FROM SURFACE SAMPLES

KEY

Muscovite

○ <20%
○ 20–50%
○ >50%

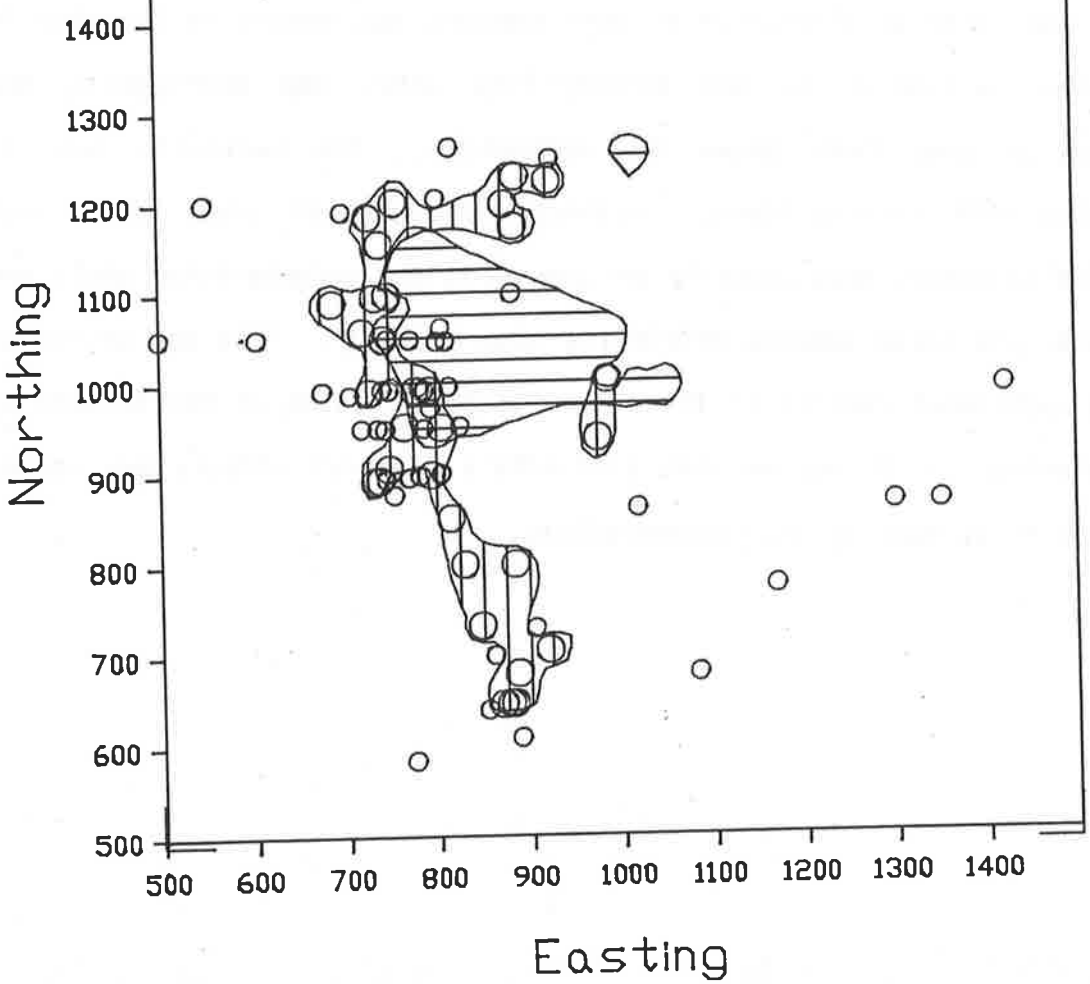

Figure 8.15 Distribution of kaolinite at Peak Hill determined from XRD of core samples and interpretation of SWIR laboratory reflectance spectra of surface samples (overlay).

Kaolinite is widespread in core samples, but occurs in quantity in a zone peripheral to the pyrophyllite zone, and overlapping the muscovite zone (both shown for reference). The kaolinite zone is hatched with sloping lines. Although the spectral study shows that kaolinite occurs most commonly peripheral to the pyrophyilite, there are several kaolinite samples within its zone boundary. This may be due to some additional control of the kaolinite distribution at the surface by weathering, or it may be that kaolinite's spectral effects are strong enough to be seen at low concentrations.

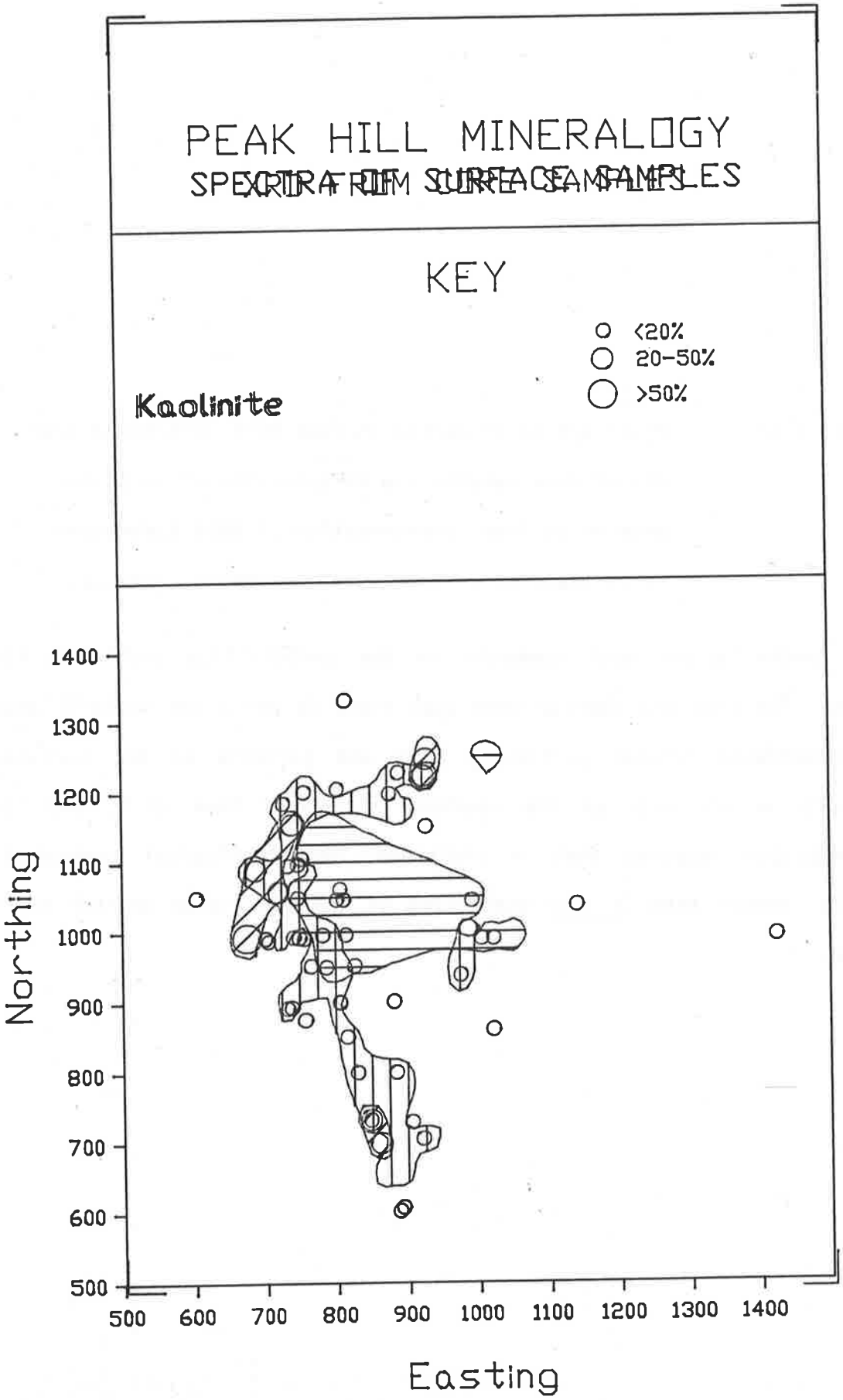
PEAK HILL MINERALOGY
SPECTRA FROM SURFACE SAMPLES
KEY
<20%
20-50%
>50%
Kaolinite
Northing
Easting
1400
1300
1200
1100
1000
900
800
700
600
500
500
600
700
800
900
1000
1100
1200
1300
1400

Figure 8.16 Distribution of pyrite at Peak Hill determined from XRD of core samples and distribution of jarosite determined from interpretation of SWIR laboratory reflectance spectra of surface samples (overlay).

Pyrite occurs most commonly in the pyrophyllite and muscovite zones. The plot and overlay show that there is not a particularly good correspondence between pyrite in core and jarosite at the surface. Jarosite occurs only on the southern slopes of Peak Hill, and its distribution suggests that an additional geomorphological control is likely, rather than *in situ* weathering of the most sulphide-rich rocks alone.

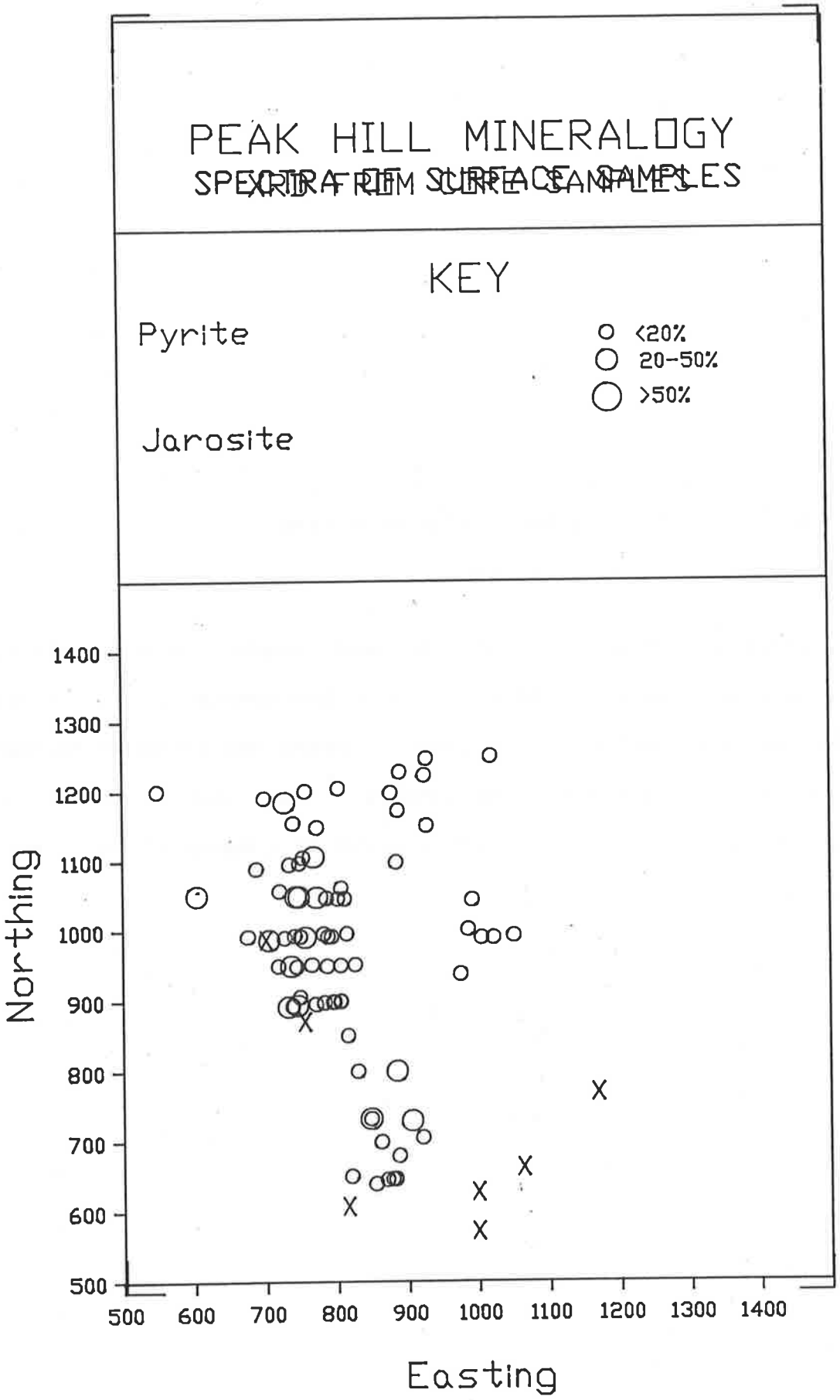
PEAK HILL MINERALOGY
SPECTRA FROM SURFACE SAMPLES
KEY
Pyrite
<20%
20-50%
>50%
Jarosite
Northing
Easting
1400
1300
1200
1100
1000
900
800
700
600
500
500
600
700
800
900
1000
1100
1200
1300
1400

Figure 8.17 Distribution of alunite at Peak Hill determined from XRD of core samples.

Alunite determined from XRD of core samples shows a strong coincidence with the muscovite distribution (see overlay). Alunite was interpreted from spectra of core samples (despite the estimated maximum content of 10% shown for these samples). The absence of alunite features in spectra of surface samples is due to a dearth of the mineral in outcrop.

PEAK HILL MINERALOGY
XRD FROM CORE SAMPLES

KEY

Alunite — All 2-10%

Muscovite

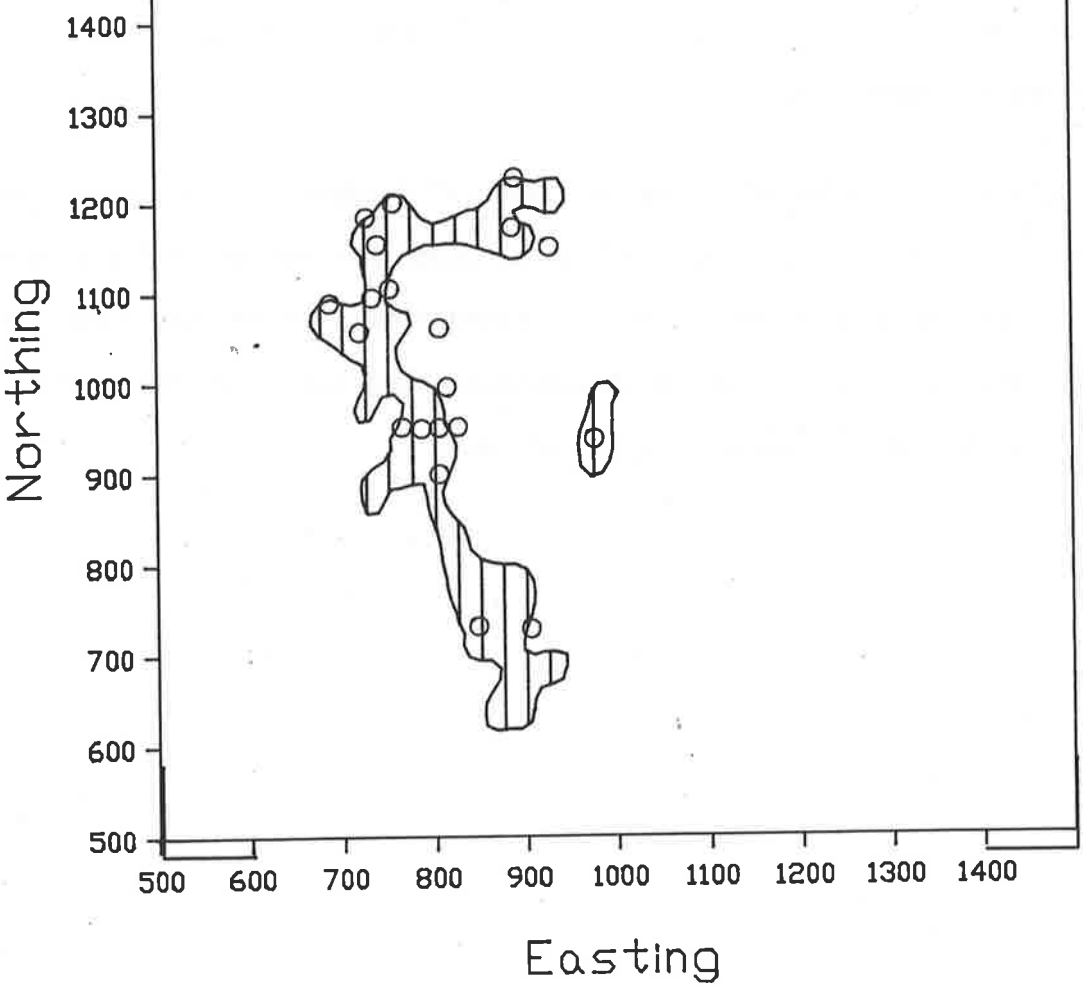

Figure 8.18 Summary diagram showing pyrophyllite, muscovite and kaolinite zones (determined from XRD analyses of core samples) compared to mineralogy interpreted from SWIR spectral features (overlay).

The results from Figs.8.14 to 8.17 have been summarised and presented together here.

Note the location of anomalous spectral features in the north and northeast of the area. Three of these samples have tentatively been interpreted as topaz- and pyrophyllite-bearing, whilst the last has tentatively been interpreted as diaspore-bearing (although XRD analysis has failed to confirm these interpretations).

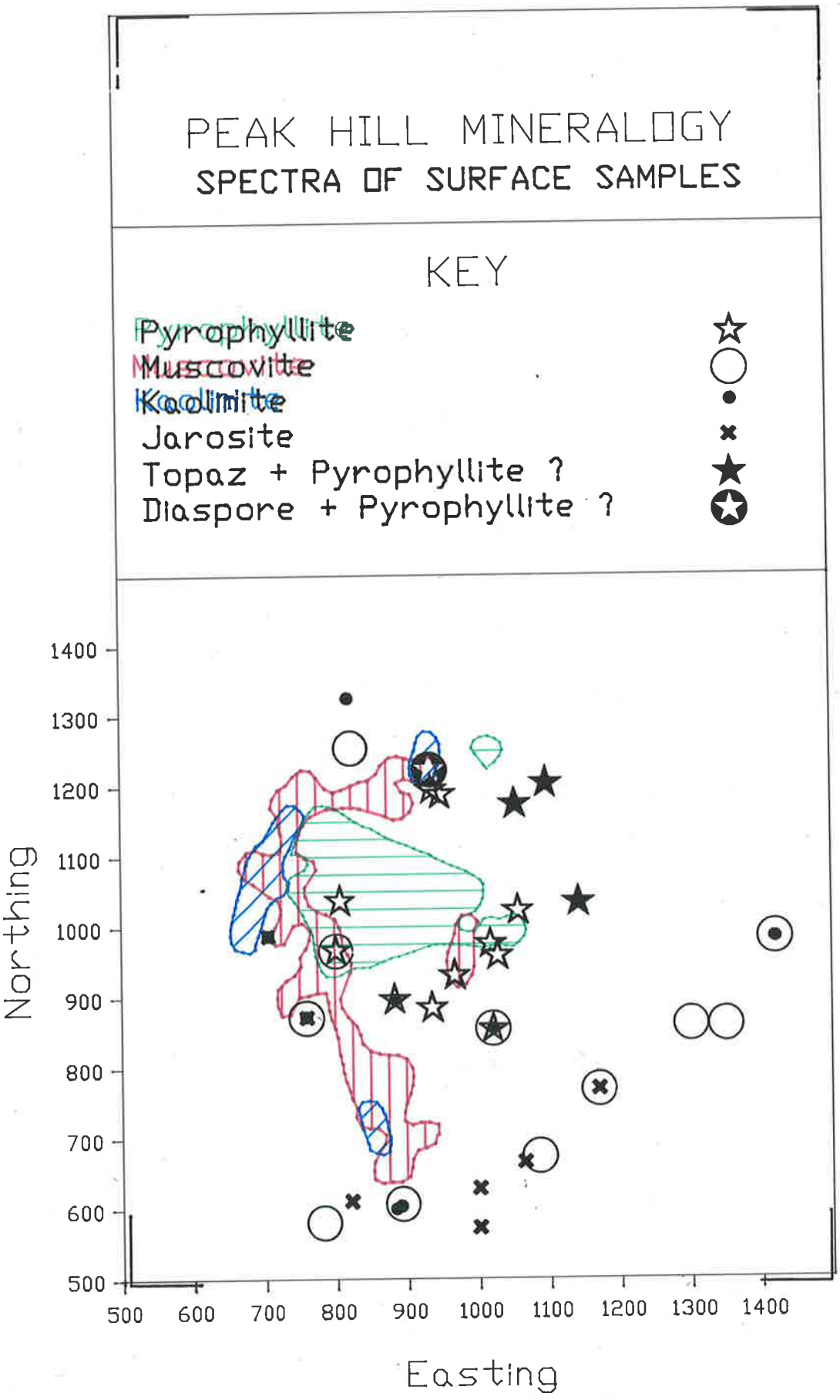
PEAK HILL MINERALOGY
SPECTRA OF SURFACE SAMPLES
KEY
Pyrophyllite
Muscovite
Kaolinite
Jarosite
Topaz + Pyrophyllite ?
Diaspore + Pyrophyllite ?
Northing
Easting
500
600
700
800
900
1000
1100
1200
1300
1400